Vergleichende molekulare Charakterisierung *Ctnnb1*- und *Ha-ras*-mutierter Mauslebertumoren

Comparative Molecular Characterization of *Ctnnb1*- and *Ha-ras*-mutated Mouse Liver Tumors

Dissertation

der Mathematisch-Naturwissenschaftlichen Fakultät
der Eberhard Karls Universität Tübingen
zur Erlangung des Grades
eines Doktors der Naturwissenschaften
(Dr. rer. nat.)

vorgelegt von
Elif Bettina Unterberger
aus Den Haag

Tübingen

2013

Tag der mündlichen Prüfung:	13.5.2013
Dekan:	Prof. Dr. Wolfgang Rosenstiel
1. Berichterstatter:	Prof. Dr. Michael Schwarz
2. Berichterstatter:	Prof. Dr. Klaus Schulze-Osthoff

The presented thesis was prepared at the Institute of Experimental and Clinical Pharmacology and Toxicology, Department of Toxicology, at the Eberhard Karls Universität Tübingen between September 2009 and March 2013 under the supervision of Prof. Dr. Michael Schwarz.

During this time period I overtook the supervision of a diploma student, Kathrin Knötzsch, who carried out mutation analysis of spontaneous mouse liver tumors.

Parts of this work have been conducted in cooperation with external partners. mRNA expression and DNA methylation profiling, as well as characterization of Meg3/Gtl2 by immunohistochemistry and *in situ* hybridization was conducted at the Novartis Institutes for BioMedical Research in Basel, Switzerland. CXR Biosciences in Dundee, Scotland, carried out miRNA expression measurements, and reverse phase protein microarray analysis was conducted at NMI, Reutlingen, Germany.

Pre-processing and statistical analysis of raw data gained from these experiments was done by Johannes Eichner, Clemens Wrzodek (University of Tübingen, Department of Computer Science, Cognitive Systems) and Raphaëlle Luisier (Department for Discovery and Investigative Safety, Novartis Institutes for BioMedical Research, Basel, Switzerland).

It is not the mountain we conquer, but ourselves.

Sir Edmund Hilary

Acknowledgements

First and foremost, I would like to thank my supervisor Prof. Michael Schwarz for giving me the opportunity to work on a fascinating and relevant topic, for his support and trust, and for generously sharing his vast knowledge about carcinogenesis.

My sincere thanks go to:

The IMI MARCAR consortium for financial support and for generating and sharing a large amount of the raw data analyzed in the course of this thesis.

Johannes Eichner and Clemens Wrzodek for their tremendous help in bioinformatically analyzing the datasets and for never growing tired of patiently answering my innumberable questions.

The members of the Novartis Institutes for BioMedical Research for their support and technical guidance in conducting immunohistochemical stainings and *in situ* hybridization.

Elke Zabinsky for excellent technical support with immunohistochemical stainings.

All members of the Department of Toxicology in Tübingen for creating a positive working atmosphere and for their constant support in all scientific, bureaucratic and personal matters.

My loving thanks go to my parents, who have always supported and encouraged me in every possible way, for their love and trust and for making me regain perspective when times were rough.

I thank Jörg, my angel, my best friend through thick and thin, for everything.

Parts of this work have been presented:

Lempiäinen H, Couttet P, Bolognani F, Müller A, Dubost V, Luisier R, Espinola Adel R, Vitry V, **Unterberger EB**, Thomson JP, Treindl F, Metzger U, Wrzodek C, Hahne F, Zollinger T, Brasa S, Kalteis M, Marcellin M, Giudicelli F, Braeuning A, Morawiec L, Zamurovic N, Längle U, Scheer N, Schübeler D, Goodman J, Chibout SD, Marlowe J, Theil D, Heard DJ, Grenet O, Zell A, Templin MF, Meehan RR, Wolf RC, Elcombe CR, Schwarz M, Moulin P, Terranova R, Moggs JG.: *Identification of Dlk1-Dio3 imprinted gene cluster non-coding RNAs as novel candidate biomarkers for liver tumor promotion*, **Toxicological Sciences 131(2), 375-386, doi: 10.1093/toxsci/kfs303**

Unterberger EB, Schwarz M: *Biomarkers and molecular tumour classification for non-genotoxic carcinogenesis*, ToxNet Baden-Württemberg Symposium, Konstanz, Germany, 2011 (**poster presentation**)

Unterberger EB, Schwarz, M: *Mechanisms of non-genotoxic carcinogenesis – novel insights from integrated genetic, transcriptomic and epigenomic profiling*, 26th GUM meeting (Society of mutational and environmental research), Mainz, Germany, 2012 **(invited lecture)**

Unterberger EB, Schwarz M: *Biomarkers and molecular tumour classification for non-genotoxic carcinogenesis*, 78th meeting of the German Society of Pharmacology and Toxicology, Dresden, Germany, 2012 (**oral presentation, awarded with the Sanofi-Aventis-Prize for best oral presentation)**

Zeller E, Kramer-Potapenja V, **Unterberger EB**, Braeuning A., Schwarz M: *Long non-docing RNA Gtl2/Meg3 and its role in hepatic cancer*, 79th meeting of the German Society of Pharmacology and Toxicology, Halle an der Saale, Germany, 2013 **(poster presentation)**

Table of contents

Abbreviations

5’-hmC	5’-hydroxymethylcytosine
5’-mC	5’-methylcytosine
APC	adenomatous polyposis coli
APS	ammonium peroxydisulfate
bp	base pairs
BSA	bovine serum albumin
°C	degree Celsius
CAR	constitutive androstane receptor
CK1	casein kinase 1
Ctnnb1	β-Catenin
Cyp	cytochrome P-450
DEN	N-Nitrosodiethylamine
Dio3	type 3 iodothyronine deiodinase
Dlk1	delta-like 1 homolog
DNA	deoxyribonucleic acid
ELK1	ETS domain-containing protein Elk-1
g	gram
GS	glutamine synthetase
GSK3β	glycogen synthase kinase 3 β
GAP	GTPase-activating protein
GTP	guanosine triphosphate
Ha-ras	Harvey rat sarcoma
HCC	hepatocellular carcinoma
IG-DMR	intergenic differentially methylated region
Igf2(r)	insulin-like growth factor 2 (receptor)
Irm	imprinted RNA near *Meg3*/*Gtl2*
l	liter
lncRNA	long non-coding RNA
M	molar
m	milli-
MAPK	mitogen-activated protein kinase
Meg3/Gtl2	maternally expressed gene 3/gene-trap locus 2
miRNA	microRNA
Mirg	microRNA-containing gene
MMTV	mouse mammary tumor virus
mRNA	messenger-RNA
µ	micro-
NGC	non-genotoxic carcinogen
PAS staining	periodic acid-Schiff staining
PB	phenobarbital
PBS	phosphate-buffered saline
Raf	rat fibrosarcoma
RFLP	restriction fragment length polymorphism
Rian	RNA imprinted and accumulated in nucleus
RNA	ribonucleic acid

Rtl1	retrotransposon-like 1
TCF/LEF	T-cell factor/lymphoid enhancer factor
TEMED	N,N,N′,N′-Tetramethylethane-1,2-diamine
TSS	transcription start site
vol/wt	volume/weight
Wnt	wingless/integration1

1. Introduction

As of 2008, cancer was the second most frequent cause of death in both sexes worldwide (WHO), with hepatocellular carcinoma (HCC) accounting for 9.2% of deaths caused by cancer (GLOBOCAN 2008 project, http://globocan.iarc.fr, status of November 2012). The term cancer describes not one but many diseases defined by very diverse genotypes and phenotypes, which, however, have one thing in common: they are triggered by a complex combination of genetic lesions and epigenetic effects. Tumor promoters, such as phenobarbital in the mouse liver, drive the selective proliferation of cells harboring specific genetic defects via indirect, non-genotoxic mechanisms. The modes of action of tumor promoters are understood to only a small extent, and their effects are extremely difficult to predict as, in contrast to mutagenicity, no reliable short-term assays exist to assess non-genotoxic carcinogenicity. In the age of high-throughput microarray technology, the integrative bioinformatic and biological analysis of large “omics” datasets to identify early molecular biomarkers is a new approach in understanding the global molecular changes during carcinogenesis and has already been applied to a number of human cancers (Kristensen et al.; Shen et al., 2007; Martín-Subero et al., 2009). As the liver is the main target organ for non-genotoxic carcinogens (NGCs), the assessment and integration of global molecular changes in liver tissue is specifically important for predicting non-genotoxic carcinogenesis (http://www.imi-marcar.eu).

1.1 Physiology of the liver

The liver is the largest gland in vertebrates and plays a crucial role in many vitally important processes in the organism, including uptake of nutrients from the intestine, biosynthesis, degradation and distribution of various biomolecules, as well as biotransformation of xenobiotics and drugs. It is composed of four lobes of unequal sizes and shapes and, in humans, constitutes 2-4% of the entire body weight. The liver is supplied with blood by two main vessels that enter at its transverse fissure, or porta: the hepatic artery which branches off the abdominal aorta and delivers oxygen-rich blood, and the portal vein delivering blood which is low in oxygen but nutrient-rich from the stomach, intestine, spleen and pancreas. Blood is transported out of the liver via the hepatic vein and flows further to the heart and lung via the caudal vena cava. Hepatocytes, also called parenchymal liver cells, are the functional hepatic cells and account for approximately 60% of all cells in the liver and 80% of the total organ volume. In addition to metabolizing both endogenous molecules and xenobiotics, an important function of hepatocytes is bile production. Secreted bile is collected

by canaliculi and eventually transported into the gall bladder via the common hepatic duct. In the gall bladder, bile is stored and, upon food uptake, discharged into the duodenum, where it acts as an emulsifier and facilitates lipid digestion. The distribution of the branches of the hepatic blood vessels and bile canaliculi in a liver section defines the smallest anatomical and functional units of the liver at the histological scale, the liver lobule and acinus, respectively (figure 1.1). The liver lobule has an idealized hexagonic shape, with the central vein in the middle. The corners of the hexagon are formed by the terminal branches of the portal vein, the hepatic artery and a bile canaliculus, a structure called portal triad. The hepatocytes are arranged in plates which radiate from the central vein to the portal triads. From the portal vein and hepatic artery in the portal triad, a mix of oxygen- and nutrient-rich blood flows through the lobule in fenestrated sinusoidal capillaries to the central vein. As bile is secreted by hepatocytes and transported to the canaliculi in the portal triad, bile flow is opposite to that of blood.

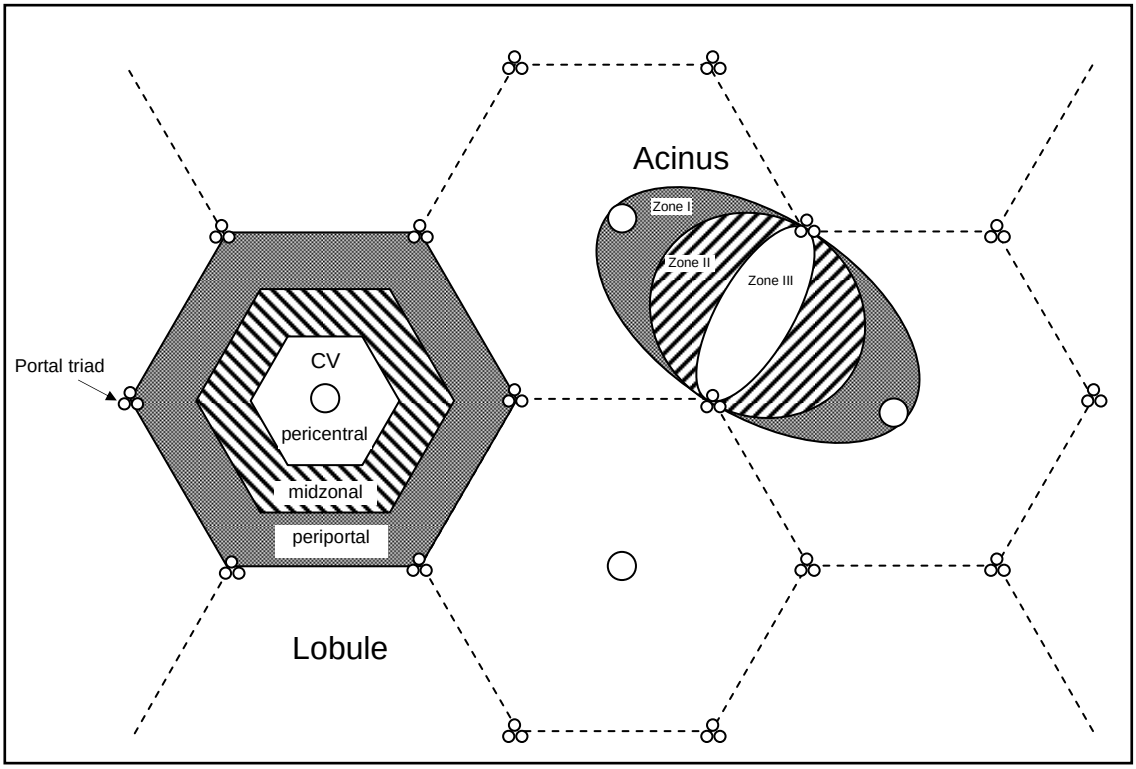

Figure 1.1. Schematic description of liver architecture according to the lobule and the acinus model, respectively. “CV” indicates the central vein.

The liver parenchyma shows heterogeneity in function which is based on the location of the hepatocytes within the lobule, and according to this, it can be divided into three arbitrary zones: the pericentral zone (surrounding the central vein, poorest in oxygen), the periportal

zone (closest to the portal triad, forming the rim of the virtual hexagon), and the midzonal area (between pericentral and periportal zone) (see figure 1.1). Periportal and pericentral hepatocytes vary in their phenotypes and gene expression patterns concerning a number of processes, such as intermediary and xenobiotic metabolism (see figure 1.2). For example, periportal hepatocytes show increased rates of gluconeogenesis and amino acid catabolism, whereas their pericentral counterparts display higher levels of glycolysis and cytochrome P450 enzymes (Jungermann et al., 1989; Gebhardt, 1992; Jungermann et al., 1996; Oinonen et al., 1998; Braeuning et al., 2006). The gene expression patterns in the periportal and pericentral hepatocytes are similar to those found in mouse liver tumors mutated in the *Ha-ras* (Harvey rat sarcoma)- and *Ctnnb1* (β-Catenin)-genes, respectively (Braeuning et al., 2007a). Indeed, recent data indicate that activation of the MAPK (mitogen-activated protein kinase) signaling pathway, which is up-regulated in *Ha-ras*-mutated tumors, maintains the periportal and inhibits the pericentral phenotype (Braeuning et al., 2007b), whereas Wnt/β-Catenin signaling, which is constitutively active in *Ctnnb1*-mutated tumors, keeps up the pericentral phenotype (Benhamouche et al., 2006a; Benhamouche et al., 2006b; Hailfinger et al., 2006; Torre et al., 2009).

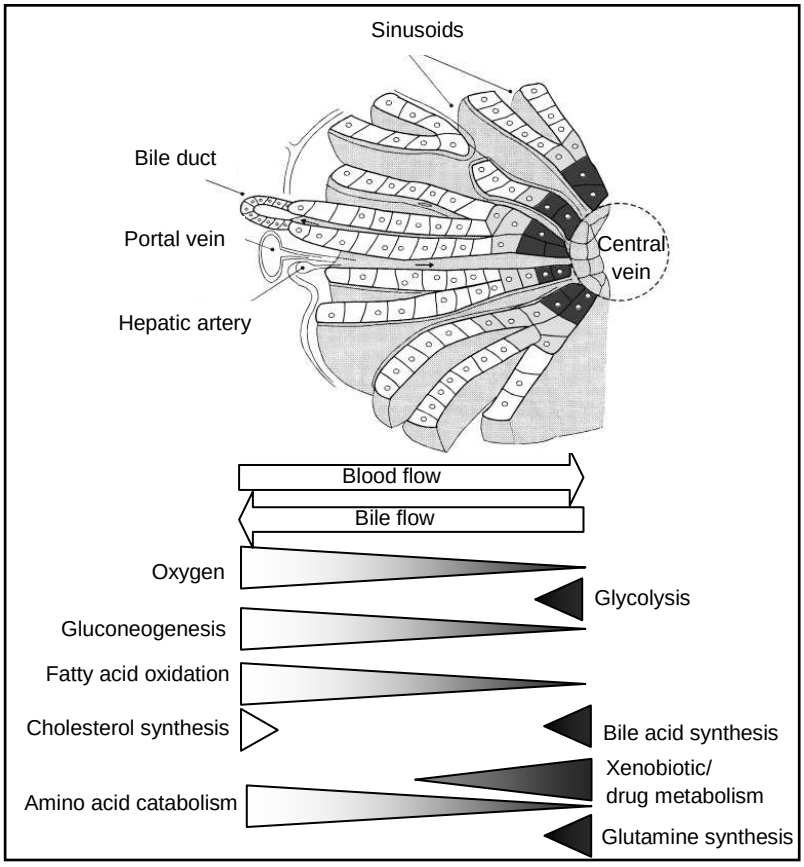

Figure 1.2. Overview of zonated gene expression in the liver.

1.2 Chemical carcinogenesis

According to the classic view, the formation of malignant tumors, or carcinogenesis, is described as a stepwise sequence of tumor initiation, promotion and progression (for reviews see Armitage, 1985; Nowell, 1976). During the first step of initiation, a single normal cell is irreversibly converted into a so-called pre-neoplastic cell by induction of mutations in either proto-oncogenes or tumor suppressor genes. Proto-oncogenes are genes which, upon initiation, are excessively transcribed or result in constitutively activated gene products, so-called oncoproteins, whereas tumor suppressor genes undergo loss or decrease of function when mutated in the course of initiation. In their normal form, these two types of genes ensure the homeostasis of central regulatory processes in the cell. For instance, the gene products of *Ha-ras* (Harvey rat sarcoma) and *B-raf* (rat fibrosarcoma) (section 1.2.2) regulate the transmission of growth-factor-mediated signaling and induce cell proliferation, whereas the proteins encoded by p53 (Vogelstein et al., 2000) or INK4a/ARF (p19(Arf)) (Sherr et al., 2000) are responsible for the physiological induction of apoptosis. Once a cell has been initiated, it is susceptible to the effects of tumor promoters, non-genotoxic agents that provide the cell with a selective proliferation advantage. This leads to clonal expansion of the pre-cancerous cell and, eventually, the formation of a well-defined, benign tumor. Finally, as the tumor progresses into a malignant state, more mutations are introduced and the tumor cells increasingly dedifferentiate and proliferate, pushing aside healthy tissue and gaining the potential to form metastases. Hanahan and Weinberg have extended the classical view of the multistep process in 2000 and 2011, respectively, hypothesizing that a cell has to acquire six characteristic capabilities before it gains independence from internal and external regulatory mechanisms and eventually becomes a cancer cell (Hanahan et al., 2000; Hanahan et al., 2011).

In the mouse model, the genotype and phenotype of chemically generated tumors can be influenced by the initiation-promotion treatment regimen (Stahl et al., 2005a). Mouse liver tumors initiated with the genotoxin N-nitrosodiethylamine (DEN) mainly harbor mutations in *Ha-ras* (~50%) or *B-raf* (~20%) (Aydinlik et al., 2001; Jaworski et al., 2005a), which lead to constitutive activation of the MAPK signaling pathway (see section 1.2.2). If DEN-initiated mice are additionally treated with the anticonvulsant phenobarbital (PB) as a tumor promoter, the resulting tumors harbor activating mutations in the proto-oncogene *Ctnnb1* (see section 1.2.1), which encodes β-Catenin, a key mediator in the canonical Wnt signaling pathway (Aydinlik et al., 2001; Strathmann et al., 2006). PB activates target gene transcription by inducing the nuclear translocation of the constitutive androstane receptor (CAR) (Honkakoski

et al., 1998) and has recently been shown to induce DNA-methylation changes in the promoter region of the CAR target gene *Cyp2b10* (cytochrome P450, family 2, subfamily b, polypeptide 10) (Lempiainen et al., 2011). However, how PB stimulates the selective outgrowth of *Ctnnb1*-mutated cells remains unknown.

1.2.1 Canonical Wnt signaling pathway

The *Wnt* gene (a portmanteau of *Wg*, *Wingless*, and *Int1*, *Integration 1*) was identified in 1982 by Nusse and Varmus, who found that *Int1* was activated in mice by insertion of the mouse mammary tumor virus (MMTV) (Nusse et al., 1982). Later, the homology between *Int1* and the *wingless* gene in drosophila melanogaster was discovered, hence the term *Wnt* (Rijsewijk et al., 1987). The protein encoded by *Wnt* is an extracellular ligand which binds to Frizzled receptors and thus activates the Wnt/β-Catenin signaling pathway, a highly conserved signaling cascade controlling development, mitogenic stimulation and differentiation of cells by regulating transcription factors of the TCF/LEF family (TCF = T-cell factor, LEF = lymphoid enhancer factor). In the absence of Wnt, an intracellular protein complex is formed, which consists of Axin, APC (adenomatous polyposis coli), GSK3β (glycogen synthase kinase 3β), CK1 (casein kinase 1) and β-Catenin (figure 1.3) (Luo et al., 2007). β-Catenin is then phosphorylated in two steps: first, CK1 acts as a "priming kinase" and phosphorylates β-Catenin at serine 45 (Amit et al., 2002). This is followed by phosphorylation of serine 33, serine 37 and threonine 41 by GSK3β (Liu et al., 2002). β-Catenin is then targeted for proteasomal degradation. Upon binding of Wnt to Frizzled, the cytoplasmic protein Dishevelled (Dvl) inhibits the formation of the protein complex, which leads to the stabilization of β-Catenin. The latter can thus translocate into the nucleus and, as a complex with TCF/LEF, activate target gene transcription (figure 1.3).

Mutations affecting the phosphorylation sites of β-Catenin, e.g. in codons 33, 37, 41, 45 or neighboring sites of the murine *Ctnnb1*-gene, can lead to the protein's stabilization and thus to a constitutive activation of β-Catenin-mediated signaling. Such activating point mutations in *Ctnnb1* are frequent in both mouse and human hepatocellular carcinoma and a number of other cancers (de La Coste et al., 1998).

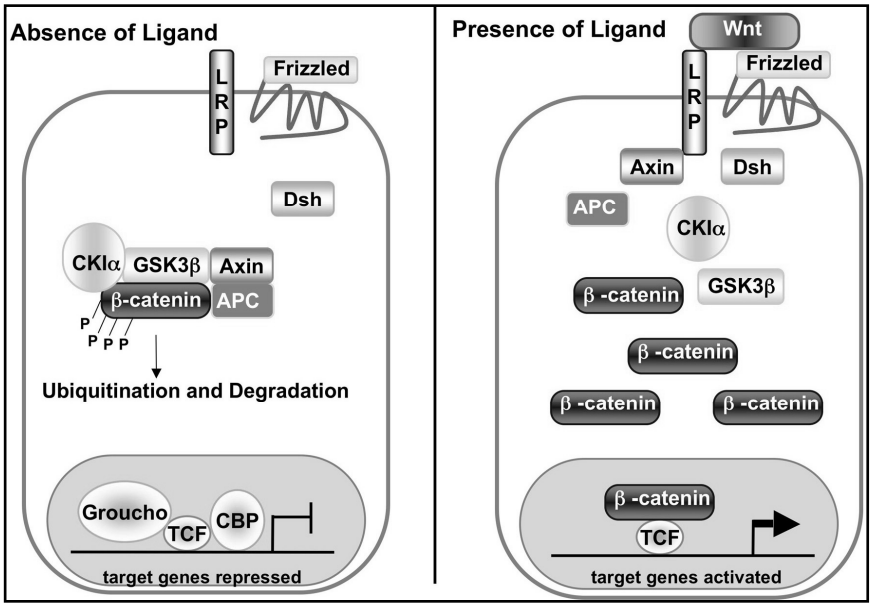

Figure 1.3: Wnt/β-Catenin signaling pathway in absence (left panel) and presence (right panel) of Wnt (modified from Eisenmann, 2005). Abbreviations: LRP, LDL-receptor-relacted protein; Dsh, dishevelled; Ck1, casein kinase 1; GSK3β, glycogen synthase kinase 3β; APC, adenomatous polyposis coli; TCF, T-cell factor; CBP, CREB-binding protein.

1.2.2 Mitogen-activated protein kinase (MAPK) signaling pathway

The mitogen-activated protein kinase (MAPK) pathway is a signaling cascade which mediates signals from cell surface receptors to the nucleus via a number of effector kinases. Small monomeric G-proteins of the Ras-family (**ra**t **s**arcoma) are transformed into their active GTP-binding forms upon receptor-mediated extracellular mitogenic stimuli (figure 1.4) (Kolch, 2000). Ras acts as a molecular switch which can bind and activate its downstream kinase Raf (**ra**t **f**ibrosarcoma). Activated Raf launches a phosphorylation cascade in the cytosol: first, Raf phosphorylates MEK (mitogen-activated protein kinase kinase, also known as MAP2K), which then phosphorylates MAPK (mitogen-activated protein kinase, also known as ERK). MAPK can phosphorylate a number of substrates, including transcription factors such as ELK1 (E twenty-six (ETS)-like transcription factor 1) and thus regulates cell growth, proliferation and differentiation. It is therefore not surprising that some genes encoding components of the MAPK pathway are proto-oncogenes, the mutation of which can lead to constitutive activation of the pathway and thus to cancer. Codons 12, 13 and 61 of the *Ha-ras*-gene (**Ha**rvey **ra**t **s**arcoma) are hotspot point mutation sites in mice. Mutations at these codons inhibit the interaction of the Ras-protein with its inactivator GAP (GTPase-activating protein) and thus lead to constitutive activity of Ras. Similarly, point mutations in codon 637 (formerly referred to as codon 624) in the murine *B-raf*-gene activate the B-raf kinase. The

MAPK pathway is constitutively activated in a large number of tumor cell lines and primary human tumors (Hoshino et al., 1999), and both *Ras*- and *Raf*-mutations have been detected in many human cancers (Bos, 1989; Davies et al., 2002; Garnett et al., 2004).

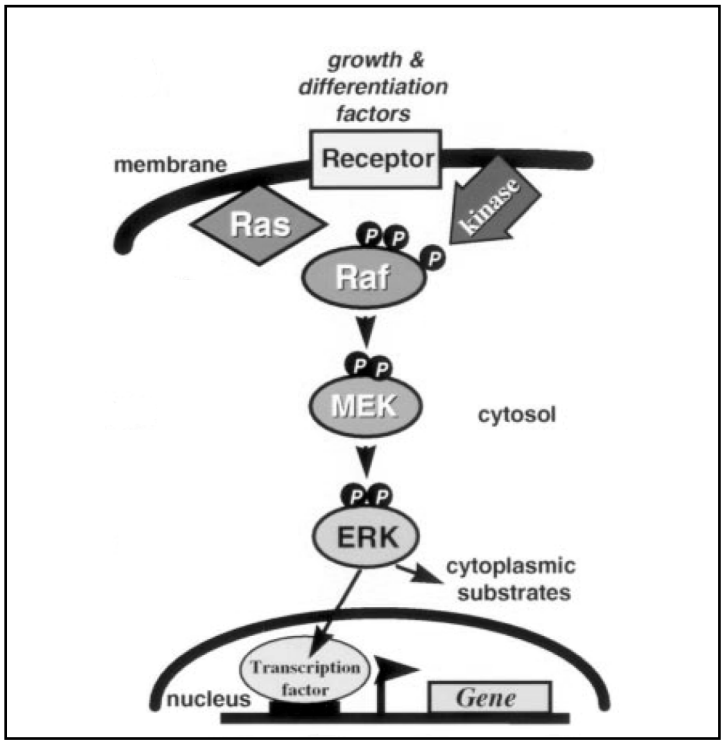

Figure 1.4: MAPK pathway (modified from Kolch, 2000).

1.3 Epigenetic mechanisms in carcinogenesis

Epigenetics, which involves DNA methylation, modification of histones and non-coding RNAs, is crucial for normal development and maintenance of cellular homeostasis. Correct DNA methylation patterns established during embryogenesis in mammals are a precondition for the maturation of healthy adult organisms (for review see Hall, 1990; Bartolomei et al., 2011), and posttranslational modification of histones is a key determinant of chromatin regulation and thus gene expression in the cell (Wolffe et al., 1999). Small non-coding RNAs, so-called microRNAs or miRNAs, negatively regulate the expression of genes containing complementary target sequences (for review see Bartel, 2004; He et al., 2004). Thus, functional impairment of any of these mechanisms can lead to severe diseases, including cancer.

A number of miRNAs have been associated with cancer, in this case termed “oncomirs” (Esquela-Kerscher et al., 2006; Braconi et al., 2011; Wang et al., 2012c). Their longer relatives, the long non-coding RNAs, or lncRNAs, also play a role in tumorigenesis, but their

function is less understood than that of miRNAs (Chen et al., 2010; Prensner et al., 2011). An observation frequently made in tumors is a global change in the methylation at the 5'-position of cytosine in the context of CG-rich sequences (Ehrlich, 2002; Esteller, 2005). 5'-methylcytosine (5'-mC) is a well characterized DNA modification and can be enzymatically transformed into a number of derivatives, including 5'-hydroxymethylcytosine (5'-hmC) (Tahiliani et al., 2009; Ito et al., 2011; Wu et al., 2011). Originally considered a mere intermediate of DNA demethylation, 5'-hmC has recently been shown to be altered in tumors (Yang et al., 2012) and is meanwhile assumed to be an independent regulatory DNA modification.

The epigenetic effects of many tumor promoters have been characterized and published. For instance, PB causes specific DNA methylation changes in the rodent liver which may underlie its capacity to promote the outgrowth of cancer cells (Watson et al., 2002; Bachman et al., 2006; Phillips et al., 2007). The chronology of epigenetic mechanisms in carcinogenesis is not entirely clear. According to the classic 3-step-model of carcinogenesis, tumor promoters can stimulate the growth of already initiated cells via non-genotoxic mechanisms, but there are also indications that epigenetic mechanisms are among the earliest events in carcinogenesis and occur long before the genotoxic events of intiation (Feinberg et al., 2006). This complexity and lack of a consistent detectable endpoint make it difficult to predict the effects of NGCs, which underlines the relevance of current endeavors to identify early and predictive biomarkers for these substances (Lempiainen et al., 2013) (www.imi-marcar.eu).

1.3.1 The *Dlk1-Dio3* imprinted gene cluster

Genomic imprinting is an epigenetic mechanism unique to mammals which causes the parent-of-origin-specific transcription of some genes by methylation and silencing of either the paternal or the maternal allele. The methylation marks leading to transcriptional inactivation of one allele are established during gametogenesis and maintained in the somatic cells of the adult organism (figure 1.5). Less than 1% of mammalian genes are imprinted (Wilkinson et al., 2007), including those encoding insulin-like growth factor 2 (*Igf2*) (DeChiara et al., 1991), insulin-like growth factor 2-receptor (*Igf2r*) (Stoger et al., 1993) and H19 (Bartolomei et al., 1991) in mice, and loss of imprinting is associated with a number of diseases, such as Prader-Willi syndrome, Angelman syndrome and cancer (Egger et al., 2004; Sharma et al., 2010).

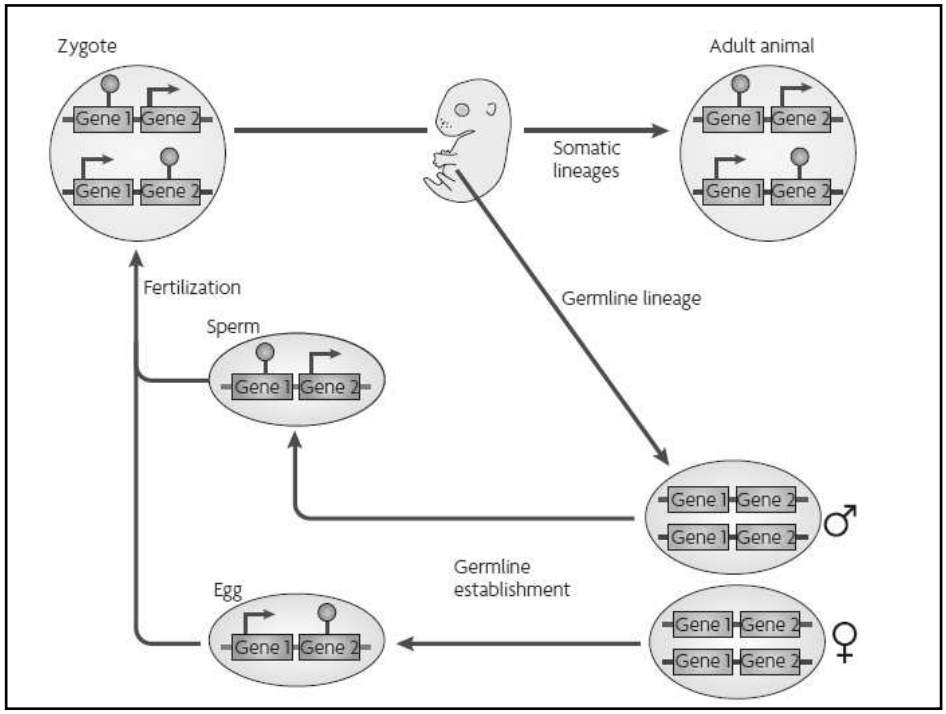

Figure 1.5: Mechanism of genomic imprinting (modified from Wilkinson et al., 2007).

The imprinted *Dlk1-Dio3* gene cluster (figure 1.6) is located on mouse distal chromosome 12 (Schuster-Gossler et al., 1998) and human chromosome 14q32, respectively (Schuster-Gossler et al., 1998; Miyoshi et al., 2000). It consists of the three paternally expressed protein-coding genes *Dlk1* (delta-like 1), *Dio3* (deiodinase, iodothyronine, type III) and *Rtl1* (retrotransposon-like 1), as well as a number of maternally expressed long non-coding RNAs (lncRNAs), microRNAs (miRNAs) and small nucleolar RNAs (snoRNAs), including *Meg3* (maternally expressed gene 3, also known as *Gtl2*, gene trap locus 2), anti-*Rtl1*, *Mirg* (microRNA-containing gene), *Rian* (RNA imprinted and accumulated in nucleus, also known as *Meg8*) and *Irm* (imprinted RNA near *Meg3*/*Gtl2*). The cluster also contains three differentially methylated regions (DMRs) which control gene expression on the locus: the Dlk1-DMR upstream of *Dlk1*, the IG-DMR (intergenic DMR) 15 kb upstream of *Meg3*/*Gtl2* and the Gtl2-DMR overlapping with the *Meg3/Gtl2*-promoter (Takada et al., 2000; Hagan et al., 2009; Takahashi et al., 2009).

Correct imprinting of the *Dlk1-Dio3* cluster is essential for embryonic development in mice. It was recently shown that maternal deletion of large parts of *Meg3/Gtl2* leads to perinatal lethality, whereas the paternal knockout seemed to have either no effect or resulted in postnatal growth retardation and perinatal death (Takahashi et al., 2009; Zhou et al., 2010).

These results indicate a crucial role of *Meg3/Gtl2* and its downstream maternally expressed genes in the regulation of *Dlk1-Dio3* cluster imprinting. Furthermore, transcriptional up-regulation of *Meg3/Gtl2* is associated with the hypertrophic phenotype in cells of PB-treated normal mouse liver (Lempiainen et al., 2013).

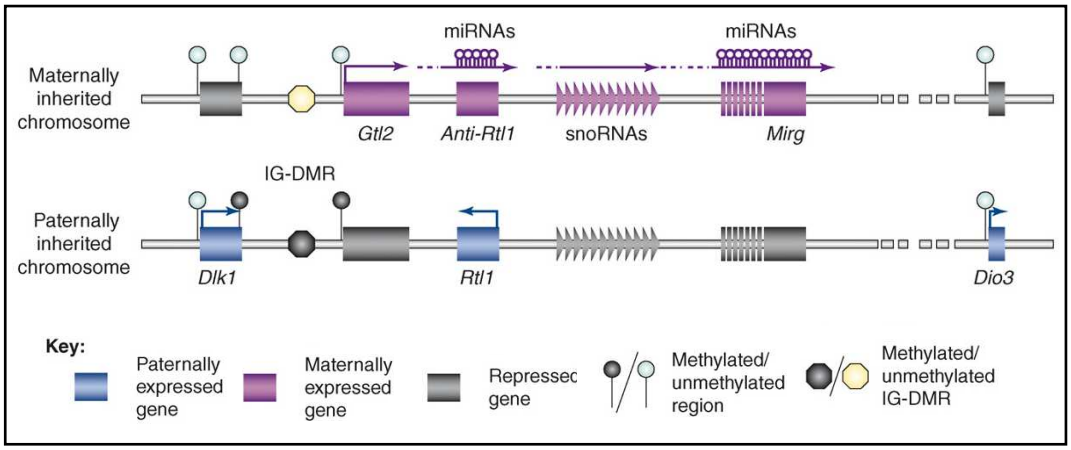

Figure 1.6: Structure of the *Dlk1-Dio3* imprinted gene cluster (modified from da Rocha et al., 2008).

1.4 Aims and objectives

The mode of action of NGCs such as PB is still widely unknown. The aim of this project was to elucidate the molecular mechanisms of NGCs by examining the differences between liver tumors that developed with or without promoter treatment. To this end, mRNA and miRNA expression, protein expression and phosphorylation, as well as DNA methylation datasets were generated for *Ha-ras*-mutated and *Ctnnb1*-mutated mouse liver tumors. The experiments were complemented by immunohistochemical staining. Furthermore, the novel bioinformatic tool InCroMAP was used to integrate the different datasets. The analyses should allow for creation of global and comprehensive molecular profiles of the two tumor types and thus for identifying characteristic differences between them. To additionally characterize epigenetic alterations in the differently mutated tumors, E-cadherin- and GS-positive tumors in fixed and embedded livers were immunohistochemically stained for 5'-methyl- (5'-mC) and 5'-hydroxymethylcytosine (5'-hmC). Another goal was to examine whether perturbations of the *Dlk1-Dio3* imprinted gene cluster play a role in PB-promoted tumorigenesis in the liver and could thus provide biomarkers which are specific for and predictive of epigenetic, non-genotoxic carcinogens. All in all, these analyses aimed at creating a global picture of the two types of tumors, thereby assessing the different molecular and biochemical programs triggered by constitutive activation of the β-Catenin and Ha-ras proteins.

2. Material

2.1 Chemicals and biochemicals

Reagent	Manufacturer
(3-Aminopropyl)triethoxysilane	Sigma, Taufkirchen, Germany
10x Taq Buffer with KCl +15 mM $MgCl_2$	Fermentas GmbH, St. Leon-Rot, Germany
3-Amino-9-ethylcarbazole	ICN Biochemicals, Aurora, OH, USA
Acetone	Sigma, Taufkirchen, Germany
Acrylamide (30%)	Roth, Karlsruhe, Germany
Agarose	Lonza, Rockland, ME, USA
Agilent RNA Pico Kit	Agilent Technologies, Santa Clara, CA, USA
Ammonium persulfate	Serva, Heidelberg, Germany
Ampuwa	Fresenius Kabi Deutschland GmbH, Bad Homburg, Germany
AMV Reverse Transcriptase 10u/µl	Promega, Madison, WI, USA
Boric acid	Merck KGaA, Darmstadt, Germany
Bovine serum albumin	Fermentas GmbH, St. Leon-Rot, Germany
Bromophenol blue	Serva, Heidelberg, Germany
BspHI (restriction endonuclease)	Fermentas GmbH, St. Leon-Rot, Germany
Chloroform	Merck KGaA, Darmstadt, Germany
dNTPs	Fermentas GmbH, St. Leon-Rot, Germany
dNTPs 2mM	Thermo Fisher Scientific, Waltham, MA, USA
dT_{20} primer	Genaxxon BioScience, Ulm, Germany
EDTA	Sigma, Taufkirchen, Germany
Entellan	Merck KGaA, Darmstadt, Germany
Ethanol	Merck KGaA, Darmstadt, Germany
Ethidium bromide	Serva, Heidelberg, Germany
Fast Red substrate	Kem-En-Tec, Copenhagen, Denmark
FastStart DNA MasterPLUS SYBR Green I kit	Roche Applied Science, Penzberg, Germany
FastStart SYBR Green Master kit	Roche Applied Science, Penzberg, Germany
Ficoll type 400	Sigma, Taufkirchen, Germany
GeneRuler 100 bp plus DNA ladder (for agarose gel electrophoresis)	Thermo Fisher Scientific, Waltham, MA, USA
H_2O_2 (30%)	Sigma, Taufkirchen, Germany
HCl	Merck KGaA, Darmstadt, Germany
HpyIII (restriction endonuclease)	Fermentas GmbH, St. Leon-Rot, Germany
Kaiser's glycerol gelatin	Merck KGaA, Darmstadt, Germany
$MgCl_2$	Roche Diagnostics, Mannheim, Germany
N,N-Dimethylformamide	Merck KGaA, Darmstadt, Germany
NaCl	Merck KGaA, Darmstadt, Germany
NaOH	Merck KGaA, Darmstadt, Germany

Reagent	Manufacturer
Orange G	Peqlab, Erlange, Germany
pBR322 DNA-MspI digest (molecular weight standard for acrylamide gel electrophoresis)	New England Biolabs, Ipswich, MA, USA
Periodic acid	Merck KGaA, Darmstadt, Germany
Phenobarbital-containing diet (0.05% w/v)	Ssniff, Soest, Germany
Phenol	Roth, Karlsruhe, Germany
Qiagen RNAse-free H_2O	Qiagen, Hilden, Germany
QuantiTect Primer Assays	Qiagen, Hilden, Germany
QuantiTect SYBR Green Mix	Qiagen, Hilden, Germany
Random hexamer primers	Genaxxon BioScience, Ulm, Germany
Restriction buffer	Fermentas GmbH, St. Leon-Rot, Germany
Restriction endonuclease buffer 4	New England Biolabs, Ipswich, MA, USA
Schiff solution	Merck KGaA, Darmstadt, Germany
SDS	Serva, Heidelberg, Germany
Sodium acetate	Merck KGaA, Darmstadt, Germany
Sucrose	Merck KGaA, Darmstadt, Germany
Swine serum (normal)	Dako, Glostrup, Denmark
Taq polymerase (1u/µl)	Fermentas GmbH, St. Leon-Rot, Germany
TaqI (restriction endonuclease)	Fermentas GmbH, St. Leon-Rot, Germany
Tetramethylethylenediamine (TEMED)	Serva, Heidelberg, Germany
TrisHCl	Sigma, Taufkirchen, Germany
TspRI (restriction endonuclease)	Fermentas GmbH, St. Leon-Rot, Germany
Tween 20	Sigma, Taufkirchen, Germany
Xylene	Merck KGaA, Darmstadt, Germany
Xylene cyanol	Sigma, Taufkirchen, Germany

2.2 Antibodies

2.2.1 Immunohistochemistry

Antigen	5'-hydroxymethylcytosine (5'-mC)
Manufacturer	Active Motif, Carlsbad, CA, USA
Catalog number	39769
Source	Rabbit, polyclonal
Application	IHC, 1:500 dilution

Antigen	5'-methylcytosine (5'-mC)
Manufacturer	Eurogentec, Seraing, Belgium
Catalog number	BI-MECY-0100
Source	Mouse, monoclonal
Application	IHC, 1:500 dilution

Antigen	E-Cadherin
Manufacturer	Cell Signaling, Danvers, MA, USA
Catalog number	3194
Source	Rabbit, monoclonal
Application	IHC, 1:25 dilution

Antigen	**Egr1 (15F7)**
Manufacturer	Cell Signaling, Danvers, MA, USA
Catalog number	4153
Source	Rabbit, monoclonal
Application	IHC, 1:100 dilution

Antigen	**Glutamine synthetase (GS)**
Manufacturer	Sigma, Taufkirchen, Germany
Catalog number	G2781
Source	Rabbit, polyclonal
Application	IHC, 1:1000 dilution

Antigen	**Phospho-p44/42 MAPK (Erk1/2) (Thr202/Tyr204)**
Manufacturer	Cell Signaling, Danvers, MA, USA
Catalog number	4376
Source	Rabbit, monoclonal
Application	IHC, 1:100 dilution

Antigen	**Rabbit IgG**
Manufacturer	Dako, Glostrup, Denmark
Catalog number	P0217
Source	Swine, polyclonal
Application	Secondary antibody for IHC, HRP-conjugated, 1:20 dilution

Antigen	**Rabbit IgG**
Manufacturer	MolMed S.p.A, Milan, Italy
Catalog number	FR14-61
Source	Goat, polyclonal
Application	Secondary antibody for IHC, biotin-conjugated, 1:200 dilution

2.2.2 Reverse phase protein microarray

Antibody	**Supplier**
4E-BP1	Epitomics (Burlingame, CA, USA)
Akt	Cell Signaling Technology
Akt - phospho S473	Cell Signaling Technology
AMPK alpha	Cell Signaling Technology
AMPK alpha - phospho T172	Cell Signaling Technology
APC	Cell Signaling Technology
ATM/ATR Substrate - phospho, S/T	Cell Signaling Technology
Aurora A - phospho T288	Cell Signaling Technology
Aurora A (AIK)	Cell Signaling Technology
Aurora A/B/C - phospho T288/T232/T198	Cell Signaling Technology
Aurora B (AIM1)	Cell Signaling Technology
Aven	Cell Signaling Technology
Bad	Cell Signaling Technology
Bax	Cell Signaling Technology
Bcl-xL	Cell Signaling Technology
β-Actin	Sigma Aldrich (St. Louis, MO, USA)

Antibody	Supplier
β -Catenin - phospho S675	Cell Signaling Technology
β -Catenin - phospho T41/S45	Cell Signaling Technology
β -Catenin	Upstate Biotechnology (Lake Placid, NY, USA)
Bik	Abcam (Cambridge, UK)
b-Raf - phospho S445	Cell Signaling Technology
Canceroembryogenic Antigen (CEA)	Dianova (Hamburg, Germany)
Caseinkinase 1 alpha	Cell Signaling Technology
CASK	BD Transduction Laboratories (San Jose, CA, USA)
CD51 (VNR alpha)	BD Transduction Laboratories
cdc25A (M-phase inducer phosphatase 1)	Applied Biological Materials (Richmond, BC, Canada)
cdc25C	Epitomics
c-Jun	Cell Signaling Technology
c-Jun - phospho S63	Cell Signaling Technology
c-Met (HGF/SF Receptor)	R&D Systems (Minneapolis, MN, USA)
c-Met (HGF/SF Receptor) - phospho Y1349	Cell Signaling Technology
c-myc	Cell Signaling Technology
c-myc - phospho T58/S62	Epitomics
c-Raf	Cell Signaling Technology
c-Raf - phospho S259	Cell Signaling Technology
CREB	Cell Signaling Technology
Cyclin A	Abcam
Cyclin D1	Cell Signaling Technology
Cyclin E2	Cell Signaling Technology
Cyp 1A1	U. Zanger, IKP, Stuttgart
Cyp 1A2	PanVera (Madison, WI, USA)
Cyp 2B1	R. Wolf, MRI, Dundee
Cyp 2B6	BD Biosciences (San Jose, CA, USA)
Cyp 2C6	R. Wolf, MRI, Dundee
Cyp 2C8	Puracyp (Carlsbad, CA, USA)
Cyp 2D6	U. Zanger, IKP, Stuttgart
Cyp 2E1	Acris (Herford, Germany)
Cyp 3A4	BD Biosciences
Cyp 3A4, 3A1, 3A11	Millipore (Billerica, MA, USA)
Cyp 3A5	BD Biosciences
Cyp 4F2	Santa Cruz Biotechnology (Santa Cruz, CA, USA)
Cytochrome b5	Oxford Biomedical Research (Rochester Hills, MI, USA)
DUSP4	Abcam
Dvl2	Cell Signaling Technology
EGFR	Epitomics
EGFR - phospho Y1068	Cell Signaling Technology
EGFR - phospho Y845	Cell Signaling Technology
EGFR - phospho, Y1045	Cell Signaling Technology

Antibody	Supplier
EGFR - phospho, Y1173	Cell Signaling Technology
eIF2 alpha	Cell Signaling Technology
eIF2 alpha - phospho S51	Cell Signaling Technology
Elk-1	Cell Signaling Technology
Erk1/2	Cell Signaling Technology
Erk1/2	Cell Signaling Technology
Erk1/2 - phospho T202/Y204	Cell Signaling Technology
Erk2 (p42 MAPK)	Cell Signaling Technology
FAK 1	Epitomics
FAK 1 - phospho, Y576, Y577	Epitomics
GAPDH	Abcam
Glutamine synthetase	Sigma Aldrich
GSK3 beta	Cell Signaling Technology
GSK3 beta - phospho S9	Cell Signaling Technology
Ha-ras	Upstate Biotechnology
Her2	Dako (Glostrup, Denmark)
Her2 - phospho Y1248	Cell Signaling Technology
Her2 - phospho Y877	Cell Signaling Technology
Histone Deacetylase 2	Epitomics
Histone Deacetylase 3	Epitomics
Histone Deacetylase 6	Millipore
Histone H2B	Epitomics
Histone H3	Cell Signaling Technology
Histone H3	Cell Signaling Technology
Histone H3 - acetyl K18	Epitomics
Histone H3 - dimethyl K4	Epitomics
Histone H3 - phospho S10	Cell Signaling Technology
Histone H3 - phospho S28	Cell Signaling Technology
Histone H3 - trimethyl K27	Cell Signaling Technology
Histone H4 - acetyl K8	Epitomics
HNF-4α	Santa Cruz Biotechnology
IGF1 Receptor	Ventana Medical Systems (Tucson, AZ, USA)
IGFBP-1	Santa Cruz Biotechnology
IkappaB alpha	Cell Signaling Technology
IkappaB alpha - phospho S32	Cell Signaling Technology
ILK1	Cell Signaling Technology
ILK1	Cell Signaling Technology
Jak 1	Cell Signaling Technology
Jak 1 - phospho Y1022/Y1023	Cell Signaling Technology
Jak 2	Cell Signaling Technology
Jak 2 - phospho Y1007/Y1008	Cell Signaling Technology
JNK/SAPK	Cell Signaling Technology
JNK/SAPK - phospho T183/Y185	Cell Signaling Technology
Ki-67	United States Biological (Swampscott, MA, USA)
Mcl-1	Cell Signaling Technology
MEK1	Cell Signaling Technology

Antibody	Supplier
MEK1/2 - phospho S217/S221	Cell Signaling Technology
MEK2	Cell Signaling Technology
MKK4	Epitomics
MKK4 - phospho, S257, T261	Cell Signaling Technology
mTOR	Cell Signaling Technology
mTOR - phospho S2448	Cell Signaling Technology
mTOR - phospho S2481	Cell Signaling Technology
N-Cadherin	BD Biosciences
Neo-P-Transferase 2	Abcam
p27 Kip1 - phospho T187	Signalway Antibody (College Park, MD, USA)
p27(Kip1) - phospho S10 - (CDKN1B)	Epitomics
p27(Kip1) (CDKN1B)	Cell Signaling Technology
p38/MAPK	Cell Signaling Technology
p38/MAPK - phospho T180,Y182	Cell Signaling Technology
p53	R&D Systems
p53 - phospho, S15	Cell Signaling Technology
p53 - phospho, S392	Cell Signaling Technology
p53 - phospho, S9	Cell Signaling Technology
p70 S6 kinase	Cell Signaling Technology
p70 S6 kinase - phospho T389	Cell Signaling Technology
PAK 1/2/3	Cell Signaling Technology
PAK1/2/3 - phospho S141	Life Technologies (Carlsbad, CA, USA)
PDK1	Cell Signaling Technology
PDK1 - phospho, S241	Cell Signaling Technology
PERK	Cell Signaling Technology
PI3-kinase p85 subunit alpha	Epitomics
PKA C alpha/beta/gamma - phospho T197	Cell Signaling Technology
PON1	Santa Cruz Biotechnology
PON3	Abcam
PP2A C - phospho Y307	R&D Systems
PPAR alpha	Abcam
PPAR alpha	Santa Cruz Biotechnology
PPAR alpha, S12	Abcam
PPAR alpha, S21	Abcam
PTEN	Cell Signaling Technology
PTEN - phospho S380	Cell Signaling Technology
Pyk2	Millipore
Rad51	Epitomics
Reduktase POR	U. Zanger, IKP, Stuttgart
RSK 1	Upstate Biotechnology
RSK 1 - phospho, T573	Epitomics
RSK 1 (p90RSK) - phospho, S380	Cell Signaling Technology
RSK 3 - phospho, T353/T356	Epitomics
RSK 4	Epitomics
RSK 4 - phospho, S235	Epitomics

Antibody	Supplier
RXR alpha	R&D Systems
S6 Ribosomal Protein	Cell Signaling Technology
S6 Ribosomal Protein - phospho S235/S236	Cell Signaling Technology
SHP-2	Epitomics
Smad2 - phospho S245/S250/S255	Cell Signaling Technology
Smad2/3	Cell Signaling Technology
SOCS-3	Cell Signaling Technology
ß-Actin	Sigma Aldrich
ß-Gal	MoBiTec (Goettingen, Germany)
STAT 1	Cell Signaling Technology
STAT 3	Cell Signaling Technology
STAT 3 - phospho S727	Cell Signaling Technology
STAT 3 - phospho Y705	Cell Signaling Technology
STAT 5	Cell Signaling Technology
STAT 5 - phospho Y694	Cell Signaling Technology
TAK1	Cell Signaling Technology
TAK1 - phospho S412	Cell Signaling Technology
UGT1A1	BD Biosciences

2.2.3 Western Blot

Antigen	Actin
Manufacturer	Santa Cruz Biotechnology,Santa Cruz, CA, USA
Catalog number	sc-1616
Source	Donkey, polyclonal
Application	Loading control for Western Blot, 1:1000 dilution

Antigen	Phospho-p44/42 MAPK (Erk1/2) (Thr202/Tyr204)
Manufacturer	Cell Signaling, Danvers, MA, USA
Catalog number	4376
Source	Rabbit, monoclonal
Application	Western Blot, 1:1000 dilution

Antigen	Phospho-MEK1/2 (Ser217/Ser221)
Manufacturer	Cell Signaling, Danvers, MA, USA
Catalog number	9121
Source	Rabbit, polyclonal
Application	Western Blot, 1:1000 dilution

Antigen	Rabbit IgG
Manufacturer	Jackson ImmunoResearch, West Grove, PA, USA
Catalog number	711-035-152
Source	Donkey, polyclonal
Application	Secondary antibody for Western Blot, conjugated with horseradish peroxidase, 1:2000 dilution

2.3 Buffers and solutions:

2.3.1 Electrophoresis

50x TAE buffer (pH 8.5) for agarose gel electrophoresis	
Tris base	242 g
EDTA (0.5 M, pH 8)	100 ml
Glacial acetic acid	57.1 ml
H_2O_{dest}	ad 1000 ml

6x loading buffer for agarose gel electrophoresis	
Sucrose	50 g
SDS	1 g
Orange G dye	0.5 g
H_2O_{dest}	ad 100 ml

GeneRuler 100 bp plus DNA ladder for agarose gels	
1 kb DNA ladder	1 µl (1 µg/µl)
6x loading buffer for agarose gel electrophoresis	1 µl
H_2O_{dest}	ad 7 µl

Ethidium bromide solution for agarose gels	
Ethidium bromide	10 mg
H_2O_{dest}	ad 1 ml

10x loading buffer for acrylamide gel electrophoresis	
Bromophenol blue	25 mg
Xylene cyanol	25 mg
Ficoll type 405	1.5 g
EDTA (0.5 M, pH 8)	1 ml
H_2O_{dest}	ad 10 ml

Ammonium persulfate for acrylamide gel electrophoresis	
APS	1.2 g
H_2O_{dest}	ad 12 ml

5x TBE buffer (pH 8.3) for acrylamide gel electrophoresis	
Tris base	54 g
EDTA (0.5 M, pH 8)	20 ml
Boric acid	27.5 g
H_2O_{dest}	ad 1000 ml

Ethidium bromide solution for acrylamide gel electrophoresis	
Ethidium bromide	0.5 mg
H_2O_{dest}	ad 1000 ml

pBR322 DNA-Msp1 Digest for acrylamide gels	
pBR322 DNA-*Msp*I Digest (1 µg/µl)	10 µl
10x Ladepuffer für Acrylamidgelelektrophorese	10 µl
H_2O_{dest}	ad 50 µl

2.3.2 Isolation of genomic DNA

Sodium acetate mixture for isolation of genomic DNA	
Sodium acetate solution (3 M)	10 ml
SDS solution (20%)	2.5 ml
EDTA solution (0.5 M, pH 8)	1 ml
H_2O_{dest}	ad 100 ml

TE buffer for isolation of genomic DNA	
TrisHCl (1 M, pH 7.5)	5 ml
EDTA solution (0.5 M, pH 8)	1 ml
H_2O_{dest}	ad 500 ml

2.3.3 Immunohistochemistry

Acetate buffer	
Sodium acetate	6.48 g
Glacial acetic acid	1.21 ml
H_2O_{dest}	ad 1000 ml

3-Amino-9-ethylcarbazole (AEC) solution	
3-Amino-9-ethylcarbazole	4 mg
N,N-Dimethylformamide	1 ml
Dissolve AEC in N,N-Dimethylformamide	
Acetate buffer	14 ml
H_2O_2 (30%)	15 µl

Alcoholic eosin solution	
Eosin Y	0.8 g
Ethanol (60%)	ad 200 ml
Filter through fluted filter paper	

Carnoy fixative	
Ethanol	60 ml
Chloroform	30 ml
Glacial acetic acid	10 ml

10x citrate buffer (0.1 M, pH 6)	
Citric acid (sodium salt)	29.41 g
H_2O_{dest}	ad 1000 ml

Coating solution for silanization of microscope slides	
(3-Aminopropyl)triethoxysilane	4 ml
Acetone	ad 200 ml

PBS/S	
NaCl	2.03 g
BSA	1 g
PBS	ad 100 ml

PBS/T	
Tween 20	1 ml
PBS	ad 1000 ml

2.3.4 Western Blot

TBS/T	
Tween 20	1 ml
NaCl	8.76 g
Tris base	2.42 g
H_2O_{dest}	ad 1000 ml

10x transfer buffer	
Tris base	30 g
Glycine	144 g
H_2O_{dest}	ad 1000 ml

2.4 Primers

2.4.1 RFLP analysis and sequencing

Gene	Forward primer (5'→3')	Reverse primer (5'→3')	Amplicon
Ctnnb1	AGCTCAGCGCAGAGCTGCTG	GAGCGCATGATGGCATGTCTG	1473 bp
Ctnnb1	ACTCTGTTTTTACAGCTGACCT	GAGCGCATGATGGCATGTCTG	248 bp
Ha-ras	GAGACATGTCTACTGGACATCCT	GCTAGCCATAGGTGGCTCACCTG	166 bp
B-raf	TTCCTTTACTTACTGCACCTCAGA	AGCAGTCACTAGTTTAGGACTG	426 bp

2.4.2 LightCycler PCR

Gene	Forward primer (5'→3') / Reverse primer (5'→3')	Amplicon
Meg3/Gtl2	Mm_Meg3_1_SG QuantiTect Primer Assay	148 bp
Rian	Mm_Rian_2_SG QuantiTect Primer Assay	149 bp
Mirg	Mm_Mirg_4_SG QuantiTect Primer Assay	168 bp
Dio3	Mm_Dio3_1_SG QuantiTect Primer Assay	143 bp
Dlk1	Mm_Dlk1_1_SG QuantiTect Primer Assay	120 bp
Rtl1	Mm_Rtl1_2_SG QuantiTect Primer Assay	88 bp

Gene	Forward primer (5'→3')	Reverse primer (5'→3')	Amplicon
18s rRNA	Mm_Rn18s_3_SG QuantiTect Primer Assay		143 bp
Cyp7a1	Mm_Cyp7a1_1_SG QuantiTect Primer Assay		67 bp
18s rRNA	CGGCTACCACATCCAAGGAA	GCTGGAATTACCGCGGCT	187 bp
Glul (glutamine synthetase)	GCGAAGACTTTGGGGTGATA	GTGCCTCTTGCTCAGTTTGTC	158 bp
H19	CTGCTGCTCTCTGGATCCTC	GTGGGTGGGTGCTATGAGTC	408 bp
CAR1	AACAACAGTCTCGGCTCCAAA	AGCATTTCATTGCCACTCCC	273 bp
Hnf6	GAGCCCAACCCTTCGGTGAC	CTCTGTCCTTCCCGTGTTCTTG	337 bp

2.5 Laboratory equipment

Device	Manufacturer	Type designation
Autoclave	Webeco, Selmsdorf, Germany	Autoclave C
Balance	Mettler-Toledo, Gießen, Germany	P1200
Balance	Sartorius, Göttingen, Germany	Analytic
Bench top portable mini-cleanroom	Safetech Limited, Hongkong SAR, China	Cleansphere CA 100
Camera	Raytest, Straubenhardt, Germany	CSC Chemoluminescense detection module
Centrifuge (for falcon tubes)	Heraeus Instruments, Hanau, Germany	Multifuge 1 L-R
Centrifuge (for Eppendorf cups)	Eppendorf, Hamburg, Germany	5417R
Electrophoresis chambers	GibcoBRL, Karlsruhe, Germany	Horizontal Gel Electrophoresis System, H6
	Bio-Rad, Munich, Germany	Mini Protean II
Magnetic stirrers	Heidolph Instruments, Schwabach, Germany	MR 80
	IKA, Staufen im Breisgau, Germany	Combimac RCT/RET
	IKA, Staufen im Breisgau, Germany	Mag RH
Microscope camera	Zeiss, Oberkochen, Germany	AxioCam MRc
Microtome	Reichert-Jung, Wetzlar, Germany	Frigocut 2800
Microwave	Bosch, Gerlingen-Schillerhöhe, Germany	600 W
PCR machine for reverse transcription	PerkinElmer, Waltham, MA, USA	GeneAmp PCR System 2400

Device	Manufacturer	Type designation
PCR machine for standard PCR	Biometra, Göttingen, Germany	UNO thermoblock
	Bio-Rad, Munich, Germany	MyCycler™ thermal cycler
pH meter	WTW, Weilheim, Germany	pH 522
Power supply for gel electrophoresis	Pharmacia, Uppsala, Sweden	LKB EPS 500/400
	Desaga, Wiesloch, Germany	Desatronic 3x500/100
	GibcoBRL, Karlsruhe, Germany	ST 305
	GibcoBRL, Karlsruhe, Germany	ST 606 T
Tissue homogenizer	B. Braun, Melsungen, Germany	Mikro-Dismembrator II
UV illuminator	Biometra, Göttingen, Germany	TI 1
Vortex mixer	Bender & Hobein AG, Zurich, Switzerland	Genie 2™
Water preparator	Merck Millipore, Billerica, MA, USA	Milli Q Plus

2.6 Expandable items and small devices

Item	Manufacturer	Type designation
15 ml tubes	BD, Franklin Lakes, NJ, USA	Falcon 2096
50 ml tubes	BD, Franklin Lakes, NJ, USA	Falcon 2070
1.5 ml reaction tubes	Eppendorf, Hamburg, Germany	-
Cages	Tecniplast, Hohenpeißenberg, Germany	Makrolon type 2
Capillaries (for LightCycler)	Roche Applied Science, Penzberg, Germany	LightCycler Capillaries (20 µl)
Centrifuge adapter	Roche Applied Science, Penzberg, Germany	LightCycler Centrifuge Adapters
Cover slips	Thermo Fisher Scientific, Waltham, MA, USA	30 mm diameter, #1
Glass Pasteur pipette	WU Mainz, Mainz, Germany	-
Glassware	Schott, Mainz, Germany	-
Metal scissors	Hauptner, Dietlikon, Switzerland	-
Metal tweezers	Eickemeyer, Tuttlingen, Germany	-
	Schnitzer Steel, Portland, OR, USA	-

Item	Manufacturer	Type designation
Microscope glasses	R. Langenbrinck, Emmendingen, Germany	26x76 mm
Needles (0.9 x 40 mm)	BD, Franklin Lakes, NJ, USA	Microlance 3™
PCR reaction tubes (0.2 ml)	Peqlab, Erlangen, Germany	-
	Bio-Rad, Munich, Germany	-
PCR reaction tubes (0.5 ml)	Eppendorf, Hamburg, Germany	-
Single channel air displacement pipettes and tips	Biozym Scientific, Hessisch Oldendorf, Germany	-
	Eppendorf, Hamburg, Germany	-
Syringes	BD, Franklin Lakes, NJ, USA	1 ml BD slip-tip syringe

2.7 Software

Adobe Systems, San Jose, CA, USA	Photoshop Elements 10
Microsoft, Redmond, WA, USA	Office 2007
Microsoft, Redmond, WA, USA	Windows Vista
Origin Lab Cooperation, Northampton, MA, USA	OriginPro 8G
PerkinElmer, Waltham, MA, USA	BioDraw Ultra 12.0
PerkinElmer, Waltham, MA, USA	NanoDrop ND-1000 V3.2.1
Premier Biosoft, Palo Alto, CA, USA	Primer Premier 5.00
Roche Diagnostics, Mannheim, Germany	Roche LightCycler Run 5.32
Zeiss, Oberkochen, Germany	AxioVision 4.5

3. Methods

3.1 Animal treatment and housing

Mice were singly kept in makrolon type 2 cages at a 12 hour light/dark cycle with water and food available *ad libitum*. At the end of an experiment, mice were anesthetized with a mix of 95% CO_2 and 5% O_2 and then killed by cervical dislocation. Animals were treated with humane care, and all protocols were in compliance with institutional guidelines.

3.1.1 Tumor tissue from previous initiation-promotion experiments

Archived frozen *Ha-ras-*, *B-raf-* or *Ctnnb1*-mutated tumor tissue and control tissues were available from previous carcinogenesis experiments conducted in our group (Jaworski et al., 2005b; Strathmann et al., 2006; Marx-Stoelting et al., 2008; Rignall et al., 2010). In brief, male C3H/HeJ mice received a single *i.p.* injection of DEN (10 or 90 µg/g body weight) at 2 or 6 weeks of age. After a treatment-free interval of 2 weeks, the mice were either kept on a diet containing 0.05% PB or on a PB-free control diet for 28 to 36 weeks before they were killed (figure 3.1). Tumors were isolated and either flash frozen in liquid nitrogen and stored at -80 °C or prepared for immunohistochemistry.

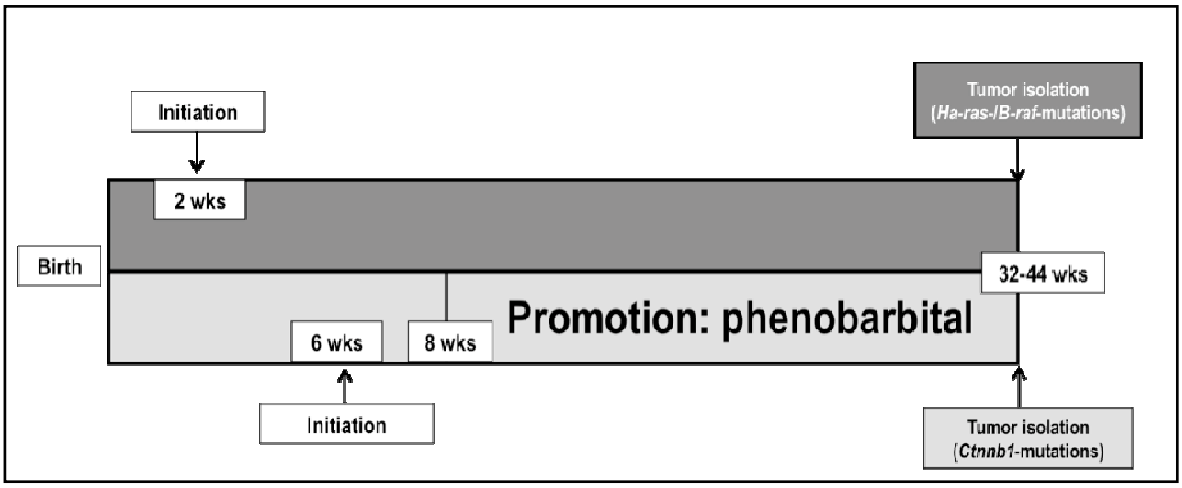

Figure 3.1. Treatment scheme for unpromoted tumors (dark gray) and PB-promoted tumors (light gray).

3.1.2 PB-treatment of Connexin32-deficient mice

Connexin32 (Cx32)-deficient mice were generated as previously described (Moennikes et al., 2000a). Male $Cx32^{Y/+}$ (wild-type) and $C32^{Y/-}$ mice (knockout) were either kept on a diet containing 0.05% PB or on a control diet for 12 weeks (five animals per group), beginning at approximately six weeks of age. At approximately 18 weeks of age, mice were killed and excised liver tissue was used for RNA isolation.

3.1.3 Obtaining of spontaneous liver tumors

Male C3H/N mice were purchased from Janvier Europe (Saint-Berthevin Cedex, France) and kept at a standard treatment-free diet. Animals were killed in four groups at approximately 52, 63, 75 and 77 weeks of age and screened for liver tumors. Tumors were isolated and either flash frozen in liquid nitrogen and stored at -80 °C or prepared for immunohistochemistry.

3.1.4 Tumors from DEN-initiated mice after withdrawal of PB-treatment

Male *Ctnnb1*$^{loxP/loxP}$, TTR-Cre-Tam mice generated in our group (Singh et al., 2013, manuscript in preparation) were initiated with a single dose of DEN (90 µg/g body weight) at the age of 5-6 weeks. After a treatment-free interval of 3 weeks, they received a PB-containing diet (0.05%) for 25 weeks. After that, the animals were kept on a PB-free control diet for another 25 weeks before they were killed and tumors were isolated and flash-frozen.

3.1.5 APC-knockout mice

Liver tissue from mice with a liver-specific tamoxifen-inducible APC-knockout was available from a previous study of our group (Zeller et al., 2012).

3.2 Mutation analysis

3.2.1 Isolation of genomic DNA

Frozen liver tissue was pulverized under liquid nitrogen using a mortar and pestle. Genomic DNA was extracted from the pulverized tissue with phenol/sodium acetate (1.25:1), chloroform/isoamyl alcohol (25:1) and finally pure chloroform. For precipitation of genomic DNA, ice-cold ethanol was added to the obtained solution. The precipitated DNA was washed, dissolved in TE buffer and quantified.

3.2.2 Standard PCR

Standard PCR was carried out on an UNO thermoblock (Biometra, Göttingen, Germany) or a MyCycler^{TM} thermal cycler (Bio-Rad, Munich, Germany). 5 µl of a 0.1 mg/ml dilution of genomic DNA were used according to the reaction mix in table 3.1. For primer sequences see section 2.4.1.

Table 3.1. Reaction mix for conventional PCR, used for *Ha-ras*-, *B-raf*- and *Ctnnb1*-specific primer pairs.

	Volume (µl)
H_2O	29
10x Taq buffer	5
dNTPs (2 mM)	5
Forward primer (10 µM)	2.5
Reverse primer (10 µM)	2.5
Taq polymerase (5 U)	1
Genomic DNA (0.1mg/ml)	5
Total volume	**50**

The temperature programs given in table 3.2 were used for the different target genes.

Table 3.2. PCR conditions for for *Ha-ras*-, *B-raf*- and *Ctnnb1*-specific primer pairs.

Target gene	**Activation**	**Temperature (℃)**	**Duration (min)**	**Number of cycles**	**Final elongation**
Ha-ras	95 ℃, 10 min	95	1	35	72 ℃, 5 min
		65	1		
		72	1		
B-raf		95	1	40	
		60	1		
		72	1		
Ctnnb1	95 ℃, 5 min	95	1	40	72 ℃, 10 min
		58	1		
		72	1		

3.2.3 RFLP analysis

To detect point mutations in codon 61 of *Ha-ras* (wildtype sequence CAA) and codon 637 of *B-raf* (wildtype sequence CTG), PCR products were fragmented in a restriction digest. Point mutations in these codons can lead to the generation of new recognition sites for restriction endonucleases or the loss of existing recognition sites and thus to altered restriction fragment lengths as compared to wildtype DNA. PCR product was mixed with H_2O, the respective restriction enzyme and, where required, NEBuffer 4 and BSA, and then incubated according to table 3.3.

Table 3.3. PCR conditions for for *Ha-ras*-, *B-raf*- and *Ctnnb1*-specific primer pairs.

	Ha-ras				***B-raf***
Restriction enzyme	TaqI	XbaI	Hpy188III	BspHI	TspRI
Codon mutation	CAA→CGA	CAA→CTA	CAA→AAA	CAA→CAT	CTG→GAG
H_2O	11 µl	11 µl	6 µl	9 µl	6 µl
NEBuffer 4	-	-	2 µl	2 µl	2 µl
BSA 1 mg/ml	-	-	2 µl	-	2 µl
Enzyme	1 µl	1 µl	2 µl	1 µl	1 µl
PCR product	8 µl	8 µl	8 µl	8 µl	9 µl
Reaction conditions	65 ℃, 1 h	37 ℃, 1 h	37 ℃, o/ n	37 ℃, 1 h	65 ℃, 2 h
Resulting fragments in wildtype (bp)	125, 41	166	129, 35	166	130, 136, 160
Resulting fragments in mutated amplicon	89, 41, 36	130, 36	166	130, 36	130, 136, 160, 266

Reaction products were separated on 10% polyacrylamide gels and stained with ethidium bromide.

Mutations in *Ctnnb1* were determined by sequencing of a 1473 bp PCR product spanning exon 3 of the *Ctnnb1* gene which encodes the critical β-Catenin phosphorylation sites. For the spontaneous tumors isolated from aged mice, a 248 bp fragment including codons 32-41 of *Ctnnb1* was sequenced. Primer sequences are indicated in 2.4.1. Sequencing was carried out by 4base lab (Reutlingen, Germany).

3.3 Quantitative Real-time PCR

3.3.1 Isolation of RNA from frozen liver

RNA (including miRNA) was isolated from frozen liver tissue using the miRNeasy Mini Kit (QIAGEN) according to the manufacturer's protocol. The concentration of eluted RNA was measured on a NanoDrop ND-1000 photometer.

3.3.2 Reverse transcription

Reverse transcription of isolated RNA was carried out using the GeneAmp PCR System 2400 (PerkinElmer, Waltham, MA, USA). The reaction was run for 1 hour at 42 °C followed by an inactivation step of 15 minutes at 95 °C. The reaction mix in table 3.4 was used:

Table 3.4. Reaction mix for reverse transcription of isolated RNA.

Reagent	Volume
H_2O (Ampuwa)	4.85 µl
$MgCl_2$ (25 mM)	3 µl
10x PCR buffer	1.5 µl
dNTPs (10 mM)	1.5 µl
dT_{20} (500 ng/µl)	0.38 µl
dN_6 (500 ng/µl)	0.38 µl
AMV-RT (10 U/µl)	0.39 µl
RNA (125 ng/µl)	3 µl
Σ	15 µl

3.3.3 LightCycler PCR

Quantitative real-time PCR was carried out on a LightCycler 1.5 instrument (Roche Applied Science, Penzberg, Germany) using either the FastStart SYBR Green Master kit (Roche), the FastStart DNA MasterPLUS SYBR Green I kit (Roche) or the QuantiTect SYBR Green PCR kit (QIAGEN, Hilden, Germany). Primers were either synthesized by Eurofins MWG GmbH (Ebersberg, Germany) or obtained as predesigned primer assays from Qiagen (Hilden, Germany) and used with the QuantiTect SYBR Green PCR kit according to the manufacturer's instructions. The temperature programs for the self-designed primers are listed in table 3.5 (for primer sequences see section 2.4.2).

Table 3.5. Temperature programs used for LightCycler PCR.

	Gene					
Step	**18s rRNA**		**H19**		**Glul (glutamine synthetase)**	
Activation	10 minutes, 95 ℃					
	Temperature (℃)	Duration (seconds)	Temperature (℃)	Duration (seconds)	Temperature (℃)	Duration (seconds)
Denaturation	95	5	95	8	95	0
Annealing	68	5	62	5	60	5
Elongation	72	8	72	10	72	10
Cycles	35		35		35	
	Gene					
Step	**Car1**		**Hnf6**			
Activation	10 minutes, 95 ℃					
	Temperature (℃)	Duration (seconds)	Temperature (℃)	Duration (seconds)		
Denaturation	95	5	95	5		
Annealing	62	10	65	6		
Elongation	72	12	72	11		
Cycles	45		50			

3.4 Global gene expression analysis

Affymetrix gene analysis was carried out as previously described by Lempiäinen et al. (Lempiainen et al., 2011) at the department for Discovery and Investigative Safety, Novartis Institutes for BioMedical Research, Basel, Switzerland. In brief, biotinylated amplified RNA (aRNA) was hybridized to the GeneChip® Mouse430_2 arrays. After washing and staining, the arrays were scanned using a solid-state laser scanner (GeneArray® Scanner 3000 combined with the GeneChip® autoloader, Affymetrix). The Affymetrix GeneChip® Operating Software (GCOS) was used to generate the primary and secondary raw data files.

3.5 miRNA expression analysis

Analysis of miRNA expression was conducted at CXR Biosciences, Dundee, Scotland. Total RNA including miRNA was isolated using the miRNeasy Mini Kit (QIAGEN, Hilden, Germany). Prior to the miRNA expression analysis, RNA integrity was checked with an Agilent 2100 Bioanalyzer using the Agilent RNA 6000 Pico Kit (Agilent Technologies, Santa Clara, CA, USA). 25 ng total RNA was end-labeled using the miRNA complete labeling and hybridization kit (Agilent# 5190-0456). Agilent unrestricted Mouse miRNA microarrays (8x15K, #G4471A) and Agilent 8x15K gasket slides (#G2534-60015) were used for the study. Arrays were hybridized using Agilent hybridization and washing buffers according to the Agilent miRNA microarray method entitled ‘miRNA Microarray System with miRNA Complete Labeling and Hyb Kit’ (G4170-90011). Following hybridization and washing, the arrays were scanned on an Agilent Microarray Scanner (#G2505B) according to the Agilent protocol (#G4170-90011). Images from the scanner were processed using Agilent Feature Extraction Software v9.5.1. Briefly, miRNA genes that were significantly expressed above background on the individual arrays were identified using Agilent Feature Extraction software. This process involved deletion control and background subtraction and calculation of a p-value reflecting the probability that there was no difference in intensity for a given feature to that of a background using a two sided t-test. The p-value calculation was based on an error calculated using an Agilent error model (Agilent Feature Extraction Software (v9.5) #G2566-90012).

3.6 Analysis of proteome and phosphoproteome

3.6.1 Reverse phase protein microarray analysis

Reverse phase protein microarray analysis was performed at the Natural and Medical Sciences Institute, Reutlingen, Germany, as described in Braeuning et al., 2011, with the following modifications: Tissue lysates were generated by adding an 8-fold excess (vol/wt) of CeLyA Lysis Buffer CLB1 (Zeptosens, Witterswil, Switzerland) containing 1 M NaCl. A microarray layout was chosen that uses two replicates of each sample at a protein concentration of 0.3 mg/ml. Antibodies used for detection of proteins and protein modifications are listed in section 2.2.2. Fluorescence signal was generated using Alexa647- (Invitrogen, Darmstadt, Germany) and Cy5- (Dianova, Hamburg, Germany) labeled anti-species secondary antibodies. Images of the microarrays were taken using the ZeptoREADER microarray imager (Zeptosens), and image analysis was performed using the ZeptoVIEW 3.1 software package (Zeptosens).

3.7 DNA methylation analysis

MeDIP analysis was carried out at the department for Discovery and Investigative Safety, Novartis Institutes for BioMedical Research, Basel, Switzerland, as previously described (Thomson et al., 2012). In brief, genomic DNA isolated from mouse liver was fragmented (mean length of around 500 bp), and 6 µg of fragmented DNA were denatured and immunoprecipitated for 3 hours at 4 °C with 15 µl mouse monoclonal antibody against 5-methylcytidine (Eurogentec, Seraing, Belgium; #BI-MECY-1000). The reaction mix was incubated with 60 µl of magnetic M-280 protein G Dynabeads (Invitrogen, Grand island, NY, USA; #100-03D) for 2 hours and then washed. Washed beads were resuspended in lysis buffer and incubated with proteinase K. Immunoprecipitated DNA fragments were then purified on DNA purification columns (Qiagen, Venlo, Netherlands) and eluted in TE. For microarray analysis, 10 µl of immunoprecipitated DNA was subjected to whole genome amplification (WGA) using the WGA2:GenomePlex Complete Whole Genome Kit (Sigma), and 6 µg of amplified material were sent to Roche Nimblegen (Iceland) for Cy3 and Cy5 labeling and hybridization on 2.1M Deluxe mouse promoter tiling arrays.

3.8 Histochemistry and *in situ* hybridization

Sections of paraffin-embedded tissue (5 µm) were cut with a microtome and transferred to silanized object slides. Before they were used for IHC, paraffin sections were incubated in xylene twice for 10 minutes for deparaffinization and then rehydratized by sequential incubation in aqueous ethanol dilutions (2 minutes each in 100%, 96%, 70%, 50% (v/v) ethanol, and finally PBS). If recommended by the antibody manufacturer, antigen demasking was carried out by boiling the sections in citrate buffer for approximately 10 minutes. Images were acquired under an Axio Imager light microscope (Imager.M1; Zeiss, Göttingen, Germany) with Axiovision Rel. 4.5 software (Zeiss).

3.8.1 Staining of E-Cadherin, phospho-MAPK, 5'-hmC, 5'-mC and Egr1

Sections were washed in PBS for 5 minutes, followed by a 5 minute incubation step in PBS/T. After that, sections were incubated in PBS/T containing 3% BSA at room temperature to avoid unspecific binding of antibodies. Primary antibody (diluted in PBS/T containing 3% BSA) was bound at 4 °C over night. Sections were washed with PBS/T for 5 minutes. Biotinylated secondary antibody (diluted 1:200 in TBS/T + 1% BSA) was bound for 1 hour at room temperature. After two short washing steps in PBS/T, sections were incubated with streptavidin-alkaline phosphatase (AP)-complexes (diluted 1:200 in TBS/T + 1% BSA) for 30 minutes at room temperature. AP enzyme activity was detected via staining with Fast Red for approximately 40 minutes.

3.8.2 Staining of glutamine synthetase

Sections were washed in PBS for 5 minutes, followed by a 5 minute incubation step in PBS/S. To inactivate endogenous peroxidase activity, sections were incubated with swine normal serum (diluted 1:30 in PBS/S) for 5 minutes. Primary antibody was bound at 4 °C over night. Sections were washed with PBS for 5 minutes. Horseradish peroxidase (HRP)-conjugated secondary antibody (diluted in 1:20 in PBS/S) was bound for 30 minutes at room temperature. After a 5 minute incubation step in acetate buffer, HRP activity was detected by incubation with AEC solution for 5-10 minutes. Sections were then washed with PBS, followed by H_2O_{dest} for 5 minutes. Finally, they were embedded in Kaiser's glycerol gelatin and covered with cover slips.

3.8.3 *Meg3/Gtl2 in situ* hybridization

ISH was performed using the fully automated instrument Ventana Discovery Ultra® (Roche Diagnostics) at the department for Discovery and Investigative Safety, Novartis Institutes for Biomedical Research, Basel. Template for *Meg3/Gtl2* probe synthesis was generated by RT-PCR on mouse brain RNA using self-priming primers flanked SP6- and T3-promoter recognition sequences (forward primer: 5'-SP6-CTCTTCTCCATCGAACGGCT, reverse primer 5'T3-AACAATAAAGAACTTGAAGAGGTTTTGAT, amplicon size: 537 bp). The PCR product was purified and then transcribed using T3-RNA polymerase (anti-sense) and SP6-RNA polymerase (sense) at 37 °C for 2 hours using dNTP containing Digoxigenin-UTP according to the manufacturer's recommendations (Roche Diagnostics, Schweiz AG, Rotkreuz, Switzerland). All chemicals were provided by Roche Diagnostics. FFPE sections were deparaffinized and rehydrated (EZprep solution). Pretreatment steps were carried out with the RiboMap™ kit according to the manufacturer's instructions. Demasking was performed by heat retrieval cycles in RiboCC solution using option mild, followed by a complementary enzymatic digestion (Protease 3 for 16 minutes at 37 °C). Hybridization was performed by adding 200 µl of RiboHybe solution containing 10 ng of DIG-riboprobe to each slide and incubating at 70 °C for 6 hours. Sections were then washed 3 times at 70 °C for 8 minutes on stringency conditions (2.0 x SSC). DIG-label probe detection was performed using an AP-conjugated sheep anti-digoxigenin antibody (Roche Diagnostics) diluted 1:500 in antibody diluent. Antibody incubation was carried out for 30 minutes at 37 °C followed by chromogenic detection using BlueMap™ Kit with a substrate incubation time of 4hours. Counterstaining using ISH nuclear fast red was performed for 2 minutes. Sections were mounted in glycerol gelatin mounting medium (Sigma-Aldrich Chemie GmbH, Buchs, Switzerland) and post-mounted using Pertex™.

3.8.4 PAS staining

Sections were dehydrated using ascending serial aquaeous dilution of ethanol (70% being the highest ethanol concentration) and then incubated in a 20% periodic acid solution for 5 minutes. They were washed under running tap water for 5 minutes and incubated in Schiff reagent for 20 minutes. After that, sections were rinsed under running tap water for 30 minutes. If applicable, a counterstaining with Mayer's haematoxylin was additionally performed (see section 3.8.5).

3.8.5 H&E staining

Sections were washed with H_2O_{dest} and then stained with Mayer's haematoxylin for 5 minutes. They were rinsed under running tap water for 10 minutes, equilibrated in 50% ethanol for 30 seconds and stained with alcoholic eosin solution for 3 minutes. Finally, the sections were dehydrated by incubation in 80%, 96% and 100% ethanol for 30 seconds each, twice incubated in xylene for 5 minutes and then embedded in Entellan and covered with cover slips.

3.9 Western Blot

Frozen tissues were pulverized using a micro-dismembrator prior to incubation with an 8-fold excess of lysis buffer (CLB1, Zeptosens) for 30 minutes on a tumbler. Afterwards, tissue lysates were centrifuged at 16 000 g and room temperature for 10 minutes. Proteins in the lyasate were separated via gel electrophoresis and then transferred to nitrocellulose membranes in NuPAGE transfer buffer (Invitrogen, Carlsbad, CA, USA) containing 10% methanol at 30V for 1 hour. Transfer to polyvinylidene difluoride (PVDF) membranes was performed in 1x transfer buffer containing 20% methanol at 100 V for 1 hour. Membranes were incubated in TBS/T buffer containing 3% bovine serum albumin (BSA) on a shaker for 30 minutes at room temperature to avoid unspecific binding. After that, membranes were incubated on a tumbler with 4 ml of diluted primary antibodies in TBS/T buffer containing 1% BSA over night at 4-8 °C. After rinsing and washing 5 times for 5 minutes each with TBS/T, the membranes were incubated with 4 ml diluted secondary antibody in TBS/T containing 1% BSA for 1 hour at room temperature on a tumbler. Rinsing and washing was repeated as described above. Finally, the membranes were incubated with 4 ml SuperSignal West Pico Chemiluminescent Substrate, Pierce (Thermo Fisher Scientific, Waltham, MA, USA) for 5 minutes. Light emission was detected with the Kodak Image Station 440 CF; image analysis was carried out using ImageJ and Adobe Photoshop.

3.10 Statistic data processing

Statistic processing of all datasets was conducted by Johannes Eichner and Clemens Wrzodek (University of Tübingen, Department of Computer Science, Cognitive Systems) and Raphaëlle Luisier (Department for Discovery and Investigative Safety, Novartis Institutes for BioMedical Research, Basel, Switzerland).

3.10.1 mRNA

Affymetrix CEL files containing the raw probe intensities were normalized using the Robust Multichip Average (RMA) method. Quality of the experiments was determined using diverse plots and statistics implemented in the package arrayQualityMetrics for R/Bioconductor (Kauffmann et al., 2009). On the basis of extensive quality controls, it was concluded that all arrays had sufficient quality. A moderated t-statistic was chosen to detect differentially expressed genes (implementation from limma package for R/Bioconductor; Smyth, 2004). In order to correct for testing multiple genes, the Benjamini-Hochberg method was applied.

3.10.2 miRNA

Background correction and pooling of probe signal levels corresponding to the individual miRNAs was conducted using the Agilent Feature Extraction (AFE) image analysis algorithm from the AgiMicroRna package for R/Bioconductor (Lopez-Romero, 2011). Probe sets flagged by the AFE software as not expressed in any samples were excluded from further analysis. Subsequently, the mean fold changes were calculated for each replicate group, and p-values were computed using a moderated t-test with FDR (false discovery rate) correction as described above for mRNA expression data. Experimentally verified mRNA targets of miRNAs were extracted and merged from three publicly available databases, namely miRecords v3 (Xiao et al., 2009), miRTarBase v2.4 (Hsu et al., 2010) and TarBase v5.0c (Hsu et al., 2010).

3.10.3 DNA methylation

In order to correct for systematic intensity biases associated with the different fluorescent dyes, within-array normalization (Loess-based) was applied to M-values (M being the difference in log-ratios between input and IP, and A being the average of the log-ratios). Smoothing over individual probe intensities was further applied to the data using the computeRunningMedians routine (Ringo package). To this end, intensity of a probe at each genomic location was replaced by the median over a region of 500 bp (expected average length of DNA fragments after sonication) centered at the given probe. This step was intended to correct for systematic biases in individual probe intensities. Smoothed data matrices were further normalized by iteratively applying quantile-normalization to groups of probes sharing both CpG content (approximated by extending the probe sequence up to 500 bp - as per DNA fragment length - and then counting the number of occurrence of “CG” within this sequence) and GC content (calculated on the basis of probe-sequence and subsequently rounded up to the first decimal to reduce number of bins). This method was designed to reduce inter-array

variation which may differ/be specific for groups of probes sharing identical GC/CpG content. MeDIP enrichment levels were determined by computing the log-ratios from the red channel (enriched methylated DNA) to the green channel (input DNA) probe intensities. As these MeDIP enrichment levels were shown to be non-linearly related with absolute DNA methylation levels, the MEDME (Model for Experimental Data with MeDIP Enrichment) approach proposed by Pelizzola and colleagues was used. In the course of this procedure, a sigmoidal model is fitted on a fully methylation dataset needed for calibration (Pelizzola et al., 2008). Based on this model, the absolute methylation levels (AML) were inferred from the computed log-ratios for each probe. After that, the mean fold-changes for each sample group (i.e., tumor type) were computed, and p-values using the same statistical method as for mRNA expression data were calculated. To reveal the interactions between differential DNA methylation and gene expression, measurements of the probes which interrogate DNA methylation in the same proximal promoter were summarized. Proximal promoters were defined as the regions spanning from 2 kbp upstream to 0.5 kbp downstream of the TSS (transcription start site). As changes in the DNA methylation are typically focused to small regulatory regions, the highest peak was used as summary value for the DNA methylation status of a promoter. To create volcano plots and Venn diagrams, regions covered by the Nimblegen Deluxe Promoter Array (-2 kpb to +0.5 kpb) were analyzed.

3.10.4 Protein expression and phosphorylation data

The data obtained from reverse phase protein microarray analysis was subjected to annotation with UniProt IDs, log-transformation and median-centering in order to ease the interpretability and obtain a symmetrical scale of the protein and protein-modification levels. Measurements for which the background noise (i.e., signal of secondary antibody) was higher than the combined foreground and background signal (i.e., signal of primary and secondary antibody), were treated as missing values (< 1%) and imputed using the k-Nearest-Neighbor (kNN) algorithm. For assessment of differential protein expression, the same procedures as for mRNA data were applied.

3.10.5 Data visualization in volcano scatter plots and Venn diagrams

For volcano scatter plots and Venn diagrams, the $\log_2$ of the fold changes of tumor vs. control tissue was computed (from now on referred to as log-ratio). Statistic significance was determined by performing a moderated t-test with Benjamini-Hochberg correction. As criteria of significance for the volcano plots, absolute log-ratios >1.0 and FDR-corrected p-values <0.05 were postulated. For the Venn diagrams, no p-values were calculated.

3.10.6 Pathway enrichment analysis of mRNA and miRNA data

Significantly dysregulated mRNAs (log-ratios >1.0, FDR-corrected p-value <0.05) were annotated to gene lists of the KEGG pathway database and displayed as lists in InCroMAP. For each gene list provided by KEGG, it was investigated if it contained one or more of the differentially expressed mRNAs measured in the present study. A “list ratio” was calculated, indicating the ratio of significantly dysregulated mRNAs to the total number of genes in a KEGG gene list. Furthermore, a “background ratio” was computed, which denotes the quotient of the number of genes in one KEGG gene list and the number of all genes in all gene lists. From these two values, p-values were calculated using a hypergeometric test with Benjamini-Hochberg FDR correction. Identified pathways were then ranked according to corrected p-values.

Enrichment of significantly up- or down-regulated miRNAs was performed on annotated mRNA targets of the respective miRNAs. Predicted targets were annotated according to the 3 databases ElMMo (Gaidatzis et al., 2007), DIANA microT (Maragkakis et al., 2011) and TargetScan (Friedman et al., 2009). The resulting mRNA pool was subjected to enrichment analysis as described above, with the exception that “list ratio” indicated the ratio of miRNAs that contain target mRNAs in a KEGG gene list and the total number of potential regulatory miRNAs in this list.

4. Results

4.1. Mutation analysis of PB-promoted and unpromoted tumors

27 liver tumors from DEN-initiated mice, 7 isolated from PB-promoted and 20 from unpromoted animals, were examined with regards to their mutation status. 100% of the PB-promoted tumors harbored activating point mutations in codons 32, 33, 37 or 41 of the *Ctnnb1*-gene, whereas most of the unpromoted tumors were either mutated in *Ha-ras*-codon 61 (35%) or *B-raf*-codon 637 (45%) (figure 4.1 and table 4.1). In four of the unpromoted tumors, no mutations in *Ctnnb1*, *Ha-ras* or *B-raf* could be detected. The outcomes of the mutation analysis presented in this thesis are in accordance with previous results (Aydinlik et al., 2001).

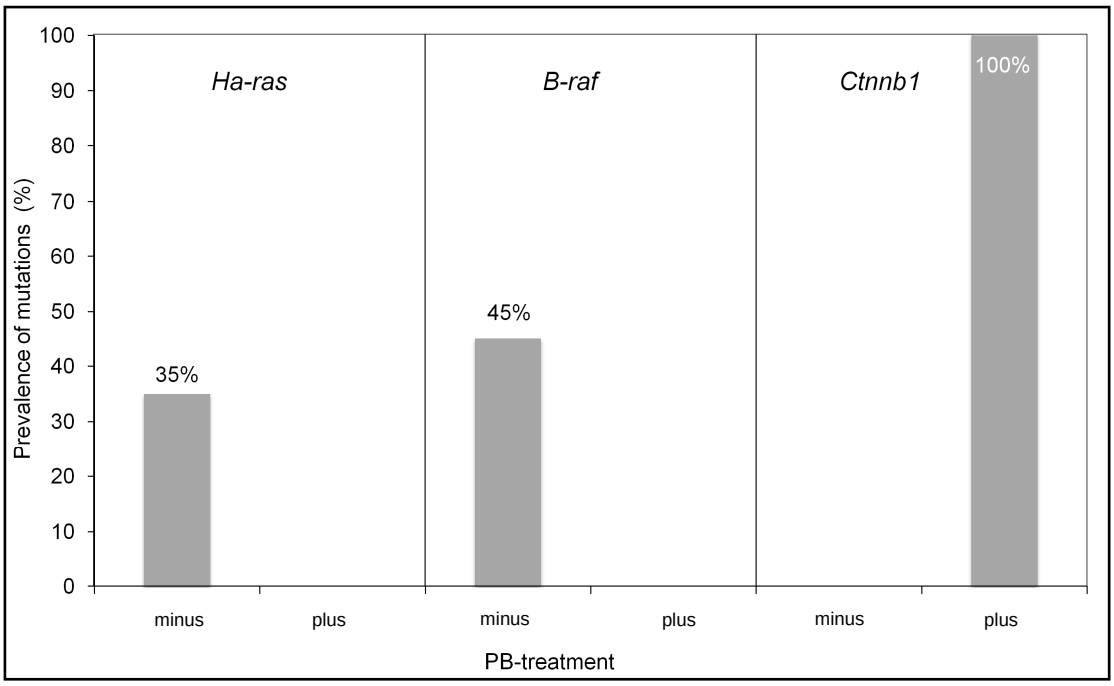

Figure 4.1. Percentages of *Ha-ras*-, *B-raf*- and *Ctnnb1*-mutations in DEN-initiated mouse liver tumors which were either PB-promoted ("plus") or unpromoted ("minus").

Table 4.1. Distribution of *Ha-ras*-, *B-raf*- and *Ctnnb1*-mutations in DEN-initiated mouse liver tumors which were either PB-promoted ("DEN+PB") or unpromoted ("DEN").

Treatment	Total number of analyzed tumors	Number of tumors			
		Mutation in *Ha-ras* (codon 61)	Mutation in *B-raf* (codon 637)	Mutations in *Ctnnb1* (codons 32, 33, 37 or 41)	Other mutations
DEN+PB	7	0	0	7	0
DEN	20	7	9	0	4

Because of the high transcriptional and phenotypic similarities between *Ha-ras*- and *B-raf*-mutated tumors (Jaworski et al., 2007; Rignall et al., 2009), a subset of 10 tumors (3 *Ha-ras*-mutated, 7 *Ctnnb1*-mutated) and 9 samples of surrounding non-tumor tissue (3 from unpromoted and 6 from PB-promoted mice) was used for further analyses. Affymetrix analysis showed very heterogenous mRNA expression patterns for the 6 samples used as control for the *Ctnnb1*-mutated tumors, 3 of them resembling the pattern in the tumors. To exclude contamination of PB-treated control tissue with tumor tissue to the greatest possible extent, mRNA levels of the non-mutation-specific liver tumor marker *Afp* (α-fetoprotein) were checked in the control tissue samples. The 3 questionable samples showed increased *Afp* levels and were thus excluded from further data analysis. To ensure that adjacent non-tumor tissues are suitable as control, independent tissues from entirely untreated mice and from mice treated with PB for 12 weeks were additionally analyzed. As no noteworthy qualitative discrepancies between the adjacent and the independent control tissues were detected in comparison with tumor tissue, the data from the adjacent tissues were used for further analyses described in section 4.2.

4.2. Global analysis of mRNA and miRNA expression, DNA methylation, and protein expression and phosphorylation in *Ha-ras*- and *Ctnnb1*-mutated tumors

The goal of the analyses presented in this section was to create a global molecular profile of *Ha-ras*- and *Ctnnb1*-mutated mouse liver tumors. The experiments conducted with these tissues included the assessment of DNA methylation via methylated DNA immunoprecipitation (MeDIP), protein expression and phosphorylation via reverse phase protein microarray, mRNA expression via DNA microarray and miRNA expression via miRNA microarray (figure 4.2).

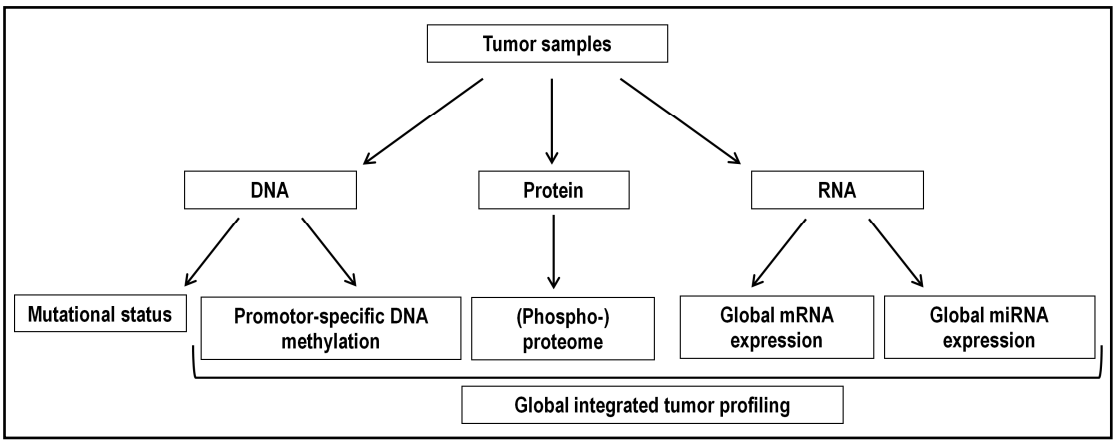

Figure 4.2. Schematic workflow of the global molecular characterisation of *Ha-ras*- and *Ctnnb1*-mutated mouse liver tumors.

To obtain a first global overview, volcano scatter plots and Venn diagrams were created for mRNA, miRNA, DNA methylation and reverse phase protein microarray data to illustrate statistically significant changes in both tumor types (figure 4.3, for detailed gene lists see appendix).

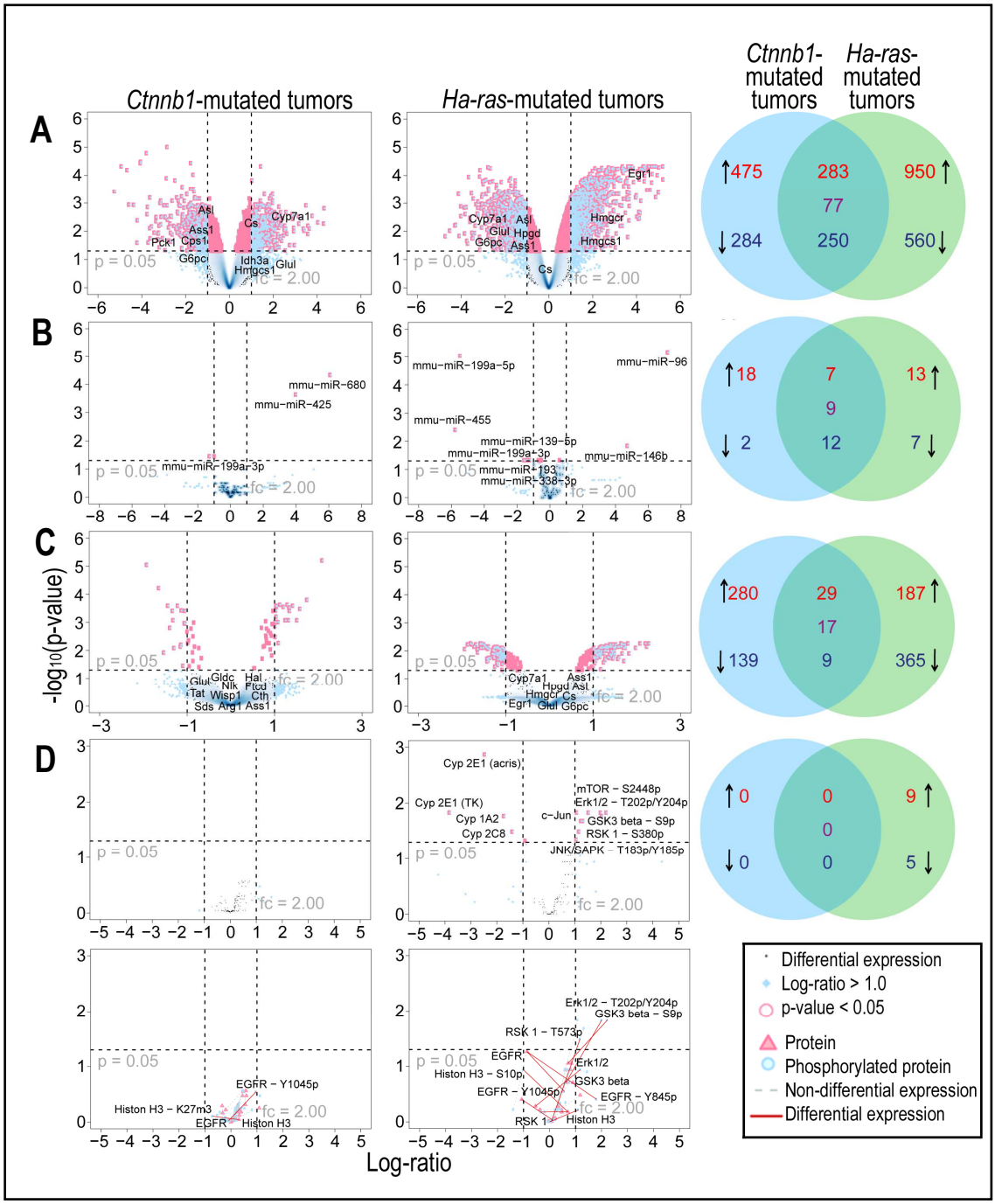

Figure 4.3. Volcano scatter plots and Venn diagrams of A) mRNA expression, B) miRNA expression, C) DNA methylation, and D) protein expression (upper panel) and phosphorylation (lower panel).
„Log-ratio" = $\log_2$ of the fold changes of tumor vs. control. As criteria of significance for the volcano plots, absolute log-ratios >1.0 and FDR-corrected (Benjamini-Hochberg correction) p-values <0.05 were required. Note that in Venn diagrams, p-values were not considered, and thus more genes may be indicated in Venn diagrams than in supplementary tables.

Comparison between *Ha-ras*- and *Ctnnb1*-mutated hepatomas showed that approximately 50 % of the down-regulated transcripts in *Ctnnb1*-mutated tumors was also decreased in the *Ha-ras*-mutated ones (250 of 534). All in all, the *Ha-ras*-mutated tumors contained 810 down-regulated RNAs. 475 transcripts were exclusively up-regulated in *Ctnnb1*-mutated and 950 exclusively in *Ha-ras*-mutated tumors, and another 284 were concomitantly increased in both types of lesions. Several general tumor markers were identified among the RNAs concurrently up-regulated in both tumor types, including the HCC serum marker *Afp* (α-fetoprotein), *Slpi* (secretory leukocyte proteinase inhibitor) which has recently been found to be up-regulated in human gastric carcinoma (Cheng et al., 2008), *Golm1* (Golgi membrane protein 1) which is used as a blood marker for liver cancer (Marrero et al., 2005) and as a tissue and urine marker for prostate cancer (Varambally et al., 2008), as well as *Gpc3* (glypican 3) which serves as a histochemical marker for HCC (Anatelli et al., 2008). Apart from that, the concomitantly up- or down-regulated RNAs in the two tumors were very diverse in function, and thus no common global changes could be defined. 77 RNAs showed anti-correlated expression, i.e., were either up-regulated in *Ha-ras*- and down-regulated in *Ctnnb1*-mutated tumors, or *vice versa*. A number of genes associated with xenobiotic metabolism were dysregulated in both types of tumors (figure 4.4). Most xenobiotic-metabolizing enzymes and transporters were transcriptionally down-regulated in the *Ha-ras*-mutated tumors whereas they were mostly unchanged or up-regulated in the *Ctnnb1*-mutated ones. mRNA changes with regards to energy metabolism are described below. The majority of changes at the mRNA level found in the present thesis were also observed in previous studies conducted in our group (Stahl et al., 2005a; Jaworski et al., 2007).

In contrast to mRNA, only few miRNAs were significantly dysregulated (log-ratio >1.0, p-values <0.05; see volcano plot in figure 4.3B), whereas the statistically less stringent Venn diagram showed that 28 miRNAs were dysregulated in both tumor types, 9 of which showed anti-correlated expression. Experimentally validated target mRNAs could be identified for 4 of the differentially expressed miRNAs in both tumor types and are listed in table 4.2.

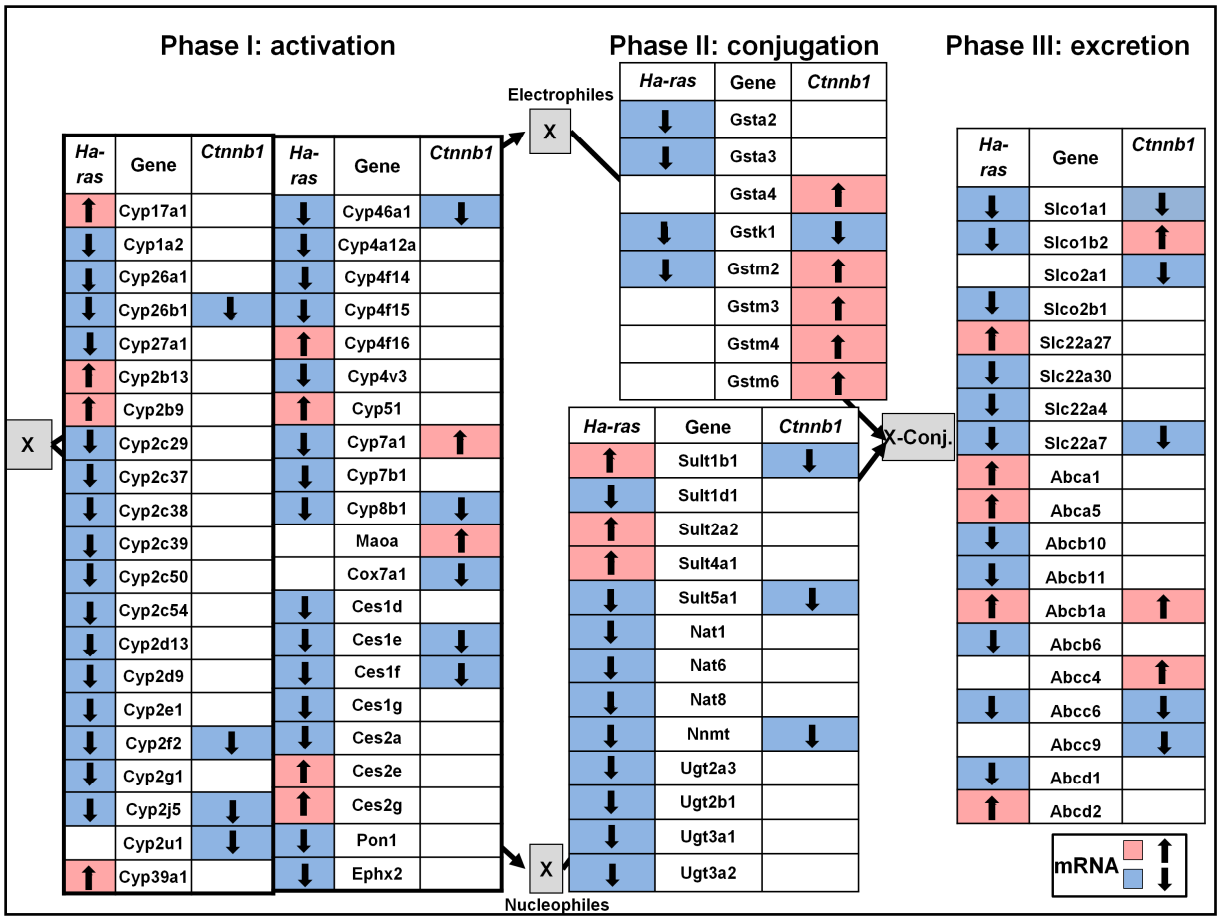

Figure 4.4. Overview of dysregulated mRNAs involved in xenobiotic metabolism in *Ha-ras*- and *Ctnnb1*-mutated tumors. Up-regulation is indicated by upward arrows in red cells, down-regulation by downward arrows in blue cells.

Table 4.2. Experimentally validated targets of significantly dysregulated miRNAs in *Ctnnb1*- and *Ha-ras*-mutated mouse liver tumors. Target mRNAs were annotated according to the miRecords v3, miRTarBase 2.4 and TarBase V5.0c databases.

Systematic miRNA name	Log-ratio in *Ctnnb1*-mutated tumors	Log-ratio in *Ha-ras*-mutated tumors	Target mRNAs
mmu-miR 199a-5p	-2.74	-5.45	*Sirt1*, *Hif1a*
mmu-miR 96	1.00	7.21	*Odf2*, *Celsr2*, *Myrip*, *Aqp5*, *Ryk*
mmu-miR 199a-3p	-1.25	-1.23	*Smad1*
mmu-miR 139-5p	-1.91	-1.21	*Foxo1*

Of the experimentally confirmed target mRNAs, only *Celsr2* in *Ha-ras*-mutated tumors was significantly changed in the present study, probably because only a small number of confirmed targets was identified altogether and the mechanisms connecting mRNA and miRNA expression are often disrupted in tumors. In addition, bioinformatically predicted mRNA targets were identified using the 3 databases ElMMo (Gaidatzis et al., 2007), DIANA microT (Maragkakis et al., 2011) and TargetScan (Friedman et al., 2009). *Tgfb2* (encoding transforming growth factor β2), one of the predicted target mRNAs of miR-199a-5p, was highly up-regulated in *Ha-ras*-mutated tumors, consistent with the decrease of its potential

regulatory miRNA. Annotation of predicted targets of miR-680 and miR-425, which were induced in *Ctnnb1*-mutated tumors, resulted in long lists of potential targets, including *Myst1* (Myst histone acetyltransferase 1), *Pbrm1* (polybromo-1), *Epc1* (enhancer of polycomb homolog 1), *Phf21a* (Phd finger protein 21A) and *Cbx6* (chromobox homolog 6), all of which play a role in chromatin remodeling. Possible targets of miR-425 included several mRNAs involved in either Ras- or Wnt-signaling, i.e. *Rap2c* (Rap2c, member of RAS oncogene family), *Smek1* (suppressor of mek1), *Mapk6* (mitogen-activated protein kinase 6) and *Fzd1* (frizzled family receptor 1).

To visualize genome-wide DNA methylation changes with Venn diagrams and volcano plots, probes within a region between 2 kbp upstream and 0.5 kbp downstream of the transcription start site (TSS) were annotated to the respective gene and then averaged to obtain the mean methylation. All in all, more genes were hypermethylated in *Ctnnb1*- than in *Ha-ras*-mutated tumors, whereas the latter showed more hypomethylated genes than their *Ctnnb1*-mutated counterparts (see Venn diagram in figure 4.3C). Only few genes were concomitantly hyper- or hypomethylated (29 of 496 and 9 of 513, respectively) in the two tumor types, and the mean methylation of 17 genes showed anti-correlated fold changes. For visualization of DNA methylation the novel cross-platform data analysis tool InCroMAP was used (Wrzodek et al., 2012; http://www.cogsys.cs.uni-tuebingen.de/software/InCroMAP/). It became obvious that, regardless of statistical significance, a number of DNA sequences - most of them gene promoter regions - showed almost mirror-image methylation patterns in *Ha-ras*- and *Ctnnb1*-mutated tumors. Four of these promoter regions, together with the absolute mRNA expression values of the downstream genes, are displayed in figure 4.5. The figure makes it clear that mRNA expression was not changed as a result of the detected DNA methylation changes. Lack of significant correlation between gene expression and promoter methylation was a general finding upon analysis of the data.

The antibodies used for reverse phase protein microarray analysis were chosen with a focus on xenobiotic-metabolizing enzymes and protein kinases with a role in signaling. Phosphorylation of several kinases was increased in the *Ha-ras*-mutated tumors (where MAPK signaling is constitutively activated) as compared to normal liver (figure 4.3D). Expectedly, since the antibody emphasis was put on signaling kinases, no proteins met the criteria of significantly differential expression or phosphorylation in *Ctnnb1*-mutated tumors (log-ratios >1.0, p-values <0.05, see figure 4.3D).

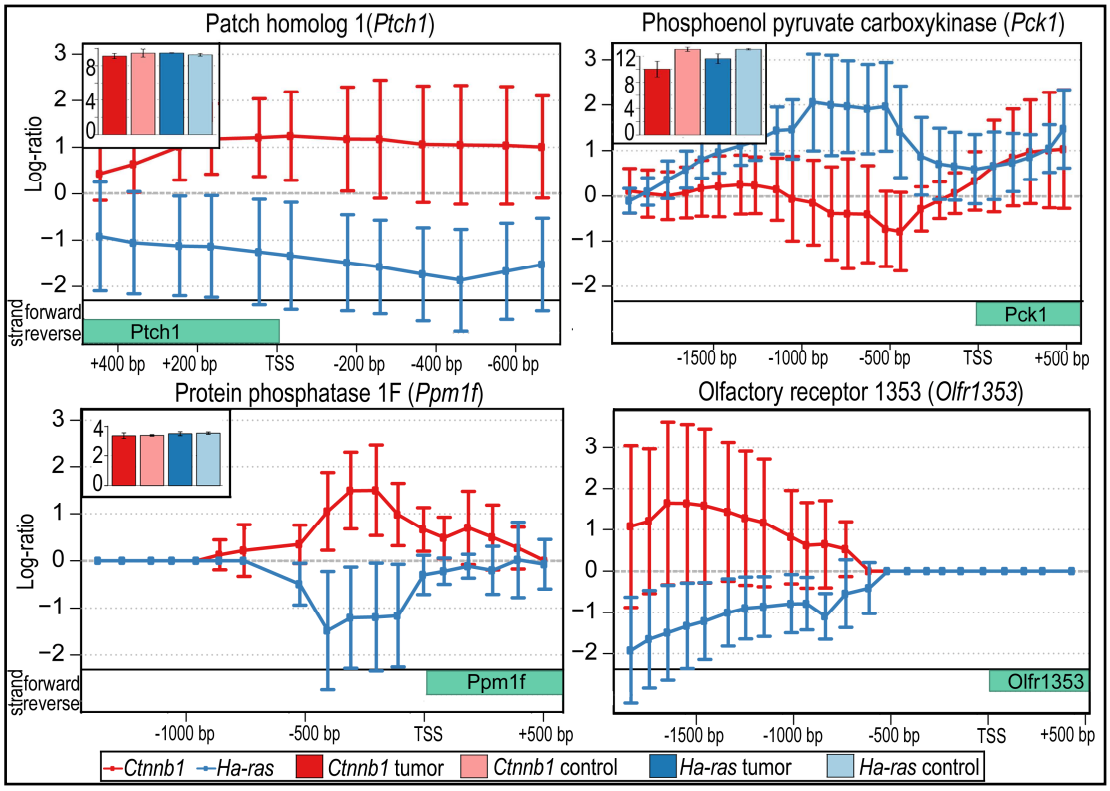

Figure 4.5. Highly anti-correlated methylation patterns in *Ha-ras*- (blue lines) and *Ctnnb1*-mutated tumors (red lines) in the promoter regions of four genes. The position of the transcribed region is indicated by the green bar („TSS“ = „transcription start site“). The absolute mRNA expression values (log-ratios) of the corresponding genes are indicated as bar diagrams in the upper left corners. Note that *Olfr1353* was not on the mRNA microarray, and hence the expression values are not indicated.

Constitutive activation of the β-Catenin and Ha-ras oncoproteins leads to disruption of Wnt- and MAPK-signaling and, as a result, to imbalances in a number of downstream processes which provide the initiated cell with a specific growth advantage. Most prominently, perturbation of metabolism is a common feature of tumors and has frequently been investigated as potential therapeutic target. In the following section, the observed changes in Wnt and MAPK signaling as well as alterations in central metabolic pathways in *Ha-ras*- and *Ctnnb1*-mutated tumors will be described.

Alterations of MAPK and Wnt signaling at the mRNA and protein level are jointly visualized in figure 4.6, based on images created with InCroMAP. As the dynamic range of the reverse phase protein microarray approach used for the detection of changes in protein expression and phosphorylation is smaller than that of the other experimental platforms (Braeuning et al., 2011), the significance criteria for protein expression and phosphorylation were eased for this visualization: Proteins were accepted as differentially expressed or phosphorylated with a log-ratio >0.5, without considering the p-value.

In *Ha-ras*-mutated tumors, activating phosphorylation of the effector kinases downstream of *Ha-ras* was increased, which is consistent with the constitutive activation of the MAPK pathway in these lesions. The same held true for Akt1 and Stat3, both of which are phosphorylation targets of MAPK and can function as transcriptional activators of Ras target genes. Accordingly, mRNA expression of the known Ras target genes *H19*, *Egr1*, *Fos* and *Jun* was significantly increased in the *Ha-ras*-mutated tumors. *Ctnnb1*-mutated tumors showed significant down-regulation of serine 445-phosphorylation of B-raf. Furthermore, an increase of the basic MAPK isoforms 8/9/10 but not the phosphorylated active forms was detected. Inhibitory phosphorylation of the kinase GSK3β at serine 9 was increased in both tumor types. β-Catenin, a target of GSK3β, was hyperphosphorylated in the *Ha-ras*-mutated tumors, which is a signal for proteasomal degradation and thus inactivation of the protein. mRNA expression of the Ras target gene *Dusp6* (dual specificity phosphatase 6) was significantly increased in the *Ha-ras*-mutated tumors as compared to control tissue. *Dusp14* mRNA was up-regulated in *Ctnnb1*-mutated tumors by a log-ratio of 1.63 and a p-value of 0.08, thereby closely missing the threshold of significance. Finally, two mRNAs encoded by Wnt-inhibitory genes, namely *Wif1* (Wnt inhibitory factor 1) and *Nlk* (Nemo-like kinase), were abundantly expressed in *Ctnnb1*-mutated tumors.

To generally elucidate which pathways apart from the Wnt and MAPK signaling cascades were affected by the molecular changes in the two tumor types, pathway enrichment analysis of the mRNA and miRNA data was conducted using the InCroMAP tool. To this end, significantly up- or down-regulated mRNAs and miRNAs were annotated to pathways corresponding to the KEGG database (Kanehisa et al., 2006). The enrichments were then ranked according to p-values (tables 4.3-4.6). Due to the comparably limited amount of significant DNA methylation and protein data, no enrichment analysis was conducted on these datasets.

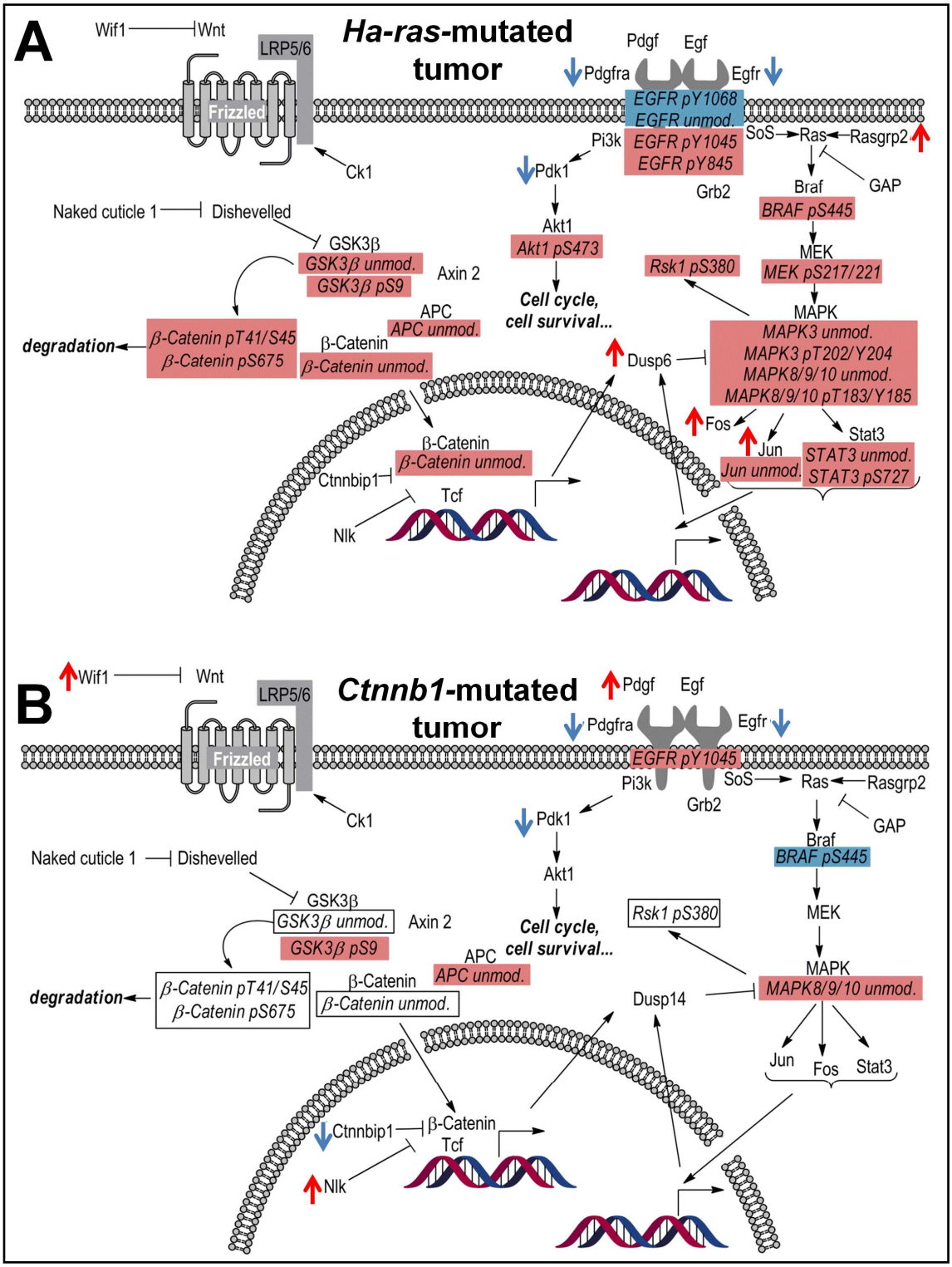

Figure 4.6. Visualization of dysregulated mRNA expression, as well as protein expression and phosphorylation in the Wnt and MAPK signaling pathways in A) *Ha-ras*- and B) *Ctnnb1*-mutated tumors. Significantly dysregulated mRNAs are indicated by red or blue arrows next to the gene name. Protein names in red or blue boxes indicate up- or down-regulated protein/phospho-protein. RNAs were considered significantly up- or down-regulated with absolute log-ratios >1.0 and p-values <0.05. Protein was considered significantly up- or down-regulated/hyper- or hypophosphorylated with absolute log-ratios >0.5 regardless of p-value.

Table 4.3. Pathway enrichments of mRNAs in *Ha-ras*-mutated tumors (top 15 pathways).

#	Name (ID)	List ratio	BG ratio	q-value	mRNAs
1	Metabolic pathways (path:mmu01100)	185/1549	1203/18080	9.12E-14	9130409I23Rik, Galnt12, Abat, Ctps2, Enpp1, Alox5, Hao2, Slc27a5, Tk1, Rgn, Plce1, Ak4, Etnk1, Cyp4f14, Mthfd2l, Dgkz, Baat, Hpse, Kynu, Cda, Hsd3b7, Akr1c6, Phgdh, Cyp4a14, Dpys, Acsl4, Ugt2a3, Mgll, Lipc, Cyp2c54, Asl, Acly, Lss, Oat, Aldh18a1, Galntl2, Chpt1, Pgd, Haao, Hsd3b2, Nat1, Pold4, Ptgds, Sds, Hexb, Hexa, Dhcr7, B3galnt1, Acsl3, Pafah2, NA, Tat, Etnk2, Acsm5, Cyp8b1, Acsl5, Bdh1, Rdh16, Alas2, Agmat, Cryl1, Rrm2, Sqle, Bdh2, Gss, Csad, Gcnt2, Gcdh, NA, Mthfd1l, Me1, Prodh, Cyp1a2, Acadsb, Rdh11, Aldh1b1, Hmgcr, Nt5e, Cyp2c50, NA, Chsy3, Hgd, Aass, NA, Psat1, Pon1, Pck1, Hibadh, Pycr1, Akr1b7, NA, P4ha2, Mgat5, Cpox, Nnmt, Ahcy, Cyp51, Cyp17a1, Smpd3, Upp2, Pigq, Uap1l1, Ggt6, Synj2, Dpyd, Lipg, Pafah1b3, NA, Cyp2b13, Fdps, Cyp2j5, Aadat, Sardh, Bcmo1, Akr1d1, Dmgdh, Sord, Hsd3b5, Cyp4f16, Cyp2b9, Fdft1, Pgm1, Gch1, Hpd, G6pdx, Afmid, B4galt6, Hmgcs1, Aldh1a7, Pld1, Ces1e, Cyp2c29, Gnpda1, Amy1, Mvd, Gmds, Acsl1, Hmgcs2, Inpp1, Ivd, Ddc, Cyp4f15, Cox5b, Aox1, Ugt2b1, Pemt, Akr1b3, Cyp4a12a, Isyna1, Cyp2e1, Sptlc2, Cth, Ido2, Dct, St6gal1, G6pc, Adh4, Cyp2c37, Glul, Cyp2c39, Cmbl, Acsm2, Cyp2c38, Gpam, Chka, Idi1, Ppap2c, Ass1, Pnpla3, Gale, Cyp27a1, Psph, Otc, Ephx2, Pck2, Nsdhl, Cyp4a31, Aldoc, Ces1d, Agps, Galnt6, Aldh1a1, Cyp7a1, Acsm1, Asns
2	Retinol metabolism (path:mmu00830)	27/1549	78/18080	9.92E-09	Cyp2c29, NA, Rdh5, Ugt2b1, Cyp4a12a, Rdh16, Cyp26a1, Cyp4a14, Retsat, NA, Cyp2b13, Ugt2a3, Adh4, Cyp2c54, Cyp2c37, Cyp2c39, Cyp2c38, Bcmo1, NA, Cyp2b9, Cyp26b1, Cyp1a2, Cyp4a31, Rdh11, Lrat, Cyp2c50, Aldh1a7
3	Primary bile acid biosynthesis (path:mmu00120)	10/1549	15/18080	2.83E-06	Baat, Hsd3b7, Slc27a5, Cyp39a1, Akr1d1, Cyp8b1, Cyp7a1, Cyp46a1, Cyp7b1, Cyp27a1
4	PPAR signaling pathway (path:mmu03320)	22/1549	82/18080	3.89E-05	NA, Pck1, Scd2, Slc27a5, Hmgcs2, Acsl1, Cyp8b1, Fabp4, Fabp7, Acsl5, Cyp27a1, Me1, Fabp5, Pck2, Fads2, Cyp4a31, Cyp4a12a, Cyp4a14, Acsl4, Cyp7a1, Acsl3, Lpl
5	Drug metabolism - cytochrome P450 (path:mmu00982)	22/1549	88/18080	1.09E-04	Cyp2c39, Cyp2c29, Cyp2c38, Gstk1, Cyp2d9, NA, Cyp2b9, Fmo1, Aox1, Ugt2b1, Cyp1a2, Cyp2e1, Gsta2, Cyp2c50, NA, Fmo4, Cyp2b13, Ugt2a3, Gsta3, Adh4, Cyp2c37, Cyp2c54
6	Arachidonic acid metabolism (path:mmu00590)	22/1549	91/18080	1.61E-04	Cyp2c29, Cyp2c39, Cyp2j5, NA, Cyp2c38, Alox5, Cyp4f15, Cyp4f14, Cyp4f16, Cyp2b9, Ephx2, Cyp4a31, Cyp4a12a, Ptgds, Gpx1, Ggt6, Cyp2e1, Cyp4a14, Cyp2c50, Cyp2b13, Cyp2c37, Cyp2c54
7	Bile secretion (path:mmu04976)	18/1549	71/18080	4.85E-04	Slc22a7, Slco1a1, Abcb1a, Abcb11, Slc27a5, Abcg5, Car2, Baat, Slco1b2, Slco1a4, Aqp9, Adcy1, Atp1b1, Hmgcr, Cyp7a1, Slc10a1, Slc10a2, Aqp4
8	p53 signaling pathway (path:mmu04115)	17/1549	70/18080	0.001265078	Ccnd1, Igfbp3, Zmat3, Bax, Ccnb1, Ccnb2, Igf1, Cdkn1a, Cdk4, Ccne1, Cdk1, Cdkn2a, Cdk6, Thbs1, Gadd45g, Serpine1, Rrm2
9	Metabolism of xenobiotics by cytochrome P450 (path:mmu00980)	18/1549	78/18080	0.001385637	Cyp2c39, Cyp2c29, Cyp2c38, Gstk1, Cyp2b9, Ugt2b1, Cyp1a2, Cyp2e1, Gsta2, Cyp2f2, Cyp2c50, NA, Cyp2b13, Ugt2a3, Gsta3, Adh4, Cyp2c54, Cyp2c37
10	Drug metabolism - other enzymes (path:mmu00983)	15/1549	59/18080	0.001574954	Ces1e, Ces2g, Tk1, NA, Ces2e, NA, Ugt2b1, Nat1, Ces1d, Cda, Upp2, Dpyd, Dpys, NA, Ugt2a3
11	Butanoate metabolism (path:mmu00650)	10/1549	31/18080	0.002745114	Acsm2, Abat, Bdh1, L2hgdh, Akr1c6, Acsm5, Hmgcs1, Bdh2, Hmgcs2, Acsm1
12	Fatty acid metabolism (path:mmu00071)	13/1549	50/18080	0.002999752	NA, Acsl1, Gcdh, Acsl5, Cyp4a31, Cyp4a12a, Acadsb, Cyp4a14, Aldh1b1, Aldh1a1, Acsl4, Acsl3, Adh4
13	Tryptophan metabolism (path:mmu00380)	12/1549	46/18080	0.004653156	Aox1, Inmt, Cyp1a2, Aadat, Kynu, Afmid, Ido2, Aldh1b1, Aldh1a1, Haao, Ddc, Gcdh
14	Glycine, serine and threonine metabolism (path:mmu00260)	10/1549	34/18080	0.00488069	Psph, Sds, Sardh, Phgdh, Cth, Gnmt, Alas2, Dmgdh, Srr, Psat1
15	Nitrogen metabolism (path:mmu00910)	8/1549	23/18080	0.005218605	Glul, Car5a, Car1, Cth, Car3, Car14, Asns, Car2

Table 4.4. Pathway enrichments of mRNAs in *Ctnnb1*-mutated tumors (top 15 pathways).

#	Name (ID)	List ratio	BG ratio	q-value	mRNAs
1	Nitrogen metabolism (path:mmu00910)	11/1077	23/18080	4.31E-06	Glul, Car5a, Cps1, Car1, Hal, Cth, Car3, Gls2, Car4, Car14, Car2
2	Metabolic pathways (path:mmu01100)	108/1077	1203/18080	4.18E-04	Atp6v0d2, Hsd17b6, Abat, Ctps2, Hao2, Plce1, Ak4, Uck2, Kynu, Cbr3, Gls2, Acsl4, Pmm2, Asl, Acly, Gldc, Arg1, Ptgds, Pold4, Sds, Arg2, Amdhd1, Sgms1, Crls1, NA, Tat, Cyp8b1, Uroc1, NA, Cryl1, Maoa, Rrm2, Rrm1, Mthfd2, Agl, Bdh2, Csad, NA, Cds2, Rdh11, Adss, Gyk, Aldh1b1, Hmgcr, Nt5e, Got1, Psat1, Aass, Cs, Pck1, Gck, Akr1b7, Acacb, Nnmt, Fbp1, Uap1l1, Upp2, Hal, Dpyd, Pnliprp1, NA, Fdps, Cyp2j5, Ahcyl1, Sardh, Gulo, Hsd3b5, Bhmt, Cyp2b9, Pycr2, St3gal5, Cbs, Hsd17b7, Hmgcs1, Acaa2, Ces1e, Cps1, Mvd, Ivd, Cyp2c65, Ept1, Aox1, St6galnac6, Pigp, Cth, Dct, St6gal1, G6pc, Pi4k2b, Glul, Cyp2c39, Aprt, Agxt, Pla2g2a, Ppap2c, Ass1, Ptgis, Aldh3a2, Otc, Idh3a, Nsdhl, Prim1, Gapdh, Ftcd, Hsd17b12, Cyp2u1, Cyp7a1, Gpat2
3	Arginine and proline metabolism (path:mmu00330)	13/1077	56/18080	7.96E-04	Glul, Asl, Cps1, Ass1, Aldh3a2, Pycr2, Otc, Arg1, Arg2, Aldh1b1, Gls2, Got1, Maoa
4	Cell cycle (path:mmu04110)	21/1077	128/18080	0.001034379	Ccnd1, Mcm6, Plk1, Ywhaq, Bub1b, Cdc6, Pttg1, Ccnb1, Cdc20, Ccnb2, Bub1, Myc, Mcm2, Rbl1, Wee1, Pcna, Cdkn2c, Cdk1, Ttk, Ccna2, Mad2l1
5	Thyroid cancer (path:mmu05216)	9/1077	30/18080	0.001506996	Tpr, Ccnd1, Pparg, Tcf7l1, Tcf7, Cdh1, Ctnnb1, Tpm3, Myc
6	Glutathione metabolism (path:mmu00480)	12/1077	54/18080	0.001732835	Ggct, Gsr, Gstm6, Mgst3, Gstm4, Gpx7, Gstk1, Gstm3, Gsta4, Gstm2, Rrm2, Rrm1
7	Alanine, aspartate and glutamate metabolism (path:mmu00250)	9/1077	34/18080	0.002705406	Asl, Glul, Cps1, Abat, Adss, Agxt, Gls2, Ass1, Got1
8	Glycine, serine and threonine metabolism (path:mmu00260)	9/1077	34/18080	0.003091892	Bhmt, Cbs, Sds, Sardh, Gldc, Cth, Agxt, Maoa, Psat1
9	Drug metabolism - cytochrome P450 (path:mmu00982)	15/1077	88/18080	0.003339641	Cyp2c39, Gstk1, Cyp2c65, NA, Cyp2b9, Aox1, Gstm6, Mgst3, Gstm4, Gstm3, NA, Gsta4, Fmo3, Maoa, Gstm2
10	Bile secretion (path:mmu04976)	13/1077	71/18080	0.003929205	Slc22a7, Slco1a1, Abcc4, Aqp1, Abcb1a, Car2, Slco1b2, Aqp9, Hmgcr, Cyp7a1, Atp1a2, Slc10a2, Aqp4
11	PPAR signaling pathway (path:mmu03320)	14/1077	82/18080	0.004345159	NA, Pparg, Cd36, Pck1, Scd2, Apoa5, Fabp2, Cyp8b1, Fabp7, Aqp7, Gyk, Cyp7a1, Acsl4, Lpl
12	Pathways in cancer (path:mmu05200)	35/1077	326/18080	0.004791806	Smo, Cdh1, Ikbkg, Myc, Col4a1, Ikbkb, Pdgfra, Pdgfa, Fgf21, Dapk1, Lama3, Araf, Wnt2, Bmp2, Tcf7l1, Tcf7, Axin2, Tpm3, Hsp90aa1, Fgfr2, Rad51, Tpr, Ccnd1, Itga6, Pparg, Casp3, Crk, Igf1, Birc5, Egfr, Tgfbr2, Ctnnb1, Zbtb16, Casp8
13	Histidine metabolism (path:mmu00340)	7/1077	28/18080	0.013665238	Uroc1, Amdhd1, Hal, Ftcd, Aldh1b1, Maoa, Aldh3a2
14	Metabolism of xenobiotics by cytochrome P450 (path:mmu00980)	12/1077	78/18080	0.021782572	Cyp2b9, Cyp2c39, Gstm6, Mgst3, Gstm4, Gstk1, Gstm3, Cyp2c65, Cyp2f2, NA, Gsta4, Gstm2
15	Prostate cancer (path:mmu05215)	13/1077	90/18080	0.023279291	Ccnd1, Ikbkg, Ikbkb, Pdgfra, Pdgfa, Igf1, Araf, Egfr, Tcf7l1, Tcf7, Ctnnb1, Hsp90aa1, Fgfr2

Table 4.5. Pathway enrichments of miRNAs in *Ctnnb1*-mutated tumors.

#	Name (ID)	List ratio	BG ratio	q-value	miRNAs
1	MAPK signaling pathway (path:mmu04010)	4/43	269/18080	0.18610429	mmu-miR-31, mmu-miR-143, mmu-let-7d*, mmu-miR-495
2	Neurotrophin signaling pathway (path:mmu04722)	3/43	132/18080	0.098679509	mmu-miR-152, mmu-let-7d*, mmu-miR-495
3	Glioma (path:mmu05214)	2/43	66/18080	0.191258049	mmu-miR-31, mmu-miR-152
4	Focal adhesion (path:mmu04510)	3/43	200/18080	0.148574037	mmu-miR-31, mmu-miR-143, mmu-miR-29c*
5	Huntington's disease (path:mmu05016)	3/43	200/18080	0.11885923	mmu-miR-199b*, mmu-let-7d*, mmu-miR-495
6	Chronic myeloid leukemia (path:mmu05220)	2/43	74/18080	0.118241193	mmu-miR-31, mmu-miR-199b*
7	ErbB signaling pathway (path:mmu04012)	2/43	87/18080	0.136273222	mmu-miR-143, mmu-miR-152
8	Prostate cancer (path:mmu05215)	2/43	90/18080	0.126782994	mmu-miR-31, mmu-miR-139-5p
9	GnRH signaling pathway (path:mmu04912)	2/43	99/18080	0.133726383	mmu-miR-143, mmu-miR-152
10	Melanogenesis (path:mmu04916)	2/43	101/18080	0.124720215	mmu-miR-31, mmu-miR-152
11	Pathways in cancer (path:mmu05200)	3/43	326/18080	0.17730514	mmu-miR-31, mmu-miR-199b*, mmu-miR-139-5p
12	Tight junction (path:mmu04530)	2/43	137/18080	0.176589314	mmu-miR-31, mmu-miR-143
13	Insulin signaling pathway (path:mmu04910)	2/43	138/18080	0.165024713	mmu-miR-143, mmu-miR-139-5p
14	Wnt signaling pathway (path:mmu04310)	2/43	154/18080	0.184108224	mmu-miR-31, mmu-miR-152

Table 4.6. Pathway enrichments of miRNAs in *Ha-ras*-mutated tumors (top 15 pathways).

#	Name (ID)	List ratio	BG ratio	q-value	miRNAs
1	Pathways in cancer (path:mmu05200)	10/41	326/18080	1.73E-07	mmu-miR-21, mmu-miR-199b*, mmu-miR-31, mmu-miR-27a, mmu-miR-486, mmu-miR-139-5p, mmu-miR-324-5p, mmu-miR-34a, mmu-miR-30c-2*, mmu-miR-31*
2	Prostate cancer (path:mmu05215)	6/41	90/18080	2.06E-06	mmu-miR-21, mmu-miR-31, mmu-miR-34a, mmu-miR-486, mmu-miR-31*, mmu-miR-139-5p
3	Focal adhesion (path:mmu04510)	7/41	200/18080	7.97E-06	mmu-miR-21, mmu-miR-31, mmu-miR-34a, mmu-miR-143, mmu-miR-29c*, mmu-miR-486, mmu-miR-31*
5	Chronic myeloid leukemia (path:mmu05220)	5/41	74/18080	1.10E-05	mmu-miR-31, mmu-miR-199b*, mmu-miR-30c-2*, mmu-miR-27a, mmu-miR-31*
4	Tight junction (path:mmu04530)	6/41	137/18080	1.24E-05	mmu-miR-21, mmu-miR-31, mmu-miR-34a, mmu-miR-143, mmu-miR-486, mmu-miR-31*
6	Glioma (path:mmu05214)	4/41	66/18080	2.02E-04	mmu-miR-21, mmu-miR-31, mmu-miR-486, mmu-miR-31*
8	Melanoma (path:mmu05218)	4/41	72/18080	2.14E-04	mmu-miR-21, mmu-miR-31, mmu-miR-486, mmu-miR-31*
7	p53 signaling pathway (path:mmu04115)	4/41	70/18080	2.19E-04	mmu-miR-21, mmu-miR-31, mmu-miR-486, mmu-miR-31*
9	Endometrial cancer (path:mmu05213)	3/41	52/18080	0.002013602	mmu-miR-21, mmu-miR-143, mmu-miR-486
10	Basal cell carcinoma (path:mmu05217)	3/41	55/18080	0.002137743	mmu-miR-31, mmu-miR-324-5p, mmu-miR-31*
11	Acute myeloid leukemia (path:mmu05221)	3/41	57/18080	0.002158356	mmu-miR-199b*, mmu-miR-30c-2*, mmu-miR-27a
12	MAPK signaling pathway (path:mmu04010)	5/41	269/18080	0.002169301	mmu-miR-21, mmu-miR-31, mmu-miR-143, mmu-let-7d*, mmu-miR-31*
13	Small cell lung cancer (path:mmu05222)	3/41	87/18080	0.006209577	mmu-miR-21, mmu-miR-34a, mmu-miR-486
14	Chagas disease (American trypanosomiasis) (path:mmu05142)	3/41	101/18080	0.008801126	mmu-miR-21, mmu-miR-31, mmu-miR-31*
15	Neurotrophin signaling pathway (path:mmu04722)	3/41	132/18080	0.017294091	mmu-miR-21, mmu-miR-34a, mmu-let-7d*

As expected, mRNAs coding for proteins involved in nitrogen and amino acid metabolism ranked very high in *Ctnnb1*-mutated tumors. In *Ha-ras*-mutated tumors, several mRNAs encoding phase I and II enzymes of xenobiotic metabolism were enriched in different pathways. mRNAs involved in general metabolic and signaling pathways associated with various cancers were significantly dysregulated in both tumor types, and only few miRNAs that regulate a number of mRNAs in different pathways were enriched. No significant enrichments of methylated DNA or protein could be detected in any pathway.

To investigate the characteristic tumor-specific perturbations in metabolism, InCroMAP was used to to visualize the data analyzed in the course of this thesis and to integrate the different datasets where applicable. First, visualizations of the changes in mRNA expression in central metabolic pathways in *Ha-ras*- or *Ctnnb1*-mutated tumors as compared to non-tumor control tissue were created (figure 4.7). These images illustrate considerable differences between the two types of tumors concerning the transcriptional regulation of genes encoding enzymes involved in energy metabolism. In the *Ha-ras*-mutated tumors, mRNA expression of *G6pc* (glucose-6-phosphatase), which catalyzes the last step of gluconeogenesis, was reduced as compared to non-tumor control tissue. Expression of *Pck1*, which encodes the rate-controlling gluconeogenic enzyme phosphoenol pyruvate carboxykinase, was decreased in *Ctnnb1*-mutated tumors. Citrate synthase (*Cs*) and a subunit of isocitrate dehydrogenase (*Idh3a*), which is the rate-limiting enzyme of the TCA cycle, were divergently expressed in the two tumor types. Both mRNAs were up-regulated in the *Ctnnb1*-mutated but down-regulated in the *Ha-ras*-mutated tumors; the fold changes in *Ha-ras*-mutated tumors were slightly below the required significance levels of +/-1.0 (-0.71 for *Idh3a* and -0.73 for *Cs*), but with significant p-values <0.04. The results of proteome analysis recently conducted in our group furthermore show that the flavoprotein subunit of succinate dehydrogenase, which represents the key interface between the TCA cycle and the respiratory chain, as well as several other proteins of the respiratory chain were down-regulated in *Ha-ras*-mutated tumors (Rignall et al., 2009).

The key enzymes of cholesterol biosynthesis were significantly dysregulated at the mRNA level in *Ha-ras*- and *Ctnnb1*-mutated tumors. The mRNA of HMG-CoA synthase 1 (*Hmgcs1*) was up-regulated in both tumor types, whereas HMG-CoA reductase (*Hmgcr*) mRNA was increased only in the *Ha-ras*-mutated ones (figure 4.7). In *Ctnnb1*-mutated tumors, the mRNA levels of cholesterol 7α-hydroxylase (*Cyp7a1*), which catalyzes the rate-limiting step

of bile acid biosynthesis from cholesterol, were elevated, while they were decreased in *Ha-ras*-mutated tumors.

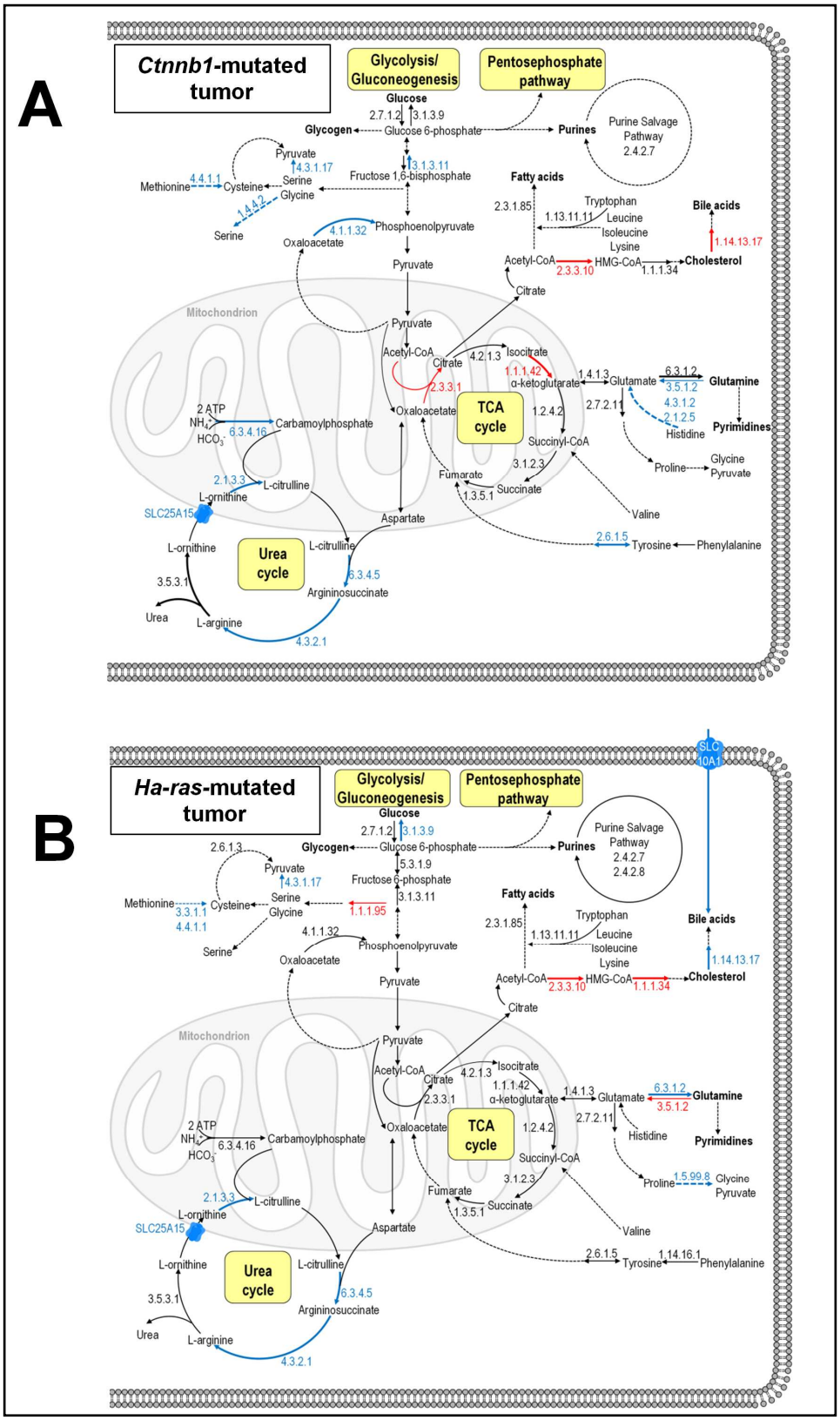

Figure 4.7. Changes in mRNA expression in the metabolism of A) *Ctnnb1*-mutated and B) *Ha-ras*-mutated tumors. Reactions catalyzed by individual enzymes are indicated by arrows and enzyme codes. Dotted arrows stand for a series of enzymatic reactions. Red arrows indicate significantly up-regulated, blue arrows significantly down-regulated mRNAs (p-value <0.05, log-ratio >1.0). For corresponding enzyme names and gene symbols see table 4.7.

Table 4.7. Enzyme names and gene symbols corresponding to the enzyme codes in figure 4.7. Entries written in bold letters indicate rate-controlling or -limiting steps.

Enzyme code	Enyme Name	Gene symbol
1.1.1.95	**3-Phosphoglycerate dehydrogenase**	*Phgdh*
4.2.1.3	Aconitase 2	*Aco2*
3.3.1.1	Adenosylhomocysteinase	*Ahcy*
2.4.2.7	Adenine phosphoribosyltransferase	*Aprt*
3.5.3.1	Arginase	*Arg*
4.3.2.1	Argininosuccinate lyase	*Asl*
6.3.4.5	Argininosuccinate synthase	*Ass*
6.3.4.16	**Carbamoyl phosphate synthetase** I	*Cpsl*
2.3.3.1	Citrate synthase	*Cs*
1.14.13.17	**CYP7A1**	*Cyp7a1*
4.4.1.1	Cystathionine γ-lyase	*Cth*
2.6.1.3	Cysteine transaminase	*Got1*
2.3.1.85	Fatty acid synthase	*Fasn*
3.1.3.11	Fructose 1,6-bisphosphatase	*Fbp1*
2.7.1.2	Glucokinase	*Gck*
3.1.3.9	Glucose 6-phosphatase	*G6pc*
5.3.1.9	Glucose-phosphate isomerase	*Gpi1*
2.7.2.11	**Glutamate 5-kinase**	*Aldh18a1*
1.4.1.3	Glutamate dehydrogenase	*Glud*
2.1.2.5	Glutamate formimino transferase (Formiminotransferase cyclodeaminase)	*Ftcd*
3.5.1.2	Glutaminase 2	*Gls2*
6.3.1.2	Glutamine synthetase	*Glul*
2.4.1.14	Glutamine-PRPP-Amidotransferase	*Ppat*
1.4.4.2	Glycine dehydrogenase	*Gldc*
2.4.1.1	Glycogen phosphorylase	*Pygl*
2.4.1.11	**Glycogen synthase**	*Gys2*
4.3.1.2	Histidine ammonia lyase	*Hal*
1.1.1.34	**HMG-CoA-reductase**	*Hgcr*
2.3.3.10	HMG-CoA-synthase	*Hgcs*
2.4.2.8	Hypoxanthine phosphoribosyltransferase	*Hprt*
1.1.1.42	**Isocitrate dehydrogenase 2**	*Idh2*
2.1.3.3	Ornithine transcarbamoylase	*Otc*
1.14.16.1	Phenylalanine hydroxylase	*Pah*
4.1.1.32	**Phosphoenolpyruvate carboxykinase**	*Pck1*
1.5.99.8	Proline dehydrogenase	*Prodh*
4.3.1.17	Serine dehydratase	*Sds*
1.3.5.1	Succinate dehydrogenase	*Sdha/b/c/d*
3.1.2.3	Succinyl-CoA hydrolase	*Acot4*
1.13.11.11	**Tryptophan 2,3-dioxygenase**	*Tdo2*
2.6.1.5	**Tyrosine aminotransferase**	*Tat*
1.2.4.2	α-ketoglutarate dehydrogenase complex	*Ogdh, Dlst, Dld*

In agreement with earlier observations (Stahl et al., 2005b), a number of mRNAs involved in amino acid catabolism were differentially expressed in the *Ctnnb1*-mutated tumors (figure 4.7). Among these were *Ftcd* (formiminotransferase cyclodeaminase), which catalyzes a step in histidine degradation, and *Sds* (serine dehydratase), which converts serine into pyruvate. Both genes were decreased in transcription. Down-regulation of Ftcd in *Ctnnb1*-mutated tumors at the protein level has also been shown previously by our group (Strathmann et al., 2007). Furthermore, an isoform of glutaminase normally expressed in kidney (*Gls1*) was up-regulated in the *Ha-ras*-mutated tumors (log-ratio 0.97, p-value= 0.01). Two key enzymes of

the urea cycle were transcriptionally down-regulated in both tumor types, namely argininosuccinate synthase (*Ass*) and argininosuccinate lyase (*Asl*). Consistently, decreased *Asl* expression in *Ha-ras*- and *Ctnnb1*-mutated tumors has been shown at the protein level in a previous study conducted in our group (Strathmann et al., 2007). Liver-type arginase (*Arg1*) was not changed at the mRNA level in either of the tumor types, however, previous studies have shown down-regulation of arginase 1 at the protein level in *Ctnnb1*-mutated tumors (Strathmann et al., 2007).

The research group of Christine Perret (Inserm, U1016, Institut Cochin, Paris, France) has identified several genes which are subject to direct control by β-Catenin via deep-sequencing of chromatin-immunoprecipitation products (unpublished data, manuscript by Torre et al. in preparation). Metabolic mRNAs that were significantly dysregulated in the *Ctnnb1*-mutated tumors in the present thesis were compared with the gene lists generated by Torre et al., and those that were identified as directly regulated by β-Catenin are listed in table 4.8

Table 4.8. Genes encoding metabolic enzymes that are differentially expressed in *Ctnnb1*-mutated tumors, identified as direct β-Catenin target genes by Torre et al.

EC	Enzyme name	Gene symbol	Log-ratio in *Ctnnb1*-mutated tumors	Log-ratio in *Ha-ras*-mutated tumors	Transcriptional regulation by β-Catenin*
3.5.3.1	Arginase 1	*Arg1*	-2.95	-	↓
2.1.3.3	Ornithine transcarbamoylase	*Otc*	-1.50	-1.31	↓
6.3.4.16	Carbamoylphosphate synthetase 1	*Cps1*	-2.17	-	↓
1.4.4.2	Glycine dehydrogenase	*Gldc*	-3.53	-	↓
4.3.1.17	Serine dehydratase	*Sds*	-4.60	-	↓
3.5.1.2	Glutaminase 2	*Gls2*	-4.18	-	↓
2.1.2.5	Glutamate formimino transferase (Formiminotransferase cyclodeaminase)	*Ftcd*	-1.47	-	↓
4.3.1.2	Histidine ammonia lyase	*Hal*	-4.35	-	↓
4.1.1.32	Phosphoenolpyruvate carboxykinase 1	*Pck1*	-3.02	-0.22	↓
4.3.2.1	Argininosuccinate lyase	*Asl*	-1.25	-1.47	↓
1.1.1.105	Retinol dehydrogenase 9	*Rdh9*	1.79	1.08	↑
1.2.1.3	Aldehyde dehydrogenase family 3, subfamily A2	*Aldh3a2*	1.86	-	↑
1.2.3.1	Aldehyde oxidase 1	*Aox1*	1.05	-1.47	↑
1.1.1.41	Isocitrate dehydrogenase 3 (NAD+) alpha	*Idh3a*	1.24	-	↑
2.4.1.1	Carbonic anhydrase 2	*Car2*	1.85	1.26	↑

*...as identified by Torre et al., manuscript in preparation

4.3. Determination of the expression levels of imprinted *Dlk1-Dio3* gene cluster RNAs

Recent work developed in cooperation with Lempiäinen and colleagues showed that several RNAs encoded on the imprinted *Dlk1-Dio3* gene cluster were up-regulated in wild-type mouse liver upon PB-treatment (Lempiainen et al., 2013). The role of these RNAs in PB-promoted tumor formation was further examined in the course of the present thesis. To this end, the expression levels of 6 RNAs, *Meg3/Gtl2*, *Dio3*, *Mirg*, *Rian*, *Dlk1* and *Rtl1*, all of which are *Dlk1-Dio3* cluster RNAs, were determined via LightCycler-PCR in tissue samples of *Ctnnb1*- and *Ha-ras*-mutated tumors, as well as adjacent non-tumor control tissue samples (figure 4.8). The *Dlk1* transcript could not be detected in any of the examined tissues, although it has previously been reported to be expressed in HCC and fetal liver (Yanai et al., 2010). RNA levels of *Meg3/Gtl2* were significantly higher in *Ctnnb1*-mutated tumors than in *Ha-ras*-mutated tumors (by a factor of 20.5) and control tissue from non-PB-treated animals (by a factor of 18.7), respectively, and expression of *Dio3* showed a significant decrease in *Ctnnb1*-mutated tumors as compared to their *Ha-ras*-mutated counterparts (by a factor of 5.9). For the other three RNAs, no significant transcriptional differences were detected between the individual tissue groups.

The PB-induced increase in *Meg3/Gtl2* transcription does not occur in livers of PB-treated mice with a liver-specific *Ctnnb1*-knockout or CAR/PXR double knockout (Lempiainen et al., 2013). Based on the knowledge that PB is a CAR agonist and selects for *Ctnnb1*-mutated cells, it was hypothesized that *Meg3/Gtl2* represents a link between the promoting agent and the resulting tumor genotype, and thus the following experiments focused on *Meg3/Gtl2*. To further characterize the potential role of *Meg3/Gtl2* in PB-mediated tumor promotion, *Meg3/Gtl2* RNA levels were determined via LightCycler-PCR in a number of normal tissues from different transgenic mouse models and various mouse tumor tissues: 1) liver tissue from mice with a liver-specific tamoxifen-inducible APC-knockout (Zeller et al., 2012), where β-Catenin is constitutively activated (figure 4.9), 2) liver tissue from Connexin32 (Cx32)-knockout mice (Moennikes et al., 2000a) which are not susceptible to tumor promotion by PB (figure 4.9), 3) mouse liver tumors isolated from entirely untreated male mice between 75 and 77 weeks of age (figure 4.10), and 4) mouse liver tumors from DEN-initiated mice which were promoted with PB for 25 weeks and then kept on a PB-free control diet for another 25 weeks before killing (figure 4.11). Liver samples of untreated mice and mice treated with PB for 12 weeks, respectively, were used as control tissues.

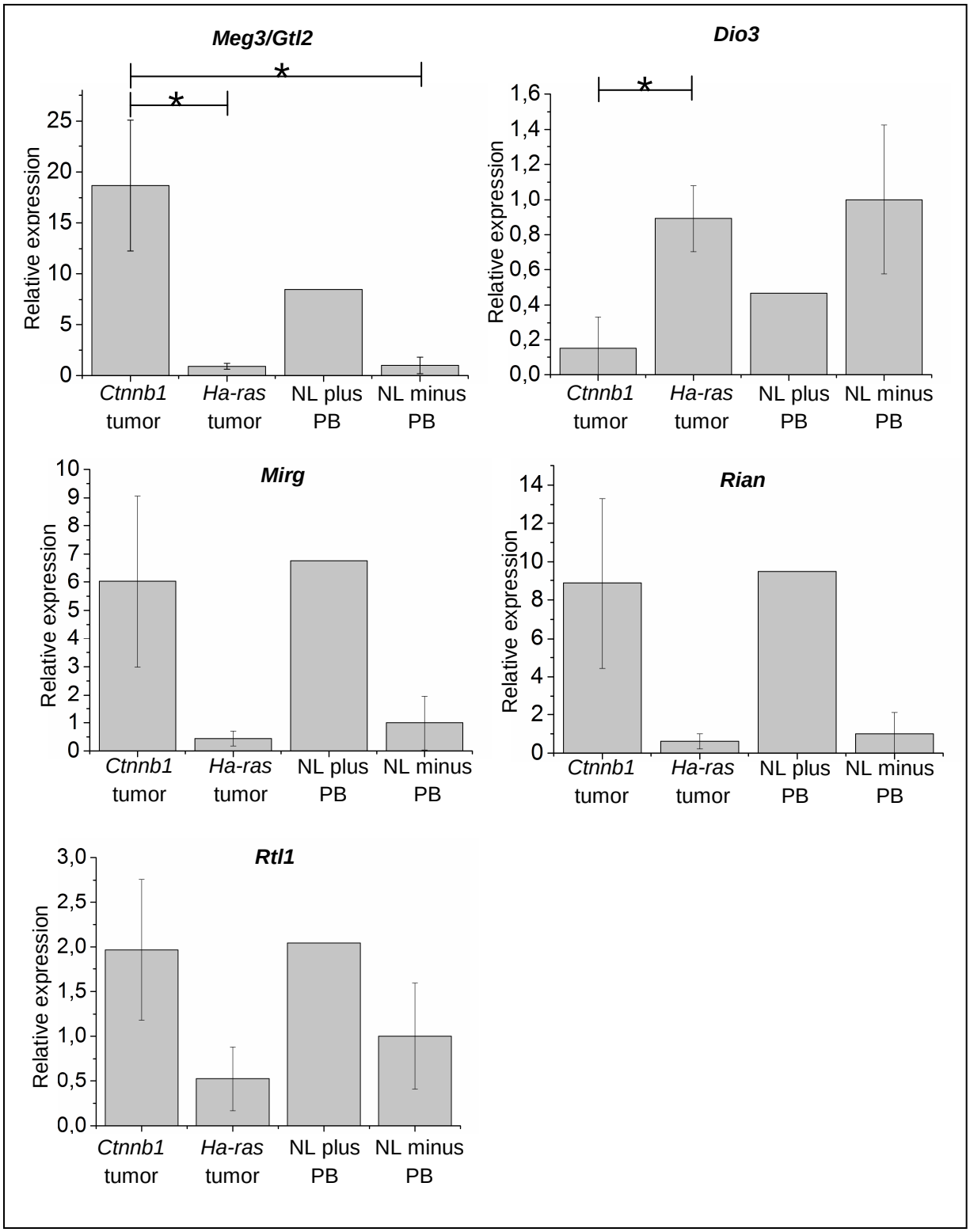

Figure 4.8. Relative expression of imprinted *Dlk1-Dio3* cluster RNAs in *Ha-ras*- and *Ctnnb1*-mutated tumors, as well as adjacent normal liver („NL plus/minus PB“).
Sample numbers: *Ctnnb1* tumors = 7; *Ha-ras* tumors = 3; NL plus PB = 2; NL minus PB = 3.
*... p-value <0.05

In APC-knockout liver, in which β-Catenin is constitutively active, *Meg3/Gtl2* RNA was up-regulated by a factor of 27.1 as compared to untreated control tissue and by a factor of 8.0 as compared to PB-treated control tissue (figure 4.9). PB-treated Cx32-knockout liver, which is insensitive to PB-promotion, showed an increase in *Meg3/Gtl2* by a factor of 3.0 as compared to untreated Cx32-knockout tissue. In this respect, tissue from Cx32-knockout mice behaved very similarly to that of wild-type mice, in which *Meg3/Gtl2* RNA was increased 3.4-fold in comparison with untreated wild-type tissue.

From the livers of two DEN-initiated mice which received a PB-containing diet for 25 weeks and were then kept on a PB-free control diet for another 25 weeks, two tumors mutated in *Ha-ras* and 3 tumors mutated in *Ctnnb1* were isolated. In both *Ha-ras*- and *Ctnnb1*-mutated tumors, *Meg3/Gtl2* was up-regulated as compared to PB-treated and untreated controls (figure 4.10), although the increase was much higher in the *Ctnnb1*-mutated (factor 441.1 as compared to untreated control) than in the *Ha-ras*-mutated tumors (factor 123.9 as compared to untreated control).

All of the tumors isolated from untreated male C3H mice of 75 to 77 weeks of age harbored *Ha-ras*-mutations. Interestingly, two tumors (tumors 2 and 6) showed increased *Meg3/Gtl2* levels as compared to untreated control, by factors of 39.9 and 5.0, respectively (figure 4.11A). To clarify the phenotypes of these two samples, mRNA levels of *H19* and *Glul* as typical markers for *Ha-ras*- and *Ctnnb1*-mutation, respectively, were determined via LightCycler-PCR. As expected, *H19* was strongly up-regulated in both samples (figure 4.11B), whereas tumor 2 showed an increase in *Glul* mRNA by a factor of 29.2 as compared to untreated control tissue (figure 4.11C).

To examine the intracellular localization of the *Meg3/Gtl2* transcript in tumors, *in situ* hybridization experiments were carried out in the laboratory of Valérie Dubost, Novartis Institutes for Biomedical Research, Basel. The experiments were conducted in fixed and embedded liver tissue from DEN-initiated mice which had either been unpromoted or promoted with PB (figure 4.12). *Meg3/Gtl2*-expressing nuclei were detected in GS-positive, *Ctnnb1*-mutated tumors but not in the GS-negative tissue surrounding the tumors. In contrast, the *Meg3/Gtl2* transcript could not be detected in nuclei of E-Cadherin-positive, *Ha-ras*-mutated tumors.

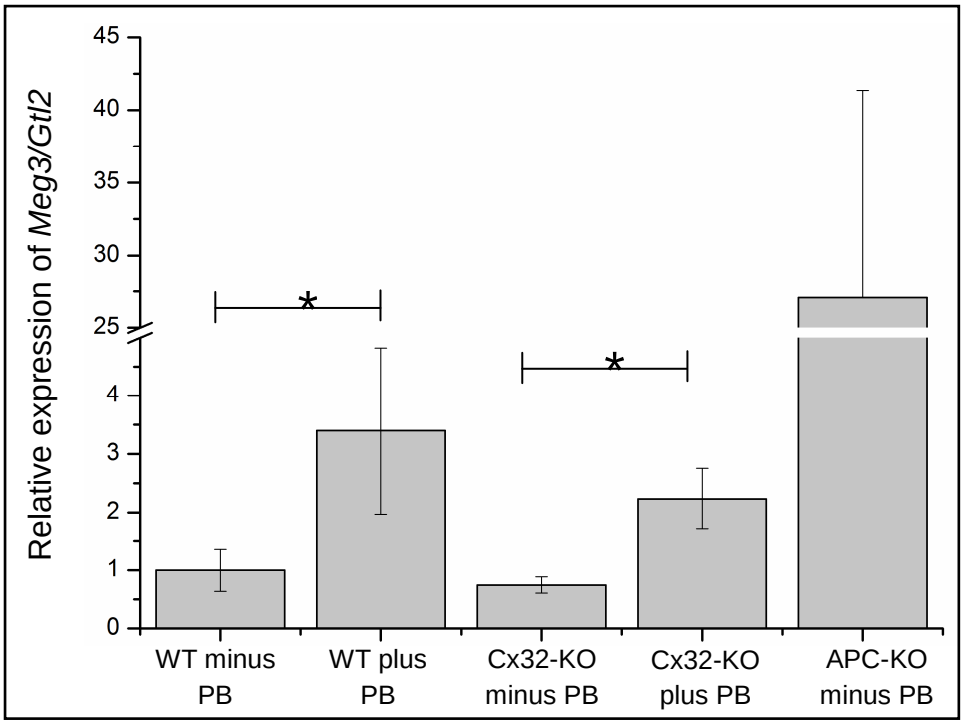

Figure 4.9. Relative expression of *Meg3/Gtl2* in normal liver from untreated wild-type mice (WT minus PB) and mice treated with PB for 12 weeks (WT plus PB), in Cx32-knockout liver with and without PB-treatment (Cx32-KO plus/minus PB), and in untreated APC-knockout liver (APC-KO minus PB).
Sample numbers: WT minus PB, WT plus PB, Cx32-KO minus PB, Cx32-KO plus PB = 4 each; APC-KO minus PB = 5.
*... p-value <0.05

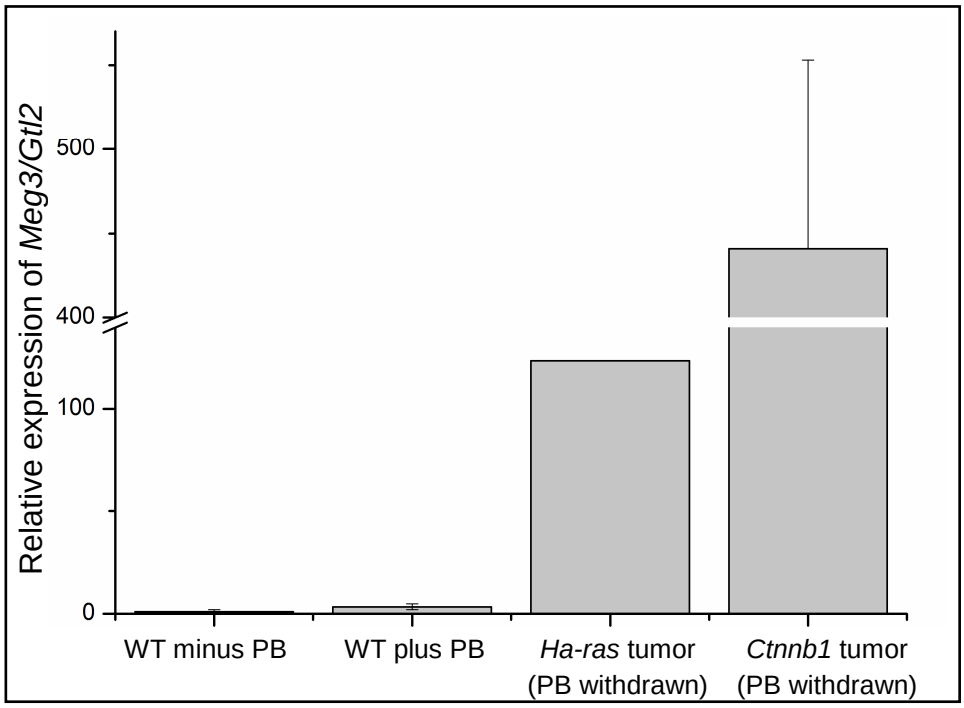

Figure 4.10. Relative expression of *Meg3/Gtl2* in *Ha-ras*- and *Ctnnb1*-mutated tumors isolated from DEN-initiated mice which were first promoted with PB for 25 weeks and then kept on a PB-free diet for 25 weeks (*Ha-ras*/*Ctnnb1* tumor (PB withdrawn)), and in normal liver from untreated wild-type mice (WT minus PB) and mice treated with PB for 12 weeks (WT plus PB).
Sample numbers: WT minus PB, WT plus PB = 4 each; *Ha-ras* tumor (PB withdrawn) = 2; *Ctnnb1* tumor (PB withdrawn) = 3.

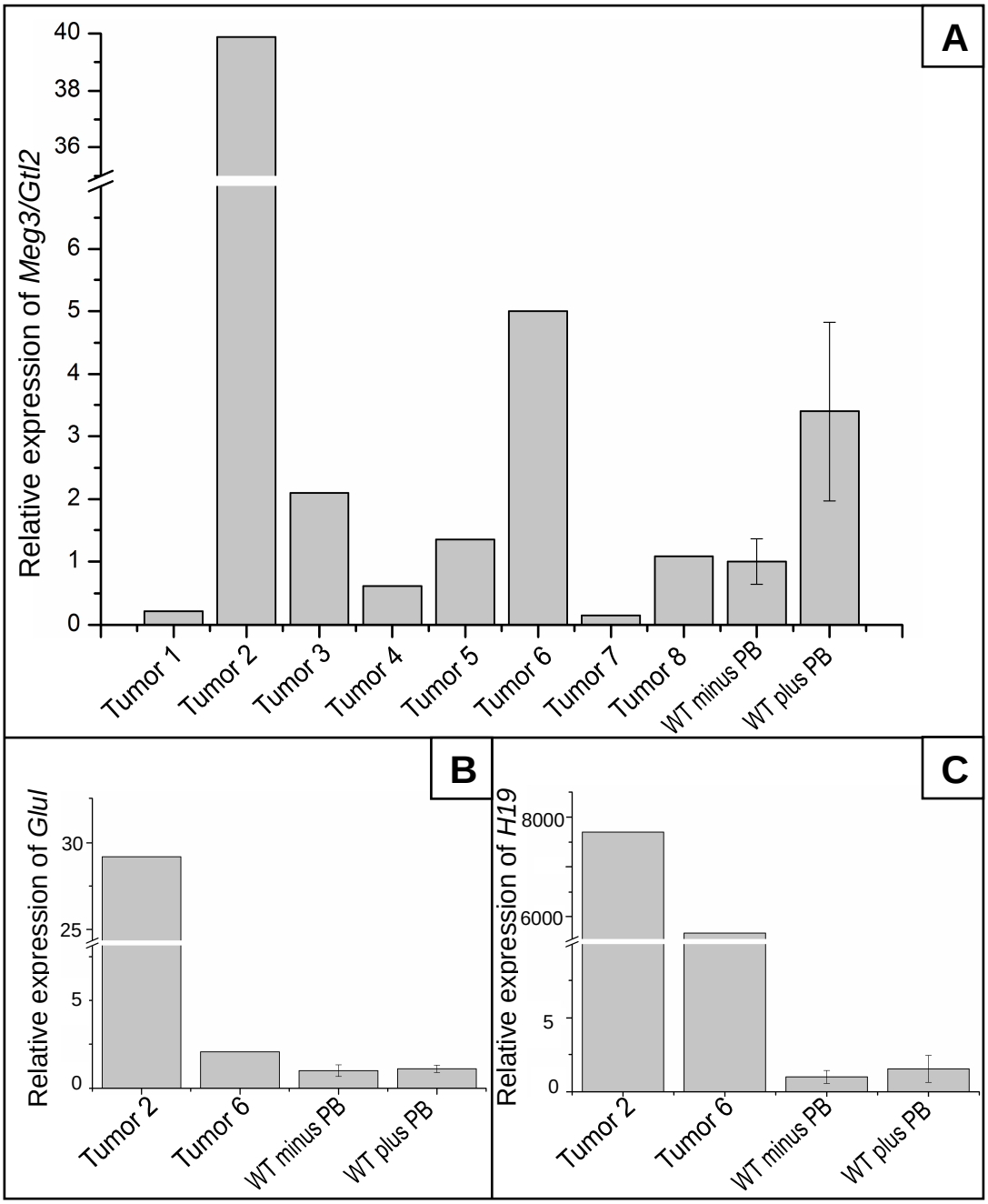

Figure 4.11. A) Relative expression of *Meg3/Gtl2* in individual spontaneous liver tumors isolated from untreated aged mice; B) relative expression of the *Ctnnb1*-mutation marker *Glul* in tumors 2 and 6; C) relative expression of the *Ha-ras*-mutation marker *H19* in tumors 2 and 6. Normal liver from untreated wild-type mice (WT minus PB) and mice treated with PB for 12 weeks (WT plus PB) were used as controls in A), B) and C).
Sample numbers: WT minus PB, WT plus PB = 4 each.

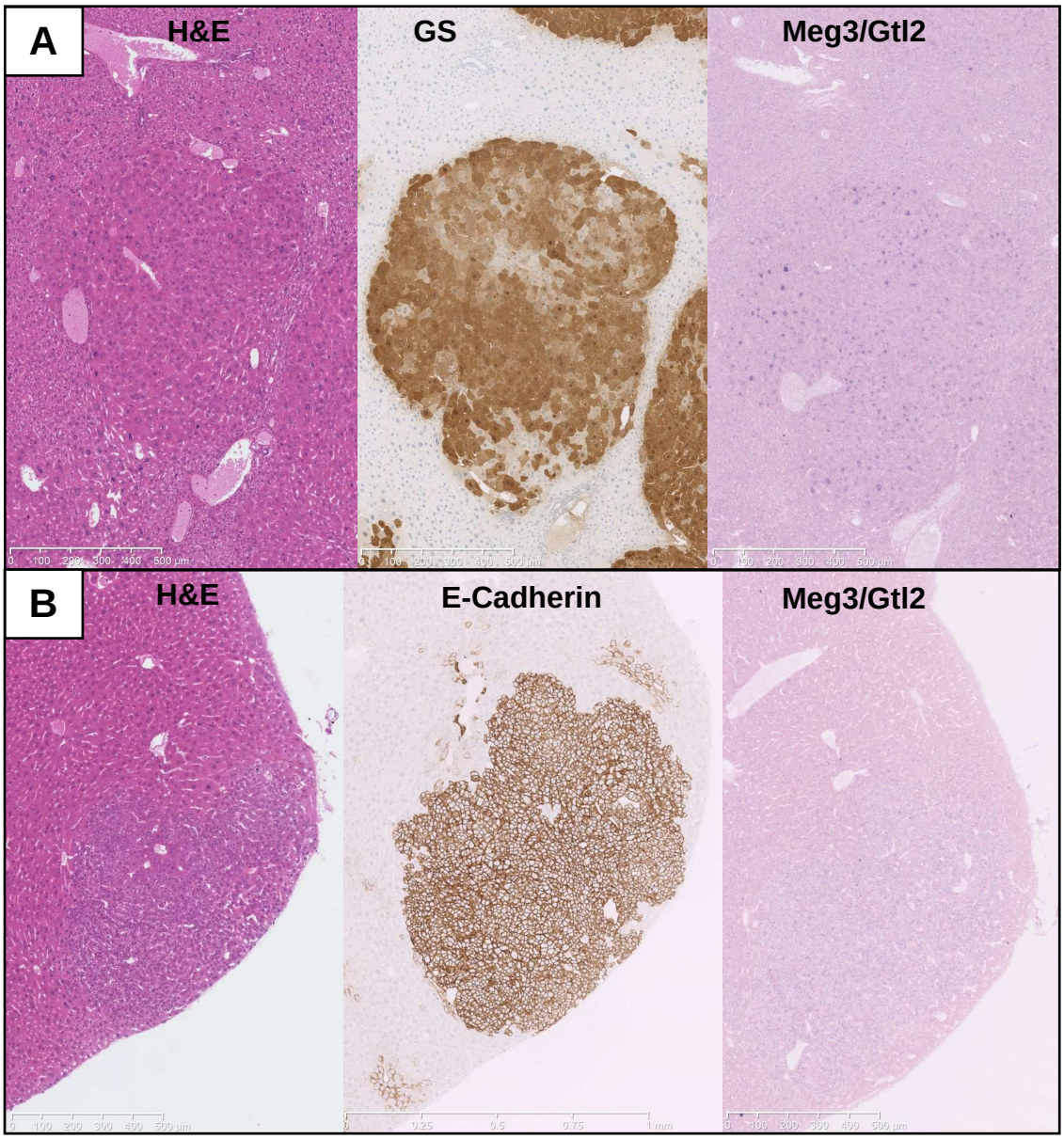

Figure 4.12. Demonstration of *Meg3/Gtl2* transcript via *in situ*-hybridization in A) GS (glutamine synthetase)-positive and B) E-Cadherin-positive tumors (fixed and embedded liver tissue). Abundantly expressed GS and E-Cadherin points to *Ctnnb1*- and *Ha-ras*- or *B-raf*-mutations, respectively. Note that *Meg3/Gtl2* is transcribed in the nuclei of GS- but not of E-Cadherin-positive tumor.

4.4. Determination of 5'-methylation and 5'-hydroxymethylation at cytidine in *Ha-ras*- and *Ctnnb1*-mutated tumors

DNA methylation is probably the most important epigenetic mechanism in mammals, and its role in the formation and treatment of cancer has been extensively studied (for reviews see Ehrlich, 2002; Esteller, 2005; McCabe et al., 2009). 5'-methylcytosine is a well-characterized modification in CpG islands (Ehrlich et al., 1981), and 5'-hydroxmethylcytosine is meanwhile referred to as the sixth DNA base (Kriaucionis et al., 2009; Tahiliani et al., 2009). As phenobarbital has been reported to cause global DNA methylation changes in the mouse liver (Watson et al., 2002; Phillips et al., 2007), the 5'-methylation and 5'-hydroxymethylation status of cytosine in *Ha-ras*- and *Ctnnb1*-mutated tumors was determined via immunohistochemstry to investigate if these modifications could serve as additional markers to stratify the two phenotypes. To this end, sections of fixed and embedded mouse livers bearing both types of tumors were stained with antibodies against 5'-mC and 5'-hmC. The results are summarized in table 4.9 and exemplified in figures 4.13 and 4.14.

Table 4.9. Immunohistochemical characterization of PB-promoted and unpromoted tumors. Overexpression of GS indicates *Ctnnb1*-mutations, overexpression of E-Cadherin indicates *Ha-ras*- or *B-raf*-mutations.

Treatment	Plus DEN, plus PB	Plus DEN, minus PB
Number of animals	4	3
Total tumors	**5**	**2**
GS-positive tumors	5	0
E-Cadherin-positive tumors	0	2
Other tumors	0	0
Tumors with decreased 5'-hmC	**5**	**2**
Tumors with decreased 5'mC	**5**	**2**

In the immunohistochemical specimens, both GS-positive and E-Cadherin-positive tumors showed reduced contents of 5'-mC and 5'-hmC as compared to surrounding non-tumor tissue. The decrease was pronounced to roughly the same extent in both tumors, although macroscopically, it appeared that in some tumors, 5'-mC was marginally less reduced that 5'-hmC, regardless of the mutation status. In the sections from mice which were promoted with PB, a slight zonation of both modifications could be detected, with increased levels of 5'-mC and 5'-hmC around the portal triad and thus directly opposed to the zonation of GS (see figure 4.13).

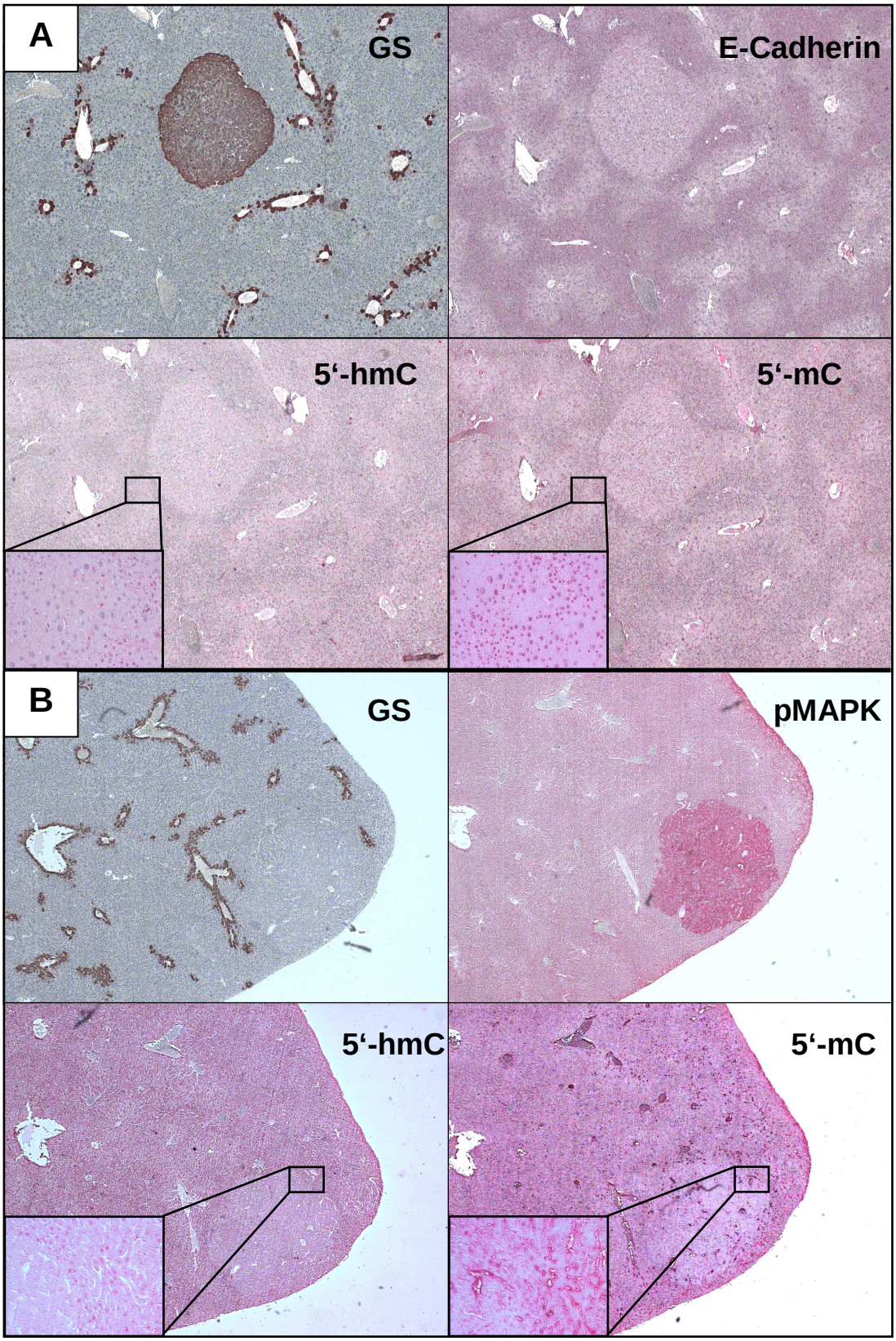

Figure 4.13. Immunohistochemical demonstration of A) GS (glutamine synthetase)-positive and B) pMAPK-positive tumors in serial sections of fixed and embedded liver tissue. Abundantly expressed GS and pMAPK points to *Ctnnb1*- and *Ha-ras*-mutations, respectively. Note the nuclear localization of 5’-mC and 5’-hmC.

4.4.1 5'-methylation and 5'-hydroxymethylation in livers of Connexin32-deficient mice

To further investigate the role of DNA methylation in tumorigenesis, 5'-mC and 5'-hmC levels were determined in tumors from Cx32-knockout mice. From a study which had previously been conducted in our group, livers of mice partly deficient in the gap junction protein connexin32 (Cx32), which is encoded by a gene located on the X-chromosome (Moennikes et al., 2000b), were available. In brief, male *Cx32* knockout mice ($Cx32^{Y/-}$) were crossed with female $Cx32^{+/+}$-mice, which led to a heterozygous *Cx32* genotype (X^+/X^- or X^-/X^+) in the females among the resulting offspring. After initiation with a single dose of DEN, the female offspring developed tumors with three different phenotypes: homogenous *Cx32* expression (48% of all lesions), complete *Cx32*-deficiency (25% of all lesions), and mosaic-like *Cx32* expression patterns with *Cx32*-positive and -negative cells within the same tumor (27% of all lesions). Assuming that in the *Cx32*-negative cells of completely *Cx32*-deficient tumors and those with the mosaic phenotype, the allele expressing *Cx32* is inactivated by cytosine methylation at the 5'-position in the course of tumor formation, one would expect to find increased 5'-mC levels in these cells as compared to *Cx32*-expressing cells. This distribution of 5'-mC-positive cells in the tumors would again result in a mosaic-like pattern, but perfectly opposed to that of *Cx32* expression. To investigate if methylation changes are responsible for the patchy *Cx32*-phenotype, sections of fixed and embedded mouse livers bearing tumors were stained with antibodies against 5'-mC and 5'-hmC, as well as GS and E-Cadherin as indicators for the tumors' mutation status. Cx32-stainings were carried out with an antibody in sections of frozen tissue from the same animals but different liver lobes. The results are summarized in table 4.10 and exemplified for the patchy phenotype in figure 4.14.

Table 4.10. Immunohistochemical analysis of female $Cx32^{+/-}$ mice, harboring the patchy Cx32-phenotype. Overexpression of GS indicates *Ctnnb1*-mutations, overexpression of E-Cadherin indicates *Ha-ras*- or *B-raf*-mutations.

Treatment	Plus DEN
Number of animals	4
Total tumors	**23**
GS-positive tumors	0
E-Cadherin-positive tumors	23
Tumors with decreased 5'-hmC	**23**
Tumors with decreased 5'-mC	**23**

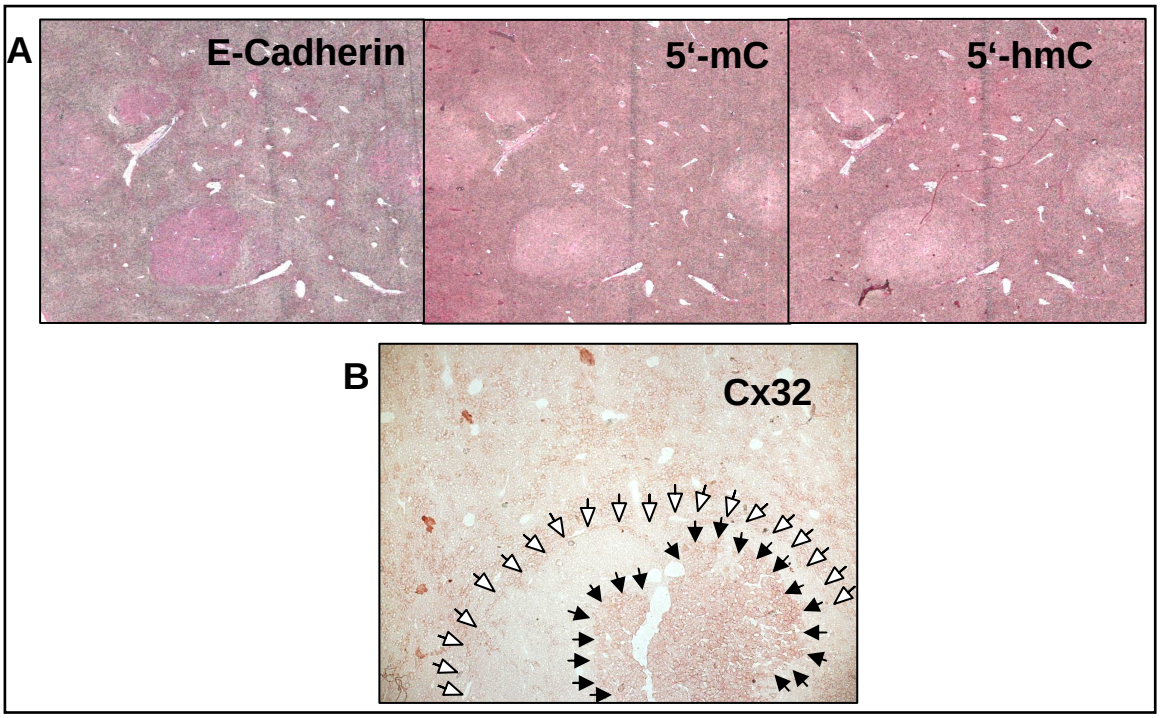

Figure 4.14. (A) Immunohistochemical demonstration of E-Cadherin, 5'-mC and 5'-hmC in liver tumors of female *Cx32*$^{+/-}$ mice. Stainings were carried out in parallel sections of fixed and embedded liver tissue. (B) Immunohistochemical demonstration of the patchy *Cx32*-phenotype in frozen tissue from the same animal but a different liver lobe. Open arrows indicate the tumor boundary. Closed arrows point towards the *Cx32*-positive area within the tumor.

In all tumors of the female Cx32$^{+/-}$ mice investigated, the content of 5'-hmC and 5'-mC was homogenously reduced as compared to surrounding non-tumor tissue, and no patchy distribution was observed.

5. Discussion

Activation of the *Ha-ras* or *Ctnnb1* proto-oncogenes results in characteristically different molecular programs which manifest themselves in tumor-specific changes on several levels, including gene expression, protein expression and modification and miRNA expression, as well as epigenetic alterations in the form of DNA methylation. As *Ctnnb1*-mutated cells are selected for by PB and no established short-term assays exist to assess the contribution of tumor promoters to carcinogenesis, the molecular stratification of tumors induced by different treatments bears a potential for predictive biomarker identification and is thus highly relevant. The present doctoral thesis comprised three projects, all of which aimed at identifying molecular markers that would allow for stratification of *Ha-ras*- and *Ctnnb1*-mutated tumors in the mouse model. In project 1, four datasets assessing mRNA expression, miRNA expression, DNA methylation and protein expression/phosphorylation obtained from the two tumor types were globally analyzed and compared. Furthermore, the datasets were integrated using a new bioinformatic tool with a focus on signaling cascades and metabolism. Project 2 aimed at characterizing the role of the lncRNA *Meg3/Gtl2*, which is a transcript encoded on the imprinted *Dlk1-Dio3* gene cluster. Since a correlation between *Meg3/Gtl2* expression and PB-treatment had previously been observed in the rodent liver, a potential role of the lncRNA in PB-mediated tumor promotion was investigated. To this end, expression of *Meg3/Gtl2* was measured and localization of the *Meg3/Gtl2* transcript was examined in *Ha-ras*- and *Ctnnb1*-mutated tumor tissue. The goal of project 3 was to elucidate whether the two tumor types differ with regards to DNA methylation. Using immunohistochemical techniques, their methylation and hydroxymethylation status at the 5'-position of cytidine (5'-mC and 5'-hmC) was determined and compared. To further examine the role of DNA methylation in tumorigenesis, it was investigated if changes in 5'-mC and 5'-hmC correlate with the observed reactivation of Cx32 in a subpopulation of tumor cells in livers from Cx32-knockout mice.

5.1 Global integrated molecular profiling of *Ha-ras*- and *Ctnnb1*-mutated tumors

The reverse phase protein microarray data presented in this thesis are a substantial supplement to the previous finding that signaling pathways regulated by Ras or Wnt were differently perturbed in *Ha-ras*- or *Ctnnb1*-mutated tumors at the mRNA level (Stahl et al., 2005a). A key characteristic of *Ha-ras*-mutated tumors is constitutive activation of MAPK signaling, and accordingly, the main kinases mediating downstream effects of Ha-ras were activated in these lesions, whereas they were unchanged or down-regulated in *Ctnnb1*-mutated tumors

(figure 4.6). Expectedly, mRNAs of the prominent Ras-target genes *Jun* and *Fos* were unchanged in *Ctnnb1*-mutated but up-regulated in *Ha-ras*-mutated tumors. Activating phosphorylation of the two proteins Stat3 (S727) and Rsk1 (T573), which act as mediators of Ras signaling, was specifically detected in *Ha-ras*- but not in *Ctnnb1*-mutated tumors (figure 4.6). In this context, a recent work by Yeh et al. has shown that phosphorylation of Stat3 at S727 mediated by Ha-ras enhances the oncogenic potential of cancer cells in culture (Yeh et al., 2009). Both tumor types investigated in the present thesis showed increased mRNA levels of one Dusp isoform: *Dusp14* in *Ctnnb1*-mutated and *Dusp6* in *Ha-ras*-mutated tumors, with the p-value for *Dusp14* expression only slightly higher than the required significance cutoff. In *Ctnnb1*-mutated tumors, the up-regulation of *Dusp14* could be explained by the activation of Ras-inhibitory mechanisms by Wnt signaling (Zeller et al., 2012). The up-regulation of *Dusp6* in *Ha-ras*-mutated tumors on the other hand indicates a feedback loop negatively regulating MAPK signaling in these lesions (Camps et al., 2000; Zhang et al., 2010). Similarly, the increased mRNA levels of the Wnt-interfering genes *Wif1* and *Nlk* (Stahl et al., 2005a), point to a negative feedback mechanism in *Ctnnb1*-mutated cells. Together with these findings, the increase of phosphorylated and thus inactivated β-Catenin and of catalytically active GSK3β in *Ha-ras*-mutated tumors, as well as the down-regulation of activating Braf kinase phosphorylation in *Ctnnb1*-mutated tumors underline that MAPK and Wnt signaling function antagonistically in HCC.

The integration of different “omics” datasets using the InCroMAP tool is a powerful approach to gain new insights into the regulation of tumor metabolism at transcriptional, translational and epigenetic levels. Global mRNA profiling of *Ctnnb1*- and *Ha-ras*-mutated tumors has already been conducted in the past (Stahl et al., 2005a), but the data analyzed in the course of the present doctoral thesis are substantially stronger as they were generated using more *Ctnnb1*-mutated tumor samples (7 instead of 3) and more appropriate control tissues. The use of adjacent non-tumor samples from PB-promoted and unpromoted mice as controls for the respective tumors allowed for the distinction between treatment effects caused by DEN alone or in combination with PB and dysregulations specifically taking place in the tumors. Moreover, this thesis presents entirely new data on DNA methylation, as well as miRNA and protein expression.

A variety of pathways were perturbed in both tumor types, as could be shown by pathway-specific enrichment of dysregulated mRNAs and miRNAs. Most notably, metabolism of nitrogen and a number of amino acids was altered at the mRNA level in *Ctnnb1*-mutated

tumors as compared to control tissue, consistently with previous results (Stahl et al., 2005a; Stahl et al., 2005b). In *Ha-ras*-mutated tumors, mRNAs coding for proteins with a role in lipid and bile acid metabolizing pathways were among those changed most in expression. The reader must bear in mind that pathway enrichments are generalizations in that genes or other regulatory molecules often have far-reaching effects in a large number of processes in the cell. Therefore, annotation to a specific pathway always harbors the risk of producing a huge amount of superficial information and is no replacement for detailed analysis of every single enriched molecule. Nevertheless, as to analyzing large microarray-based datasets, pathway enrichment analysis is extremely useful in providing a global overview of the processes perturbed in the examined tissue.

Comparison of the mRNA expression data presented in this thesis with the results of deep-sequencing of chromatin-immunoprecipitation products conducted by Torre et al. (2013, manuscript in preparation) revealed that a number of genes encoding metabolic enzymes altered in mRNA expression in the *Ctnnb1*-mutated tumors are direct targets of the β-Catenin/TCF4 transcription factor complex (table 4.7). Generally, fundamental metabolic changes were found upon analysis of the mRNA data in the course of the present study (figure 4.7). Together with the frequent observation that glucose-6-phosphatase activity is reduced in liver tumors at the enzyme level, the decreased mRNA expression of phosphoenolpyruvate carboxykinase (*Pck1*) in *Ctnnb1*-mutated tumors and of glucose-6-phosphatase (*G6pc*) in *Ha-ras*-mutated tumors indicates a global down-regulation of gluconeogenesis in both tumor types. This is supported by the fact that the rate-limiting enzyme of glycogen synthesis in the cytosol, glycogen synthase (*Gys2*), was unchanged in both tumors at the mRNA level. Consistently with the observed reduction of gluconeogenesis in *Ctnnb1*-mutated tumors, Chafey and colleagues have identified several gluconeogenic genes as negatively regulated by Wnt signaling in mouse liver (Chafey et al., 2009). In the *Ha-ras*-mutated tumors investigated in the present thesis, a substantial decrease in glycogen storage could be detected via periodic acid-Schiff staining (figure 5.1A), another indication for lowered gluconeogenesis rates. A mechanism for the inhibition of glucose synthesis from pyruvate recently demonstrated in human HCCs (Wang et al., 2012a) could also be identified in *Ha-ras*-mutated mouse tumors via integration of mRNA, miRNA and protein data (figure 5.1B): Stat3, which was activated in these lesions, blocks translation of the *G6pc* transcript by inducing the expression of miR-23a, which was increased by a log-ratio of 1.08 and only closely missed the significance cutoff with a p-value of 0.63. As *G6pc* mRNA is a target transcript of miR-23a, its conversion into a functional enzyme is inhibited, which is in accordance with the previously described

observations. As mentioned above, loss of mRNA expression and enzyme activity of glucose-6-phosphatase is a common yet poorly understood feature of many liver tumors, and these interactions between protein, miRNA and mRNA provide possible mechanisms in *Ha-ras*-mutated tumors. However, miR-23a could only be found to be up-regulated in *Ha-ras*-mutated tumors, which indicates that alternative mechanisms exist in *Ctnnb1*-mutated lesions.

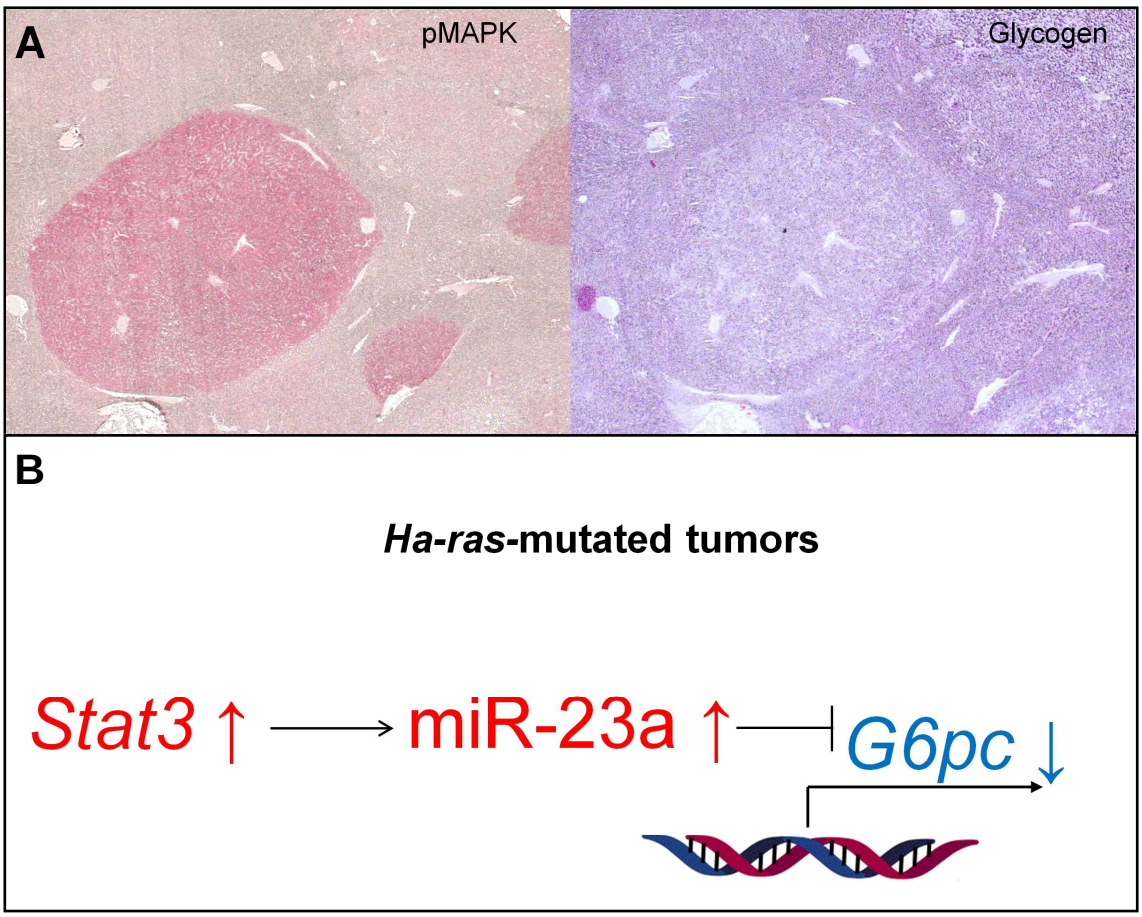

Figure 5.1. A) Histochemical demonstration of glycogen in a pMAPK-positive, *Ha-ras*-mutated tumor via periodic acid-Schiff-staining. B) Proposed mechanism for down-regulation of *G6pc* transcription in *Ha-ras*-mutated tumors via Stat3 and miRNA 23a.

Transcription of genes involved in the central metabolic processes of amino acid degradation, urea cycle and gluconeogenesis is zonated in normal liver, where it mainly takes place in periportal hepatocytes (Gebhardt, 1992). The list of negative β-Catenin target genes in table 4.7, all of which play a role in the mentioned metabolic pathways, is thus consistent with the observation that *Ctnnb1*-mutated tumor tissue corresponds to the perivenous phenotype and periportal gene expression is inhibited in these tumors, whereas the periportal phenotype is stimulated in *Ha-ras*-mutated tumors (Braeuning et al., 2007a).

In *Ha-ras*-mutated tumors, expression of the mRNAs encoding the two key enzymes of cholesterol biosynthesis, *Hmgcs1* and *Hmgcr*, was significantly increased, and expression of

Hmgcs1 was elevated also in *Ctnnb1*-mutated tumors (figure 4.7). At the protein level, Hmgcs1 could neither be detected by immunohistochemical staining nor by Western Blot using commercially available antibodies. However, two previously conducted studies confirm the up-regulation of *Hmgcs1* in *Ha-ras*-mutated tumors versus normal liver at the mRNA level (Stahl et al., 2005a; Jaworski et al., 2007). *Ha-ras*- and *Ctnnb1*-mutated tumors differed with regards to mRNA expression of the gene encoding the key enzyme of bile acid biosynthesis, Cyp7a1, which was up-regulated at the mRNA level in *Ctnnb1*-mutated (figure 5.3.B) and transcriptionally down-regulated in *Ha-ras*-mutated tumors. Accordingly, accumulation of cholesterol in *Ha-ras*-mutated but not in *Ctnnb1*-mutated mouse liver tumors has been shown previously by our group (Jaworski et al., 2007). These findings indicate that usage of cholesterol for bile acid synthesis is regulated differently in *Ha-ras*- and *Ctnnb1*-mutated tumors (figure 5.3). Strikingly, most mRNAs encoding proteins involved in bile acid biosynthesis were down-regulated in *Ha-ras*-mutated tumors, except for *Cyp39a1*, which was increased in transcription (table 5.1). In addition to the present study, these results were found consistently in two other experiments of our group (Stahl et al., 2005a; Jaworski et al., 2007). Previous mRNA expression measurements showed that *Cyp39a1* transcription is repressed in perivenous as compared to periportal hepatocytes (Braeuning et al., 2006). As *Ha-ras*-mutated tumors show a periportal phenotype, this is in consistence with the selective up-regulation of Cyp39a1 in these tumors. In *Ctnnb1*-mutated tumors, mRNAs coding for enzymes of bile acid synthesis were largely unchanged in the present study and the study conducted by Stahl et al. (Stahl et al., 2005a), with the exception of the key enzyme Cyp7a1 (figure 4.7, table 5.1), as well as Cyp46a1 and Cyp8b1 (table 5.1). The fact that bile acid biosynthesis is significantly down-regulated at the mRNA level in *Ha-ras*-mutated tumors corresponds to the observed storage of cholesterol in these lesions (Jaworski et al., 2007).

Table 5.1. Significantly dysregulated mRNAs involved in bile acid biosynthesis. Study 1 = Stahl et al., 2005a; study 2 = Jaworski et al., 2007; pv vs. pp = perivenous versus periportal hepatocytes (Braeuning et al., 2006). For scheme of bile acid biosynthesis see figure 5.2.

Enzyme name	Gene symbol	Enzyme code	*Ha-ras*-mutated tumor			pv vs. pp	*Ctnnb1*-mutated tumor	
			Study 1	Study 2	Present study		Study 1	Present study
cytochrome P450, family 7, subfamily a, polypeptide 1	Cyp7a1	1.14.15.6	**-6.74**	**-3.23**	**-3.21; -3.13**	**3.42**	**-**	**2.36; 1.62**
cytochrome P450, family 46, subfamily a, polypeptide 1	Cyp46a1	1.14.13.30	**-3.74**	**-2.33**	**-3.30**	-	**-2.92**	**-3.32**
cytochrome P450, family 27, subfamily a, polypeptide 1	Cyp27a1	4.2.1.92	**-3.42**	**-2.60**	**-2.47**	-	-	**-**
cytochrome P450, family 39, subfamily a, polypeptide 1	Cyp39a1	4.2.1.92	**1.59**	**5.09**	**2.28**	**-2.38**	-	-
cytochrome P450, family 7, subfamily b, polypeptide 1	Cyp7b1	1.14.13.30	**-6.18; -6.36**	**-4.39; -6.01**	**-3.68; -3.72**	-	-	-
hydroxy-delta-5-steroid dehydrogenase, 3 beta- and steroid delta-isomerase 7	Hsd3b7	5.1.3.3	-	**-1.67**	**-1.18**	-	-	-
cytochrome P450, family 8, subfamily b, polypeptide 1	Cyp8b1	1.14.15.4	**-5.74**	**-5.20**	**-3.57**	-	-	**-1.20**
aldo-keto reductase family 1, member D1	Akr1d1	1.3.99.6	**-3.49; -1.88**	**-1.72; -1.88**	**-1.22; -1.10**	-	-	-
solute carrier family 27 (fatty acid transporter), member 5, bile acyl CoA synthase	Slc27a5	6.3.2.20	**-1.19**	**-1.16**	**-1.09**	-	**-**	-

Hmgcs1 and *Hmgcr* are known target genes of the transcription factor EGR1 (early growth response protein 1) (Gokey et al., 2011). In *Ha-ras*-mutated tumors in the present study, Egr1 mRNA was found up-regulated, and increased levels of the protein were detected immunohistochemically in the tumors but not in adjacent non-tumor tissue (figure 5.3B). On its part, Egr1 mRNA expression is induced by SRF (serum response factor) and other transcription factors which act as downstream mediators of MAPK signaling and bind to a serum response element in the promoter region of the *Egr1* gene (Qureshi et al., 1991; Gregg et al., 2011; Gregg et al., 2012). This is consistent with the detected increase of activated MAPK protein and up-regulated *Egr1* mRNA expression in *Ha-ras*-mutated tumors, and, consequently, explains the increase of Hmgcs at the mRNA level in this tumor type.

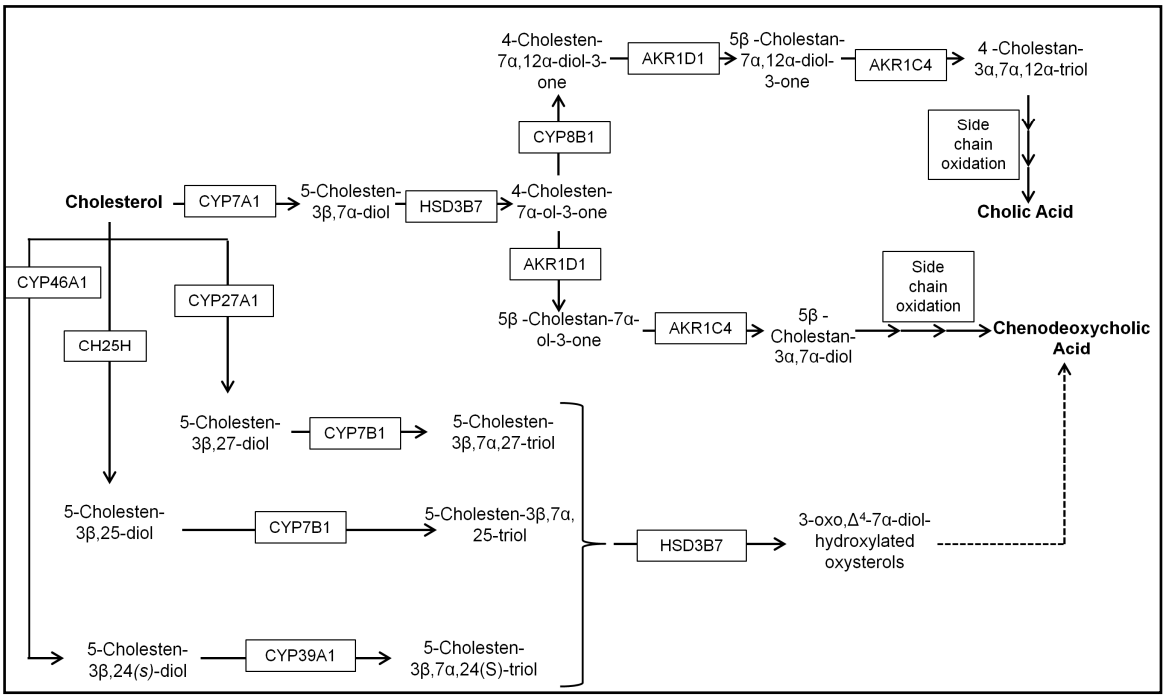

Figure 5.2. Schematic demonstration of bile acid synthesis from cholesterol (modified from Schwarz, 2004).

Several observations support the idea that the *Cyp7a1* gene is regulated by β-Catenin. Comparison of *Cyp7a1* mRNA levels in wild-type mouse liver and liver tissue from mice harboring a *Ctnnb1*-knockout (Rignall et al., 2010) shows significantly decreased *Cyp7a1* expression in the knockout (log-ratio = -1.25). Furthermore, *Cyp7a1* is a pericentrally expressed gene (figure 1.2), and accordingly, its mRNA expression was up-regulated by a log-ratio of 3.42 in enriched populations of pericentral as compared to periportal hepatocytes (figure 5.3B; Braeuning et al., 2006). Pericentral gene expression patterns are maintained in *Ctnnb1*-mutated tumors, which is consistent with the up-regulation of *Cyp7a1* in these lesions in the present study. Interaction between the transcription factor HNF4 and Wnt-signaling has recently been shown to regulate zonal gene expression in liver (Colletti et al., 2009). In that work, it was shown that expression of the model pericentral gene *Cyp1a1* was induced by joint binding of the HNF4 and TCF-4 transcription factors in the gene's promoter region upon activation of Wnt-signaling. In the present study, bioinformatic analysis of the *Cyp7a1* gene promoter using the ModuleMaster tool (Wrzodek et al., 2010) revealed binding sites for HNF4 and TCF-4 in close proximity to one another, about 240 bp and 150 bp upstream of the transcription start site, respectively. To confirm the theory that *Cyp7a1* transcription is directly activated by β-Catenin, mRNA levels of *Cyp7a1* were determined by qPCR measurements in cultured 70.4 and 53.2b hepatoma cells which had been treated with LiCl to

stimulate β-Catenin. It was not possible to detect *Cyp7a1* mRNA in cell culture at all (data not shown). However, the presence of a TCF binding site in the promoter and the fact that *Cyp7a1* transcription is decreased in murine *Ctnnb1*-knockout liver tissue strongly indicate a regulatory function of β-Catenin.

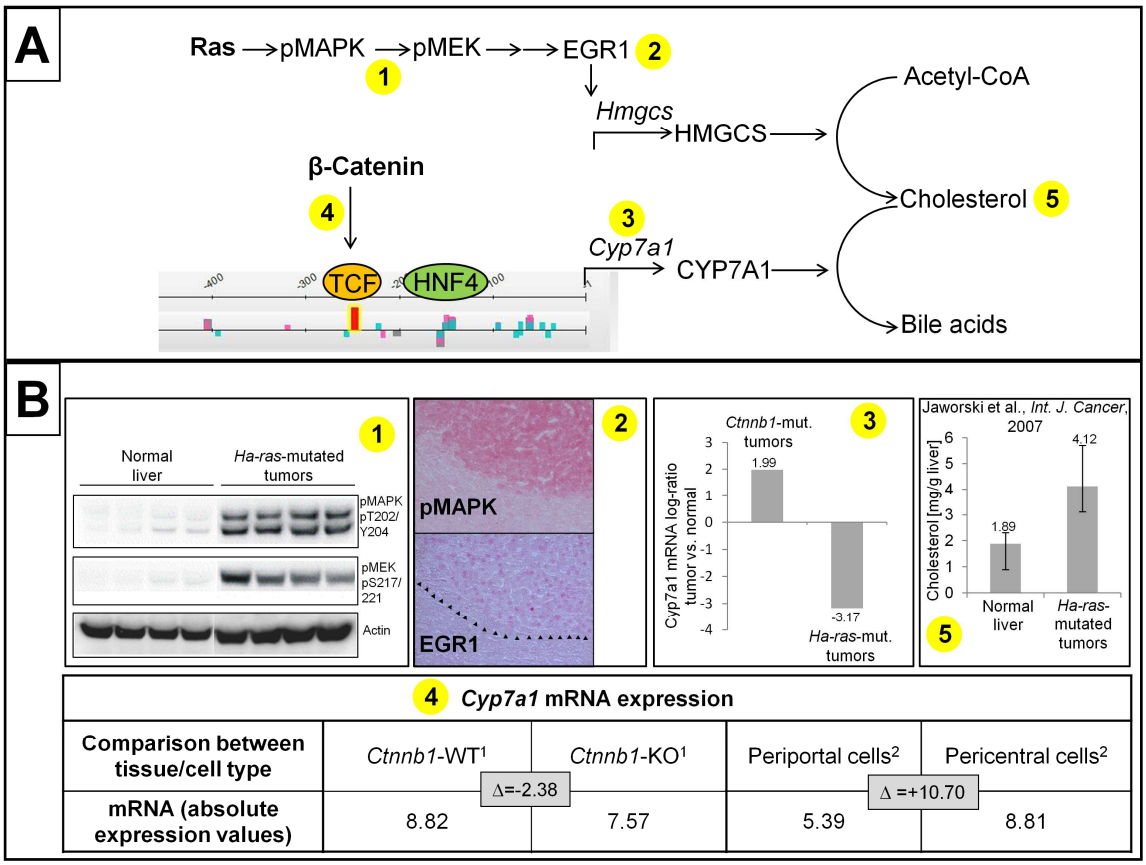

Figure 5.3. A) Demonstration of cholesterol synthesis in *Ha-ras*-mutated tumors by integration of mRNA, protein and metabolite data. mRNAs are written in italics, proteins in regular capitals. B) (1) Detection of pMAPK and pMEK in *Ha-ras*-mutated tumors via Western Blot; (2) Immunohistochemical demonstration of transcription factor EGR1 in pMAPK-positive (*Ha-ras*-mutated tumors); (3) *Cyp7a1* mRNA expression in *Ctnnb1*- and *Ha-ras*-mutated tumors; (4) absolute *Cyp7a1* mRNA expression values in *Ctnnb1*-wildtype and knockout tissue, as well as in periportal and perivenous hepatocytes; (5) Cholesterol levels in Ha-ras-mutated tumors and normal liver, obtained from Jaworski et al., 2007.
[1]…data obtained from Rignall et al., 2010
[2]…data obtained from Braeuning et al., 2006

An interaction between MAPK-signaling and Cyp7a1 transcription has previously been proposed (De Fabiani et al., 2001). In this model, *Cyp7a1* transcription is subject to feedback regulation, whereby bile acids lead to activation of the MAP-kinase Jun. Jun then activates transcription of the nuclear receptor SHP (small heterodimer partner), which represses *Cyp7a1* transcription. Activation of Jun via phosphorylation was detected in *Ha-ras*-mutated tumors in a previous study conducted in our group (Thomas Knorpp, University of Tübingen, unpublished data). However, no dysregulation of the potential downstream effectors in the model mentioned above could be detected in the present study. Thus, a MAPK-stimulatory

feedback mechanism mediated by bile acids does not provide sufficient molecular explanation for the down-regulation of *Cyp7a1* in *Ha-ras*-mutated tumors.

The sodium/bile acid cotransporter Slc10a1 (solute carrier 10 familiy member 1), which mediates the reabsorption of bile acids into hepatocytes via the basolateral membrane was down-regulated at the mRNA level in *Ha-ras*-mutated tumors (figure 4.7). As bile salts have previously been reported to activate MAPK signaling (Kurz et al., 2000), this might indicate another negative feedback mechanism in these lesions. Acetyl-CoA is the precursor of cholesterol biosynthesis and provided in the cytosol in the form of citrate subtracted from the TCA cycle via the citrate-pyruvate shuttle system in the mitochondrial membrane (figure 4.7). Since citrate synthase is slightly down-regulated at the mRNA level in the *Ha-ras*-mutated tumors, the question arises if in this case acetyl-CoA is really obtained from the mitochondria. To definitely clarify this, one would have to collect and analyze enzyme activity data for citrate synthase, ATP citrate lyase, which catalyzes the formation of Acetyl-CoA from citrate, as well as the carriers involved in the mitochondrial shuttle system. The abundant synthesis of cholesterol on the one hand and the lack of "drainage" into bile acid synthesis on the other leads to the observed accumulation in the cell, where it can be used as a precursor for the biosynthesis of cellular structures, such as membranes. Furthermore, several tumors are dependent on the presence of isoprenoids (Gibbs et al., 1997; Larner et al., 1998), which are formed as intermediates in the pathway leading to cholesterol, the mevalonate pathway, and are used for prenylation of proteins. Interactions between cholesterol metabolism and Ras, which itself is anchored in the cell membrane with, among others, a prenyl anchor, have been described previously (Shack et al., 1999; Clendening et al., 2010). The observations made in the course of the present study indicate that by up-regulation of *Hmgcs* and *Hmgcr Ha-ras*-mutated tumors are provided with a selective proliferation advantage. The potential use of statins, which inhibit the major regulatory step in cholesterol biosynthesis catalyzed by Hmgcr, as chemotherapeutics is currently a prominent topic of research and has been so for several years (Lonardo et al., 2012). The data shown in the present thesis corroborate that this approach is promising for *Ha-ras*-mutated but not for *Ctnnb1*-mutated tumors. The fact that cholesterol production is increased in *Ha-ras*-mutated but not in *Ctnnb1*-mutated tumors shows that the metabolic adaptations contributing to a tumor cell's growth advantage can be very diverse. All in all, this underlines the fundamental differences between the two types of lesions analyzed here.

In the beginning of the 20th century, Otto Warburg postulated that, regardless of oxygen supply, proliferating tumor cells would metabolize glucose via conversion to lactate and subsequent anaerobic fermentation, rather than generating pyruvate, which feeds into the TCA cycle and oxidative phosphorylation in the mitochondria (Warburg, 1956). This theory is commonly known as the Warburg Hypothesis and attributes the metabolic shift observed in tumors to mitochondrial dysfunction. In neither of the two tumor types analyzed in the course of this thesis, the mRNA levels of the enzyme catalyzing the conversion of pyruvate into lactate, lactate dehydrogenase (*Ldh*), was significantly changed. While the mRNA levels of two key enzymes of the TCA cycle, isocitrate dehydrogenase (*Idh3a*) and citrate synthase (*Cs*), were slightly decreased in *Ha-ras*-mutated lesions, transcriptional up-regulation of these two genes was observed in *Ctnnb1*-mutated tumors. Contrary to Warburg's hypothesis, the latter finding rather points to oxidative glucose metabolism than to lactate fermentation in *Ctnnb1*-mutated lesions. At the protein and metabolite level, these results are supported by a recent report by Yuneva and colleagues who conducted metabolic profiling of MET-induced mouse liver tumors which contain activated β-Catenin, similar to the system investigated in the present thesis. They were unable to detect elevated lactate levels in these tumors, despite an increase in enzyme activity of lactate dehydrogenase (Yuneva et al., 2012). Furthermore, it was recently shown that Ldh enzyme activity is increased in mice harboring a liver-specific APC-knockout, which results in constitutive activation of β-Catenin (Chafey et al., 2009). Overall, these observations indicate that *Ctnnb1*-mutated prefer the energetically more efficient pathway of oxidative phosphorylation for glucose catabolism to lactate fermentation, while *Ha-ras*-mutated cells, showing a repression of the TCA cycle and the respiratory chain, carry out glycolysis in the cytosol only, without involving the mitochondria. Do these observations allow the conclusion that *Ctnnb1*-mutated tumors function contrary to the Warburg Hypothesis? As a matter of fact, our current knowledge demands that Warburg's model be viewed in a more differentiated manner, looking beyond the aspect of efficiency of ATP production. In most tumors, the functionality of mitochondria is not impaired but, on the contrary, essential for highly proliferating cells (Schulze et al., 2012; Ward et al., 2012). They require an enormous amount of biomolecules and depend on the mitochondria as key biosynthesis organelles. The present study indicates that *Ha-ras*- and *Ctnnb1*-mutated tumors have developed very different strategies to meet these requirements. *Ha-ras*-mutated tumors carried out massive cholesterol synthesis (figure 5.3), they increasingly produced glycine and serine as C1 and C3 components for further biosyntheses and, finally, they degraded glutamine via kidney-type glutaminase (*Gls*), while the mRNA levels of glutamine synthetase

(*Glul*) were down-regulated. Glutamine could fulfill the function of a key energy source, as ATP is gained from the oxidation of its degradation product α-ketoglutarate in the mitochondria. It could also play an important role in the tumor's defense against oxidative stress by being deaminated to glutamate, which is part of the antioxidative tripeptide glutathione. Furthermore, glutamine is required for a number of biosyntheses, including that of purines. With the transcriptional down-regulation of glutamine synthesis (*Glul*) and up-regulation of its degradation (*Gls*), the question arises as to where glutamine is obtained from in the first place. The liver's main glutamine transporter Slc38a1 was unchanged at the mRNA level, so it remains unclear if the tumor still withdraws glutamine from the blood stream, if the transporter is activated at the protein level, or if the tumor receives glutamine via some other mechanism, such as protein degradation. *Ctnnb1*-mutated tumors differed from their *Ha-ras*-mutated counterparts in that they showed elevated mRNA levels of enzymes forming TCA-cycle intermediates from glucose and excessively synthesized glutamine. The fact that bile acid biosynthesis from cholesterol was increased in the *Ctnnb1*-mutated tumors (*Cyp7a1*) indicates that, in contrast to the *Ha-ras*-mutated ones, excessive storage of cholesterol does not result in a specific proliferation advantage for these tumor cells. Both tumor types investigated in this study showed lowered mRNA levels of genes encoding some key enzymes of amino acid degradation. Accordingly, some mRNAs of genes involved in the urea cycle, where amino acid-derived ammonia is detoxified, were down-regulated. This could be a sign of increased protein synthesis, which would make perfect sense for proliferating cells.

The results discussed here underline that the Warburg Hypothesis as such is a too simplistic model to describe the energetic and metabolic adaptations a cell undergoes in the course of transformation. According to this model, most tumor cells, regardless of their genetic modification or phenotype, reprogram their metabolism to follow one specific route with the priority objective of maximizing ATP-production. The comparison between *Ctnnb1*- and *Ha-ras*-mutated mouse liver tumors provides evidence that cancer cells in fact develop very diverse metabolic strategies, not all of which exclude oxidative glucose metabolism in the mitochondria. Whether the metabolic alterations are a transcriptional consequence of changes in upstream signaling or in fact an initial feature selected for during tumorigenesis is unclear. There is currently an ever-growing body of evidence for a direct interaction between signaling proteins and metabolism, without transcriptional mechanisms being activated (Ward et al., 2012). However, as exemplified for cholesterol synthesis in *Ha-ras*-mutated tumors (figure 5.3), regulation of gene expression by transcription factors is still a valid mechanism. In

conclusion, the results of data set-spanning analysis and comparison of the two tumor types emphasize that altered metabolism is a mutation-specific fingerprint of tumor cells.

5.2 The role of the imprinted *Dlk1-Dio3*-Cluster in the formation of *Ha-ras*- and *Ctnnb1*-mutated tumors

The relevance of epigenetic mechanisms such as genomic imprinting, histone modification or ncRNAs during carcinogenesis is commonly recognized, although their effects appear to be more complex than originally thought. While miRNA-mediated regulation of gene expression is well-established, the function and mechanism of lncRNAs remains enigmatic. The imprinted *Dlk1-Dio3* gene cluster plays a pivotal role in developmental processes (Kagami et al., 2008) and encodes a number of protein-coding RNAs, miRNAs and lncRNAs, the latter including *Meg3/Gtl2*. A connection between *Meg3/Gtl2* and carcinogenesis has been observed in a number of tumor cells and tissues from different species (Zhou et al., 2007; Anwar et al., 2012; Wang et al., 2012b; Ying et al., 2013), but the reported findings are in part inconsistent and have so far failed to present a mechanism for this lncRNA. One of the goals of the present thesis was to investigate a potential function of *Meg3/Gtl2* as a biomarker for PB-promoted tumors.

A recent study conducted in cooperation with the Novartis Institutes for Biomedical Research in Basel has shown that *Meg3/Gtl2* is expressed in the GS-positive, hypertrophic hepatocytes surrounding the central vein in normal mouse liver tissue treated with PB (Lempiainen et al., 2013). Together with the observation that the induction of *Meg3/Gtl2* and other cluster ncRNAs is genetically dependent on CAR and β-Catenin, these findings provide strong evidence of a potential role of this locus in PB-promoted tumor formation. This is corroborated by the specific increase in *Meg3/Gtl2* expression in *Ctnnb1*- but not *Ha-ras*-mutated mouse liver tumors, demonstrated on the basis of qPCR measurements and histochemical experiments in this work (figures 4.8 and 4.12). A potential link between *Meg3/Gtl2* and β-Catenin is further emphasized by transcriptional induction of the gene in APC knockout tissue where β-Catenin is constitutively active (figure 4.9). Interestingly, PB had a very similar effect on *Meg3/Gtl2* expression in the liver of transgenic mice lacking the major gap junction protein Cx32 and wild-type mice, leading to a moderate but significant increase of expression. This was unexpected in the light of the outcome of an initiation-promotion experiment with Cx32 knockout mice previously conducted in our group, which showed that Cx32 is essential for liver tumor promotion by PB (Moennikes et al., 2000a). The

results of both experiments allow the conclusion that for PB-mediated transactivation of *Meg3/Gtl2*, CAR and β-Catenin but not Cx32 is required. Furthermore, if the *Meg3/Gtl2* transcript is a mediator of PB in the course of tumor formation in the mouse liver, its effects are dependent on the presence of functional Cx32 and cannot circumvent gap junctional intercellular communication.

In normal mouse liver, the up-regulation of *Meg3/Gtl2* is completely reversible when PB-treatment is abandoned (Lempiainen et al., 2013). However, in tumors which were promoted with PB for 25 weeks and then proliferated for another 25 weeks in the absence of PB before they were isolated, the levels of *Meg3/Gtl2* remained increased as compared to untreated and PB-treated normal liver (figure 4.10). Interestingly, this was the case both in *Ctnnb1*- and *Ha-ras*-mutated tumors, while *Ha-ras*-mutated tumors that had formed in non-PB-treated animals showed no induction of *Meg3/Gtl2* (figure 4.8). Under the assumption that PB-treatment stimulates the outgrowth of *Ctnnb1*-mutated and inhibits proliferation of *Ha-ras*-mutated cells, it is imaginable that during the 25 PB-free weeks the *Ha-ras*-mutated cells regained the capacity to proliferate and form a tumor (figure 5.4). Since *Meg3/Gtl2* was detected in the PB-treated *Ha-ras*-mutated tumors, the activating effect of PB on this lncRNA appears to not be exclusive to *Ctnnb1*-mutated cells but takes place in *Ha-ras*-mutated cells as well, at least when treated with PB over a longer period of time.

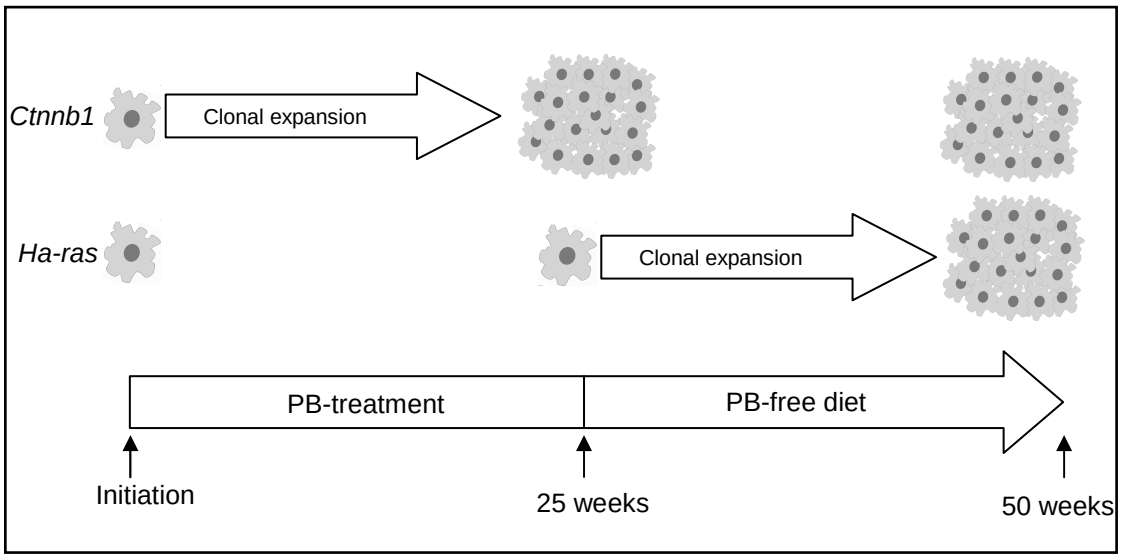

Figure 5.4. Scheme of proliferation of *Ctnnb1*- and *Ha-ras*-mutated cells during PB-promotion and when PB-treatment is abandoned.

All of the spontaneously formed tumors isolated from untreated aged male C3H mice were *Ha-ras*-mutated, and most of them showed similar or slightly lower levels of *Meg3/Gtl2* mRNA than untreated control tissue (figure 4.11A). In two tumors, however, *Meg3/Gtl2* expression was increased by factors of 40 and 9, respectively, as compared to the untreated control and was thus even higher than in the PB-treated control samples. As expected, these two samples showed up-regulated mRNA levels of the *Ha-ras*-mutation marker gene *H19* as compared to non-tumor control tissue (figure 4.11C). Interestingly however, the *Ha-ras*-mutated tumor with the 40-fold induction of *Meg3/Gtl2* showed a significant increase in the expression of *Glul*, which is characteristically up-regulated in *Ctnnb1*-mutated tumors (figure 4.11B). In consideration of the finding that unpromoted *Ha-ras*-mutated tumors usually do not overexpress *Meg3/Gtl2*, the question arose as to why this particular spontaneous tumor sample did anyway. The percentage of *Ctnnb1*-mutated tumors in the livers of non-PB-promoted mice is very low, and no activating point mutations were detected in the spontaneous tumors. However, aside from single base substitutions in codons 32, 33, 37 and 41, which predominate under the experimental conditions used, larger deletions in the *Ctnnb1*-gene, which also lead to activation of β-Catenin, may occur rarely. Thus, in addition to the *Ha-ras*-mutated cells that were identified via RFLP-analysis, the spontaneous tumor isolated from untreated mice could contain a population of cells harboring large deletions in *Ctnnb1* which were not detected with the primers used in this study. Another explanation for the elevated *Meg3/Gtl2* levels in the *Ha-ras*-mutated tumor would be that it harbored additional unknown mutations which lead to a stabilization of β-Catenin, for instance in the *Apc* gene. The results gained from spontaneous tumors and from those which developed under the regimen with PB-promotion and subsequent PB-withdrawal must be regarded with reservations as the sample numbers were very small. This made it impossible to statistically assess the effects seen in these tissues in a reasonable manner.

All in all, the investigation of *Meg3/Gtl2* showed that its activation can neither be assigned exclusively to one specific type of mutation nor to treatment with PB. This is consistent with the outcomes of other studies, which have shown *Meg3/Gtl2* to be dysregulated in a variety of tissues and tumors. However, two facts still strongly support its role as a potential early and predictive biomarker for PB as a tumor promoter: first, up-regulation of *Meg3/Gtl2* can be observed in normal liver after only two weeks of PB-treatment and thus long before a tumor has actually formed, and second, it is significantly increased in PB-promoted tumors.

The data presented in this work point to a tumor-driving function of *Meg3/Gtl2* as it is always up-regulated in the context of PB-treatment or tumor formation. This is in contrast to other studies showing that *Meg3/Gtl2* is significantly down-regulated in human liver cancer cell lines as compared to non-tumor cells (Braconi et al., 2011), inhibits cell proliferation in glioma cells *in vitro* (Wang et al., 2012b), induces apoptosis via activation of p53 (Zhou et al., 2007), and has thus been suggested as a tumor suppressor (Zhou et al., 2012). However, the data from PB-driven *Ctnnb1*-mutated tumors provide a strong body of evidence that *Meg3/Gtl2* functions as a promoter in these tumors, or at least is an essential component of PB-mediated tumor promotion in mouse liver. To definitely test this hypothesis, one would have to run an initiation-promotion experiment using DEN and PB in mice with a liver-specific *Meg3/Gtl2* knockout and check if tumor formation is impaired in these animals.

5.3 5'-methylation and 5'-hydroxymethylation of cytidine in *Ha-ras*- and *Ctnnb1*-mutated tumors

The 5'-hmC patterns in murine and human brain are subject to defined dynamics in the course of postnatal neurodevelopment (Szulwach et al., 2011), which indicates that 5'-hmC is a self-contained epigenetic modification and not a mere intermediate in the demethylation of 5'-mC. However, the functional significance of 5'-hmC is currently unknown. Impaired methylation at the 5'-position of cytosine is a frequently found feature in many cancer cell lines and tumors (Goelz et al., 1985; Barciszewska et al., 2007; Braconi et al., 2011), and a number of human cancers show a global decrease in 5'-hmC (Yang et al., 2012). Correspondingly, a comprehensive reduction of both 5'-mC and 5'-hmC was detected in *Ha-ras*- and *Ctnnb1*-mutated tumors as compared to surrounding non-tumor tissue in the present work. The decrease in 5'-hmC has been reported to be accompanied by a down-regulation of *Tet* (ten-eleven translocation) gene expression in various human cancers (Yang et al., 2012); however, no differential expression of the *Tet* genes was found in the two tumor types investigated in this study. The fact that *Ctnnb1*-mutated tumors showed reduced 5'-mC and 5'-hmC levels along with up-regulated expression of *Meg3/Gtl2* indicates a causal relationship between these two phenomena. This is corroborated by a recent work by Braconi and colleagues, who have shown that decreased expression of *Meg3/Gtl2* in human cancer cell lines could be re-induced by treatment with a methylation inhibitor or siRNAs targeting the transcripts of *Dnmt1* and *3b* (DNA methyltransferases 1 and 3b) (Braconi et al., 2011).

In the livers of both unpromoted and PB-promoted mice, 5'-hmC and 5'-mC were zonated in a periportally dominated pattern. Affymetrix® mRNA datasets of enriched populations of

periportal and pericentral mouse hepatocytes were available from an earlier experiment (Braeuning et al., 2006). To determine if the zonated methylation pattern was due to zonated expression of the enzymes that synthesize 5'-mC (*Tet*) or convert it to 5'-hmC (*Dnmt*), it was checked if these genes were differentially expressed in either of the cell types, but this was not the case. It is, however, possible that the catalytic activity of these enzymes is subject to differential regulation at the protein level in periportal and pericentral hepatocytes.

To further analyze how DNA methylation influences the phenotype of a tumor, an interesting unpromoted tumor type with patchy Cx32-expression was investigated with regards to its 5'-mC and 5'-hmC status. These analyses aimed at elucidating if DNA methylation is responsible for inactivation of the functional Cx32 allele in liver tumors of Cx32-heterozygous female mice (X^+/X^- or X^-/X^+). Immunohistochemical stainings showed no correlation between cytidine methylation or hydroxymethylation and the expression of Cx32 in the tumors harboring the mixed Cx32-phenotype. The determination of the global contents of 5'-mC and 5'-hmC in tissue sections is a rather unspecific method and does not allow an exact-to-the-nucleotide identification of local methylation changes in a specific genetic region. If the Cx32 promoter is very selectively methylated in only the Cx32-negative subpopulation of cells in the investigated tumors, these changes may not be visible in an antibody staining. In the course of integrated data analysis of *Ha-ras*- and *Ctnnb1*-mutated tumors, no significant correlation between methylation of a promoter region and expression of the downstream gene was detected (see figure 4.3 and section 4.2). This indicates that regulation of mRNA expression by DNA methylation is a more complex mechanism than described in textbooks and might work indirectly via intermediate steps, which could be another explanation for the lack of a direct correspondence between Cx32-expression and DNA methylation.

The data discussed in this section show that *Ha-ras*- and *Ctnnb1*-mutated tumors cannot be stratified by means of global visual assessment of their 5'-mC and 5'-hmC contents. Nevertheless, it is known that PB causes significant changes in 5'-hydroxymethylation and 5'-methylation in the promoter regions of selected genes in normal mouse liver (Thomson et al., 2012), which cannot be detected by immunohistochemical staining. This implies that PB as a NGC does in fact mediate specific epigenetic mechanisms that contribute to the substantial molecular differences between *Ha-ras*- and *Ctnnb1*-mutated tumors.

5.4 Conclusions and outlook

Comprehensive molecular characterization of *Ha-ras*- and *Ctnnb1*-mutated tumors, with a focus on metabolism and signaling, revealed distinctive differences, but also similarities between the two tumor types. The identified tumor-specific features, especially in combination with further metabolite data, may be a valuable contribution to the development of future cancer therapies as they provide very selective drug targets.

The function of *Meg3/Gtl2* is not fully understood, and its characterization is complicated by ambivalent results: Does it function as a tumor suppressor or an oncogene? Whatever its mechanism may be, *Meg3/Gtl2* definitely qualifies as a predictive biomarker for PB-promoted tumor formation. An *in vivo* carcinogenesis experiment in a *Meg3/Gtl2*-knockout mouse model would bring clarity to the question of this lncRNA's mechanism and relevance in tumorigenesis. The generation of such a mouse model, however, poses a challenge since the *Dlk1-Dio3* locus is subject to genomic imprinting and thus needs to be deleted allele-specifically, and furthermore, the locus is essential for embryonic development. *In situ* knockdown techniques, at which siRNAs complementary to the target transcript are administered to a wild-type animal via tail vein injection, could serve as alternative to stable genetic modification (Zhang et al., 1999).

The global reduction in methylation and hydroxymethylation is a common feature of many tumors, and visualization of 5'-mC and 5'-hmC in fixed and embedded liver specimens does not allow a distinction between *Ha-ras*- and *Ctnnb1*-mutated tumors. Nevertheless, PB causes very specific epigenetic changes in rodent liver, and it is thus likely that PB-promoted and unpromoted tumors diverge in that each tumor type shows a different DNA methylation fingerprint. Current technology provides the possibility of high resolution DNA methylation analysis (Akalin et al., 2012; Llamas et al., 2012). A detailed, exact-to-the-nucleotide methylation chart of *Ha-ras*- and *Ctnnb1*-mutated tumors would allow for precise localization of hyper- or hypomethylated regions respective to transcription factor binding sites and other important regulatory sequences in the genome. Thus, the tumors could be characterized more accurately with regards to their DNA methylation status and the consequences thereof.

The results of the analyses presented here also bear a methodic relevance with respect to personalized tumor therapy. Screening for specific markers is already a frequently used technique in tumor patients to evaluate the necessity and predict the effectiveness of chemotherapy and, if possible, to spare the patients a long and arduous treatment. Bioinformatic tools like InCroMAP could allow for fast and easy integration of large datasets

obtained from isolated tumor specimens and thus for more targeted and efficient therapeutic measures for the individual patient.

Summary

Oncogene mutations in chemically induced mouse liver tumors strongly depend on the experimental regimen. Treatment of mice with a single dose of the genotoxin DEN mainly gives rise to *Ha-ras*- (~50%) or *B-raf*- (~20%) mutated tumors, in which the mitogen-activated protein kinase (MAPK) pathway is permanently activated. However, if DEN-treatment is followed by continuous application of the tumor promoter PB, selective proliferation of cells harboring activating mutations in *Ctnnb1*, which results in constitutive activation of the Wnt/β-Catenin signaling pathway, is observed. The mechanisms of tumor promotion are still widely unsolved. Comprehensive molecular characterization of *Ctnnb1*- and *Ha-ras*-mutated mouse liver tumors was conducted with the goal of identifying tumor-specific differences that could help elucidate the molecular mechanism of PB and PB-like promoters.

Analysis of large mRNA and miRNA (microRNA) expression, DNA methylation and protein expression/phosphorylation datasets using the novel bioinformatic data integration tool InCroMAP revealed characteristic changes in metabolism and signaling in the tumors, as well as tumor-specific differences. Most notably, mRNA data in *Ctnnb1*- but not *Ha-ras*-mutated tumors indicated that glucose is oxidatively metabolized in the TCA cycle. In contrast to *Ctnnb1*-mutated tumors, *Ha-ras*-mutated lesions displayed excessive production and trapping of cholesterol in the cell. Integration of miRNA, mRNA and protein data provided a possible mechanism for the down-regulation of glucose-6-phosphatase at the transcription and enzyme level in *Ha-ras*-mutated tumors, by which the transcription factor Stat3 transactivates miR-23a, which on its part targets and inhibits *G6pc* mRNA. Joint analysis of mRNA and protein data showed that *Ha-ras*-mutated tumors activate feedback mechanisms, which negatively regulate MAPK signaling, while *Ctnnb1*-mutated tumors show an activation of *Wnt*-inhibitory genes. Furthermore, the data supported a previously proposed crosstalk between the two signaling cascades mediated by dual-specificity phosphatases.

The relevance of the lncRNA *Meg3/Gtl2* in PB-mediated tumor promotion was investigated by qPCR measurements and *in situ* hybridization in *Ctnnb1*- and *Ha-ras*-mutated tumors as well as non-tumor control tissues. The main result of these experiments is that *Meg3/Gtl2* was consistently and reproducibly up-regulated in all *Ctnnb1*-mutated tumors from PB-promoted mice but in none of the *Ha-ras*-mutated lesions from unpromoted animals. Together with the previous observation that *Meg3/Gtl2* is increased in pericentral hypertrophic hepatocytes in

PB-treated normal mouse liver, the described findings corroborate the relevance of this lncRNA as a predictive biomarker for PB-mediated tumor promotion.

Ha-ras- and *Ctnnb1*-mutated tumors showed a ubiquitous reduction of methylation and hydroxymethylation at the 5'-position of cytidine relative to normal liver tissue, as determined by immunohistochemical staining. This suggests that global visual assessment of the DNA methylation and hydroxymethylation status is not suited as a means of stratification between the two tumor types.

In conclusion, the data presented in this thesis underline that tumors harboring different oncogene mutations develop in part fundamentally different survival strategies. Comprehensive analysis of these substantial differences, including bioinformatic integration of large "omics" datasets, is extremely helpful in understanding the molecular processes that drive tumorigenesis and has led to identification of at least one promising new predictive biomarker for PB-mediated tumor formation.

Zusammenfassung

Der Onkogen-Mutationsstatus in chemikalieninduzierten Mauslebertumoren wird stark vom vorangegangen Behandlungsschema bestimmt. Werden Mäuse mit einer Einzeldosis des gentoxischen Initiators DEN behandelt, führt dies hauptsächlich zu *Ha-ras*- (~50%) oder *B-raf*- (~20%) mutierten Tumoren, in welchen der MAPK-Signalweg dauerhaft aktiviert ist. Folgt jedoch auf die DEN-Einzeldosis eine kontinuierliche Behandlung mit dem Tumorpromotor PB, wird selektives Auswachsen von Tumoren mit aktivierenden Mutationen im *Ctnnb1*-Gen beobachtet, welche zur konstitutiven Aktivierung des Wnt/β-Catenin-Signalwegs führen. Da die genaue Wirkungsweise von Tumorpromotoren weitgehend unbekannt ist, wurden *Ctnnb1*- und *Ha-ras*-mutierte Mauslebertumoren einer umfassenden molekularen Charakterisierung unterzogen. Ziel dessen war es, tumorspezifische Unterschiede aufzuzeigen, die ein genaueres Verständnis des molekularen Mechanismus von PB und PB-ähnlichen Promotoren ermöglichen.

Mit Hilfe der neuentwickelten Datenintegrations-Software InCroMAP wurden große Datensätze, die mRNA- und miRNA (microRNA)-Expression, DNA-Methylierung sowie Proteinexpression und -phosphorylierung umfassten, zusammenhängend analysiert. Dabei wurden in den Tumoren charakteristische Veränderungen und tumorspezifische Unterschiede im Bezug auf Stoffwechsel und Signaltransduktion gefunden. Die mRNA-Daten deuteten insbesondere darauf hin, dass in *Ctnnb1*- aber nicht in *Ha-ras*-mutierten Tumoren Glucose oxidativ im Citratzyklus abgebaut wird. Außerdem zeigten *Ha-ras*-mutierte im Gegensatz zu *Ctnnb1*-mutierten Tumoren eine deutlich erhöhte Produktion und Speicherung von Cholesterin. Aus der Integration von miRNA-, mRNA- und Proteindaten ergab sich ein möglicher Mechanismus für die Inhibierung der Glucose-6-Phosphatase (*G6pc*) in *Ha-ras*-mutierten Tumoren auf Transkriptions- und Enzymnebene, im Zuge dessen der Transkriptionsfaktor Stat3 die Expression von miR-23a aktiviert, die ihrerseits das G6pc-Transkript und damit dessen Translation blockiert. In *Ha-ras*-mutierten Tumoren konnte auf mRNA- und Proteinebene die Aktivierung von Rückkopplungsmechanismen, die den MAPK-Signalweg negativ regulieren, gezeigt werden. In *Ctnnb1*-mutierten Tumoren wurde wiederum die Transaktivierung Wnt-inhibitorischer Gene festgestellt. Die Daten stützten des Weiteren das Modell einer durch *dual-specificity*-Phosphatasen vermittelten Wechselwirkung zwischen diesen beiden Signalwegen.

Die Bedeutung der lncRNA *Meg3/Gtl2* in der PB-vermittelten Tumorpromotion wurde mittels qPCR-Messungen und *In-situ*-Hybridisierung in *Ctnnb1*- und *Ha-ras*-mutierten Tumoren

sowie nicht-mutierten Kontrollgeweben untersucht. Der eindeutige und reproduzierbare Befund dieser Experimente war, dass *Meg3/Gtl2* in PB-promovierten *Ctnnb1*-mutierten, jedoch nicht in unpromovierten *Ha-ras*-mutierten Tumoren induziert wird. In Anbetracht vorangegangener Experimente, in denen *Meg3/Gtl2*-Transkription durch PB-Behandlung in den perizentralen hypertrophen Zellen in Mäusenormalleber aktiviert werden konnte, untermauern die beschriebenen Ergebnisse die Bedeutung dieser lncRNA als prädiktiven Biomarker für PB-vermittelte Tumorpromotion.

In immunhistochemischen Färbungen wurde eine flächendeckende Reduktion der Methylierung und Hydroxymethylierung an der 5'-Position von Cytidin sowohl in *Ha-ras*- als auch *Ctnnb1*-mutierten Tumoren demonstriert. Dies deutet darauf hin, dass die globale visuelle Erfassung von DNA-Methylierung und -Hydroxymethylierung sich nicht zur Unterscheidung von *Ha-ras*- und *Ctnnb1*-mutierten Tumoren eignet.

Zusammenfassend unterstreichen die in dieser Arbeit präsentierten Daten die Tatsache, dass Tumore mit unterschiedlichen Onkogenmutationen teilweise grundlegend verschiedene Überlebensstrategien entwickeln. Die umfassende Analyse dieser beträchtlichen Unterschiede, unter anderem durch bioinformatische Integration großer "-omik"-Datensätze, ist extrem hilfreich für das Verständnis der molekularen Vorgänge, welche die Tumorgenese antreiben, und hat zur Identifikation mindestens eines neuen vielversprechenden prädiktiven Biomarkers für PB-vermittelte Tumorbildung geführt.

6. Curriculum vitae

Personal data

Name:	Elif Bettina Unterberger
Born:	March 28 1986, Den Haag, Netherlands
Nationality:	Austrian
Parents:	Stephan Unterberger, Arzu Unterberger (née Doğusoy)

Education

1992-1996	Volksschule Schendlingen, Bregenz, Austria
1996-2004	Bundesgymnasium Blumenstraße, Bregenz, Austria
06/2004	General qualification for university entrance (Matura)
10/2004-10/2006	Basic study biochemistry, Eberhard Karls Universität Tübingen
10/2006-11/2008	Main study biochemistry, Eberhard Karls Universität Tübingen
12/2008-08/2009	Diploma thesis at the Institute of Experimental and Clinical Pharmacology and Toxicology, Department Toxicology, Eberhard Karls Universität Tübingen. Supervision by PD Dr. Peter Münzel. Title of thesis: “Das *hairless*-Gen und seine mögliche Rolle bei der Kanzerogenese“
09/2009-03/2013	PhD thesis at the Institute of Experimental and Clinical Pharmacology and Toxicology, Department Toxicology, Eberhard Karls Universität Tübingen. Supervision by Prof. Dr. Michael Schwarz. Title of thesis: “Comparative Molecular Characterization of *Ctnnb1*- and *Ha-ras*-mutated Mouse Liver Tumors“

7. Literature

Akalin, A., F. E. Garrett-Bakelman, M. Kormaksson, J. Busuttil, L. Zhang, I. Khrebtukova, T. A. Milne, Y. Huang, D. Biswas, J. L. Hess, C. D. Allis, R. G. Roeder, P. J. Valk, B. Lowenberg, R. Delwel, H. F. Fernandez, E. Paietta, M. S. Tallman, G. P. Schroth, C. E. Mason, A. Melnick and M. E. Figueroa (2012). "Base-pair resolution DNA methylation sequencing reveals profoundly divergent epigenetic landscapes in acute myeloid leukemia." PLoS Genet **8**(6): e1002781.

Amit, S., A. Hatzubai, Y. Birman, J. S. Andersen, E. Ben-Shushan, M. Mann, Y. Ben-Neriah and I. Alkalay (2002). "Axin-mediated CKI phosphorylation of beta-catenin at Ser 45: a molecular switch for the Wnt pathway." Genes Dev **16**(9): 1066-76.

Anatelli, F., S. T. Chuang, X. J. Yang and H. L. Wang (2008). "Value of glypican 3 immunostaining in the diagnosis of hepatocellular carcinoma on needle biopsy." Am J Clin Pathol **130**(2): 219-23.

Anwar, S. L., T. Krech, B. Hasemeier, E. Schipper, N. Schweitzer, A. Vogel, H. Kreipe and U. Lehmann (2012). "Loss of imprinting and allelic switching at the DLK1-MEG3 locus in human hepatocellular carcinoma." PLoS One **7**(11): e49462.

Armitage, P. (1985). "Multistage models of carcinogenesis." Environ Health Perspect **63**: 195-201.

Aydinlik, H., T. D. Nguyen, O. Moennikes, A. Buchmann and M. Schwarz (2001). "Selective pressure during tumor promotion by phenobarbital leads to clonal outgrowth of β-catenin-mutated mouse liver tumors." Oncogene **20**(53): 7812-7816.

Bachman, A. N., J. M. Phillips and J. I. Goodman (2006). "Phenobarbital induces progressive patterns of GC-rich and gene-specific altered DNA methylation in the liver of tumor-prone B6C3F1 mice." Toxicol Sci **91**(2): 393-405.

Barciszewska, A. M., D. Murawa, I. Gawronska, P. Murawa, S. Nowak and M. Z. Barciszewska (2007). "Analysis of 5-methylcytosine in DNA of breast and colon cancer tissues." IUBMB Life **59**(12): 765-70.

Bartel, D. P. (2004). "MicroRNAs: genomics, biogenesis, mechanism, and function." Cell **116**(2): 281-97.

Bartolomei, M. S. and A. C. Ferguson-Smith (2011). "Mammalian genomic imprinting." Cold Spring Harb Perspect Biol **3**(7).

Bartolomei, M. S., S. Zemel and S. M. Tilghman (1991). "Parental imprinting of the mouse H19 gene." Nature **351**(6322): 153-5.

Benhamouche, S., T. Decaens, C. Godard, R. Chambrey, D. S. Rickman, C. Moinard, M. Vasseur-Cognet, C. J. Kuo, A. Kahn, C. Perret and S. Colnot (2006a). "Apc tumor suppressor gene is the "zonation-keeper" of mouse liver." Dev Cell **10**(6): 759-70.

Benhamouche, S., T. Decaens, C. Perret and S. Colnot (2006b). "[Wnt/beta-catenin pathway and liver metabolic zonation: a new player for an old concept]." Med Sci (Paris) **22**(11): 904-6.

Bos, J. L. (1989). "ras oncogenes in human cancer: a review." Cancer Res **49**(17): 4682-9.

Braconi, C., T. Kogure, N. Valeri, N. Huang, G. Nuovo, S. Costinean, M. Negrini, E. Miotto, C. M. Croce and T. Patel (2011). "microRNA-29 can regulate expression of the long non-coding RNA gene MEG3 in hepatocellular cancer." Oncogene **30**(47): 4750-6.

Braeuning, A., Y. Heubach, T. Knorpp, M. A. Kowalik, M. Templin, A. Columbano and M. Schwarz (2011). "Gender-specific interplay of signaling through beta-catenin and CAR in the regulation of xenobiotic-induced hepatocyte proliferation." Toxicol Sci **123**(1): 113-22.

Braeuning, A., C. Ittrich, C. Kohle, A. Buchmann and M. Schwarz (2007a). "Zonal gene expression in mouse liver resembles expression patterns of Ha-ras and beta-catenin mutated hepatomas." Drug Metab Dispos **35**(4): 503-7.

Braeuning, A., C. Ittrich, C. Kohle, S. Hailfinger, M. Bonin, A. Buchmann and M. Schwarz (2006). "Differential gene expression in periportal and perivenous mouse hepatocytes." FEBS J **273**(22): 5051-61.

Braeuning, A., M. Menzel, E. M. Kleinschnitz, N. Harada, Y. Tamai, C. Kohle, A. Buchmann and M. Schwarz (2007b). "Serum components and activated Ha-ras antagonize expression of perivenous marker genes stimulated by beta-catenin signaling in mouse hepatocytes." FEBS J **274**(18): 4766-77.

Camps, M., A. Nichols and S. Arkinstall (2000). "Dual specificity phosphatases: a gene family for control of MAP kinase function." FASEB J **14**(1): 6-16.

Chafey, P., L. Finzi, R. Boisgard, M. Cauzac, G. Clary, C. Broussard, J. P. Pegorier, F. Guillonneau, P. Mayeux, L. Camoin, B. Tavitian, S. Colnot and C. Perret (2009). "Proteomic analysis of beta-catenin activation in mouse liver by DIGE analysis identifies glucose metabolism as a new target of the Wnt pathway." Proteomics **9**(15): 3889-900.

Chen, L. L. and G. G. Carmichael (2010). "Long noncoding RNAs in mammalian cells: what, where, and why?" Wiley Interdiscip Rev RNA **1**(1): 2-21.

Cheng, W. L., C. S. Wang, Y. H. Huang, Y. Liang, P. Y. Lin, C. Hsueh, Y. C. Wu, W. J. Chen, C. J. Yu, S. R. Lin and K. H. Lin (2008). "Overexpression of a secretory leukocyte protease inhibitor in human gastric cancer." Int J Cancer **123**(8): 1787-96.

Clendening, J. W., A. Pandyra, P. C. Boutros, S. El Ghamrasni, F. Khosravi, G. A. Trentin, A. Martirosyan, A. Hakem, R. Hakem, I. Jurisica and L. Z. Penn (2010). "Dysregulation of the mevalonate pathway promotes transformation." Proc Natl Acad Sci U S A **107**(34): 15051-6.

Colletti, M., C. Cicchini, A. Conigliaro, L. Santangelo, T. Alonzi, E. Pasquini, M. Tripodi and L. Amicone (2009). "Convergence of Wnt signaling on the HNF4alpha-driven transcription in controlling liver zonation." Gastroenterology **137**(2): 660-72.

da Rocha, S. T., C. A. Edwards, M. Ito, T. Ogata and A. C. Ferguson-Smith (2008). "Genomic imprinting at the mammalian Dlk1-Dio3 domain." Trends Genet **24**(6): 306-16.

Davies, H., G. R. Bignell, C. Cox, P. Stephens, S. Edkins, S. Clegg, J. Teague, H. Woffendin, M. J. Garnett, W. Bottomley, N. Davis, E. Dicks, R. Ewing, Y. Floyd, K. Gray, S. Hall, R. Hawes, J. Hughes, V. Kosmidou, A. Menzies, C. Mould, A. Parker, C. Stevens, S. Watt, S. Hooper, R. Wilson, H. Jayatilake, B. A. Gusterson, C. Cooper, J. Shipley, D. Hargrave, K. Pritchard-Jones, N. Maitland, G. Chenevix-Trench, G. J. Riggins, D. D. Bigner, G. Palmieri, A. Cossu, A. Flanagan, A. Nicholson, J. W. Ho, S. Y. Leung, S. T. Yuen, B. L. Weber, H. F. Seigler, T. L. Darrow, H. Paterson, R. Marais, C. J. Marshall, R. Wooster, M. R. Stratton and P. A. Futreal (2002). "Mutations of the BRAF gene in human cancer." Nature **417**(6892): 949-54.

De Fabiani, E., N. Mitro, A. C. Anzulovich, A. Pinelli, G. Galli and M. Crestani (2001). "The negative effects of bile acids and tumor necrosis factor-alpha on the transcription of cholesterol 7alpha-hydroxylase gene (CYP7A1) converge to hepatic nuclear factor-4: a novel mechanism of feedback regulation of bile acid synthesis mediated by nuclear receptors." J Biol Chem **276**(33): 30708-16.

de La Coste, A., B. Romagnolo, P. Billuart, C. A. Renard, M. A. Buendia, O. Soubrane, M. Fabre, J. Chelly, C. Beldjord, A. Kahn and C. Perret (1998). "Somatic mutations of the beta-catenin gene are frequent in mouse and human hepatocellular carcinomas." Proc Natl Acad Sci U S A **95**(15): 8847-51.

DeChiara, T. M., E. J. Robertson and A. Efstratiadis (1991). "Parental imprinting of the mouse insulin-like growth factor II gene." Cell **64**(4): 849-59.

Egger, G., G. Liang, A. Aparicio and P. A. Jones (2004). "Epigenetics in human disease and prospects for epigenetic therapy." Nature **429**(6990): 457-63.

Ehrlich, M. (2002). "DNA methylation in cancer: too much, but also too little." Oncogene **21**(35): 5400-13.

Ehrlich, M. and R. Y. Wang (1981). "5-Methylcytosine in eukaryotic DNA." Science **212**(4501): 1350-7.

Eisenmann, D. M. (2005). "Wnt signaling." WormBook: 1-17.

Esquela-Kerscher, A. and F. J. Slack (2006). "Oncomirs - microRNAs with a role in cancer." Nat Rev Cancer **6**(4): 259-69.

Esteller, M. (2005). "Aberrant DNA methylation as a cancer-inducing mechanism." Annu Rev Pharmacol Toxicol **45**: 629-56.
Feinberg, A. P., R. Ohlsson and S. Henikoff (2006). "The epigenetic progenitor origin of human cancer." Nat Rev Genet **7**(1): 21-33.
Friedman, R. C., K. K. Farh, C. B. Burge and D. P. Bartel (2009). "Most mammalian mRNAs are conserved targets of microRNAs." Genome Res **19**(1): 92-105.
Gaidatzis, D., E. van Nimwegen, J. Hausser and M. Zavolan (2007). "Inference of miRNA targets using evolutionary conservation and pathway analysis." BMC Bioinformatics **8**: 69.
Garnett, M. J. and R. Marais (2004). "Guilty as charged: B-RAF is a human oncogene." Cancer Cell **6**(4): 313-9.
Gebhardt, R. (1992). "Metabolic zonation of the liver: regulation and implications for liver function." Pharmacol Ther **53**(3): 275-354.
Gibbs, J. B. and A. Oliff (1997). "The potential of farnesyltransferase inhibitors as cancer chemotherapeutics." Annu Rev Pharmacol Toxicol **37**: 143-66.
Goelz, S. E., B. Vogelstein, S. R. Hamilton and A. P. Feinberg (1985). "Hypomethylation of DNA from benign and malignant human colon neoplasms." Science **228**(4696): 187-90.
Gokey, N. G., C. Lopez-Anido, A. L. Gillian-Daniel and J. Svaren (2011). "Early growth response 1 (Egr1) regulates cholesterol biosynthetic gene expression." J Biol Chem **286**(34): 29501-10.
Gregg, J. and G. Fraizer (2011). "Transcriptional Regulation of EGR1 by EGF and the ERK Signaling Pathway in Prostate Cancer Cells." Genes Cancer **2**(9): 900-9.
Gregg, J. and G. Fraizer (2012). "Transcriptional Regulation of EGR1 by EGF and the ERK Signaling Pathway in Prostate Cancer Cells." Genes Cancer **2**(9): 900-9.
Hagan, J. P., B. L. O'Neill, C. L. Stewart, S. V. Kozlov and C. M. Croce (2009). "At least ten genes define the imprinted Dlk1-Dio3 cluster on mouse chromosome 12qF1." PLoS One **4**(2): e4352.
Hailfinger, S., M. Jaworski, A. Braeuning, A. Buchmann and M. Schwarz (2006). "Zonal gene expression in murine liver: lessons from tumors." Hepatology **43**(3): 407-14.
Hall, J. G. (1990). "Genomic imprinting: review and relevance to human diseases." Am J Hum Genet **46**(5): 857-73.
Hanahan, D. and R. A. Weinberg (2000). "The hallmarks of cancer." Cell **100**(1): 57-70.
Hanahan, D. and R. A. Weinberg (2011). "Hallmarks of cancer: the next generation." Cell **144**(5): 646-74.
He, L. and G. J. Hannon (2004). "MicroRNAs: small RNAs with a big role in gene regulation." Nat Rev Genet **5**(7): 522-31.
Honkakoski, P., I. Zelko, T. Sueyoshi and M. Negishi (1998). "The nuclear orphan receptor CAR-retinoid X receptor heterodimer activates the phenobarbital-responsive enhancer module of the CYP2B gene." Mol Cell Biol **18**(10): 5652-8.
Hoshino, R., Y. Chatani, T. Yamori, T. Tsuruo, H. Oka, O. Yoshida, Y. Shimada, S. Ari-i, H. Wada, J. Fujimoto and M. Kohno (1999). "Constitutive activation of the 41-/43-kDa mitogen-activated protein kinase signaling pathway in human tumors." Oncogene **18**(3): 813-22.
Hsu, S. D., F. M. Lin, W. Y. Wu, C. Liang, W. C. Huang, W. L. Chan, W. T. Tsai, G. Z. Chen, C. J. Lee, C. M. Chiu, C. H. Chien, M. C. Wu, C. Y. Huang, A. P. Tsou and H. D. Huang (2010). "miRTarBase: a database curates experimentally validated microRNA-target interactions." Nucleic Acids Res **39**(Database issue): D163-9.
Ito, S., L. Shen, Q. Dai, S. C. Wu, L. B. Collins, J. A. Swenberg, C. He and Y. Zhang (2011). "Tet proteins can convert 5-methylcytosine to 5-formylcytosine and 5-carboxylcytosine." Science **333**(6047): 1300-3.
Jaworski, M., A. Buchmann, P. Bauer, O. Riess and M. Schwarz (2005a). "*B-raf* and *Ha-ras* mutations in chemically induced mouse liver tumors." Oncogene **24**: 1290-1295.
Jaworski, M., S. Hailfinger, A. Buchmann, M. Hergenhahn, M. Hollstein, C. Ittrich and M. Schwarz (2005b). "Human p53 knock-in (hupki) mice do not differ in liver tumor

response from their counterparts with murine p53." Carcinogenesis **26**(10): 1829–1834.
Jaworski, M., C. Ittrich, S. Hailfinger, M. Bonin, A. Buchmann, M. Schwarz and C. Kohle (2007). "Global gene expression in Ha-ras and B-raf mutated mouse liver tumors." Int J Cancer **121**(6): 1382-5.
Jungermann, K. and N. Katz (1989). "Functional specialization of different hepatocyte populations." Physiol Rev **69**(3): 708-64.
Jungermann, K. and T. Kietzmann (1996). "Zonation of parenchymal and nonparenchymal metabolism in liver." Annu Rev Nutr **16**: 179-203.
Kagami, M., Y. Sekita, G. Nishimura, M. Irie, F. Kato, M. Okada, S. Yamamori, H. Kishimoto, M. Nakayama, Y. Tanaka, K. Matsuoka, T. Takahashi, M. Noguchi, K. Masumoto, T. Utsunomiya, H. Kouzan, Y. Komatsu, H. Ohashi, K. Kurosawa, K. Kosaki, A. C. Ferguson-Smith, F. Ishino and T. Ogata (2008). "Deletions and epimutations affecting the human 14q32.2 imprinted region in individuals with paternal and maternal upd(14)-like phenotypes." Nat Genet **40**(2): 237-42.
Kanehisa, M., S. Goto, M. Hattori, K. F. Aoki-Kinoshita, M. Itoh, S. Kawashima, T. Katayama, M. Araki and M. Hirakawa (2006). "From genomics to chemical genomics: new developments in KEGG." Nucleic Acids Res **34**(Database issue): D354-7.
Kauffmann, A., R. Gentleman and W. Huber (2009). "arrayQualityMetrics--a bioconductor package for quality assessment of microarray data." Bioinformatics **25**(3): 415-6.
Kolch, W. (2000). "Meaningful relationships: the regulation of the Ras/Raf/MEK/ERK pathway by protein interactions." Biochem J **351 Pt 2**: 289-305.
Kriaucionis, S. and N. Heintz (2009). "The nuclear DNA base 5-hydroxymethylcytosine is present in Purkinje neurons and the brain." Science **324**(5929): 929-30.
Kristensen, V. N., C. J. Vaske, J. Ursini-Siegel, P. Van Loo, S. H. Nordgard, R. Sachidanandam, T. Sorlie, F. Warnberg, V. D. Haakensen, A. Helland, B. Naume, C. M. Perou, D. Haussler, O. G. Troyanskaya and A. L. Borresen-Dale "Integrated molecular profiles of invasive breast tumors and ductal carcinoma in situ (DCIS) reveal differential vascular and interleukin signaling." Proc Natl Acad Sci U S A **109**(8): 2802-7.
Kurz, A. K., C. Block, D. Graf, S. V. Dahl, F. Schliess and D. Haussinger (2000). "Phosphoinositide 3-kinase-dependent Ras activation by tauroursodesoxycholate in rat liver." Biochem J **350 Pt 1**: 207-13.
Larner, J., J. Jane, E. Laws, R. Packer, C. Myers and M. Shaffrey (1998). "A phase I-II trial of lovastatin for anaplastic astrocytoma and glioblastoma multiforme." Am J Clin Oncol **21**(6): 579-83.
Lempiainen, H., P. Couttet, F. Bolognani, A. Muller, V. Dubost, R. Luisier, A. Del Rio Espinola, V. Vitry, E. Unterberger, J. P. Thomson, F. Treindl, U. Metzger, C. Wrzodek, F. Hahne, T. Zollinger, S. Brasa, M. Kalteis, M. Marcellin, F. Giudicelli, A. Braeuning, L. Morawiec, N. Zamurovic, U. Langle, N. Scheer, D. Schubeler, J. Goodman, S. D. Chibout, J. Marlowe, D. Theil, D. J. Heard, O. Grenet, A. Zell, M. F. Templin, R. R. Meehan, C. R. Wolf, C. R. Elcombe, M. Schwarz, P. Moulin, R. Terranova and J. G. Moggs (2013). "Identification of Dlk1-Dio3 imprinted gene cluster non-coding RNAs as novel candidate biomarkers for liver tumor promotion." Toxicol Sci.
Lempiainen, H., A. Muller, S. Brasa, S. S. Teo, T. C. Roloff, L. Morawiec, N. Zamurovic, A. Vicart, E. Funhoff, P. Couttet, D. Schubeler, O. Grenet, J. Marlowe, J. Moggs and R. Terranova (2011). "Phenobarbital mediates an epigenetic switch at the constitutive androstane receptor (CAR) target gene Cyp2b10 in the liver of B6C3F1 mice." PLoS One **6**(3): e18216.
Liu, C., Y. Li, M. Semenov, C. Han, G. H. Baeg, Y. Tan, Z. Zhang, X. Lin and X. He (2002). "Control of beta-catenin phosphorylation/degradation by a dual-kinase mechanism." Cell **108**(6): 837-47.
Llamas, B., M. L. Holland, K. Chen, J. E. Cropley, A. Cooper and C. M. Suter (2012). "High-resolution analysis of cytosine methylation in ancient DNA." PLoS One **7**(1): e30226.

Lonardo, A. and P. Loria (2012). "Potential for statins in the chemoprevention and management of hepatocellular carcinoma." J Gastroenterol Hepatol **27**(11): 1654-64.

Lopez-Romero, P. (2011). "Pre-processing and differential expression analysis of Agilent microRNA arrays using the AgiMicroRna Bioconductor library." BMC Genomics **12**: 64.

Luo, J., J. Chen, Z. L. Deng, X. Luo, W. X. Song, K. A. Sharff, N. Tang, R. C. Haydon, H. H. Luu and T. C. He (2007). "Wnt signaling and human diseases: what are the therapeutic implications?" Lab Invest **87**(2): 97-103.

Maragkakis, M., T. Vergoulis, P. Alexiou, M. Reczko, K. Plomaritou, M. Gousis, K. Kourtis, N. Koziris, T. Dalamagas and A. G. Hatzigeorgiou (2011). "DIANA-microT Web server upgrade supports Fly and Worm miRNA target prediction and bibliographic miRNA to disease association." Nucleic Acids Res **39**(Web Server issue): W145-8.

Marrero, J. A., P. R. Romano, O. Nikolaeva, L. Steel, A. Mehta, C. J. Fimmel, M. A. Comunale, A. D'Amelio, A. S. Lok and T. M. Block (2005). "GP73, a resident Golgi glycoprotein, is a novel serum marker for hepatocellular carcinoma." J Hepatol **43**(6): 1007-12.

Martín-Subero, J. I., M. Kreuz, M. Bibikova, S. Bentink, O. Ammerpohl, E. Wickham-Garcia, M. Rosolowski, J. Richter, L. Lopez-Serra, E. Ballestar, H. Berger, X. Agirre, H.-W. Bernd, V. Calvanese, S. B. Cogliatti, H. G. Drexler, J.-B. Fan, M. F. Fraga, M. L. Hansmann, M. Hummel, W. Klapper, B. Korn, R. Küppers, R. A. F. MacLeod, P. Möller, G. Ott, C. Pott, F. Prosper, A. Rosenwald, C. Schwaenen, D. Schübeler, M. Seifert, B. Stürzenhofecker, M. Weber, S. Wessendorf, M. Loeffler, L. Trümper, H. Stein, R. Spang, M. Esteller, D. Barker, D. Hasenclever and R. Siebert (2009). "New insights into the biology and origin of mature aggressive B-cell lymphomas by combined epigenomic, genomic, and transcriptional profiling." Blood **113**: 2488-2497.

Marx-Stoelting, P., J. Mahr, T. Knorpp, S. Schreiber, M. F. Templin, T. Ott, A. Buchmann and M. Schwarz (2008). "Tumor Promotion in Liver of Mice with a Conditional Cx26 Knockout." Toxicological Sciences **103**(2): 260–267.

McCabe, M. T., J. C. Brandes and P. M. Vertino (2009). "Cancer DNA methylation: molecular mechanisms and clinical implications." Clin Cancer Res **15**(12): 3927-37.

Miyoshi, N., H. Wagatsuma, S. Wakana, T. Shiroishi, M. Nomura, K. Aisaka, T. Kohda, M. A. Surani, T. Kaneko-Ishino and F. Ishino (2000). "Identification of an imprinted gene, Meg3/Gtl2 and its human homologue MEG3, first mapped on mouse distal chromosome 12 and human chromosome 14q." Genes Cells **5**(3): 211-20.

Moennikes, O., A. Buchmann, A. Romualdi, T. Ott, J. Werringloer, K. Willecke and M. Schwarz (2000a). "Lack of Phenobarbital-mediated Promotion of Hepatocarcinogenesis in Connexin32-Null Mice." Cancer Research **60**: 5087–5091.

Moennikes, O., A. Buchmann, K. Willecke, O. Traub and M. Schwarz (2000b). "Hepatocarcinogenesis in female mice with mosaic expression of connexin32." Hepatology **32**(3): 501-6.

Nowell, P. C. (1976). "The clonal evolution of tumor cell populations." Science **194**(4260): 23-8.

Nusse, R. and H. E. Varmus (1982). "Many tumors induced by the mouse mammary tumor virus contain a provirus integrated in the same region of the host genome." Cell **31**(1): 99-109.

Oinonen, T. and K. O. Lindros (1998). "Zonation of hepatic cytochrome P-450 expression and regulation." Biochem J **329 (Pt 1)**: 17-35.

Pelizzola, M., Y. Koga, A. E. Urban, M. Krauthammer, S. Weissman, R. Halaban and A. M. Molinaro (2008). "MEDME: an experimental and analytical methodology for the estimation of DNA methylation levels based on microarray derived MeDIP-enrichment." Genome Res **18**(10): 1652-9.

Phillips, J. M., Y. Yamamoto, M. Negishi, R. R. Maronpot and J. I. Goodman (2007). "Orphan nuclear receptor constitutive active/androstane receptor-mediated alterations in DNA methylation during phenobarbital promotion of liver tumorigenesis." Toxicol Sci **96**(1): 72-82.

Prensner, J. R. and A. M. Chinnaiyan (2011). "The emergence of lncRNAs in cancer biology." Cancer Discov **1**(5): 391-407.
Qureshi, S. A., X. M. Cao, V. P. Sukhatme and D. A. Foster (1991). "v-Src activates mitogen-responsive transcription factor Egr-1 via serum response elements." J Biol Chem **266**(17): 10802-6.
Rignall, B., A. Braeuning, A. Buchmann and M. Schwarz (2010). "Tumor formation in liver of conditional beta-catenin-deficient mice exposed to a diethylnitrosamine/phenobarbital tumor promotion regimen." Carcinogenesis **32**(1): 52-7.
Rignall, B., C. Ittrich, E. Krause, K. E. Appel, A. Buchmann and M. Schwarz (2009). "Comparative transcriptome and proteome analysis of Ha-ras and B-raf mutated mouse liver tumors." J Proteome Res **8**(8): 3987-94.
Rijsewijk, F., M. Schuermann, E. Wagenaar, P. Parren, D. Weigel and R. Nusse (1987). "The Drosophila homolog of the mouse mammary oncogene int-1 is identical to the segment polarity gene wingless." Cell **50**(4): 649-57.
Schulze, A. and A. L. Harris (2012). "How cancer metabolism is tuned for proliferation and vulnerable to disruption." Nature **491**(7424): 364-73.
Schuster-Gossler, K., P. Bilinski, T. Sado, A. Ferguson-Smith and A. Gossler (1998). "The mouse Gtl2 gene is differentially expressed during embryonic development, encodes multiple alternatively spliced transcripts, and may act as an RNA." Dev Dyn **212**(2): 214-28.
Schwarz, M. (2004). "Pathways and defects of bile acid synthesis: insights from in vitro and in vivo experimental models." Drug Discovery Today: Disease Models **1**(3): 205-212.
Shack, S., M. Gorospe, T. W. Fawcett, W. R. Hudgins and N. J. Holbrook (1999). "Activation of the cholesterol pathway and Ras maturation in response to stress." Oncogene **18**(44): 6021-8.
Sharma, S., T. K. Kelly and P. A. Jones (2010). "Epigenetics in cancer." Carcinogenesis **31**(1): 27-36.
Shen, L., M. Toyota, Y. Kondo, E. Lin, L. Zhang, Y. Guo, N. S. Hernandez, X. Chen, S. Ahmed, K. Konishi, S. R. Hamilton and J.-P. J. Issa (2007). "Integrated genetic and epigenetic analysis identifies three different subclasses of colon cancer." Proceedings of the National Academy of Sciences **104**(47): 18654–18659.
Sherr, C. J. and J. D. Weber (2000). "The ARF/p53 pathway." Curr Opin Genet Dev **10**(1): 94-9.
Smyth, G. K. (2004). "Linear models and empirical bayes methods for assessing differential expression in microarray experiments." Stat Appl Genet Mol Biol **3**: Article3.
Stahl, S., C. Ittrich, P. Marx-Stoelting, C. Kohle, O. Altug-Teber, O. Riess, M. Bonin, J. Jobst, S. Kaiser, A. Buchmann and M. Schwarz (2005a). "Genotype-phenotype relationships in hepatocellular tumors from mice and man." Hepatology **42**(2): 353-61.
Stahl, S., C. Ittrich, P. Marx-Stoelting, C. Köhle, T. Ott, A. Buchmann and M. Schwarz (2005b). "Effect of the tumor promoter phenobarbital on the pattern of global gene expression in liver of connexin32-wild-type and connexin32-deficient mice." International Journal of Cancer **115**: 861–869.
Stoger, R., P. Kubicka, C. G. Liu, T. Kafri, A. Razin, H. Cedar and D. P. Barlow (1993). "Maternal-specific methylation of the imprinted mouse Igf2r locus identifies the expressed locus as carrying the imprinting signal." Cell **73**(1): 61-71.
Strathmann, J., K. Paal, C. Ittrich, E. Krause, K. E. Appel, H. P. Glauert, A. Buchmann and M. Schwarz (2007). "Proteome analysis of chemically induced mouse liver tumors with different genotype." Proteomics **7**(18): 3318-31.
Strathmann, J., M. Schwarz, J. C. Tharappel, H. P. Glauert, B. T. Spear, L. W. Robertson, K. E. Appel and A. Buchmann (2006). "PCB 153, a non-dioxin-like tumor promoter, selects for beta-catenin (Catnb)-mutated mouse liver tumors." Toxicol Sci **93**(1): 34-40.
Szulwach, K. E., X. Li, Y. Li, C. X. Song, H. Wu, Q. Dai, H. Irier, A. K. Upadhyay, M. Gearing, A. I. Levey, A. Vasanthakumar, L. A. Godley, Q. Chang, X. Cheng, C. He and P. Jin (2011). "5-hmC-mediated epigenetic dynamics during postnatal neurodevelopment and aging." Nat Neurosci **14**(12): 1607-16.

Tahiliani, M., K. P. Koh, Y. Shen, W. A. Pastor, H. Bandukwala, Y. Brudno, S. Agarwal, L. M. Iyer, D. R. Liu, L. Aravind and A. Rao (2009). "Conversion of 5-methylcytosine to 5-hydroxymethylcytosine in mammalian DNA by MLL partner TET1." Science **324**(5929): 930-5.

Takada, S., M. Tevendale, J. Baker, P. Georgiades, E. Campbell, T. Freeman, M. H. Johnson, M. Paulsen and A. C. Ferguson-Smith (2000). "Delta-like and gtl2 are reciprocally expressed, differentially methylated linked imprinted genes on mouse chromosome 12." Curr Biol **10**(18): 1135-8.

Takahashi, N., A. Okamoto, R. Kobayashi, M. Shirai, Y. Obata, H. Ogawa, Y. Sotomaru and T. Kono (2009). "Deletion of Gtl2, imprinted non-coding RNA, with its differentially methylated region induces lethal parent-origin-dependent defects in mice." Hum Mol Genet **18**(10): 1879-88.

Thomson, J. P., H. Lempiainen, J. A. Hackett, C. E. Nestor, A. Muller, F. Bolognani, E. J. Oakeley, D. Schubeler, R. Terranova, D. Reinhardt, J. G. Moggs and R. R. Meehan (2012). "Non-genotoxic carcinogen exposure induces defined changes in the 5-hydroxymethylome." Genome Biol **13**(10): R93.

Torre, C., C. Perret and S. Colnot (2009). "Transcription dynamics in a physiological process: beta-catenin signaling directs liver metabolic zonation." Int J Biochem Cell Biol **43**(2): 271-8.

Varambally, S., B. Laxman, R. Mehra, Q. Cao, S. M. Dhanasekaran, S. A. Tomlins, J. Granger, A. Vellaichamy, A. Sreekumar, J. Yu, W. Gu, R. Shen, D. Ghosh, L. M. Wright, R. D. Kladney, R. Kuefer, M. A. Rubin, C. J. Fimmel and A. M. Chinnaiyan (2008). "Golgi protein GOLM1 is a tissue and urine biomarker of prostate cancer." Neoplasia **10**(11): 1285-94.

Vogelstein, B., D. Lane and A. J. Levine (2000). "Surfing the p53 network." Nature **408**(6810): 307-10.

Wang, B., S. H. Hsu, W. Frankel, K. Ghoshal and S. T. Jacob (2012a). "Stat3-mediated activation of microRNA-23a suppresses gluconeogenesis in hepatocellular carcinoma by down-regulating Glucose-6-phosphatase and peroxisome proliferator-activated receptor gamma, coactivator 1 alpha." Hepatology **56**(1): 186-97.

Wang, P., Z. Ren and P. Sun (2012b). "Overexpression of the long non-coding RNA MEG3 impairs in vitro glioma cell proliferation." J Cell Biochem **113**(6): 1868-74.

Wang, W., L. J. Zhao, Y. X. Tan, H. Ren and Z. T. Qi (2012c). "Identification of deregulated miRNAs and their targets in hepatitis B virus-associated hepatocellular carcinoma." World J Gastroenterol **18**(38): 5442-53.

Warburg, O. (1956). "On the origin of cancer cells." Science **123**(3191): 309-14.

Ward, P. S. and C. B. Thompson (2012). "Metabolic reprogramming: a cancer hallmark even warburg did not anticipate." Cancer Cell **21**(3): 297-308.

Watson, R. E. and J. I. Goodman (2002). "Effects of phenobarbital on DNA methylation in GC-rich regions of hepatic DNA from mice that exhibit different levels of susceptibility to liver tumorigenesis." Toxicol Sci **68**(1): 51-8.

Wilkinson, L. S., W. Davies and A. R. Isles (2007). "Genomic imprinting effects on brain development and function." Nat Rev Neurosci **8**(11): 832-43.

Wolffe, A. P. and J. J. Hayes (1999). "Chromatin disruption and modification." Nucleic Acids Res **27**(3): 711-20.

Wrzodek, C., J. Eichner and A. Zell (2012). "Pathway-based visualization of cross-platform microarray datasets." Bioinformatics.

Wrzodek, C., A. Schroder, A. Drager, D. Wanke, K. W. Berendzen, M. Kronfeld, K. Harter and A. Zell (2010). "ModuleMaster: a new tool to decipher transcriptional regulatory networks." Biosystems **99**(1): 79-81.

Wu, H. and Y. Zhang (2011). "Mechanisms and functions of Tet protein-mediated 5-methylcytosine oxidation." Genes Dev **25**(23): 2436-52.

Xiao, F., Z. Zuo, G. Cai, S. Kang, X. Gao and T. Li (2009). "miRecords: an integrated resource for microRNA-target interactions." Nucleic Acids Res **37**(Database issue): D105-10.

Yanai, H., K. Nakamura, S. Hijioka, A. Kamei, T. Ikari, Y. Ishikawa, E. Shinozaki, N. Mizunuma, K. Hatake and A. Miyajima (2010). "Dlk-1, a cell surface antigen on foetal hepatic stem/progenitor cells, is expressed in hepatocellular, colon, pancreas and breast carcinomas at a high frequency." J Biochem **148**(1): 85-92.

Yang, H., Y. Liu, F. Bai, J. Y. Zhang, S. H. Ma, J. Liu, Z. D. Xu, H. G. Zhu, Z. Q. Ling, D. Ye, K. L. Guan and Y. Xiong (2012). "Tumor development is associated with decrease of TET gene expression and 5-methylcytosine hydroxylation." Oncogene.

Yeh, H. H., R. Giri, T. Y. Chang, C. Y. Chou, W. C. Su and H. S. Liu (2009). "Ha-ras oncogene-induced Stat3 phosphorylation enhances oncogenicity of the cell." DNA Cell Biol **28**(3): 131-9.

Ying, L., Y. Huang, H. Chen, Y. Wang, L. Xia, Y. Chen, Y. Liu and F. Qiu (2013). "Downregulated MEG3 activates autophagy and increases cell proliferation in bladder cancer." Mol Biosyst.

Yuneva, M. O., T. W. Fan, T. D. Allen, R. M. Higashi, D. V. Ferraris, T. Tsukamoto, J. M. Mates, F. J. Alonso, C. Wang, Y. Seo, X. Chen and J. M. Bishop (2012). "The metabolic profile of tumors depends on both the responsible genetic lesion and tissue type." Cell Metab **15**(2): 157-70.

Zeller, E., K. Mock, M. Horn, S. Colnot, M. Schwarz and A. Braeuning (2012). "Dual-specifi city phosphatases are targets of the Wnt/β-catenin pathway and candidate mediators of β-catenin/Ras signaling interactions." Biological Chemistry **393**: 1183-1191.

Zhang, G., V. Budker and J. A. Wolff (1999). "High levels of foreign gene expression in hepatocytes after tail vein injections of naked plasmid DNA." Hum Gene Ther **10**(10): 1735-7.

Zhang, Z., S. Kobayashi, A. C. Borczuk, R. S. Leidner, T. Laframboise, A. D. Levine and B. Halmos (2010). "Dual specificity phosphatase 6 (DUSP6) is an ETS-regulated negative feedback mediator of oncogenic ERK signaling in lung cancer cells." Carcinogenesis **31**(4): 577-86.

Zhou, Y., P. Cheunsuchon, Y. Nakayama, M. W. Lawlor, Y. Zhong, K. A. Rice, L. Zhang, X. Zhang, F. E. Gordon, H. G. Lidov, R. T. Bronson and A. Klibanski (2010). "Activation of paternally expressed genes and perinatal death caused by deletion of the Gtl2 gene." Development **137**(16): 2643-52.

Zhou, Y., X. Zhang and A. Klibanski (2012). "MEG3 noncoding RNA: a tumor suppressor." J Mol Endocrinol **48**(3): R45-53.

Zhou, Y., Y. Zhong, Y. Wang, X. Zhang, D. L. Batista, R. Gejman, P. J. Ansell, J. Zhao, C. Weng and A. Klibanski (2007). "Activation of p53 by MEG3 non-coding RNA." J Biol Chem **282**(34): 24731-42.

Appendix

A) Genes significantly dysregulated in *Ctnnb1*-mutated tumors vs. adjacent non-tumor tissue (log-ratio >1.0, p-value <0.05).

Gene symbol	EntrezGene ID	Log-ratio	p-value	Gene name
Abca8a	217258	-1.09	0.05	ATP-binding cassette, sub-family A (ABC1), member 8a
Abcb1a	18671	1.84	0.01	ATP-binding cassette, sub-family B (MDR/TAP), member 1a
Abcc4	239273	2.78	0.03	ATP-binding cassette, sub-family C, member 4
Abcc9	20928	-1.40/-1.01	0.01	ATP-binding cassette, sub-family C, member 9
Abhd12	76192	1.67	0.01	Abhydrolase domain containing 12
Abi3bp	320712	-1.71	0.00	ABI family, member 3 (NESH) binding protein
Acacb	100705	-1.09	0.02	Acetyl-CoA carboxylase beta
Accn5	58170	-1.24	0.02	Amiloride-sensitive cation channel 5, intestinal
Acly	104112	-1.00	0.01	ATP citrate lyase
Acot9	56360	1.59	0.01	Acyl-CoA thioesterase
Acsl4	50790	1.35/1.01/1.63	0.02	Long-chain-fatty-acid-CoA ligase 4
Adam23	23792	-1.99	0.01	Disintegrin and metalloproteinase domain-containing protein 23
Adamdec1	58860	-2.04	0.00	A disintegrin and metalloproteinase domain-like protein decysin-1
Adamtsl1	77739	-1.47	0.00	A disintegrin and metalloproteinase with thrombospondin motifs)-like 1
Adamtsl4	229595	2.60	0.00	A disintegrin and metalloproteinase with thrombospondin motifs)-like 4
Adra2b	11552	-1.04	0.01	alpha-2B adrenergic receptor
Adss	11566	1.11	0.00	Adenylosuccinate synthase
Afp	11576	3.61/4.33/4.35	0.01/0.01/0.00	Alpha-Fetal Protein
Agfg1	15463	1.00	0.01	Arf-GAP domain and FG repeats-containing protein 1
Agl	77559	1.11/1.01/1.09	0.01/0.02/0.01	Glycogen debranching enzyme
Agxt	11611	-1.53	0.01	Serine—pyruvate aminotransferase
Agxt2l1	71760	-5.23/-4.91	0.00	Alanine-glyoxylate aminotransferase 2-like 1
Ahr	11622	1.44	0.00	Aryl hydrocarbon receptor
AI413582	106672	1.20	0.04	N/A
Airn	104103	1.96	0.00	Antisense of IGF2R
Ak4	11639	-2.80/-2.75	0.00/0.01	Adenylate kinase 4
Akap7	432442	-1.11	0.02	A-kinase anchor protein 7
Akr1b7	11997	2.02	0.01	Aldo-keto reductase family 1, member B7
Akr1e1	56043	1.29	0.03	Aldo-keto reductase family 1, member E1
Aldh1b1	72535	-3.61	0.01	Aldehyde dehydrogenase 1 family, member B1
Aldh3a2	11671	1.86	0.00	Aldehyde dehydrogenase 3 family, member A2
Amdhd1	71761	-2.90/-2.69	0.00/0.01	Amidohydrolase domain containing 1
Amigo1	229715	-1.01	0.01	Adhesion molecule with Ig-like domain 1
Angptl6	70726	-1.09	0.01	Angiopoietin-like 6
Ankrd33b	67434	-1.12	0.03	Ankyrin repeat domain 33B
Anln	68743	1.46	0.02	Actin-binding protein anillin
Anxa13	69787	-1.48	0.01	Annexin A13
Anxa2	12306	2.28	0.00	Annexin A2
Anxa7	11750	1.04	0.01	Annexin A7
Anxa9	71790	1.31	0.01	Annexin A9
Aox1	11761	1.05	0.02	Aldehyde oxidase 1
Aph1b	208117	1.06	0.01	Anterior pharynx defective 1 homolog B
Aplnr	23796	3.60	0.01	Apelin receptor
Apoa5	66113	-1.16	0.02	Apolipoprotein A-V
Aprt	11821	1.01	0.02	Adenine phosphoribosyltransferase
Aqp4	11829	-3.76	0.00	Aquaporin 4
Aqp7	11832	1.19/1.79	0.02/0.03	Aquaporin 7
Arf6	11845	1.44	0.05	ADP-ribosylation factor 6
Arg2	11847	2.99/3.43	0.03/0.01	Arginase 2
Arhgap11a	228482	1.49	0.01	Rho GTPase activating protein 11A
Arhgef2	16800	1.19/1.01	0.00/0.02	Rho guanine nucleotide exchange factor 2
Arl2bp	107566	1.07	0.05	ADP-ribosylation factor-like 2 binding protein
Armcx3	71703	-1.24	0.00	Armadillo repeat-containing X-linked protein 3
As3mt	57344	-1.51	0.04	Arsenic (+3 oxidation state) methyltransferase
Asl	109900	-1.25	0.00	Argininosuccinate lyase
Aspg	104816	-3.73	0.00	Asparaginase homolog

Gene symbol	EntrezGene ID	Log-ratio	p-value	Gene name
Aspm	12316	2.10	0.00	Abnormal spindle-like microcephaly-associated protein
Ass1	11898	-1.66/-1.27	0.01/0.04	Argininosuccinate synthase 1
Atp2b2	11941	1.41	0.04	Ca(2+)-pumping ATPase isoform PMCA2
Atp6v0d2	242341	1.29	0.04	ATPase, H+ transporting, lysosomal 38kDa, V0 subunit d2
Atrnl1	226255	-1.89	0.01	Attractin-like 1
Aurka	20878	1.59	0.01	Aurora kinase a
Aurkb	20877	1.11	0.05	Aurora kinase b
Avpr1a	54140	1.93/2.19	0.01/0.01	Arginine vasopressin receptor 1A
Bace2	56175	1.37	0.01	beta-site APP-cleaving enzyme 2
Bag4	67384	-1.03	0.00	BAG family molecular chaperone regulator 4
Bche	12038	-1.09	0.01	*Butyrylcholinesterase*
Bdh2	69772	-2.96	0.00	3-hydroxybutyrate dehydrogenase, type 2
Bgn	12111	-1.41/-1.38/-1.27	0.01/0.01/0.00	biglycan
Bik	12124	-1.79	0.02	Bcl-2-interacting killer
Birc5	11799	1.90	0.02	Baculoviral IAP repeat containing 5
Blvrb	233016	1.86	0.00	biliverdin reductase B (flavin reductase (NADPH))
Bmp2	12156	-1.76	0.01	Bone morphogenetic protein 2
Bmp5	12160	-1.52	0.01	Bone morphogenetic protein 5
Btc	12223	1.25	0.02	Betacellulin
Btg1	12226	-1.03	0.04	B-cell translocation gene 1, anti-proliferative
Bub1	12235	1.81	0.01	Budding uninhibited by benzimidazoles 1 homolog
C8a	230558	-1.47	0.03	Bomplement component 8, alpha polypeptide
Cadm1	54725	-1.08	0.02	Cell adhesion molecule 1
Cadps2	320405	-3.19	0.01	Ca2+-dependent activator protein for secretion 2
Calcrl	54598	-1.12	0.01	Calcitonin receptor-like
Calml4	75600	3.52	0.00	Calmodulin-like 4
Camkk2	207565	-1.80/-1.33/-1.10	0.00/0.00/0.01	Calcium/calmodulin-dependent protein kinase kinase 2, beta
Car14	23831	-1.43	0.04	Carbonic anhydrase 14
Car2	12349	1.85	0.00	Carbonic anhydrase 2
Casp1	12362	2.09	0.01	Caspase 1
Casp12	12364	2.35/2.38	0.01/0.01	Caspase 12
Casp4	12363	1.11	0.05	Caspase 4
Cav1	12389	1.06	0.02	Caveolin 1
Cbs	12411	-1.28	0.04	Cystathionine-β-synthase
Ccbe1	320924	-1.45	0.00	Collagen and calcium binding EGF domains 1
Ccdc120	54648	1.76	0.01	Coiled-coil domain containing 120
Ccdc28b	66264	-1.08	0.02	Coiled-coil domain containing 28b
Ccdc99	70385	1.20	0.01	Coiled-coil domain containing 99
Ccna2	12428	1.20/1.30	0.04/0.01	Cyclin-A2
Ccnb1	268697	1.79/2.23/2.28	0.02/0.00/0.01	Cyclin-B1
Ccnb2	12442	2.27	0.00	Cyclin-B2
Ccnl2	56036	-1.04	0.01	Cyclin-L2
Cd163	93671	-1.67	0.01	Cluster of Differentiation 163
Cd200	17470	1.28	0.04	Cluster of Differentiation 200
Cd2ap	12488	1.05/1.47/1.71	0.00/0.00/0.00	CD2-associated protein
Cd34	12490	1.24	0.04	Hematopoietic progenitor cell antigen CD34
Cd5l	11801	-1.43	0.04	CD5 antigen-like
Cd9	12527	1.24	0.03	CD9 antigen
Cd93	17064	1.14/1.17	0.01/0.01	CD93 antigen
Cdc20	107995	1.43	0.03	Cell-division cycle protein 20
Cdc6	23834	1.04	0.03	Cell-division cycle protein 6
Cdca3	14793	1.53	0.02	Cell division cycle associated 3
Cdca8	52276	1.08/1.14/1.84	0.02/0.02/0.00	Cell division cycle associated 8
Cdhr2	268663	2.11	0.02	Cadherin-related family member 2
Cdk1	12534	1.71	0.01	Cyclin-dependent kinase 1
Cdkn2c	12580	1.50	0.00	Cyclin-dependent kinase 4 inhibitor C
Cdkn3	72391	1.96	0.01	Cyclin-dependent kinase 3 inhibitor
Cds2	110911	1.13	0.00	CDP-diacylglycerol synthase (phosphatidate cytidylyltransferase) 2
Celsr1	12614	-1.43	0.02	Cadherin EGF LAG seven-pass G-type receptor 1
Cenpa	12615	1.08	0.04	Centromere protein A
Cenpf	108000	1.51	0.03	Centromere protein F
Cenpi	102920	1.20	0.02	Centromere protein I
Cenpl	70454	1.90	0.00	Centromere protein L
Cenpp	66336	1.13/1.51	0.04/0.01	Centromere protein P
Cenpt	320394	1.12	0.01	Centromere protein T
Cep192	70799	1.31	0.04	Centrosomal protein of 192 kDa
Cep55	74107	1.83	0.01	Centrosomal protein of 55 kDa
Ces1e	13897	-2.67	0.00	Carboxylesterase 1E
Ces1f	234564	-2.15	0.04	Carboxylesterase 1F
Cfhr2	545366	-1.12	0.00	Complement factor H-related protein 2

Gene symbol	EntrezGene ID	Log-ratio	p-value	Gene name
Cgrrf1	68755	1.03	0.03	Cell growth regulator with ring finger domain 1
Chrna4	11438	-1.15	0.01	Neuronal acetylcholine receptor subunit alpha-4
Cib2	56506	2.12	0.02	Calcium and integrin binding family member 2
Cisd1	52637	-1.13	0.02	CDGSH iron sulfur domain 1
Ckap2	80986	1.71	0.02	Cytoskeleton-associated protein 2
Cldn2	12738	1.14	0.02	Claudin-2
Clec1b	56760	-1.10	0.01	C-type lectin domain family 1 member B
Clec4b1	69810	1.09	0.05	C-type lectin domain family 1 member B1
Clec4f	51811	-1.95	0.02	C-type lectin domain family 4, member F
Clmn	94040	-1.69/-1.67	0.01/0.01	Calmin (calponin-like, transmembrane)
Cln6	76524	1.24	0.03	Ceroid-lipofuscinosis neuronal protein 6
Cmah	12763	-1.14	0.01	Putative cytidine monophosphate-N-acetylneuraminic acid hydroxylase-like protein
Col13a1	12817	-1.06	0.00	Collagen, type XIII, alpha 1
Col14a1	12818	-1.15	0.02	Collagen, type XIV, alpha 1
Col27a1	373864	-1.23/-1.18	0.00/0.01	Collagen, type XXVII, alpha 1
Col4a1	12826	1.01	0.03	Collagen, type IV, alpha 1
Col4a3bp	68018	1.11	0.05	Collagen type IV alpha-3-binding protein
Colec10	239447	-3.14	0.02	Collectin sub-family member 10
Colec11	71693	-1.79/-1.34	0.00/0.01	Collectin sub-family member 11
Cox7a1	12865	-1.13	0.03	Cytochrome c oxidase polypeptide 7A1, mitochondrial
Cps1	227231	-2.17	0.02	Carbamoyl-phosphate synthase 1
Crem	12916	-1.08	0.04	cAMP responsive element modulator
Crim1	50766	1.32	0.02	Cysteine-rich motor neuron 1 protein
Crls1	66586	1.16	0.05	Cardiolipin synthase 1
Cryl1	68631	-3.14/-2.83/-1.55	0.00/0.00/0.00	Crystallin, lambda 1
Cs	12974	1.08	0.01	Citrate synthase
Csad	246277	1.58	0.03	Cysteine sulfinic acid decarboxylase
Csn3	12994	1.30	0.02	Kappa-casein
Csprs	114564	1.04	0.01	Component of Sp100-rs
Csrp2	13008	1.43	0.03	Cysteine and glycine-rich protein 2
Cstb	13014	1.45/1.92	0.00/0.00	Cystatin B
Ctbs	74245	1.28/1.37	0.03/0.02	Di-N-acetylchitobiase
Cth	107869	-1.10	0.02	Cystathionine gamma-lyase
Ctnnbip1	67087	-1.46/-1.44	0.00/0.00	Beta-catenin-interacting protein 1
Ctps2	55936	1.51	0.01	CTP synthase 2
Ctsc	13032	-1.57	0.01	Cathepsin C
Cttn	13043	1.01	0.03	Cortactin
Cxcl10	15945	1.79	0.02	C-X-C motif chemokine 10
Cxcl12	20315	-1.80/-1.51	0.01/0.01	C-X-C motif chemokine 12
Cyfip2	76884	-2.36/-2.41	0.01/0.01	Cytoplasmic FMR1-interacting protein 2
Cyp2f2	13107	-4.19	0.03	Cytochrome P450 2F2
Cyp2j5	13109	-1.49	0.04	Cytochrome P450 2J5
Cyp2u1	71519	-1.28	0.00	Cytochrome P450 2U1
Cyp46a1	13116	-3.32	0.00	Cytochrome P450 46A1
Cyp7a1	13122	1.62/2.36	0.03/0.00	Cytochrome P450 7A1 (Cholesterol 7 alpha-hydroxylase)
Cyp8b1	13124	-1.20	0.01	Cytochrome P450 8B1
Dab2ip	69601	1.08	0.01	Disabled homolog 2-interacting protein
Dach2	93837	-1.42	0.04	Dachshund homolog 2
Dapk1	69635	-1.23	0.01	Death-associated protein kinase 1
Dcdc2a	195208	-1.25	0.00	Doublecortin domain containing 2a
Dclk3	245038	-1.79	0.00	Doublecortin-like kinase 3
Dcn	13179	-2.04	0.01	Decorin
Dct	13190	-3.25	0.02	Dopachrome tautomerase
Ddi2	68817	-1.35/-1.02	0.00/0.00	DNA-damage inducible 1 homolog 2
Dhrs1	52585	1.09	0.02	Dehydrogenase/reductase SDR family member 1
Dhx32	101437	1.08	0.04	Putative pre-mRNA-splicing factor ATP-dependent RNA helicase
Dmrta1	242523	-1.74	0.00	DMRT-like family A1
Dnajc10	66861	1.01	0.01	DnaJ homolog subfamily C member 10
Dnajc24	99349	1.01	0.01	DnaJ homolog subfamily C member 24
Dnase1l3	13421	-1.37	0.02	Deoxyribonuclease gamma
Dnase2a	13423	1.04	0.03	Deoxyribonuclease II alpha
Dpp7	83768	1.21	0.00	Dipeptidyl-peptidase 2
Dpt	56429	-2.01	0.01	Dermatopontin
Dpyd	99586	-1.12	0.01	Dihydropyrimidine dehydrogenase [NADP+]
Dynll1	56455	1.24	0.00	Dynein light chain 1, cytoplasmic
Dyrk3	226419	2.00	0.00	Dual specificity tyrosine-phosphorylation-regulated kinase 3
E130308A19Rik	230259	-1.02	0.05	N/A
Ecm1	13601	-1.51	0.01	Extracellular matrix protein 1
Ect2	13605	2.11	0.01	Epithelial cell transforming sequence 2 oncogene
Efemp1	216616	-2.36	0.01	EGF containing fibulin-like extracellular matrix protein 1

Gene symbol	EntrezGene ID	Log-ratio	p-value	Gene name
Efna5	13640	-1.36	0.01	Ephrin-A5
Egfr	13649	-1.80/-1.62	0.00/0.00	Epidermal growth factor receptor
Ehd4	98878	1.33	0.02	EH-domain containing 4
Emcn	59308	1.77	0.01	Endomucin
Emp1	13730	1.18	0.04	Epithelial membrane protein 1
Emp2	13731	1.38	0.03	Epithelial membrane protein 2
Enah	13800	-1.14	0.01	Protein enabled homolog
Endod1	71946	1.18/1.44/1.59/1.74/1.82	0.01/0.01/0.00/0.01/0.00	Endonuclease domain containing 1
Enho	69638	-1.42/-1.18	0.02/0.03	Energy homeostasis associated
Entpd5	12499	1.41/1.05/1.20	0.01/0.01/0.00	ctonucleoside triphosphate diphosphohydrolase 5
Epcam	17075	-1.35	0.01	Epithelial cell adhesion molecule
Erp27	69187	-1.47	0.00	Endoplasmic reticulum protein 27
Esco2	71988	2.52	0.01	Establishment of cohesion 1 homolog 2
Esm1	71690	1.31	0.05	Endothelial cell-specific molecule 1
Etl4	208618	1.02	0.01	Enhancer trap locus 4
Ets2	23872	1.04	0.00	Protein C-ets-2
Fam101b	76566	1.30	0.00	Family with sequence similarity 101, member B
Fam171a1	269233	1.92	0.00	Family with sequence similarity 171, member A1
Fam198b	68659	1.16	0.03	Family with sequence similarity 198, member B
Fam25c	69134	1.51	0.05	Family with sequence similarity 25, member C
Fam46a	212943	-1.56	0.04	Family with sequence similarity 46, member A
Fam46c	74645	-1.63	0.03	Family with sequence similarity 46, member C
Fam47e	384198	-1.63	0.03	Family with sequence similarity 47, member E
Fam55b	78252	2.59	0.01	Family with sequence similarity 55, member B
Fam89a	69627	1.12	0.03	Family with sequence similarity 89, member A
Fbp1	14121	-1.26	0.01	Fructose-1,6-bisphosphatase 1
Fbxo31	76454	-1.12	0.00	F-box protein 31
Fcna	14133	-1.15	0.05	Ficolin A
Fdps	110196	1.52	0.05	Farnesyl diphosphate synthase
Fez2	225020	1.03	0.00	Fasciculation and elongation protein zeta-2
Fgf21	56636	1.87	0.05	Fibroblast growth factor 21
Fgfr2	14183	-2.30/-1.36	0.00/0.03	Fibroblast growth factor 2
Fhl1	14199	-1.06	0.04	Four and a half LIM domains 1
Fkbp11	66120	1.29	0.01	FK506 binding protein 11
Fkbp1a	14225	1.14	0.01	Peptidyl-prolyl cis-trans isomerase
Fn3k	63828	-1.09	0.00	Fructosamine-3-kinase
Folh1	53320	1.75	0.02	Folate hydrolase (prostate-specific membrane antigen) 1
Folr2	14276	-1.42	0.01	Folate receptor beta
Foxp1	108655	-1.20/-1.00	0.03/0.03	Forkhead box protein P1
Foxp2	114142	-1.21	0.02	Forkhead box protein P2
Frk	14302	1.11/1.66	0.00/0.01	Fyn-related kinase
Ftcd	14317	-1.47	0.03	Formiminotransferase cyclodeaminase
Fundc1	72018	1.08	0.01	FUN14 domain containing 1
Gabra3	14396	-1.53	0.02	Gamma-aminobutyric acid receptor subunit alpha-3
Gars	353172	1.10	0.00	Glycyl-tRNA synthetase
Gas1	14451	-2.85/-1.75	0.00/0.00	Growth arrest-specific protein 1
Gas7	14457	1.36	0.02	Growth arrest-specific protein 7
Gca	227960	1.45/1.54	0.00/0.01	Grancalcin
Gdf10	14560	-2.34	0.00	Growth differentiation factor 10
Gdf2	12165	-1.42	0.00	Growth differentiation factor 2
Gins2	272551	1.38	0.02	GINS complex subunit 2 (Psf2 homolog)
Gipc2	54120	3.67	0.01	GIPC PDZ domain containing family, member 2
Gldc	104174	-3.53	0.01	Glycine dehydrogenase (decarboxylating)
Gls2	216456	-4.18	0.00	Glutaminase 2
Golm1	105348	1.95	0.01	Golgi membrane protein 1
Got1	14718	-3.17	0.04	Aspartate aminotransferase, cytoplasmic
Gpat2	215456	-1.09	0.00	glycerol-3-phosphate acyltransferase 2, mitochondrial
Gpc3	14734	4.06	0.00	Glypican-3
Gpm6a	234267	-1.70	0.00	Glycoprotein M6A
Gpx7	67305	1.63	0.00	Glutathione peroxidase 7
Gramd1b	235283	1.65/1.55	0.01/0.01	GRAM domain containing 1B
Grhl1	195733	1.21	0.01	Grainyhead-like 1
Grm8	14823	-2.11	0.00	Glutamate receptor, metabotropic 8
Gsn	227753	-2.12/-2.06/-2.05/-1.40	0.00/0.00/0.01/0.00	Gelsolin
Gsr	14782	1.33	0.05	Glutathione reductase
Gsta4	14860	1.08	0.03	Glutathione S-transferase A4
Gstk1	76263	-1.04	0.01	Glutathione S-transferase kappa 1
Gstm2	14863	1.79	0.00	Glutathione S-transferase Mu 2

Gene symbol	EntrezGene ID	Log-ratio	p-value	Gene name
Gstm3	14864	2.00	0.00	Glutathione S-transferase Mu 3
Gstm4	14865	1.18	0.01	Glutathione S-transferase Mu 4
Gstm6	14867	1.86	0.02	Glutathione S-transferase Mu 6
Gulo	268756	1.45	0.01	L-gulonolactone oxidase
Gyg	27357	1.44	0.00	Glycogenin 1
Gyk	14933	1.54	0.01	Glycerol kinase
Gypc	71683	-1.19	0.01	Glycophorin C
Hal	15109	-4.35	0.00	Histidine ammonia lyase
Hamp	84506	-3.23/-3.20	0.01/0.01	Hepcidin
Hamp2	66438	-3.61	0.00	Hepcidin 2
Hand2	15111	-1.83	0.00	Heart- and neural crest derivatives-expressed protein 2
Hfe2	69585	1.28	0.01	Hemochromatosis type 2
Hist1h1c	50708	1.27/1.58	0.05/0.00	Histone cluster 1, H1c
Hmgb2	97165	1.31	0.03	High-mobility group protein B2
Hmgcs1	208715	1.37/1.45	0.01/0.03	3-hydroxy-3-methylglutaryl-CoA synthase 1
Hmmr	15366	1.22/1.22/1.46	0.01/0.05/0.01	Hyaluronan-mediated motility receptor
Hn1	15374	1.26	0.00	Hematological and neurological expressed 1 protein
Hsd17b13	243168	-1.63/-1.31	0.01/0.02	Hydroxysteroid (17-beta) dehydrogenase 13
Hsd17b7	15490	1.07	0.04	Hydroxysteroid (17-beta) dehydrogenase 7
Hsf2bp	74377	1.93	0.01	Heat shock transcription factor 2 binding protein
Iars	105148	1.26	0.04	Isoleucyl-tRNA synthetase
Ica1	15893	1.51	0.03	Islet cell autoantigen 1
Icos	54167	-1.04	0.00	Inducible T-cell co-stimulator
Idh3a	67834	1.24	0.01	Isocitrate dehydrogenase [NAD] subunit alpha
Ifi27l2b	217845	1.39	0.00	Interferon, alpha-inducible protein 27 like 2B
Ifitm1	68713	-1.87	0.00	Interferon-induced transmembrane protein 1
Ifngr1	15979	1.40	0.00	Interferon gamma receptor 1
Ifngr2	15980	1.10	0.03	Interferon gamma receptor 2
Igf1	16000	-2.15/-1.90	0.04/0.05	Insulin-like growth factor 1
Igf2r	16004	1.55	0.00	Insulin-like growth factor 2 receptor
Igfbp1	16006	1.55	0.00	Insulin-like growth factor-binding protein 1
Ikbkb	16150	1.26	0.02	Inhibitor of kappa light polypeptide gene enhancer in B-cells, kinase beta
Ikbkg	16151	1.01	0.05	Inhibitor of kappa light polypeptide gene enhancer in B-cells, kinase gamma
Il13ra1	16164	-1.42/-1.17	0.01/0.02	Interleukin 13 receptor, alpha 1
Il1rap	16180	-1.09	0.02	Interleukin-1 receptor accessory protein
Impact	16210	1.10	0.01	Impact homolog
Irf2	16363	-1.17	0.00	Interferon regulatory factor 2
Islr	26968	-1.15	0.03	Immunoglobulin superfamily containing leucine-rich repeat
Itga6	16403	1.06	0.01	Integrin alpha-6
Ivd	56357	-1.09	0.04	Isovaleryl-CoA dehydrogenase
Jub	16475	2.08	0.02	Ajuba
Kalrn	545156	-1.43	0.00	Kalirin
Kcnk1	16525	2.01/2.12	0.01/0.00	Potassium channel subfamily K member 1
Kcnt2	240776	-1.75	0.00	Potassium channel subfamily T, member 2
Kctd12b	207474	1.01	0.03	Kctd12b potassium channel tetramerisation domain containing 12b
Kif11	16551	1.05/1.41	0.02/0.01	Kinesin family member 11
Kif20a	19348	1.95	0.01	Kinesin family member 20A
Kif20b	240641	1.39	0.04	Kinesin family member 20B
Kif22	110033	1.09/1.32	0.03/0.01	Kinesin family member 22
Klf10	21847	-1.37	0.01	Krueppel-like factor 10
Klf6	23849	1.39/1.80	0.02/0.01	Krueppel-like factor 6
Kpnb1	16211	1.06	0.04	Karyopherin (importin) beta 1
Krt4	16682	3.80/2.96	0.00/0.01	Keratin 4
Kynu	70789	-1.88/-1.77	0.01/0.00	Kynureninase
Lama3	16774	-1.57	0.01	Laminin, alpha 3
Lats2	50523	1.08	0.03	Large tumor suppressor, homolog 2
Lcn2	16819	2.96	0.01	Lipocalin-2
Lect2	16841	1.59	0.01	Leukocyte cell-derived chemotaxin-
Lepr	16847	-1.77	0.01	Leptin receptor
Lgals3	16854	2.23	0.02	Galectin-3
Lgr5	14160	2.57	0.05	Leucine-rich repeat-containing G-protein coupled receptor 5
Lhx2	16870	-1.61	0.00	LIM homeobox 2
Lix1l	280411	-1.02	0.00	Lix1 homolog (mouse)- like
Lmod3	320502	-1.65	0.02	Leiomodin-3
Lpin2	64898	1.27	0.00	Lipin 2
Lpl	16956	2.00/1.33	0.00/0.01	Lipoprotein lipase
Lrat	79235	-2.13	0.01	Lecithin retinol acyltransferase
Lrrc39	109245	1.50	0.03	Leucine-rich repeat-containing protein 39

Gene symbol	EntrezGene ID	Log-ratio	p-value	Gene name
Lrtm1	319476	-1.68	0.00	Leucine-rich repeats and transmembrane domains 1
Lum	17022	-1.29	0.04	Lumican
Ly6d	17068	3.40	0.01	Lymphocyte antigen 6 complex, locus D
Ly75	17076	1.00	0.04	Lymphocyte antigen 75
Mab21l3	242125	2.03	0.01	Mab-21-like 3
Macrod1	107227	-1.45	0.01	MACRO domain containing 1
Mad2l1	56150	1.64	0.00	MAD2 mitotic arrest deficient-like 1
Maf	17132	-1.03	0.05	V-maf musculoaponeurotic fibrosarcoma oncogene homolog
Mafb	16658	-1.42	0.01	V-maf musculoaponeurotic fibrosarcoma oncogene homolog B
Maged2	80884	1.06	0.04	Melanoma-associated antigen D2
Mamdc2	71738	-2.11	0.00	Melanoma-associated antigen C2
Maoa	17161	2.33/2.50	0.02/0.01	Monoamine oxidase A
Mapre2	212307	-1.47/-1.46	0.00/0.03	Microtubule- associated protein, RP/EB family, member 2
Mark1	226778	-1.11	0.00	MAP/microtubule affinity -regulating kinase 1
Marveld3	73608	-1.85	0.00	MARVEL domain containing 3
Masp1	17174	-1.26/-1.24	0.01/0.05	Mannan-binding lectin serine protease 1
Mcart1	230125	-2.82/-1.63/-1.62	0.00/0.00/0.00	Mitochondrial carrier triple repeat 1
Mcm10	70024	-1.43	0.04	Minichromosome maintenance complex component 10
Mcm2	17216	1.18	0.01	Minichromosome maintenance complex component 2
Mcm6	17219	1.38	0.02	Minichromosome maintenance complex component 6
Mfsd2a	76574	-3.41	0.01	Major facilitator superfamily domain-containing protein 2
Mgst3	66447	1.47	0.01	Microsomal glutathione S-transferase 3
Mis18bp1	217653	1.02/1.24	0.04/0.03	MIS18 binding protein 1
Mki67	17345	1.50	0.03	Antigen identified by monoclonal antibody Ki-67
Mmd2	75104	-1.29	0.02	Monocyte to macrophage differentiation-associated 2
Mmgt1	236792	1.10	0.05	Membrane magnesium transporter 1
Mmp13	17386	1.79	0.01	Matrix metallopeptidase 13
Mmp15	17388	-1.16	0.04	Matrix metallopeptidase 15
Mn1	433938	-2.59	0.00	Meningioma (disrupted in balanced translocation) 1
Mosc1	66112	-2.22	0.00	MOCO sulphurase C-terminal domain containing 1
Mpp1	17524	1.23	0.00	Membrane protein, palmitoylated 1, 55kDa
Mrps18a	68565	1.07	0.03	Mitochondrial ribosomal protein S18A
Ms4a4d	66607	-1.73	0.00	Membrane-spanning 4-domains, subfamily A, member 4D
Msi2	76626	-1.07	0.01	Musashi homolog 2
Mt1	17748	-1.22	0.05	Melatonin receptor 1A
Mthfd2	17768	1.53	0.01	Methylenetetrahydrofolate dehydrogenase (NADP+ dependent) 2
Mtmr11	194126	1.86	0.00	Myotubularin related protein 11
Mup10	100039008	-3.68	0.03	Major urinary protein 10
Mup3	17842	-2.74	0.02	Major urinary protein 3
Mup5	17844	-1.71	0.01	Major urinary protein 5
Mustn1	66175	-1.02	0.01	Musculoskeletal, embryonic nuclear protein 1
Mybl1	17864	1.36	0.02	V-myb myeloblastosis viral oncogene homolog (avian)-like 1
Myc	17869	1.64	0.00	V-myc myelocytomatosis viral oncogene homolog
Mycn	18109	2.17	0.00	V-myc myelocytomatosis viral related oncogene, neuroblastoma derived
Myo15b	217328	1.04	0.00	Myosin XVB pseudogene
N6amt2	68043	1.24	0.02	N-6 adenine-specific DNA methyltransferase 2 (putative)
Nap1l1	53605	1.03	0.02	Nucleosome assembly protein 1-like 1
Napepld	242864	1.22	0.00	N-acyl phosphatidylethanolamine phospholipase D
Ncapg2	76044	1.55	0.00	Non-SMC condensin II complex, subunit G2
Ndn	17984	-1.20/-1.20/-1.18	0.00/0.00/0.00	Necdin
Ndrg1	17988	1.37/1.47/1.93	0.03/0.04/0.01	N-myc downstream regulated 1
Neat1	66961	1.65	0.00	Nuclear enriched abundant transcript 1
Neb	17996	-2.24	0.01	Nebulin
Nek2	18005	1.53	0.01	NIMA (never in mitosis gene a)-related kinase 2
Nek6	59126	1.17	0.00	NIMA (never in mitosis gene a)-related kinase 6
Net1	56349	1.23	0.01	Neuroepithelial cell transforming 1
Nfia	18027	-1.14	0.01	Nuclear factor I/A
Nhp2	52530	1.13	0.01	NHP2 ribonucleoprotein homolog

Gene symbol	EntrezGene ID	Log-ratio	p-value	Gene name
Nid1	18073	1.33/1.98	0.03/0.00	Nidogen 1
Nlk	18099	1.36	0.03	Nemo-like kinase
Nnmt	18113	-3.59	0.02	Nicotinamide N- methyltransferase
Npc1l1	237636	1.91	0.05	Niemann-Pick C1-like protein 1
Npdc1	18146	1.94	0.00	Neural proliferation, differentiation and control, 1
Nptx1	18164	1.59/3.18	0.01/0.00	Neuronal pentraxin I
Nqo1	18104	1.96	0.04	NAD(P)H dehydrogenase , quinone 1
Nsdhl	18194	1.33	0.03	Sterol-4-alpha-carboxylate 3-dehydrogenase
Nt5e	23959	2.55/1.69	0.01/0.02	5'-nucleotidase
Ntn1	18208	-1.60	0.00	Netrin-1
Nubp1	26425	1.02	0.04	Nucleotide binding protein 1
Nudt7	67528	-1.03	0.01	Nudix (nucleoside diphosphate linked moiety X)-type motif 7
Nusap1	108907	2.46	0.00	Nucleolar and spindle associated protein 1
Odf3b	70113	-1.59	0.00	Outer dense fiber of sperm tails 3B
Olfm1	56177	-1.27	0.01	Olfactomedin 1
Olfm3	229759	-4.04/-4.03	0.00/0.00	Olfactomedin 3
Ostc	66357	1.04	0.01	Oligosaccharyltransferase complex subunit
Otc	18416	-1.46/-1.53	0.03/0.03	Ornithine carbamoyltransferase
Pbk	52033	1.65	0.02	PDZ binding kinase
Pbld2	67307	-1.24	0.01	Phenazine biosynthesis-like protein domain containing 2
Pcdh17	219228	1.74/1.76	0.00/0.00	Protocadherin-17
Pck1	18534	-3.02	0.02	Phosphoenolpyruvate carboxykinase 1 (soluble)
Pclo	26875	-1.03	0.00	Piccolo (presynaptic cytomatrix protein)
Pcolce2	76477	-1.38	0.02	Procollagen C- endopeptidase enhancer 2
Pde7b	29863	-1.48	0.01	Phosphodiesterase 7B
Pdgfa	18590	1.03/1.05	0.02/0.02	Platelet-derived growth factor subunit A
Pdgfra	18595	-1.66	0.00	Alpha-type platelet-derived growth factor receptor
Pdk1	228026	-1.30/-1.22/-2.13	0.00/0.00/0.00	Pyruvate dehydrogenase lipoamide kinase isozyme 1, mitochondrial
Pdlim7	67399	1.17	0.01	PDZ and LIM domain protein 7
Pdp1	381511	1.24	0.02	Pyruvate dehyrogenase phosphatase catalytic subunit 1
Peli2	93834	-1.26	0.03	Pellino homolog 2
Pes1	64934	1.08	0.01	Pescadillo homolog 1, containing BRCT domain
Pgm3	109785	1.33	0.00	Phosphoglucomutase 3
Phlda2	22113	1.79	0.00	Pleckstrin homology-like domain family A member 2
Pi4k2b	67073	1.06	0.03	Phosphatidylinositol 4- kinase type 2 beta
Pigp	56176	1.04	0.03	Phosphatidylinositol glycan anchor biosynthesis, class P
Pigr	18703	-2.67/-2.65	0.01/0.02	Polymeric immunoglobulin receptor
Pir	69656	1.30	0.01	Pirin
Plagl1	22634	-1.48	0.04	Pleiomorphic adenoma gene-like 1
Plbd1	66857	1.27	0.00	Phospholipase B domain containing 1
Plce1	74055	-1.85	0.00	Phospholipase C, epsilon 1
Plcxd1	403178	-1.17	0.01	Phosphatidylinositol- specific phospholipase C, X domain containing 1
Plk1	18817	1.03	0.01	Polo-like kinase 1
Plk4	20873	1.01	0.01	Polo-like kinase 4
Pls1	102502	1.87	0.00	Plastin 1
Plscr1	22038	1.03/1.07	0.01/0.01	Phospholipid scramblase 1
Pold4	69745	1.24	0.02	DNA polymerase delta subunit 4
Ppap2c	50784	1.07	0.00	Phosphatidic acid phosphatase type 2C
Pparg	19016	1.49	0.03	Peroxisome proliferator-activated receptor gamma
Ppargc1b	170826	-1.80	0.01	Peroxisome proliferator-activated receptor gamma coactivator 1-beta
Ppl	19041	1.22	0.00	Periplakin
Ppm1l	242083	-1.09	0.03	Protein phosphatase, Mg2+/Mn2+ dependent, 1L
Prc1	233406	1.33	0.02	Protein regulator of cytokinesis 1
Prickle1	106042	-1.01	0.01	Prickle homolog 1
Prkcdbp	109042	1.19	0.00	Protein kinase C, delta binding protein
Psmd8	57296	1.40	0.00	Proteasome (prosome, macropain) 26S subunit, non-ATPase, 8
Psmd9	67151	-1.52	0.03	Proteasome (prosome, macropain) 26S subunit, non-ATPase, 9
Ptbp1	19205	-2.18	0.01	Polypyrimidine tract binding protein 1
Ptgds	19215	-1.54/-1.15	0.03/0.04	Prostaglandin D2 synthase 21kDa (brain)
Ptger2	19217	-1.37	0.01	Prostaglandin E receptor 2 (subtype EP2), 53kDa
Ptgis	19223	-1.01	0.02	Prostaglandin I2 (prostacyclin) synthase
Pth1r	19228	-1.87	0.00	Parathyroid hormone 1 receptor

Gene symbol	EntrezGene ID	Log-ratio	p-value	Gene name
Ptplb	70757	1.28/1.20	0.01/0.00	Protein tyrosine phosphatase-like (proline instead of catalytic arginine), member b
Ptpn14	19250	2.57	0.01	Protein tyrosine phosphatase, non-receptor type 14
Pttg1	30939	1.98	0.01	Pituitary tumor- transforming 1
Pycr2	69051	-1.04	0.01	Pyrroline-5-carboxylate reductase family, member 2
Rab27b	80718	-1.26	0.00	RAB27B, member RAS oncogene family
Racgap1	26934	1.60	0.01	Rac GTPase activating protein 1
Rad51	19361	1.54	0.01	RAD51 homolog
Rad51ap1	19362	1.07	0.01	RAD51 associated protein 1
Ralgps2	78255	1.32	0.00	Ral GEF with PH domain and SH3 binding motif 2
Ramp1	51801	-1.35	0.01	Receptor activity modifying protein 1
Ranbp3l	223332	-1.57	0.00	RAN binding protein 3-like
Rasgef1b	320292	-1.69	0.01	RasGEF domain family, member 1B
Rasgrp2	19395	-1.19	0.01	RAS guanyl-releasing protein 2
Rbbp8	225182	1.06	0.01	Retinoblastoma binding protein 8
Rbl1	19650	1.56	0.00	Retinoblastoma-like 1
Rbm24	666794	1.08	0.01	RNA binding motif protein 24
Rbms3	207181	-2.27/-1.55	0.00/0.00	RNA binding motif, single stranded interacting protein 3
Rbp1	19659	1.48	0.00	Retinol binding protein 1
Rbp7	63954	1.74	0.03	Retinol binding protein 7
Rdh9	103142	1.79	0.01	Retinol dehydrogenase 9
Reck	53614	-2.46	0.00	Reversion-inducing- cysteine-rich protein with kazal motifs
Rfc4	106344	1.05	0.02	Replication factor C (activator 1) 4, 37kDa
Rgs2	19735	-1.05	0.01	Regulator of G-protein signaling 2
Rgs4	19736	-1.85	0.01	Regulator of G-protein signaling 4
Rgs5	19737	-2.10/-1.19/-1.72	0.00/0.03/0.04	Regulator of G-protein signaling 5
Rhoc	11853	1.08	0.02	Ras homolog gene family, member C
Rian	75745	2.65	0.01	RNA imprinted and accumulated in nucleus
Rnf14	56736	1.16	0.04	Ring finger protein 14
Rnf43	207742	1.23	0.03	Ring finger protein 43
Rnpep	215615	1.24	0.00	Arginyl aminopeptidase (aminopeptidase B)
Rp2h	19889	1.26/1.46	0.00/0.03	Retinitis pigmentosa 2 homolog
Rpl12	269261	1.01	0.03	Ribosomal protein L12
Rpl22l1	68028	1.21	0.00	Ribosomal protein L22- like 1
Rps4y2	66184	-2.16	0.00	Ribosomal protein S4, Y-linked 2
Rras	20130	1.31	0.01	Related RAS viral (r-ras) oncogene homolog
Rrm1	20133	1.36	0.02	Ribonucleotide reductase M1
Rrm2	20135	1.42/1.63	0.02/0.03	Ribonucleotide reductase M2
Rspo3	72780	-2.12	0.00	R-spondin 3
Rtn4	68585	1.54	0.03	Reticulon 4
S100a10	20194	1.30	0.01	S100 calcium binding protein A10
S100a11	20195	2.10	0.03	S100 calcium binding protein A11
Samd4	74480	1.34	0.02	Sterile alpha motif domain containing 4A
Sardh	192166	-1.09	0.01	Sarcosine dehydrogenase
Scamp5	56807	1.22	0.00	Secretory carrier membrane protein 5
Scara3	219151	-1.81	0.03	Scavenger receptor class A, member 3
Scara5	71145	1.65	0.02	Scavenger receptor class A, member 5
Sco2	100126824	-1.33	0.00	SCO cytochrome oxidase deficient homolog 2
Scoc	56367	1.37	0.02	Short coiled-coil protein
Sdc1	20969	-1.07	0.01	Syndecan 1
Sds	231691	-4.57	0.00	Serine dehydratase
Sdsl	257635	-2.38	0.00	Serine dehydratase-like
Sectm1a	209588	1.89	0.01	Secreted and transmembrane 1A
Sema3b	20347	1.53	0.02	Semaphorin-3B
Sema3d	108151	-1.42	0.01	Semaphorin-3D
Sema3e	20349	-1.83/-1.73/-1.36	0.03/0.01/0.01	Semaphorin-3E
Serpina4-ps1	321018	-2.52/-2.30/-1.58	0.01/0.01/0.02	Serine (or cysteine) peptidase inhibitor, clade A, member 4, pseudogene 1
Serpinb6a	20719	1.98	0.01	Serine (or cysteine) peptidase inhibitor, clade B, member 6a
Setd7	73251	-1.05	0.01	SET domain containing (lysine methyltransferase) 7
Sftpd	20390	-1.25	0.03	Surfactant protein D
Sfxn1	14057	-3.33/-3.09	0.00/0.00	Sideroflexin 1
Sfxn2	94279	-1.42/-1.31	0.01/0.03	Sideroflexin 2
Sgms1	208449	1.04/1.16	0.02/0.02	Sphingomyelin synthase 1
Sgol2	68549	1.18	0.03	Shugoshin-like 2
Shcbp1	20419	1.41	0.00	SHC SH2-domain binding protein 1
Sidt1	320007	2.03	0.02	SID1 transmembrane family, member 1
Slc10a2	20494	2.00	0.00	Solute carrier family 10 (sodium/bile acid cotransporter family), member 2

Gene symbol	EntrezGene ID	Log-ratio	p-value	Gene name
Slc11a1	18173	1.30	0.03	Solute carrier family 11 (proton-coupled divalent metal ion transporters), member 1
Slc12a2	20496	-1.05	0.02	Solute carrier family 12 (sodium/potassium/chloride transporters), member 2
Slc13a2	20500	-1.26	0.00	Solute carrier family 13 (sodium-dependent dicarboxylate transporter), member 2
Slc13a3	114644	2.06/2.24	0.02/0.00	Solute carrier family 13 (sodium-dependent dicarboxylate transporter), member 3
Slc16a7	20503	1.12	0.05	Solute carrier family 16, member 7 (monocarboxylic acid transporter 2)
Slc1a4	55963	1.94/2.37/2.90	0.00/0.00/0.00	Solute carrier family 1 (glutamate/neutral amino acid transporter), member 4
Slc22a7	108114	-1.33	0.04	Solute carrier family 22 (organic anion transporter), member 7
Slc25a15	18408	-1.14	0.00	Solute carrier family 25 (mitochondrial carrier; ornithine transporter) member 15
Slc25a25	227731	-1.00	0.04	Solute carrier family 25 (mitochondrial carrier; phosphate carrier), member 25
Slc25a30	67554	1.57	0.03	Solute carrier family 25 (mitochondrial carrier; phosphate carrier), member 30
Slc36a1	215335	1.00	0.00	Solute carrier family 36 (proton/amino acid symporter), member 1
Slc37a4	14385	-1.00	0.02	Solute carrier family 37 (glucose-6-phosphate transporter), member 4
Slc38a3	76257	-1.51	0.00	Solute carrier family 38 (sodium-coupled neutral amino acid transporter), member 3
Slc39a2	214922	2.21	0.04	Solute carrier family 39 (zinc transporter), member 2
Slc39a4	72027	1.48	0.01	Solute carrier family 39 (zinc transporter), member 4
Slc48a1	67739	1.10/1.21	0.04/0.01	Solute carrier family 48 (heme transporter), member 1
Slc5a3	53881	-1.24	0.01	Solute carrier family 5 (sodium/myo-inositol cotransporter), member 3
Slc7a2	11988	-1.96/-1.50	0.00/0.01	Solute carrier family 7 (cationic amino acid transporter, y+ system), member 2
Slc7a4	224022	-1.17	0.01	Solute carrier family 7 (cationic amino acid transporter, y+ system), member 4
Slc8a3	110893	-1.18	0.01	Solute carrier family 8 (sodium/calcium exchanger), member 3
Slco2a1	24059	-1.68	0.03	Solute carrier organic anion transporter family, member 2A1
Slpi	20568	2.20	0.03	Secretory leukocyte peptidase inhibitor
Smc2	14211	1.02	0.03	Structural maintenance of chromosomes protein 2
Smo	319757	-1.10	0.02	Smoothened, frizzled family receptor
Snhg11	319317	1.45	0.03	Small nucleolar RNA host gene 11 (non-protein coding)
Snhg8	69895	-1.07	0.03	Small nucleolar RNA host gene 8 (non-protein coding)
Sntg2	268534	-1.60	0.00	Syntrophin, gamma 2
Socs5	56468	-1.00	0.02	Suppressor of cytokine signaling 5
Sod3	20657	-1.06	0.03	Superoxide dismutase 3, extracellular
Spa17	20686	1.06	0.04	Sperm autoantigenic protein 17
Sparcl1	13602	2.17	0.01	SPARC-like 1
Spc25	66442	1.30	0.01	NDC80 kinetochore complex component, homolog
Sprr1a	20753	2.54	0.01	Small proline-rich protein 1A
Srxn1	76650	2.11/2.29	0.04/0.04	Sulfiredoxin 1
St3gal5	20454	-1.58/-1.49	0.01/0.01	ST3 beta-galactoside alpha-2,3-sialyltransferase 5
Steap2	74051	-1.78	0.00	STEAP family member 2, metalloreductase
Stmn1	16765	1.25	0.04	Stathmin 1
Strbp	20744	1.47	0.04	Spermatid perinuclear RNA binding protein
Sulf2	72043	-1.42/-1.35	0.00/0.00	Sulfatase 2
Sult5a1	57429	-1.85	0.02	Sulfotransferase family 5A, member 1
Susd1	634731	-1.46	0.02	Sushi domain containing 1
Susd4	96935	-2.62/-2.32	0.00/0.00	Sushi domain containing 4
Syde2	214804	-1.47	0.00	Synapse defective 1, Rho GTPase, homolog 2
Synpo	104027	1.09	0.01	Synaptopodin
Tat	234724	-1.57	0.02	Tyrosine aminotransferase
Tbc1d8	54610	-1.01	0.04	TBC1 domain family, member 8 (with GRAM domain)
Tbcel	272589	1.02	0.02	Tubulin folding cofactor E-like
Tbx20	57246	-1.30	0.01	T-box 20
Tcf21	21412	-1.71	0.01	Transcription factor 21
Tcf7	21414	1.32	0.02	Transcription factor 7

Gene symbol	EntrezGene ID	Log-ratio	p-value	Gene name
Tcf7l1	21415	-1.49	0.00	Transcription factor 7-like 1
Tead1	21676	-1.42	0.01	TEA domain family member 1
Tes	21753	1.05	0.01	Testis derived transcript
Tgfbi	21810	-1.33/-1.12/-1.08/-1.17	0.03/0.04/0.01/0.01	Transforming growth factor, beta-induced, 68kDa
Tgfbr2	21813	1.01	0.01	Transforming growth factor, beta receptor II
Tgfbr3	21814	-1.32	0.02	Transforming growth factor, beta receptor III
Them5	66198	-1.80	0.00	Thioesterase superfamily member 5
Tiam2	24001	-1.93	0.03	T-cell lymphoma invasion and metastasis 2
Timd4	276891	-1.15	0.05	T-cell immunoglobulin and mucin domain containing 4
Timm8a1	30058	1.25	0.01	Translocase of inner mitochondrial membrane 8 homolog a1
Timp2	21858	-1.07	0.05	TIMP metallopeptidase inhibitor 2
Tinag	26944	2.92	0.00	Tubulointerstitial nephritis antigen
Tle4	21888	-1.03	0.03	Transducin-like enhancer of split 4
Tmem204	407831	-1.03	0.05	Transmembrane protein 204
Tmem25	71687	-1.37	0.02	Transmembrane protein 25
Tmem37	170706	1.18	0.05	Transmembrane protein 37
Tmem43	74122	1.06	0.02	Transmembrane protein 43
Tmem45a	56277	-1.40	0.03	Transmembrane protein 45A
Tmem47	192216	-1.26	0.01	Transmembrane protein 47
Tmem63a	208795	-1.10	0.00	Transmembrane protein 63A
Tmem97	69071	1.20	0.01	Transmembrane protein 97
Tmpo	21917	1.05	0.02	Thymopoietin
Tmprss2	50528	1.16/1.21	0.00/0.00	Transmembrane protease, serine 2
Tmprss4	214523	-1.09	0.03	Transmembrane protease, serine 4
Tmtc2	278279	-1.12	0.02	Transmembrane and tetratricopeptide repeat containing 2
Tmtc4	70551	1.49/1.70	0.01/0.01	Transmembrane and tetratricopeptide repeat containing 4
Tnfrsf11b	18383	-1.08	0.01	Tumor necrosis factor receptor superfamily, member 11b
Tnfrsf12a	27279	1.35/1.48	0.03/0.02	Tumor necrosis factor receptor superfamily, member 12a
Tnfrsf19	29820	1.67	0.01	Tumor necrosis factor receptor superfamily, member 19
Tns1	21961	-1.17	0.00	Tensin 1
Tnxb	81877	-1.26	0.00	Tenascin XB
Top2a	21973	1.86	0.00	DNA topoisomerase 2-alpha
Tpd52	21985	1.22	0.01	Tumor protein D52
Tpm1	22003	1.30/1.58	0.00/0.00	Tropomyosin 1 (alpha)
Tpr	108989	1.13/1.24	0.01/0.01	Translocated promoter region (to activated MET oncogene)
Tpx2	72119	1.35	0.02	Targeting protein for Xklp2
Trim2	80890	1.01/1.48	0.01/0.03	Tripartite motif containing 2
Trpm7	58800	1.18	0.04	Transient receptor potential cation channel, subfamily M, member 7
Tshz2	228911	-1.76/-1.03	0.01/0.01	Teashirt zinc finger homeobox 2
Tspan33	232670	-1.32	0.01	Tetraspanin 33
Tspyl4	72480	-1.62	0.03	TSPY-like 4
Tstd1	226654	-2.63	0.00	Thiosulfate sulfurtransferase (rhodanese)-like domain containing 1
Ttc39a	230603	1.46	0.01	Tetratricopeptide repeat domain 39A
Ttk	22137	1.68	0.01	TTK protein kinase
Tubb4b	227613	1.35	0.02	Tubulin, beta 4B class IVb
Uap1l1	227620	1.63	0.00	UDP-N-acteylglucosamine pyrophosphorylase 1-like 1
Ubd	24108	3.20	0.01	Ubiquitin D
Ube2c	68612	1.95	0.00	Ubiquitin-conjugating enzyme E2 C
Ube2t	67196	1.30	0.03	Ubiquitin-conjugating enzyme E2 T
Uck2	80914	-1.77	0.02	Uridine-cytidine kinase 2
Uroc1	243537	-2.59/-2.17	0.01/0.01	Urocanase domain containing 1
Vipr1	22354	-1.38	0.01	Vasoactive intestinal polypeptide receptor 1
Vma21	67048	1.05	0.02	VMA21 vacuolar H+-ATPase homolog
Vopp1	232023	1.26/1.95	0.01/0.00	Vesicular, overexpressed in cancer, prosurvival protein 1
Vwf	22371	-1.10	0.02	Von Willebrand factor
Wdr1	22388	1.05	0.01	WD repeat domain 1
Wdr67	210544	1.12	0.03	WD repeat domain 67
Wfdc15b	192201	-1.57	0.01	WAP four-disulfide core domain 15B
Wfdc2	67701	-2.05	0.00	WAP four-disulfide core domain 2
Wisp1	22402	2.23/2.41	0.01/0.02	WNT1-inducible-signaling pathway protein 1
Wsb1	78889	-1.89	0.00	WD repeat and SOCS box containing 1
Zdhhc14	224454	-1.96/-1.90/-1.86	0.01/0.01/0.02	Zinc finger, DHHC-type containing 14
Zfand2a	100494	1.03/1.22	0.01/0.00	Zinc finger, AN1-type domain 2A
Zfp259	22687	-1.27	0.00	Zinc finger protein 259
Zfp54	22712	1.21	0.02	Zinc finger protein 54

Gene symbol	EntrezGene ID	Log-ratio	p-value	Gene name
Zfpm2	22762	-1.09	0.01	Zinc finger protein, multitype 2
Zswim6	67263	-1.07	0.01	Zinc finger, SWIM-type containing 6
Zwilch	68014	1.75	0.00	Zwilch, kinetochore associated, homolog

B) Genes significantly dysregulated in *Ha-ras*-mutated tumors vs. adjacent non-tumor tissue (log-ratio >1.0, p-value <0.05).

Gene symbol	EntrezGene ID	Log-ratio	p-value	Gene name
Aadat	23923	-2.25	0.00	Aminoadipate aminotransferase
Aass	30956	-1.26	0.00	Aminoadipate-semialdehyde synthase
Abat	268860	-1.45	0.00	4-aminobutyrate aminotransferase
Abca5	217265	1.39	0.00	ATP-binding cassette, sub-family A (ABC1), member 5
Abcb10	56199	-1.42/-1.13	0.00/0.01	ATP-binding cassette, sub-family B (MDR/TAP), member 10
Abcb11	27413	-1.40	0.04	ATP-binding cassette, sub-family B (MDR/TAP), member 11
Abcb1a	18671	1.88/2.17	0.02/0.01	ATP-binding cassette, sub-family B (MDR/TAP), member 1A
Abcb6	74104	-1.13	0.00	ATP-binding cassette, sub-family B (MDR/TAP), member 6
Abcc5	27416	1.16	0.00	ATP-binding cassette, sub-family C (CFTR/MRP), member 5
Abcd2	26874	3.38/3.64/4.74	0.00/0.00/0.00	ATP-binding cassette, sub-family D (ALD), member 2
Abhd15	67477	-2.07	0.01	Abhydrolase domain containing 15
Abhd2	54608	1.32/1.43/1.90	0.00/0.00/0.00	Abhydrolase domain containing 2
Abhd5	67469	1.60/1.74	0.00/0.00	Abhydrolase domain containing 5
Abi2	329165	2.75/2.78	0.00/0.00	Abl-interactor 2
Abi3bp	320712	-2.75/-1.54	0.00/0.00	ABI family, member 3 (NESH) binding protein
Ablim3	319713	-1.96	0.00	Actin binding LIM protein family, member 3
Acadsb	66885	-1.29	0.00	Acyl-CoA dehydrogenase, short/branched chain
Acbd3	170760	1.20/1.20/1.42	0.00/0.02/0.02	Acyl-CoA binding domain containing 3
Accn5	58170	-2.83	0.00	Amiloride-sensitive cation channel 5
Acot1	26897	-2.37	0.00	Acyl-CoA thioesterase 1
Acot9	56360	1.07	0.00	Acyl-CoA thioesterase 9
Acsl1	14081	-1.10/-1.05	0.02/0.01	Acyl-CoA synthetase long-chain family member 1
Acsl3	74205	1.74/1.85	0.01/0.02	Acyl-CoA synthetase long-chain family member 3
Acsl4	50790	1.79/1.97/2.03	0.00/0.00/0.00	Acyl-CoA synthetase long-chain family member 4
Acsl5	433256	1.23	0.00	Acyl-CoA synthetase long-chain family member 5
Acsm1	117147	-2.06	0.00	Acyl-CoA synthetase medium-chain family member 1
Acsm2	233799	-1.48	0.00	Acyl-CoA synthetase medium-chain family member 2
Acsm5	272428	-2.31	0.00	Acyl-CoA synthetase medium-chain family member 5
Actn1	109711	1.04	0.00	Actinin, alpha 1
Adam11	11488	-1.10	0.00	ADAM metallopeptidase domain 11
Adamdec1	58860	-2.05	0.01	ADAM-like, decysin 1
Adamts5	23794	-1.10	0.03	ADAM metallopeptidase with thrombospondin type 1 motif, 5
Adck3	67426	-1.22	0.04	AarF domain containing kinase 3
Adck4	76889	2.32	0.00	AarF domain containing kinase 4
Add3	27360	-1.09	0.01	Adducin 3 (gamma)
Adh4	26876	-2.19	0.00	Alcohol dehydrogenase 4 (class II), pi polypeptide
Adhfe1	76187	-1.57/-1.38	0.01/0.01	Alcohol dehydrogenase, iron containing, 1
Adrbk2	320129	1.27/1.79/2.09	0.00/0.00/0.00	Adrenergic, beta, receptor kinase 2
Aebp1	11568	1.36/2.00	0.00/0.00	AE binding protein 1
Afmid	71562	-1.53/-1.12	0.01/0.04	Arylformamidase
Afp	11576	1.13/3.43/4.17/4.81	0.02/0.00/0.00/0.00	Alpha-fetoprotein
Agbl3	76223	-1.20	0.00	ATP/GTP binding protein-like 3
Agfg1	15463	1.18/1.41/1.47/1.75/ 1.92	0.00/0.00/0.00/0.00/0.00	ArfGAP with FG repeats 1
Agmat	75986	-1.89	0.00	Agmatine ureohydrolase (agmatinase)
Agps	228061	1.06	0.01	Alkylglycerone phosphate synthase
Agxt2l1	71760	-4.50	0.01	Alanine-glyoxylate aminotransferase 2-like 1
Ahcy	269378	-1.17	0.02	Adenosylhomocysteinase
AI132709	101494	3.60	0.00	N/A
AI195470	107131	-1.07	0.02	N/A
AI464131	329828	-1.19	0.00	N/A
AI597468	103266	1.31	0.01	N/A
Aifm3	72168	-1.53	0.00	Apoptosis-inducing factor, mitochondrion-associated, 3
Aig1	66253	1.40	0.00	Androgen-induced 1
Airn	104103	1.73	0.00	Antisense of IGF2R RNA (non-protein coding)
Ak4	11639	1.08	0.02	Adenylate kinase 4
Akr1b3	11677	1.72/1.82/2.30	0.01/0.00/0.00	Aldo-keto reductase family 1, member B3
Akr1b7	11997	1.37	0.01	Aldo-keto reductase family 1, member 7

Gene symbol	EntrezGene ID	Log-ratio	p-value	Gene name
Akr1c18	105349	5.04	0.00	Aldo-keto reductase family 1, member C18
Akr1c19	432720	-1.56	0.03	Aldo-keto reductase family 1, member C19
Akr1c6	83702	-1.45	0.00	Aldo-keto reductase family 1, member C6
Akr1d1	208665	-1.22/-1.10	0.02/0.02	Aldo-keto reductase family 1, member D1 (delta 4-3-ketosteroid-5-beta-reductase)
Alas2	11656	-2.31	0.00	Aminolevulinate, delta-, synthase 2
Alcam	11658	1.59/1.81/1.92/2.04/2.09	0.00/0.00/0.00/0.00/0.00	Activated leukocyte cell adhesion molecule
Aldh16a1	69748	-1.08	0.00	Aldehyde dehydrogenase 16 family, member A1
Aldh18a1	56454	1.28/2.34	0.01/0.00	Aldehyde dehydrogenase 18 family, member A1
Aldh1a1	11668	-1.20	0.01	Aldehyde dehydrogenase 1 family, member A1
Aldh1a7	26358	-1.18	0.00	Aldehyde dehydrogenase family 1, subfamily A7
Aldh1b1	72535	1.99	0.00	Aldehyde dehydrogenase 1 family, member B1
Aldoc	11676	1.37	0.01	Aldolase C, fructose-bisphosphate
Alox5	11689	2.66	0.00	Arachidonate 5-lipoxygenase
Amn	93835	1.37	0.01	Amnionless homolog (mouse)
Amot	27494	1.56	0.00	Angiomotin
Amy1	11722	-1.29	0.00	Amylase 1, salivary, alpha-amylase
Ang	11727	-2.76	0.00	Angiogenin, ribonuclease, RNase A family, 5
Angptl6	70726	-1.16	0.01	Angiopoietin-like 6
Ankrd33b	67434	-2.08/-1.76	0.00/0.01	Ankyrin repeat domain 33B
Ano1	101772	-1.03	0.00	Anoctamin 1, calcium activated chloride channel
Anxa2	12306	2.64	0.00	Annexin A2
Anxa3	11745	1.55	0.00	Annexin A3
Anxa4	11746	1.27/1.38	0.00/0.00	Annexin A4
Anxa5	11747	1.13	0.00	Annexin A5
Anxa9	71790	1.29	0.00	Annexin A9
Aox1	11761	-1.47	0.00	Aldehyde oxidase 1
Aox3	71724	-3.04	0.01	Aldehyde oxidase 3
Aph1b	208117	1.65/1.83	0.00/0.00	Anterior pharynx defective 1 homolog B (C. elegans)
Aplnr	23796	3.07	0.04	Apelin receptor
Apoa4	11808	1.70/2.18	0.00/0.00	Apolipoprotein A-IV
Apoc2	11813	1.47	0.00	Apolipoprotein C-II
Apom	55938	1.51	0.00	Apolipoprotein M
App	11820	1.80/2.01	0.00/0.00	Amyloid beta (A4) precursor protein
Aqp4	11829	-2.69/-1.97	0.00/0.02	Aquaporin 4
Aqp9	64008	-1.38/-1.30	0.01/0.00	Aquaporin 9
Ar	11835	-2.53/-2.46/-1.00	0.00/0.00/0.01	Androgen receptor
Arhgap12	75415	1.08	0.01	Rho GTPase activating protein 12
Arhgap22	239027	1.66	0.00	Rho GTPase activating protein 22
Arhgap42	71544	-1.28	0.01	Rho GTPase activating protein 42
Arhgef37	328967	-2.43	0.00	Rho guanine nucleotide exchange factor (GEF) 37
Arl2bp	107566	1.27	0.00	ADP-ribosylation factor-like 2 binding protein
Armcx3	71703	1.67/1.80	0.00/0.01	Armadillo repeat containing, X-linked 3
Arntl2	272322	1.61	0.00	Aryl hydrocarbon receptor nuclear translocator-like 2
Arpc1b	11867	1.78	0.00	Actin related protein 2/3 complex, subunit 1B, 41kDa
As3mt	57344	1.04	0.01	Arsenic (+3 oxidation state) methyltransferase
Asl	109900	-1.47	0.00	Argininosuccinate lyase
Aspa	11484	-1.48	0.01	Aspartoacylase
Asph	65973	1.16	0.00	Aspartate beta-hydroxylase
Ass1	11898	-1.45	0.01	Argininosuccinate synthase 1
Atf3	11910	1.40	0.02	Activating transcription factor 3
Atp11c	320940	-1.33/-1.21	0.00/0.00	ATPase, class VI, type 11C
Atp1b1	11931	1.10/1.10/1.14/1.22	0.01/0.00/0.00/0.00	ATPase, Na+/K+ transporting, beta 1 polypeptide
Atp8b4	241633	-2.06	0.03	ATPase, class I, type 8B, member 4
Atpif1	11983	1.35	0.00	ATPase inhibitory factor 1
Atrnl1	226255	-1.59	0.00	Attractin-like 1
Avpi1	69534	1.33	0.00	Arginine vasopressin-induced 1
Avpr1a	54140	-1.59	0.04	Arginine vasopressin receptor 1A
B3galnt1	26879	1.11	0.00	Beta-1,3-N-acetylgalactosaminyltransferase 1 (globoside blood group)
B4galt6	56386	1.77/2.45/2.87/2.93	0.00/0.00/0.00/0.00	UDP-Gal:betaGlcNAc beta 1,4- galactosyltransferase, polypeptide 6
Baat	12012	-1.67/-1.49	0.00/0.00	Bile acid CoA: amino acid N-acyltransferase (glycine N-choloyltransferase)
Bace1	23821	-1.14	0.02	Beta-site APP-cleaving enzyme 1
Bach1	12013	1.31/1.40	0.01/0.01	BTB and CNC homology 1, basic leucine zipper transcription factor 1
Bach2	12014	1.02/1.04	0.02/0.02	BTB and CNC homology 1, basic leucine zipper transcription factor 2
Bag4	67384	-1.50/-1.41	0.000.00	BCL2-associated athanogene 4
Bax	12028	1.08	0.01	BCL2-associated X protein
Baz1a	217578	1.00	0.00	Bromodomain adjacent to zinc finger domain, 1A
BB319198	100503607	1.84	0.00	
Bbox1	170442	-1.04	0.03	Butyrobetaine (gamma), 2-oxoglutarate dioxygenase (gamma-butyrobetaine hydroxylase) 1
Bcas1	76960	1.50	0.01	Breast carcinoma amplified sequence 1
Bcl10	12042	1.18/1.37/1.54	0.00/0.00/0.00	B-cell CLL/lymphoma 10
Bcl2	12043	1.41/1.71	0.00/0.00	B-cell CLL/lymphoma 2
Bcl2l11	12125	1.03/1.27/1.30/2.00	0.02/0.01/0.01/0.00	BCL2-like 11 (apoptosis facilitator)
Bcl2l14	66813	1.62/1.73	0.00/0.00	BCL2-like 14 (apoptosis facilitator)

Gene symbol	EntrezGene ID	Log-ratio	p-value	Gene name
Bcmo1	63857	2.23	0.00	Beta-carotene 15,15'-monooxygenase 1
Bco2	170752	-1.51	0.01	Beta-carotene oxygenase 2
Bdh1	71911	1.06	0.00	3-hydroxybutyrate dehydrogenase, type 1
Bdh2	69772	-1.80	0.00	3-hydroxybutyrate dehydrogenase, type 2
Bdnf	12064	-1.45	0.00	Brain-derived neurotrophic factor
Bex1	19716	5.23	0.00	Brain expressed, X-linked 1
Bex2	12069	2.55	0.00	Brain expressed X-linked 2
Bgn	12111	-1.18/-1.08	0.02/0.01	Biglycan
Bicc1	83675	1.49/1.68	0.00/0.00	Bicaudal C homolog 1 (Drosophila)
Blnk	17060	1.94	0.03	B-cell linker
Bmf	171543	-1.95	0.00	Bcl2 modifying factor
Bmp4	12159	1.14	0.01	Bone morphogenetic protein 4
Bmp5	12160	-1.94	0.00	Bone morphogenetic protein 5
Bmp7	12162	1.49/2.55	0.00/0.00	Bone morphogenetic protein 7
Bmp8b	12164	1.27/1.56	0.00/0.00	Bone morphogenetic protein 8b
Btc	12223	1.34/1.44	0.00/0.00	Betacellulin
Btg2	12227	2.86/3.25	0.00/0.00	BTG family, member 2
Btnl9	237754	1.46	0.03	Butyrophilin-like 9
Bub1	12235	1.83	0.05	Budding uninhibited by benzimidazoles 1 homolog (yeast)
C1ql3	227580	1.05	0.03	Complement component 1, q subcomponent-like 3
C4b	12268	-1.67	0.00	Complement component 4B (Chido blood group)
C6	12274	-1.83	0.03	Complement component 6
C8b	110382	-2.06	0.01	Complement component 8, beta polypeptide
C9	12279	-1.33	0.01	Complement component 9
Cab39	12283	1.08	0.01	Calcium binding protein 39
Cacna1b	12287	2.85/2.94	0.03/0.02	Calcium channel, voltage-dependent, N type, alpha 1B subunit
Cacna1c	12288	1.51	0.00	Calcium channel, voltage-dependent, L type, alpha 1C subunit
Calml4	75600	2.79	0.00	Calmodulin-like 4
Capn10	23830	1.01	0.03	Calpain 10
Caprin2	232560	1.39	0.00	Caprin family member 2
Capsl	75568	1.22	0.01	Calcyphosine-like
Car1	12346	-2.88	0.00	Cysteinyl-tRNA synthetase
Car14	23831	-1.61	0.05	Carbonic anhydrase 14
Car2	12349	1,26	0,00	Carbonic anhydrase 2
Car3	12350	-2,67/-2,39/-1,82/-1,35	0,01/0,03/0,03/0,03	Carbonic anhydrase 3
Car5a	12352	-2,14	0,00	Carbonic anhydrase 5a, mitochondrial
Card10	105844	1,32	0,00	Caspase recruitment domain family, member 10
Cars	27267	1,03	0,01	Cysteinyl-tRNA synthetase
Casc4	319996	3,88	0,00	Cancer susceptibility candidate 4
Casp12	12364	1,98/2,27	0,00/0,00	Caspase 12 (gene/pseudogene)
Casp4	12363	1,76	0,00	Caspase 4, apoptosis-related cysteine peptidase
Cav1	12389	1,82	0,02	Caveolin 1, caveolae protein, 22kDa
Cav2	12390	2,54	0,00	Caveolin 2
Ccbe1	320924	-1,47	0,04	Collagen and calcium binding EGF domains 1
Ccdc120	54648	2,36	0,00	Coiled-coil domain containing 120
Ccdc125	76041	1,01	0,02	Coiled-coil domain containing 125
Ccdc149	100503884	2,07	0,00	Coiled-coil domain containing 149
Ccdc162	75973	-1,61	0,01	Coiled-coil domain containing 162, pseudogene
Ccdc164	381738	2,21	0,00	Coiled-coil domain containing 164
Ccdc25	67179	1,38	0,01	Coiled-coil domain containing 25
Ccdc51	66658	1,31	0,00	Coiled-coil domain containing 51
Ccdc68	381175	1,77	0,00	Coiled-coil domain containing 68
Ccdc88c	68339	1,19	0,02	Coiled-coil domain containing 88C
Ccdc99	70385	1,08	0,02	Coiled-coil domain containing 99
Ccna2	12428	1,31/1,98	0,03/0,04	Cyclin A2
Ccnb1	268697	2,12	0,05	Cyclin B1
Ccnb2	12442	2,58	0,03	Cyclin B2
Ccnd1	12443	2,19/2,32/2,43	0,01/0,00/0,01	Cyclin D1
Ccne1	12447	2,11	0,00	Cyclin E1
Cd14	12475	3,11	0,00	CD14 molecule
Cd163	93671	-2,43	0,01	CD163 molecule
Cd1d2	12480	2,31	0,00	CD1d2 antigen
Cd209b	69165	-1,32	0,01	N/A
Cd24a	12484	1,34	0,04	CD24a antigen
Cd276	102657	1,71	0,01	CD276 molecule
Cd2ap	12488	1,26/1,43/1,67	0,00/0,00/0,00	CD2-associated protein
Cd40	21939	2,05/2,06/2,72	0,00/0,00/0,00	CD40 molecule
Cd9	12527	1,17	0,00	CD9 molecule
Cd93	17064	1,42/1,55	0,01/0,01	CD93 molecule
Cd97	26364	1,02	0,01	CD97 molecule
Cda	72269	1,06	0,00	Cytidine deaminase
Cdc20	107995	1,29/1,86	0,04/0,02	Cell division cycle 20 homolog (S. cerevisiae)
Cdca3	14793	1,64	0,03	Cell division cycle associated 3
Cdca4	71963	1,14	0,00	Cell division cycle associated 4
Cdca8	52276	1,05/1,28	0,01/0,04	Cell division cycle associated 8
Cdh1	12550	3,38	0,01	Cadherin 1, type 1, E-cadherin (epithelial)
Cdh17	12557	3,34	0,00	Cadherin 17, LI cadherin (liver-intestine)

Gene symbol	EntrezGene ID	Log-ratio	p-value	Gene name
Cdhr2	268663	2,59	0,00	Cadherin-related family member 2
Cdhr5	72040	-1,06	0,01	Cadherin-related family member 5
Cdk1	12534	1,33	0,05	Cyclin-dependent kinase 1.
Cdk2ap2	52004	1,05	0,01	Cyclin-dependent kinase 2 associated protein 2
Cdk4	12567	1,02	0,01	Cyclin-dependent kinase 4
Cdk6	12571	1,19	0,02	Cyclin-dependent kinase 6
Cdkn1a	12575	1,59/1,95	0,00/0,00	Cyclin-dependent kinase inhibitor 1A (p21, Cip1)
Cdkn2a	12578	2,65	0,00	Cyclin-dependent kinase inhibitor 2A (melanoma, p16, inhibits CDK4)
Cdkn2b	12579	4,65	0,00	Cyclin-dependent kinase inhibitor 2B (p15, inhibits CDK4)
Cdkn2c	12580	2,18	0,00	Cyclin-dependent kinase inhibitor 2C (p18, inhibits CDK4)
Cdkn3	72391	2,24	0,02	Cyclin-dependent kinase inhibitor 3
Celf2	14007	-2,14/-1,68/-1,53	0,02/0,04/0,02	CUGBP, Elav-like family member 2
Celsr2	53883	1,87	0,00	Cadherin, EGF LAG seven-pass G-type receptor 2 (flamingo homolog, Drosophila)
Cenpa	12615	2,07	0,00	Centromere protein A
Cep170	545389	1,03	0,03	Centrosomal protein 170kDa
Cep192	70799	1,04	0,00	Centrosomal protein 192kDa
Cerk	223753	1,38	0,01	Ceramide kinase
Ces1d	104158	-1,93/-1,78	0,03/0,04	Carboxylesterase 1D
Ces1e	13897	-3,50	0,00	Carboxylesterase 1E
Ces1f	234564	-2,46	0,00	Carboxylesterase 1F
Ces1g	12623	-2,91	0,00	Carboxylesterase 1G
Ces2a	102022	-1,76	0,01	Carboxylesterase 2A
Ces2e	234673	2,52	0,00	Carboxylesterase 2E
Ces2g	72361	1,25	0,00	Carboxylesterase 2G
Cfhr1	50702	-1,50	0,00	Complement factor H-related 1
Cgref1	68567	1,90/2,47	0,00/0,00	Cell growth regulator with EF-hand domain 1
Chka	12660	2,42/2,45	0,04/0,04	Choline kinase alpha
Chmp2b	68942	1,05/1,21	0,03/0,00	Charged multivesicular body protein 2B
Chmp4c	66371	1,47/2,26/2,54	0,01/0,00/0,00	Charged multivesicular body protein 4C
Chmp6	208092	1,24	0,00	Charged multivesicular body protein 6
Chpt1	212862	-2,31/-2,24/-2,03/-1,84	0,00/0,00/0,00/0,00	Choline phosphotransferase 1
Chrna2	110902	-1,05	0,00	Cholinergic receptor, nicotinic, alpha 2 (neuronal)
Chrna4	11438	1,75	0,02	Cholinergic receptor, nicotinic, alpha 4 (neuronal)
Chsy3	78923	1,67	0,00	Chondroitin sulfate synthase 3
Cib2	56506	-1,75	0,00	Calcium and integrin binding family member 2
Cidea	12683	4,72	0,00	Cell death-inducing DFFA-like effector a
Cidec	14311	2,18	0,01	Cell death-inducing DFFA-like effector c
Cisd1	52637	-1,03	0,00	CDGSH iron sulfur domain 1
Ckap2	80986	1,78	0,03	Cytoskeleton associated protein 2
Cks1b	54124	1,16	0,01	CDC28 protein kinase regulatory subunit 1B
Clcf1	56708	1,75	0,00	Cardiotrophin-like cytokine factor 1
Clcn2	12724	-1,95	0,01	Chloride channel 2
Cldn14	56173	1,40	0,00	Claudin 14
Cldn15	60363	1,01	0,00	Claudin 15
Cldn7	53624	1,78	0,04	Claudin 7
Clec1b	56760	-1,69	0,05	C-type lectin domain family 1, member B
Clec4f	51811	-2,46	0,04	C-type lectin domain family 4, member F
Clic5	224796	-1,19/-1,04	0,01/0,04	Chloride intracellular channel 5
Clint1	216705	1,13	0,01	Clathrin interactor 1
Cmah	12763	-1,84/-1,55	0,00/0,03	Cytidine monophospho-N-acetylneuraminic acid hydroxylase, pseudogene
Cmbl	69574	-1,51	0,00	Carboxymethylenebutenolidase homolog (Pseudomonas)
Cml1	66116	-1,78	0,00	Camello-like 1
Cml2	93673	-2,72/-2,43/-2,36	0,00/0,00/0,00	Camello-like 2
Cml5	69049	-1,13	0,00	Camello-like 5
Cobl	12808	1,79	0,00	Cordon-bleu homolog (mouse)
Col13a1	12817	-1,06	0,01	Collagen, type XIII, alpha 1
Col14a1	12818	-1,04/-1,00	0,03/0,02	Collagen, type XIV, alpha 1
Col27a1	373864	-1,20	0,01	Collagen, type XXVII, alpha 1
Col4a1	12826	1,14/1,55	0,04/0,01	Collagen, type IV, alpha 1
Col4a2	12827	1,19	0,03	Collagen, type IV, alpha 2
Col4a3	12828	2,93/3,17	0,00/0,00	Collagen, type IV, alpha 3 (Goodpasture antigen)
Col4a4	12829	1,63/2,04	0,00/0,00	Collagen, type IV, alpha 4
Col4a5	12830	1,54/3,10	0,00/0,00	Collagen, type IV, alpha 5
Col5a3	53867	-1,35	0,00	Collagen, type V, alpha 3
Colec10	239447	-3,48	0,02	Collectin sub-family member 10 (C-type lectin)
Colec11	71693	-1,80/-1,12	0,00/0,02	Collectin sub-family member 11
Comtd1	69156	1,07	0,00	Catechol-O-methyltransferase domain containing 1
Copb2	50797	1,07	0,01	Coatomer protein complex, subunit beta 2 (beta prime)
Coq10a	210582	-1,31	0,00	Coenzyme Q10 homolog A (S. cerevisiae)
Corin	53419	-3,03	0,00	Corin, serine peptidase
Cox5b	12859	2,26	0,00	Cytochrome c oxidase subunit Vb
Cp	12870	1,28/1,63	0,02/0,02	Ceruloplasmin (ferroxidase)
Cpd	12874	1,10/1,21	0,00/0,01	Carboxypeptidase D
Cpox	12892	-1,17/-1,07	0,01/0,01	Coproporphyrinogen oxidase

Gene symbol	EntrezGene ID	Log-ratio	p-value	Gene name
Cpsf4l	52670	-1,33	0,00	Cleavage and polyadenylation specific factor 4-like
Creb3l2	208647	1,14	0,01	cAMP responsive element binding protein 3-like 2
Crisp2	22024	1,37	0,01	Cysteine-rich secretory protein 2
Crp	12944	-1,04	0,00	C-reactive protein, pentraxin-related
Crygn	214301	-2,05	0,02	Crystallin, gamma N
Cryl1	68631	-1,03	0,01	Crystallin, lambda 1
Csad	246277	-2,07	0,00	Cysteine sulfinic acid decarboxylase
Csn3	12994	4,12	0,00	Casein kappa
Csrp2	13008	-1,93	0,00	Cysteine and glycine-rich protein 2
Csrp3	13009	-2,61	0,00	Cysteine and glycine-rich protein 3 (cardiac LIM protein)
Cstb	13014	1,07	0,00	Cystatin B (stefin B)
Cth	107869	-1,30	0,00	Cystathionase (cystathionine gamma-lyase)
Ctps2	55936	1,99	0,00	CTP synthase II
Ctsc	13032	1,42/1,80	0,00/0,00	Cathepsin C
Cxadr	13052	1,31/1,38/1,61	0,04/0,04/0,00	Coxsackie virus and adenovirus receptor
Cxcl1	14825	1,11/1,33	0,02/0,01	Chemokine (C-X-C motif) ligand 1 (melanoma growth stimulating activity, alpha)
Cxcl12	20315	-1,74/-1,48	0,00/0,01	Chemokine (C-X-C motif) ligand 12
Cxcl14	57266	2,73	0,02	Chemokine (C-X-C motif) ligand 14
Cxcl17	232983	1,91	0,05	Chemokine (C-X-C motif) ligand 17
Cyb561	13056	2,99	0,00	Cytochrome b-561
Cyb5r1	72017	1,41	0,00	Cytochrome b5 reductase 1
Cyfip2	76884	-1,26	0,02	Cytoplasmic FMR1 interacting protein 2
Cyp17a1	13074	2,73	0,01	Cytochrome P450, family 17, subfamily A, polypeptide 1
Cyp1a2	13077	-2,62	0,00	Cytochrome P450, family 1, subfamily A, polypeptide 2
Cyp26a1	13082	-2,13	0,02	Cytochrome P450, family 26, subfamily A, polypeptide 1
Cyp26b1	232174	-1,17	0,02	Cytochrome P450, family 26, subfamily B, polypeptide 1
Cyp27a1	104086	-2,47	0,00	Cytochrome P450, family 27, subfamily A, polypeptide 1
Cyp2b13	13089	3,01	0,00	Cytochrome P450, family 2, subfamily B, polypeptide 13
Cyp2b9	13094	3,69	0,00	Cytochrome P450, family 2, subfamily B, polypeptide 9
Cyp2c29	13095	-1,16	0,04	Cytochrome P450, family 2, subfamily C, polypeptide 29
Cyp2c37	13096	-3,12	0,00	Cytochrome P450, family 2. subfamily C, polypeptide 37
Cyp2c38	13097	-2,18	0,00	Cytochrome P450, family 2, subfamily C, polypeptide 38
Cyp2c39	13098	-2,91	0,00	Cytochrome P450, family 2, subfamily C, polypeptide 39
Cyp2c50	107141	-2,99	0,00	Cytochrome P450, family 2, subfamily C, polypeptide 50
Cyp2c54	404195	-2,85	0,00	Cytochrome P450, family 2, subfamily C, polypeptide 54
Cyp2d13	68444	-1,70/-1,38	0,01/0,02	Cytochrome P450, family 2, subfamily D, polypeptide 13
Cyp2d9	13105	-1,41	0,02	Cytochrome P450, family 2, subfamily D, polypeptide 9
Cyp2e1	13106	-1,41	0,02	Cytochrome P450, family 2, subfamily E, polypeptide 1
Cyp2f2	13107	-2,85	0,01	Cytochrome P450, family 2, subfamily F, polypeptide 1
Cyp2g1	13108	-2,74	0,01	Cytochrome P450, family 2, subfamily G, polypeptide 1
Cyp2j5	13109	-1,98/-1,75	0,01/0,00	Cytochrome P450, family 2, subfamily J, polypeptide 5
Cyp39a1	56050	2,28	0,01	Cytochrome P450, family 39, subfamily A, polypeptide 1
Cyp46a1	13116	-3,30	0,00	Cytochrome P450, family 46, subfamily A, polypeptide 1
Cyp4a12a	277753	-3,80	0,00	Cytochrome P450, family 4, subfamily A, polypeptide 12a
Cyp4f14	64385	-3,21	0,00	Cytochrome P450, family 4, subfamily F, polypeptide 14
Cyp4f15	106648	-1,66	0,01	Cytochrome P450, family 4, subfamily F, polypeptide 15
Cyp4f16	70101	1,57	0,00	Cytochrome P450, family 4, subfamily F, polypeptide 16
Cyp4v3	102294	-1,33/-1,12	0,00/0,00	Cytochrome P450, family 4, subfamily V, polypeptide 3
Cyp51	13121	1,59	0,04	Cytochrome P450, family 51
Cyp7a1	13122	-3,21/-3,13	0,00/0,02	Cytochrome P450, family 7, subfamily A, polypeptide 1
Cyp7b1	13123	-3,72/-3,68	0,02/0,03	Cytochrome P450, family 7, subfamily B, polypeptide 1
Cyp8b1	13124	-3,57	0,00	Cytochrome P450, family 8, subfamily B, polypeptide 1
Dab1	13131	1,39/1,40/2,37/3,58/ 3,69	0,01/0,01/0,00/0,00/0,00	Disabled homolog 1 (Drosophila)
Dach2	93837	-1,98	0,00	Dachshund homolog 2 (Drosophila)
Dapk2	13143	1,50	0,00	Death-associated protein kinase 2
Dbndd2	52840	1,01	0,00	Dysbindin (dystrobrevin binding protein 1) domain containing 2
Dcbld1	66686	1,14/1,33	0,00/0,00	Discoidin, CUB and LCCL domain containing 1
Dcn	13179	-2,21	0,00	Decorin
Ddah1	69219	1,04/1,13	0,01/0,02	Dimethylarginine dimethylaminohydrolase 1

Gene symbol	EntrezGene ID	Log-ratio	p-value	Gene name
Ddhd2	72108	-1,49	0,03	DDHD domain containing 2
Ddit4l	73284	1,47/1,67	0,00/0,00	DNA-damage-inducible transcript 4-like
Ddr1	12305	1,18/1,91/2,64	0,00/0,00/0,00	Discoidin domain receptor tyrosine kinase 1
Ddx1	104721	1,07	0,01	DEAD (Asp-Glu-Ala-Asp) box polypeptide 1
Ddx25	30959	1,34	0,04	DEAD (Asp-Glu-Ala-Asp) box polypeptide 25
Dera	232449	-1,09	0,00	Deoxyribose-phosphate aldolase (putative)
Det1	76375	1,00	0,01	De-etiolated homolog 1 (Arabidopsis)
Dgkz	104418	1,15	0,00	Diacylglycerol kinase, zeta
Dhcr7	13360	1,64	0,01	7-dehydrocholesterol reductase
Dhtkd1	209692	-2,05	0,01	Dehydrogenase E1 and transketolase domain containing 1
Dkk4	234130	-1,72	0,00	Dickkopf homolog 4 (Xenopus laevis)
Dleu2	668253	-1,20/-1,15	0,00/0,01	Deleted in lymphocytic leukemia 2 (non-protein coding)
Dlgap4	228836	1,01	0,00	Discs, large (Drosophila) homolog-associated protein 4
Dlx4	13394	1,07/1,35	0,01/0,00	Distal-less homeobox 4
Dmgdh	74129	-1,55	0,00	Dimethylglycine dehydrogenase
Dmrta1	242523	-1,73	0,00	DMRT-like family A1
Dmxl2	235380	-1,42	0,02	Dmx-like 2
Dnajc10	66861	1,03	0,00	DnaJ (Hsp40) homolog, subfamily C, member 10
Dnase1	13419	-1,31	0,01	Deoxyribonuclease I
Dnase2a	13423	-1,65	0,01	Deoxyribonuclease II alpha
Dntt	21673	1,97	0,04	Deoxynucleotidyltransferase, terminal
Dock8	76088	-2,26	0,00	Dedicator of cytokinesis 8
Dopey2	70028	-1,00	0,04	Dopey family member 2
Dpp4	13482	-2,30/-1,84/-1,39	0,01/0,01/0,02	Dipeptidyl-peptidase 4
Dpy19l1	244745	-1,13/-1,02	0,01/0,01	Dpy-19-like 1 (C. elegans)
Dpy19l3	233115	-1,94/-1,23	0,00/0,03	Dpy-19-like 3 (C. elegans)
Dpyd	99586	-1,71/-1,51	0,00/0,00	Dihydropyrimidine dehydrogenase
Dpys	64705	-2,33/-1,88/-1,84	0,04/0,00/0,01	Dihydropyrimidinase
Dse	212898	-1,07	0,04	Dermatan sulfate epimerase
Dusp16	70686	1,26	0,01	Dual specificity phosphatase 16
Dusp5	240672	1,85	0,00	Dual specificity phosphatase 5
Dusp6	67603	2,57	0,00	Dual specificity phosphatase 6
Dynll1	56455	2,19	0,00	Dynein, light chain, LC8-type 1
E2f8	108961	-1,44	0,01	E2F transcription factor 8
Ecm1	13601	-1,63	0,01	Extracellular matrix protein 1
Ednra	13617	-1,18	0,00	Endothelin receptor type A
Efemp1	216616	-1,36	0,01	EGF containing fibulin-like extracellular matrix protein 1
Efnb2	13642	1,33	0,01	Ephrin-B2
Egfr	13649	-1,47/-1,11/-1,04	0,00/0,01/0,04	Epidermal growth factor receptor
Egr1	13653	3,88	0,00	Early growth response 1
Ehd4	98878	1,47	0,01	EH-domain containing 4
Eif2c2	239528	1,11	0,01	Eukaryotic translation initiation factor 2C, 2
Elovl3	12686	-3,12	0,05	ELOVL fatty acid elongase 3
Elovl7	74559	1,62/1,76/2,04/2,40/ 2,59	0,00/0,01/0,00/0,00/0,00	ELOVL fatty acid elongase 7
Emcn	59308	2,02	0,01	Endomucin
Enc1	13803	1,95/2,45	0,00/0,00	Ectodermal-neural cortex 1 (with BTB-like domain)
Enpep	13809	-1,37	0,00	Glutamyl aminopeptidase (aminopeptidase A)
Enpp1	18605	1,05/1,24/1,52	0,00/0,00/0,00	Ectonucleotide pyrophosphatase/phosphodiesterase 1
Enpp2	18606	1,41	0,00	Ectonucleotide pyrophosphatase/phosphodiesterase 2
Enpp5	83965	-1,04	0,01	Ectonucleotide pyrophosphatase/phosphodiesterase 5 (putative)
Entpd2	12496	1,86	0,00	Ectonucleoside triphosphate diphosphohydrolase 2
Epas1	13819	1,49	0,00	Endothelial PAS domain protein 1
Ephx2	13850	-1,13	0,01	Epoxide hydrolase 2, cytoplasmic
Ergic1	67458	-1,09	0,03	Endoplasmic reticulum-golgi intermediate compartment (ERGIC) 1
Ero1lb	67475	-1,65/-1,07	0,00/0,02	ERO1-like beta (S. cerevisiae)
Erp27	69187	-1,72	0,01	Endoplasmic reticulum protein 27
Esm1	71690	4,13	0,00	Endothelial cell-specific molecule 1
Etl4	208618	1,09	0,00	Enhancer trap locus 4
Etnk1	75320	1,06	0,04	Ethanolamine kinase 1
Etnk2	214253	-1,23	0,02	Ethanolamine kinase 2
Ets2	23872	1,05/1,42	0,02/0,00	V-ets erythroblastosis virus E26 oncogene homolog 2 (avian)
Etv5	104156	1,57	0,00	Ets variant 5
Exph5	320051	-1,05	0,02	Exophilin 5
Extl1	56219	-1,00	0,00	Exostoses (multiple)-like 1
F11r	16456	1,65	0,00	F11 receptor
F2r	14062	1,24	0,00	Coagulation factor II (thrombin) receptor
F2rl1	14063	3,81	0,00	Coagulation factor II (thrombin) receptor-like 1
Fabp4	11770	1,33/2,10/2,24	0,01/0,01/0,00	Fatty acid binding protein 4, adipocyte
Fabp5	16592	2,16	0,00	Fatty acid binding protein 5 (psoriasis-associated)
Fabp7	12140	-1,92	0,05	Fatty acid binding protein 7, brain
Fads1	76267	1,16	0,01	Fatty acid desaturase 1
Fads2	56473	1,36/1,54/1,88	0,01/0,01/0,00	Fatty acid desaturase 2
Fam110c	104943	1,56/1,61	0,00/0,00	Family with sequence similarity 110, member C

Gene symbol	EntrezGene ID	Log-ratio	p-value	Gene name
Fam114a1	68303	1,01	0,00	Family with sequence similarity 114, member A1
Fam118a	73225	1,05	0,00	Family with sequence similarity 118, member A
Fam126a	84652	1,01	0,00	Family with sequence similarity 126, member A
Fam176a	232146	-1,07	0,00	Family with sequence similarity 176, member A
Fam19a5	106014	-1,26	0,00	Family with sequence similarity 19 (chemokine (C-C motif)-like), member A5
Fam25c	69134	-2,87	0,00	Family with sequence similarity 25, member C
Fam3c	27999	1,77/1,99	0,00/0,00	Family with sequence similarity 3, member C
Fam43a	224093	1,18	0,01	Family with sequence similarity 43, member A
Fam46a	212943	2,31	0,00	Family with sequence similarity 46, member A
Fam46c	74645	1,56/1,96	0,01/0,00	Family with sequence similarity 46, member C
Fam59a	381126	1,24	0,00	Family with sequence similarity 59, member A
Fam65b	193385	-1,91	0,02	Family with sequence similarity 65, member B
Fam69a	67266	-1,76	0,05	Family with sequence similarity 69, member A
Fam81a	76886	1,50	0,00	Family with sequence similarity 81, member A
Fam82a1	381110	-1,50/-1,48/-1,42	0,01/0,02/0,00	Family with sequence similarity 82, member A1
Fam84b	399603	2,32	0,00	Family with sequence similarity 84, member B
Farp2	227377	-1,41/-1,00	0,00/0,00	FERM, RhoGEF and pleckstrin domain protein 2
Fat1	14107	1,33	0,00	FAT tumor suppressor homolog 1 (Drosophila)
Fblim1	74202	1,88/2,20	0,00/0,00	Filamin binding LIM protein 1
Fdft1	14137	1,18/1,27	0,04/0,04	Farnesyl-diphosphate farnesyltransferase 1
Fgf1	14164	-1,59/-1,34	0,00/0,00	Fibroblast growth factor 1 (acidic)
Fgf21	56636	1,32	0,04	Fibroblast growth factor 21
Fgfr2	14183	1,26	0,00	Fibroblast growth factor receptor 2
Fgl2	14190	2,31/2,69	0,01/0,01	Fibrinogen-like 2
Fitm1	68680	-1,71	0,00	Fat storage-inducing transmembrane protein 1
Fkbp11	66120	2,31	0,00	FK506 binding protein 11, 19 kDa
Fmn1	14260	1,11	0,03	Formin 1
Fmn2	54418	-2,51/-2,49	0,04/0,02	Formin 2
Fmnl2	71409	1,29	0,00	Formin-like 2
Fmo1	14261	-1,20	0,02	Flavin containing monooxygenase 1
Fn3k	63828	-2,16	0,01	Fructosamine 3 kinase
Fndc3b	72007	2,08/2,16	0,00/0,00	Fibronectin type III domain containing 3B
Folr2	14276	-1,18	0,03	Folate receptor 2 (fetal)
Fos	14281	2,38	0,00	FBJ murine osteosarcoma viral oncogene homolog
Foxa3	15377	1,07	0,00	Forkhead box A3
Foxp2	114142	-1,77/-1,62/-1,21	0,00/0,00/0,00	Forkhead box P2
Frk	14302	1,05/1,09	0,00/0,01	Fyn-related kinase
Frmd6	319710	1,07	0,01	FERM domain containing 6
Frmd8	67457	1,10	0,01	FERM domain containing 8
Fscn1	14086	1,67	0,01	Fascin homolog 1, actin-bundling protein (Strongylocentrotus purpuratus)
Fst	14313	3,53/4,19	0,00/0,00	Follistatin
Fubp1	51886	1,02	0,01	Far upstream element (FUSE) binding protein 1
Fxyd1	56188	-1,14	0,00	FXYD domain containing ion transport regulator 1
Fzd3	14365	1,13/2,00	0,01/0,00	Frizzled family receptor 3
Fzd5	14367	1,11	0,01	Frizzled family receptor 5
G6pc	14377	-2,71	0,01	Glucose-6-phosphatase, catalytic subunit
G6pdx	14381	1,77	0,00	Glucose-6-phosphate dehydrogenase X-linked
Gabarapl1	57436	-1,39/-1,27	0,01/0,01	GABA(A) receptor-associated protein like 1
Galm	319625	-1,08	0,00	Galactose mutarotase (aldose 1-epimerase)
Galnt12	230145	1,40	0,00	UDP-N-acetyl-alpha-D-galactosamine:polypeptide N-acetylgalactosaminyltransferase 12 (GalNAc-T12)
Galnt6	207839	1,65/2,55	0,00/0,00	UDP-N-acetyl-alpha-D-galactosamine:polypeptide N-acetylgalactosaminyltransferase 6 (GalNAc-T6)
Galntl2	78754	1,12	0,02	UDP-N-acetyl-alpha-D-galactosamine:polypeptide N-acetylgalactosaminyltransferase-like 2
Gas1	14451	-3,13/-1,75	0,00/0,00	Growth arrest-specific 1
Gas2	14453	-2,01	0,00	Growth arrest-specific 2
Gca	227960	1,13	0,00	Grancalcin, EF-hand calcium binding protein
Gcdh	270076	-1,18	0,02	Glutaryl-CoA dehydrogenase
Gch1	14528	-1,20	0,00	GTP cyclohydrolase 1
Gcnt2	14538	1,00/1,14/1,29	0,02/0,00/0,01	Glucosaminyl (N-acetyl) transferase 2, I-branching enzyme (I blood group)
Gde1	56209	-1,10	0,02	Glycerophosphodiester phosphodiesterase 1
Gdf10	14560	-2,39	0,00	Growth differentiation factor 10
Gdf2	12165	-1,33	0,01	Growth differentiation factor 2
Gem	14579	-1,41	0,01	GTP binding protein overexpressed in skeletal muscle
Ggct	110175	1,39	0,01	Gamma-glutamylcyclotransferase
Ggnbp1	70772	-1,12	0,03	Gametogenetin binding protein 1
Ggt6	71522	-1,22	0,01	Gamma-glutamyltransferase 6
Ggta1	14594	1,69	0,00	Glycoprotein, alpha-galactosyltransferase 1 pseudogene
Ghr	14600	-1,99/-1,31/-1,12	0,00/0,00/0,00	Growth hormone receptor
Glipr1	73690	1,94	0,00	Glioma pathogenesis-related protein 1
Glis3	226075	1,57	0,00	GLIS family zinc finger 3
Glo1	109801	-1,62	0,00	Glyoxalase I
Glrx	93692	-1,17/-1,17	0,00/0,01	Glutaredoxin (thioltransferase)
Glul	14645	-1,96/-1,34	0,01/0,02	Glutamate-ammonia ligase
Gmfb	63985	1,10	0,00	Glia maturation factor, beta

Gene symbol	EntrezGene ID	Log-ratio	p-value	Gene name
Gna14	14675	-2,70/-2,32/-2,24	0,00/0,01/0,00	Guanine nucleotide binding protein (G protein), alpha 14
Gnai1	14677	-1,23	0,02	Guanine nucleotide binding protein (G protein), alpha inhibiting activity polypeptide 1
Gnmt	14711	-1,61	0,01	Glucosaminyl (N-acetyl) transferase 3
Gnpda1	26384	-1,30	0,00	Glucosamine-6-phosphate deaminase 1
Golm1	105348	3,51	0,00	Golgi membrane protein 1
Gpam	14732	1,22	0,03	Glycerol-3-phosphate acyltransferase, mitochondrial
Gpc1	14733	1,18	0,02	Glypican 1
Gpc3	14734	4,23	0,00	Glypican 3
Gpc6	23888	1,64/1,73/2,16	0,01/0,04/0,00	Glypican 6
Gpr110	77596	1,19	0,03	G protein-coupled receptor 110
Gpr12	14738	-1,03	0,00	G protein-coupled receptor 12
Gpr39	71111	1,02	0,01	G protein-coupled receptor 39
Gpr98	110789	-1,64	0,00	G protein-coupled receptor 98
Gprc5b	64297	2,54/4,38	0,00/0,00	G protein-coupled receptor, family C, group 5, member B
Gprc5c	70355	1,10	0,01	G protein-coupled receptor, family C, group 5, member C
Gpx1	14775	-1,09	0,01	Glutathione peroxidase 1
Gramd1b	235283	1,26	0,02	GRAM domain containing 1B
Greb1l	381157	1,46	0,01	Growth regulation by estrogen in breast cancer-like
Grhl1	195733	1,59	0,00	Grainyhead-like 1 (Drosophila)
Gria3	53623	1,66/3,31	0,02/0,00	Glutamate receptor, ionotropic, AMPA 3
Grm8	14823	-1,47	0,00	Glutamate receptor, metabotropic 8
Gsn	227753	-1,71/-1,67/-1,48	0,04/0,05/0,04	Gelsolin
Gspt2	14853	2,27/2,47	0,00/0,00	G1 to S phase transition 2
Gss	14854	1,02	0,00	Glutathione synthetase
Gsta2	14858	-2,59	0,00	Glutathione S-transferase alpha 2
Gsta3	14859	-1,58/-1,20	0,00/0,01	Glutathione S-transferase alpha 3
Gstk1	76263	-1,24	0,01	Glutathione S-transferase kappa 1
Gucy1a3	60596	-1,17	0,00	Guanylate cyclase 1, soluble, alpha 3
Gucy1b3	54195	-1,03	0,01	Guanylate cyclase 1, soluble, beta 3
H19	14955	3,28	0,00	H19, imprinted maternally expressed transcript (non-protein coding)
Haao	107766	-1,01	0,01	3-hydroxyanthranilate 3,4-dioxygenase
Habp2	226243	-1,26	0,01	Hyaluronan binding protein 2
Hacl1	56794	-1,99	0,02	2-hydroxyacyl-CoA lyase 1
Hand2	15111	-1,52	0,01	Heart and neural crest derivatives expressed 2
Hao2	56185	1,37	0,02	Hydroxyacid oxidase 2 (long chain)
Haus7	73738	1,09	0,00	HAUS augmin-like complex, subunit 7
Hcfc1r1	353502	-1,26/-1,23	0,00/0,01	Host cell factor C1 regulator 1 (XPO1 dependent)
Hebp1	15199	-1,08	0,01	Heme binding protein 1
Hes1	15205	1,44	0,00	Hairy and enhancer of split 1, (Drosophila)
Hes6	55927	-1,11	0,01	Hairy and enhancer of split 6 (Drosophila)
Hexa	15211	1,29	0,00	Hexosaminidase A (alpha polypeptide)
Hexb	15212	1,06	0,01	Hexosaminidase B (beta polypeptide)
Hgd	15233	-1,25	0,01	Homogentisate 1,2-dioxygenase
Hgf	15234	-1,21	0,00	Hepatocyte growth factor (hepapoietin A; scatter factor)
Hgfac	54426	1,19	0,00	HGF activator
Hhip	15245	-1,37	0,00	Hedgehog interacting protein
Hibadh	58875	-1,33/-1,25	0,00/0,00	3-hydroxyisobutyrate dehydrogenase
Hilpda	69573	1,61	0,00	Hypoxia inducible lipid droplet-associated
Hmgcr	15357	2,28	0,00	3-hydroxy-3-methylglutaryl-CoA reductase
Hmgcs1	208715	1,75/1,79/1,92/2,28/2,59	0,02/0,02/0,02/0,03/0,02	3-hydroxy-3-methylglutaryl-CoA synthase 1 (soluble)
Hmgcs2	15360	-1,35	0,01	3-hydroxy-3-methylglutaryl-CoA synthase 2 (mitochondrial)
Hn1	15374	1,16	0,00	Hematological and neurological expressed 1
Homer2	26557	-1,78/-1,52	0,03/0,02	Homer homolog 2 (Drosophila)
Hpd	15445	-1,86	0,01	4-hydroxyphenylpyruvate dioxygenase
Hpgd	15446	-1,50/-1,36	0,01/0,01	Hydroxyprostaglandin dehydrogenase 15-(NAD)
Hps4	192232	-1,29	0,02	Hermansky-Pudlak syndrome 4
Hsbp1l1	66255	2,18	0,00	Heat shock factor binding protein 1-like 1
Hsd17b13	243168	1,41	0,00	Hydroxysteroid (17-beta) dehydrogenase 13
Hsd3b2	15493	-2,28	0,00	Hydroxy-delta-5-steroid dehydrogenase, 3 beta- and steroid delta-isomerase 2
Hsd3b3	15494	-1,40	0,00	Hydroxy-delta-5-steroid dehydrogenase, 3 beta- and steroid delta-isomerase 3
Hsd3b5	15496	-4,07	0,01	Hydroxy-delta-5-steroid dehydrogenase, 3 beta- and steroid delta-isomerase 5
Hsd3b7	101502	-1,18	0,03	Hydroxy-delta-5-steroid dehydrogenase, 3 beta- and steroid delta-isomerase 7
Hsf2bp	74377	1,57	0,03	Heat shock transcription factor 2 binding protein
Hspa4l	18415	1,14/1,21/1,53	0,02/0,02/0,00	Heat shock 70kDa protein 4-like
Hspa8	15481	1,06/1,24	0,03/0,01	Heat shock 70kDa protein 8
Hspb1	15507	-1,09	0,04	Heat shock 27kDa protein 1
Hspb6	243912	-1,40	0,00	Heat shock protein, alpha-crystallin-related, B6
Ica1	15893	1,59/1,72	0,01/0,00	Islet cell autoantigen 1, 69kDa
Id1	15901	2,28	0,01	Inhibitor of DNA binding 1, dominant negative helix-loop-helix protein

Gene symbol	EntrezGene ID	Log-ratio	p-value	Gene name
Ido2	209176	-1,11	0,01	Indoleamine 2,3-dioxygenase 2
Ier3	15937	1,87	0,02	Immediate early response 3
Ier5	15939	1,00/1,43	0,02/0,00	Immediate early response 5
Ifi27l2b	217845	3,35	0,00	Alpha-inducible protein 27 like 2B
Ifi44	99899	1,48	0,00	Interferon-induced protein 44
Ifitm1	68713	-2,03	0,00	Interferon induced transmembrane protein 1
Ifngr1	15979	1,71	0,00	Interferon gamma receptor 1
Ifrd1	15982	1.03	0.04	Interferon-related developmental regulator 1
Ift122	81896	1.47	0.00	Intraflagellar transport 122 homolog
Igdcc4	56741	4.41/4.71	0.00/0.00	Immunoglobulin superfamily, DCC subclass, member 4
Igf1	16000	-1.54/-1.47/-1.27/-1.24	0.00/0.00/0.01/0.01	Insulin-like growth factor 1
Igfals	16005	-3.00	0.00	Insulin-like growth factor binding protein, acid labile subunit
Igfbp1	16006	3.11	0.00	Insulin-like growth factor-binding protein 1
Igfbp5	16011	-2.15	0.04	Insulin-like growth factor-binding protein 5
Ighm	16019	-1.24/-1.09	0.02/0.05	Immunoglobulin heavy constant mu
Igsf5	72058	1.16	0.00	Immunoglobulin superfamily member 5
Igsf8	140559	1.17	0.00	Immunoglobulin superfamily member 8
Ikbip	67454	1.17/1.27	0.00/0.00	IKBKB interacting protein
Il18	16173	-1.13	0.05	Interleukin 18 (interferon-gamma-inducing factor)
Il1r1	16177	-1.00	0.02	Interleukin 1 receptor, type I
Il1rap	16180	-1.36	0.00	Interleukin 1 receptor accessory protein
Il1rn	16181	1.50/2.97/3.60	0.03/0.00/0.00	Interleukin 1 receptor antagonist
Il33	77125	1.92	0.00	Interleukin 33
Il6st	16195	-1.00	0.03	Interleukin 6 signal transducer (gp130, oncostatin M receptor)
Ildr2	100039795	-2.00/-1.88	0.02/0.02	Immunoglobulin-like domain containing receptor 2
Inca1	103844	-1.09	0.02	Inhibitor of CDK, cyclin A1 interacting protein 1
Inf2	70435	1.11	0.01	Inverted formin, FH2 and WH2 domain containing
Inhbb	16324	3.10	0.01	Inhibin, beta B
Inpp1	16329	1.52	0.00	Inositol polyphosphate-1-phosphatase
Ipcef1	320495	4.54	0.00	Interaction protein for cytohesin exchange factors 1
Iqgap1	29875	1.05	0.02	IQ motif containing GTPase activating protein 1
Irx3	16373	3.22	0.00	Iroquois homeobox 3
Islr	26968	-1.17	0.01	Immunoglobulin superfamily containing leucine-rich repeat
Isyna1	71780	1.24	0.00	Inositol-3-phosphate synthase 1
Itga6	16403	1.94/2.73	0.00/0.00	Integrin, alpha 6
Itih5	209378	3.60/3.67/3.89	0.00/0.00/0.00	Inter-alpha-trypsin inhibitor heavy chain family, member 5
Itm2c	64294	1.43	0.00	Integral membrane protein 2C
Itpripl2	319622	1.61	0.00	Inositol 1,4,5-trisphosphate receptor interacting protein-like 2
Ivd	56357	-1.06	0.02	Isovaleryl-CoA dehydrogenase
Ivns1abp	117198	1.14	0.04	Influenza virus NS1A binding protein
Jazf1	231986	1.17	0.02	JAZF zinc finger 1
Jub	16475	2.35	0.00	Ajuba
Jun	16476	1.12/1.27	0.01/0.00	Jun proto-oncogene
Junb	16477	1.18	0.01	Jun B proto-oncogene
Kalrn	545156	-1.16	0.02	Kalirin, RhoGEF kinase
Kazald1	107250	1.93	0.02	Kazal-type serine peptidase inhibitor domain 1
Kbtbd13	74492	1.65	0.02	Kelch repeat and BTB (POZ) domain containing 13
Kbtbd8	243574	1.07	0.00	Kelch repeat and BTB (POZ) domain containing 8
Kcnj8	16523	1.28	0.02	Potassium inwardly-rectifying channel, subfamily J, member 8
Kcnk1	16525	-1.39	0.01	Potassium channel, subfamily K, member 1
Kcnk5	16529	-1.23	0.01	Potassium channel, subfamily K, member 5
Kcnt2	240776	-2.28	0.00	Potassium channel, subfamily T, member 2
Kctd12	239217	1.27	0.02	Potassium channel tetramerisation domain containing 12
Kctd12b	207474	1.34	0.01	Potassium channel tetramerisation domain containing 12B
Kctd15	233107	-1.34	0.00	Potassium channel tetramerisation domain containing 15
Kctd3	226823	1.31/1.72	0.00/0.00	Potassium channel tetramerisation domain containing 3
Kdelr3	105785	2.21	0.00	KDEL (Lys-Asp-Glu-Leu) endoplasmic reticulum protein retention receptor 3
Keg1	64697	-1.96	0.00	Kidney expressed gene 1
Khdrbs3	13992	-1.49	0.01	KH domain containing, RNA binding, signal transduction associated 3
Kif13a	16553	1.73	0.04	Kinesin family member 13A
Kif20a	19348	1.75	0.05	Kinesin family member 20A
Kif21a	16564	1.05	0.00	Kinesin family member 21A
Kif5c	16574	3.64/4.89	0.00/0.00	Kinesin family member 5C
Kifc3	16582	1.30	0.00	Kinesin family member C3
Klc3	232943	1.28	0.01	Kinesin light chain 3
Klf1	16596	-1.90	0.00	Krueppel-like factor 1
Klf4	16600	1.22/1.57	0.00/0.00	Krueppel-like factor 4

Gene symbol	EntrezGene ID	Log-ratio	p-value	Gene name
Klf6	23849	1.05/1.22/1.35/1.49/ 1.66	0.01/0.00/0.00/0.00/0.00	Krueppel-like factor 6
Klhdc2	69554	1.20/1.48	0.00/0.00	Kelch domain containing 2
Klhl13	67455	2.29/2.74	0.00/0.00	Kelch-like 13
Klhl4	237010	1.11	0.03	Kelch-like 4
Klk1b4	18048	2.96/3.01	0.00/0.00	Kallikrein 1-related peptidase b4
Klk1b5	16622	1.18	0.00	Kallikrein 1-related peptidase b5
Krt18	16668	1.48	0.00	Keratin 18
Krt23	94179	2.69	0.01	Keratin 23
Krtap16-4	170654	-1.03	0.00	Keratin associated protein 16-4
Kynu	70789	-1.46	0.01	Kynureninase
L2hgdh	217666	-1.03	0.00	L-2-hydroxyglutarate dehydrogenase
L3mbtl3	237339	1.23	0.00	L(3)mbt-like 3
Lama1	t16772	-1.01	0.01	Laminin, alpha 1
Lama3	16774	-2.73	0.00	Laminin, alpha 3
Lass6	241447	1.74	0.01	Longevity assurance homolog 6
Lbp	16803	-1.21/-1.08	0.01/0.02	Lipopolysaccharide binding protein
Lcn13	227627	-3.82	0.01	Lipocalin 13
Lcn2	16819	2.64	0.03	Lipocalin 2
Lcp1	18826	-1.50/-1.26	0.02/0.01	Lymphocyte cytosolic protein 1 (L-plastin)
Ldhd	52815	-2.08/-2.03	0.00/0.00	Lactate dehydrogenase D
Leap2	259301	-2.00	0.00	Liver expressed antimicrobial peptide 2
Lect1	16840	-2.15	0.03	Leukocyte cell-derived chemotaxin 1
Lect2	16841	-1.83	0.00	Leukocyte cell-derived chemotaxin 2
Lepr	16847	3.01/3.43	0.00/0.00	Leptin receptor
Leprot	230514	1.15/1.31/1.35	0.01/0.00/0.00	Leptin receptor overlapping transcript
Lgals1	16852	1.41/1.44	0.00/0.00	Lectin, galactoside-binding, soluble, 1
Lgmn	19141	1.27	0.00	Legumain
Lgr5	14160	-1.61	0.00	Leucine-rich repeat containing G protein-coupled receptor 5
Lhpp	76429	-2.40	0.00	Phospholysine phosphohistidine inorganic pyrophosphate phosphatase
Lhx2	16870	-1.53	0.00	LIM homeobox 2
Lif	16878	1.02	0.00	Leukemia inhibitory factor
Lifr	16880	-1.24	0.01	Leukemia inhibitory factor receptor alpha
Limd1	29806	1.16/1.35	0.01/0.00	LIM domains containing 1
Lims2	225341	-1.18	0.03	LIM and senescent cell antigen-like domains 2
Lin7a	108030	-1.63/-1.59/-1.37	0.03/0.00/0.00	Lin-7 homolog A
Lipc	15450	-2.48	0.01	Lipase, hepatic
Lipg	16891	-1.12	0.01	Lipase, endothelial
Lmna	16905	1.07/1.26	0.00/0.00	Lamin A/C
Lphn1	330814	-1.03	0.00	Latrophilin 1
Lpl	16956	1.86/2.29	0.03/0.01	Lipoprotein lipase
Lrat	79235	-2.13	0.00	Lecithin retinol acyltransferase
Lrit1	239037	-2.29	0.01	Leucine-rich repeat, immunoglobulin-like and transmembrane domains 1
Lrit2	239038	-1.90	0.01	Leucine-rich repeat, immunoglobulin-like and transmembrane domains 2
Lrp11	237253	1.25	0.00	Low density lipoprotein receptor-related protein 11
Lrp12	239393	1.10	0.01	Low density lipoprotein receptor-related protein 12
Lrrc24	378937	2.10	0.00	Leucine rich repeat containing 24
Lrrc8c	100604	1.09	0.00	Leucine rich repeat containing 8 family, member C
Lrrc8e	72267	1.10/1.21	0.03/0.01	Leucine rich repeat containing 8 family, member E
Lrtm1	319476	-2.17	0.04	Leucine-rich repeats and transmembrane domains 1
Lss	16987	1.07/2.36/2.67	0.03/0.01/0.00	Lanosterol synthase (2,3-oxidosqualene-lanosterol cyclase)
Ltb	16994	2.52	0.01	Lymphotoxin beta (TNF superfamily, member 3)
Lum	17022	-1.78	0.00	Lumican
Ly6a	110454	-2.42	0.03	Lymphocyte antigen 6 complex, locus A
Ly6d	17068	4.37	0.00	Lymphocyte antigen 6 complex, locus D
Lysmd2	70082	2.26	0.00	Putative peptidoglycan-binding, domain containing 2
Lyve1	114332	1.40	0.04	Lymphatic vessel endothelial hyaluronan receptor 1
Macrod1	107227	-2.24	0.00	MACRO domain containing 1
Macrod2	72899	-1.10	0.01	MACRO domain containing 2
Mad2l1	56150	1.27	0.00	MAD2 mitotic arrest deficient-like 1
Maff	17133	1.64	0.00	V-maf musculoaponeurotic fibrosarcoma oncogene homolog F (avian)
Maged1	94275	1.00/1.20	0.00/0.00	Melanoma antigen family H, 1
Magi3	99470	1.18	0.00	Membrane associated guanylate kinase, WW and PDZ domain containing 3
Mamdc2	71738	-2.65	0.00	MAM domain containing 2
Mansc1	67729	1.74	0.00	MANSC domain containing 1
Map2k6	26399	-1.07	0.03	Mitogen-activated protein kinase kinase 6
Map4k4	26921	1.06/1.79	0.00/0.00	Mitogen-activated protein kinase kinase kinase kinase 4
Marveld2	218518	1.07	0.01	MARVEL domain containing 2
Marveld3	73608	1.56	0.00	MARVEL domain containing 3
Mast3	546071	-1.21	0.01	Microtubule associated serine/threonine kinase 3
Mbl1	17194	-1.68	0.00	Mannose-binding lectin (protein A) 1
Mcart1	230125	-1.14	0.02	Mitochondrial carrier triple repeat 1
Mcm10	70024	-2.43/-1.40	0.00/0.00	Minichromosome maintenance complex component 10

Gene symbol	EntrezGene ID	Log-ratio	p-value	Gene name
Mcm2	17216	1.76	0.00	Minichromosome maintenance complex component 2
Me1	17436	-1.48/-1.23	0.03/0.02	Malic enzyme 1, NADP(+)-dependent, cytosolic
Meg3	17263	-1.07	0.01	Maternally expressed 3
Mep1b	17288	2.69	0.00	Meprin A subunit beta
Mfge8	17304	1.30	0.03	Milk fat globule-EGF factor 8
Mfn2	170731	-1.16	0.00	Mitofusin 2
Mfsd6	98682	1.18	0.00	Major facilitator superfamily domain containing 6
Mgat5	107895	1.20/1.49	0.00/0.00	Mannosyl (alpha-1,6-)-glycoprotein beta-1,6-N-acetyl-glucosaminyltransferase
Mgll	23945	-1.12/-1.04	0.05/0.03	Monoacylglycerol lipase
Minpp1	17330	1.14	0.00	Multiple inositol-polyphosphate phosphatase 1
Miox	56727	2.75	0.00	Myo-inositol oxygenase
Mlkl	74568	1.15	0.02	Mixed lineage kinase domain-like
Mllt3	70122	1.40/1.61/1.96	0.00/0.00/0.00	Myeloid/lymphoid or mixed-lineage leukemia (trithorax homolog, Drosophila); translocated to, 3
Mmd	67468	-1.20	0.01	Monocyte to macrophage differentiation-associated
Mmd2	75104	-1.89/-1.48	0.02/0.01	Monocyte to macrophage differentiation-associated 2
Mmp12	17381	1.76	0.03	Matrix metalloproteinase 12
Mmp13	17386	1.97	0.01	Matrix metalloproteinase 13
Mmp14	17387	1.16/1.36	0.00/0.01	Matrix metalloproteinase 14
Mob3a	208228	1.08	0.00	MOB kinase activator 3A
Mob3b	214944	1.21	0.01	MOB kinase activator 3B
Morc4	75746	1.02	0.00	MORC family CW-type zinc finger 4
Morf4l2	56397	1.01/1.01	0.01/0.01	Mortality factor 4 like 2
Mpdz	17475	-1.55/-1.04	0.00/0.01	Multiple PDZ domain protein
Mpeg1	17476	1.46	0.01	Macrophage-expressed *gene* 1
Mpp1	17524	1.19	0.01	Membrane protein, palmitoylated 1 (MAGUK p55 subfamily member 4)
Mpp4	227157	-1.22	0.04	Membrane protein, palmitoylated 4 (MAGUK p55 subfamily member 4)
Mpped1	223726	1.47	0.00	Metallophosphoesterase domain containing 1
Mreg	381269	-1.24	0.05	Melanoregulin
Ms4a4d	66607	-1.44	0.01	Membrane-spanning 4-domains, subfamily A, member 4D
Msrb3	320183	1.60	0.00	Methionine sulfoxide reductase B3
Mst1r	19882	1.38	0.02	Macrophage stimulating 1 receptor
Mthfd2l	665563	1.23	0.00	Methylenetetrahydrofolate dehydrogenase (NADP+ dependent) 2-like
Mtmr11	194126	3.53	0.00	Myotubularin related protein 11
Mtmr2	77116	1.06	0.00	Myotubularin related protein 2
Mtmr4	170749	-1.04	0.01	Myotubularin related protein 4
Mtpn	14489	1.45	0.00	Myotrophin
Mtx3	382793	-1.07	0.01	Metaxin 3
Mup10	100039008	-4.70	0.02	Major urinary protein 10
Mup3	17842	-2.16/-1.77	0.00/0.01	Major urinary protein 3
Mup4	17843	-1.49	0.00	Major urinary protein 4
Mup5	17844	-1.60	0.01	Major urinary protein 5
Mustn1	66175	-1.18	0.02	Musculoskeletal, embryonic nuclear protein 1
Mvd	192156	1.46	0.03	Mevalonate (diphospho) decarboxylase
Myadm	50918	1.87/1.98	0.00/0.00	Myeloid-associated differentiation marker
Mycn	18109	2.45	0.00	V-myc myelocytomatosis viral related oncogene, neuroblastoma derived
Myef2	17876	1.05	0.01	Myelin expression factor 2
Myh9	17886	1.01/1.09/1.24	0.00/0.00/0.00	Myosin, heavy chain 9, non-muscle
Myo5c	208943	2.13	0.00	Myosin VC
Myzap	102371	1.27	0.01	Myocardial zonula adherens protein
N4bp2l1	100637	-1.09	0.01	NEDD4 binding protein 2-like 1
Nagpa	27426	-1.05	0.00	N-acetylglucosamine-1-phosphodiester alpha-N-acetylglucosaminidase
Naip2	17948	1.46	0.00	NLR family, apoptosis inhibitory protein 2
Nars2	244141	-1.04	0.00	Asparaginyl-tRNA synthetase 2, mitochondrial (putative)
Nat1	17960	-1.78	0.00	N-acetyltransferase 1 (arylamine N-acetyltransferase)
Nat6	56441	-1.00	0.02	N-acetyltransferase 6 (GCN5-related)
Nat8	68396	-2.97	0.00	N-acetyltransferase 8 (GCN5-related, putative)
Ncam2	17968	-1.07	0.01	Neural cell adhesion molecule 2
Ncapg2	76044	1.36	0.01	Non-SMC condensin II complex, subunit G2
Ndn	17984	-1.90/-1.70/-1.57/-1.53	0.00/0.00/0.00/0.00	Necdin
Ndrg2	29811	-1.76	0.00	NDRG family member 2
Neat1	66961	1.67	0.00	Nuclear enriched abundant transcript 1
Neb	17996	-3.74	0.00	Nebulin
Nebl	74103	-1.50	0.00	Nebulette
Nedd9	18003	1.47/1.49	0.04/0.02	Neural precursor cell expressed, developmentally down-regulated 9
Neto1	246317	1.20	0.00	Neuropilin (NRP) and tolloid (TLL)-like 1
Nfe2	18022	2.49	0.00	Nuclear factor (erythroid-derived 2), 45kDa
Nfil3	18030	-1.05	0.03	Nuclear factor, interleukin 3 regulated
Nfix	18032	-1.45/-1.12/-1.06	0.01/0.02/0.01	Nuclear factor I/X (CCAAT-binding transcription factor)
Ngfrap1	12070	1.92	0.00	Nerve growth factor receptor (TNFRSF16) associated protein 1
Nid1	18073	2.42/3.42	0.00/0.00	Nidogen 1

Gene symbol	EntrezGene ID	Log-ratio	p-value	Gene name
Nipal1	70701	2.89/3.00	0.00/0.00	NIPA-like domain containing 1
Nlrp12	378425	1.84	0.00	NLR family, pyrin domain containing 12
Nnmt	18113	-3.37	0.01	Nicotinamide N-methyltransferase
Noa1	56412	-1.12	0.00	Nitric oxide associated 1
Nop58	55989	1.10	0.02	*NOP58* ribonucleoprotein homolog
Notch4	18132	1.04	0.03	Neurogenic locus notch homolog protein 4
Notum	77583	-1.01	0.01	Notum pectinacetylesterase homolog
Nox4	50490	-2.15/-2.06	0.00/0.00	NADPH oxidase 4
Npc1l1	237636	2.09	0.00	NPC1 (Niemann-Pick disease, type C1, gene)-like 1
Npdc1	18146	2.34	0.00	Neural proliferation differentiation and control 1
Npr2	230103	-1.90	0.00	Natriuretic peptide receptor B/guanylate cyclase B
Nr1i3	12355	-2.46	0.00	Nuclear receptor subfamily 1, group I, member 3
Nrarp	67122	1.22	0.02	NOTCH-regulated ankyrin repeat protein
Nrg1	211323	2.20	0.00	Neuregulin 1
Nrip2	60345	1.18	0.03	Nuclear receptor-interacting protein 2
Nt5e	23959	1.54	0.04	5'-nucleotidase, ecto (CD73)
Ntn1	18208	-1.85	0.00	Netrin 1
Ntn4	57764	1.00/1.43	0.01/0.00	Netrin 4
Ntrk2	18212	-1.15	0.05	Neurotrophic tyrosine kinase, receptor, type 2
Nucb2	53322	2.63	0.00	Nucleobindin 2
Nudt7	67528	-2.27/-1.97/-1.23	0.00/0.00/0.01	Nudix (nucleoside diphosphate linked moiety X)-type motif 7
Nup93	71805	1.14	0.00	Nucleoporin 93kDa
Nupl1	71844	1.52	0.00	Nucleoporin like 1
Nupr1	56312	1.37/1.79	0.02/0.01	Nuclear protein, transcriptional regulator, 1
Nxn	18230	1.60/1.73	0.00/0.00	Nucleoredoxin
Oat	18242	-2.95	0.00	Ornithine aminotransferase
Odz3	23965	-1.67/-1.63	0.01/0.03	Odz, odd Oz/ten-m homolog 3
Ogfrl1	70155	-1.09	0.02	Opioid growth factor receptor-like 1
Ogn	18295	-1.92/-1.13	0.04/0.05	Osteoglycin
Olfm1	56177	-1.19/-1.13	0.03/0.02	Olfactomedin 1
Olfm3	229759	-2.59/-2.26	0.00/0.00	Olfactomedin 3
Olig1	50914	-1.81	0.00	Oligodendrocyte transcription factor 1
Omd	27047	-1.16	0.00	Osteomodulin
Onecut2	225631	-1.88/-1.84/-1.77	0.04/0.02/0.01	One cut homeobox 2
Orai2	269717	1.23	0.02	ORAI calcium release-activated calcium modulator 2
Orm3	18407	-2.16	0.01	Orosomucoid 3
Osbpl10	74486	1.01	0.00	Oxysterol-binding protein-related protein 10
Osbpl3	71720	2.01	0.04	Oxysterol-binding protein-related protein 3
Osgin1	71839	1.47	0.03	Oxidative stress induced growth inhibitor 1
Osgin2	209212	1.48	0.02	Oxidative stress induced growth inhibitor 2
Otc	18416	-1.40/-1.22	0.01/0.02	Ornithine carbamoyltransferase
Otud7b	229603	1.18/1.39	0.00/0.01	OTU domain containing 7B
P2rx7	18439	2.04/2.88	0.00/0.00	Purinergic receptor P2X, ligand-gated ion channel, 7
Pafah1b3	18476	1.39	0.00	Platelet-activating factor acetylhydrolase IB subunit gamma
Pafah2	100163	-1.11	0.00	Platelet-activating factor acetylhydrolase 2, cytoplasmic
Pak1	18479	1.36/1.53	0.05/0.02	p21 protein (Cdc42/Rac)-activated kinase 1
Panx1	55991	1.76	0.00	Pannexin 1
Paqr9	75552	-1.31	0.01	Progestin and adipoQ receptor family member IX
Pard3b	72823	-1.50	0.00	Par-3 partitioning defective 3 homolog B
Parva	57342	-1.00	0.00	Parvin, alpha
Pawr	114774	1.77	0.00	PRKC, apoptosis, WT1, regulator
Pbk	52033	1.69	0.03	PDZ binding kinase
Pbld1	68371	-1.19	0.01	Phenazine biosynthesis-like protein domain containing 1
Pbld2	67307	-1.35	0.00	Phenazine biosynthesis-like protein domain containing 2
Pcdh17	219228	2.03/2.39	0.00/0.00	Protocadherin-17
Pcdhgc4	93707	1.00	0.05	Protocadherin gamma subfamily C, 4
Pck1	18534	-1.69/-1.44/2.46	0.04/0.03/0.00	Phosphoenolpyruvate carboxykinase 1 (soluble)
Pck2	74551	1.26/1.82	0.00/0.00	Phosphoenolpyruvate carboxykinase 2 (mitochondrial)
Pcolce2	76477	-1.85	0.02	Procollagen C-endopeptidase enhancer 2
Pcsk9	100102	1.63	0.02	Proprotein convertase subtilisin/kexin type 9
Pde6c	110855	3.56	0.00	Phosphodiesterase 6C, cGMP-specific, cone, alpha prime
Pde6h	78600	-1.28	0.02	Phosphodiesterase 6H, cGMP-specific, cone, gamma
Pdgfra	18595	-1.70	0.00	Platelet-derived growth factor receptor, alpha polypeptide
Pdilt	71830	-3.08/-2.11	0.00/0.00	Protein disulfide isomerase-like, testis expressed
Pdk1	228026	-1.22	0.03	Pyruvate dehydrogenase kinase, isozyme 1
Pdlim7	67399	1.19/1.88	0.00/0.00	PDZ and LIM domain 7 (enigma)
Pdp1	381511	1.27/2.28	0.01/0.00	Pyruvate dehyrogenase phosphatase catalytic subunit 1
Pdpr	319518	-1.26/-1.20/-1.08	0.01/0.04/0.05	Pyruvate dehydrogenase phosphatase regulatory subunit
Pdzk1ip1	67182	1.53	0.00	PDZK1 interacting protein 1
Pdzrn3	55983	-1.76	0.05	PDZ domain containing ring finger 3
Pea15a	18611	1.10	0.00	Phosphoprotein enriched in astrocytes 15A
Pebp1	23980	-1.09/-1.02	0.00/0.00	Phosphatidylethanolamine binding protein 1

Gene symbol	EntrezGene ID	Log-ratio	p-value	Gene name
Pecr	111175	-1.93	0.00	Peroxisomal trans-2-enoyl-CoA reductase
Peg3	18616	1.42/2.08	0.02/0.03	Paternally expressed gene 3
Pemt	18618	-1.49	0.00	phosphatidylethanolamine N-methyltransferase
Pgd	110208	1.09/1.16	0.00/0.00	Phosphogluconate dehydrogenase
Pglyrp1	21946	1.18	0.01	Peptidoglycan recognition protein 1
Pgm1	66681	1.71	0.00	Phosphoglucomutase 1
Pgm3	109785	1.75	0.00	Phosphoglucomutase 3
Phf3	213109	1.16	0.01	PHD finger protein 3
Phgdh	236539	1.32/3.36/3.70	0.02/0.00/0.00	3-Phosphoglycerate dehydrogenase
Phlda2	22113	1.12	0.01	Pleckstrin homology-like domain, family A, member 2
Phlda3	27280	1.56	0.00	Pleckstrin homology-like domain, family A, member 3
Pigq	14755	-1.30	0.00	Phosphatidylinositol glycan anchor biosynthesis, class Q
Pik3r1	18708	-1.01	0.01	Phosphoinositide-3-kinase, regulatory subunit 1 (alpha)
Pim3	223775	-1.24/-1.23	0.02/0.00	Pim-3 oncogene
Pitpnm1	18739	1.19	0.02	Phosphatidylinositol transfer protein, membrane-associated 1
Pkhd1	241035	1.10	0.04	Polycystic kidney and hepatic disease 1
Pkp2	67451	1.02	0.01	Plakophilin 2
Pla1a	85031	1.05	0.01	Phospholipase A1 member A
Plat	18791	1.40	0.01	Plasminogen activator, tissue
Plce1	74055	1.11	0.04	Phospholipase C, epsilon 1
Plch1	269437	1.65	0.00	Phospholipase C, eta 1
Pld1	18805	1.28/1.56	0.00/0.00	Phospholipase D1, phosphatidylcholine-specific
Plek2	27260	2.15	0.00	Pleckstrin 2
Plekhb1	27276	-2.44/1.22	0.00/0.00	pleckstrin homology domain containing, family B (evectins) member 1
Plin2	11520	1.07	0.00	Perilipin 2
Pls1	102502	2.62	0.00	Plastin 1
Plscr1	22038	2.00/2.10	0.01/0.00	Phospholipid scramblase 1
Plxnb1	235611	3.04	0.00	Plexin B1
Pm20d2	242377	-2.10	0.00	Peptidase M20 domain containing 2
Pnpla3	116939	2.28	0.00	Patatin-like phospholipase domain containing 3
Pnpla5	75772	3.68	0.00	Patatin-like phospholipase domain containing 5
Pold4	69745	2.84	0.00	Polymerase (DNA-directed), delta 4
Pon1	18979	-2.75	0.00	Paraoxonase 1
Pou3f1	18991	1.35	0.00	POU domain, class 3, transcription factor 1
Ppap2c	50784	1.93	0.00	Phosphatidic acid phosphatase type 2C
Ppl	19041	1.77	0.00	Periplakin
Ppm1h	319468	1.23	0.03	Protein phosphatase, Mg2+/Mn2+ dependent, 1H
Ppm1k	243382	-1.80/-1.66	0.00/0.01	Protein phosphatase, Mg2+/Mn2+ dependent, 1K
Ppp1r13b	21981	1.20	0.00	Protein phosphatase 1 regulatory subunit 13B
Ppp1r14a	68458	-1.27	0.01	Protein phosphatase 1 regulatory subunit 14A
Ppp1r14b	18938	1.01	0.00	Protein phosphatase 1 regulatory subunit 14B
Pprc1	226169	1.16	0.00	Peroxisome proliferator-activated receptor gamma coactivator-related protein 1
Pqlc3	217430	1.77	0.00	PQ loop repeat containing 3
Prelid2	77619	1.84	0.01	PRELI domain containing 2
Prkab1	19079	1.00	0.00	Protein kinase, AMP-activated, beta 1 non-catalytic subunit
Prkca	18750	1.35	0.00	Protein kinase C, alpha
Prlr	19116	-2.76/-2.29/-2.28/-1.43/-1.27/-1.11	0.00/0.00/0.00/0.04/0.02/0.00	Prolactin receptor
Prodh	19125	-3.57	0.00	Proline dehydrogenase (oxidase) 1
Prom1	19126	4.06	0.00	Prominin 1
Prom2	192212	2.82	0.00	Prominin 2
Prr5l	72446	1.23	0.01	Proline rich 5 like
Prrg1	546336	1.41	0.00	Proline rich Gla (G-carboxyglutamic acid) 1
Prss8	76560	1.58	0.03	Protease, serine, 8
Prtn3	19152	1.86	0.01	Proteinase 3
Psat1	107272	3.45/3.61	0.00/0.00	Phosphoserine aminotransferase 1
Psg18	26438	1.90	0.01	Pregnancy specific glycoprotein 18
Psph	100678	2.13	0.00	Phosphoserine phosphatase
Psrc1	56742	1.42/4.40	0.00/0.00	Proline/serine-rich coiled-coil 1
Ptbp1	19205	-3.05	0.00	Polypyrimidine tract binding protein 1
Ptger2	19217	-1.18	0.04	Prostaglandin E receptor 2 (subtype EP2), 53kDa
Ptgfrn	19221	2.19	0.00	Prostaglandin F2 receptor negative regulator
Ptgr1	67103	2.41	0.00	Prostaglandin reductase 1
Pth1r	19228	-1.51	0.00	Parathyroid hormone 1 receptor
Pth2r	213527	1.26	0.01	Parathyroid hormone 2 receptor
Ptk2b	19229	-1.48	0.01	Protein tyrosine kinase 2 beta
Ptpla	30963	-1.19/-1.19	0.00/0.01	Protein tyrosine phosphatase-like (proline instead of catalytic arginine), member A
Ptprd	19266	-1.50/-1.47/-1.35	0.01/0.01/0.00	Protein tyrosine phosphatase, receptor type, D
Ptpre	19267	2.23/2.77	0.00/0.00	Protein tyrosine phosphatase, receptor type, E
Ptprk	19272	1.04/1.13	0.00/0.01	Protein tyrosine phosphatase, receptor type, K
Pycr1	209027	1.16	0.02	Pyrroline-5-carboxylate reductase 1
Pygb	110078	2.76	0.00	Phosphorylase, glycogen; brain
Rab11fip5	52055	1.06	0.02	RAB11 family interacting protein 5 (class I)
Rab23	19335	1.28/1.50	0.00/0.00	Ras-related protein *Rab-23*

Gene symbol	EntrezGene ID	Log-ratio	p-value	Gene name
Rab34	19376	1.73/1.76	0.00/0.00	Ras-related protein *Rab-34*
Rab3d	19340	1.28/1.82	0.00/0.00	Ras-related protein Rab-3D
Rad51l1	19363	2.16	0.01	RAD51 homolog B
Rai2	24004	-1.22	0.00	Retinoic acid-induced protein 2
Ramp1	51801	-1.30	0.00	Receptor activity modifying protein 1
Ranbp3l	223332	-1.52	0.01	RAN binding protein 3-like
Rap2a	76108	-1.08	0.00	Ras-related protein Rap-2a
Rapgef5	217944	1.47/1.69	0.01/0.00	Rap guanine nucleotide exchange factor (GEF) 5
Rasa2	114713	1.79/1.83	0.00/0.00	RAS p21 protein activator 2
Rasgrp2	19395	2.69/2.98/3.22	0.00/0.00/0.00	RAS guanyl-releasing protein 2
Rassf5	54354	-1.34/-1.22	0.02/0.02	Ras association domain-containing protein 5
Rbfox2	93686	1.24	0.00	RNA binding protein, fox-1 homolog (C. elegans) 2
Rbl1	19650	1.23	0.02	Retinoblastoma-like 1
Rbm24	666794	1.09/1.16	0.00/0.00	RNA binding motif protein 24
Rbms3	207181	-1.19/-1.06	0.01/0.00	RNA binding motif, single stranded interacting protein 3.
Rbp1	19659	3.39	0.00	Retinol binding protein 1
Rcan3	53902	2.08	0.00	RCAN family member 3
Rcn2	26611	1.00	0.00	Reticulocalbin 2
Rdh16	19683	-1.20	0.02	Retinol dehydrogenase 16
Rdh5	19682	1.33	0.00	Retinol dehydrogenase 5
Rdh9	103142	1.08	0.02	Retinol dehydrogenase 9
Reep5	13476	1.19/1.36	0.00/0.00	Receptor accessory protein 5
Rell1	100532	1.42/1.49	0.00/0.00	RELT-like 1
Retsat	67442	-1.89/-1.67	0.00/0.00	All-trans-retinol 13,14-reductase
Rfx4	71137	-2.79	0.00	Regulatory factor X, 4 (influences HLA class II expression)
Rgn	19733	-2.08	0.00	Regucalcin
Rgs16	19734	1.42/1.67/1.70	0.00/0.00/0.00	Regulator of G-protein signaling 16
Rgs20	58175	2.85	0.00	Regulator of G-protein signaling 20
Rgs4	19736	-1.17	0.05	Regulator of G-protein signaling 4
Rgs5	19737	-1.70/-1.66/-1.65/-1.13	0.00/0.00/0.01/0.03	Regulator of G-protein signaling 5
Rhbdf1	13650	1.90	0.00	Rhomboid 5 homolog 1
Rhoc	11853	2.37/2.45	0.00/0.00	Ras homolog gene family, member C
Rhod	11854	1.23	0.01	Ras homolog gene family, member D
Rims2	116838	1.51	0.02	Regulating synaptic membrane exocytosis 2
Rims4	241770	1.28	0.02	Regulating synaptic membrane exocytosis 4
Rnase4	58809	-1.76	0.03	Ribonuclease, RNase A family, 4
Rnf152	320311	-1.07	0.01	Ring finger protein 152
Rnf39	386454	2.36	0.00	Ring finger protein 39
Robo1	19876	2.55	0.00	Roundabout homolog 1
Rogdi	66049	2.02	0.00	*Rogdi* homolog
Rora	19883	1.05	0.00	RAR-related orphan receptor A
Rp2h	19889	1.10/1.36/1.61	0.01/0.00/0.00	Retinitis pigmentosa 2 homolog
Rpain	69723	-1.13/-1.03	0.00/0.00	RPA interacting protein
Rpap3	71919	1.09	0.00	RNA polymerase II associated protein 3
Rpp21	67676	1.02	0.00	Ribonuclease P/MRP 21kDa subunit
Rrbp1	81910	1.11/1.16/1.22	0.00/0.00/0.01	Ribosome binding protein 1 homolog 180kDa
Rsph3a	66832	1.45	0.01	Radial spoke 3A homolog
Rspo3	72780	-1.82	0.01	R-spondin-3
Rtkn	20166	1.52	0.00	Rhotekin
Rundc3b	242819	1.82	0.05	RUN domain containing 3B
Runx2	12393	1.86	0.01	Runt-related transcription factor 2
S100a1	20193	-1.25/-1.22	0.00/0.00	S100 calcium binding protein A1
S100a11	20195	2.24	0.00	S100 calcium binding protein A11
S100g	12309	1.19	0.05	S100 calcium binding protein G
S1pr3	13610	1.89/2.61	0.00/0.00	Sphingosine-1-phosphate receptor 3
Saa1	20208	-2.54	0.01	Serum amyloid A1
Saa4	20211	-1.33/-1.05	0.00/0.01	Serum amyloid A4, constitutive
Sall1	58198	1.09	0.00	Sal-like 1
Samd4	74480	1.11/1.17/1.67	0.01/0.00/0.00	Sterile alpha motif domain containing 4
Sardh	192166	-1.29/-1.11	0.01/0.01	Sarcosine dehydrogenase, mitochondrial
Satb2	212712	1.14	0.00	Special AT-rich sequence-binding protein 2
Scamp5	56807	1.14	0.00	Secretory carrier-associated membrane protein 5
Scara5	71145	-1.41	0.02	Scavenger receptor class A, member 5 (putative)
Sccpdh	109232	2.23	0.00	Saccharopine dehydrogenase (putative)
Scd2	20250	3.70/4.02	0.00/0.00	Stearoyl-CoA desaturase (delta-9-desaturase)
Scel	64929	2.73	0.00	Sciellin
Scn8a	20273	1.80/2.70/4.57	0.00/0.00/0.00	Sodium channel, voltage gated, type VIII, alpha subunit
Scnn1a	20276	-1.00	0.00	Sodium channel, nonvoltage-gated 1 alpha
Sdpr	20324	1.09/1.20/1.65	0.00/0.00/0.00	Serum deprivation response
Sdr9c7	70061	-1.86/-1.74	0.03/0.02	Short chain dehydrogenase/reductase family 9C, member 7
Sec14l4	103655	-1.32	0.01	SEC14-like 4
Sectm1a	209588	1.68	0.01	Secreted and transmembrane 1A
Sel1l3	231238	1.57	0.00	Sel-1 suppressor of lin-12-like 3
Sema3d	108151	-2.05	0.00	Sema domain, immunoglobulin domain (Ig), short basic domain, secreted, (semaphorin) 3D

Gene symbol	EntrezGene ID	Log-ratio	p-value	Gene name
Sema3e	20349	-2.34/-1.75/-1.46	0.00/0.00/0.01	Sema domain, immunoglobulin domain (Ig), short basic domain, secreted, (semaphorin) 3E
Sepn1	74777	1.03	0.01	Selenoprotein N, 1
Sepw1	20364	-1.09/-1.04	0.01/0.00	Selenoprotein W, 1
Serpina11	380780	-1.18	0.01	Serpin peptidase inhibitor, clade A (alpha-1 antiproteinase, antitrypsin), member 11
Serpina12	68054	1.12/2.18	0.02/0.00	Serpin peptidase inhibitor, clade A (alpha-1 antiproteinase, antitrypsin), member 12
Serpina3k	20714	-1.90	0.01	Serine (or cysteine) peptidase inhibitor, clade A, member 3k
Serpina4-ps1	321018	-3.99/-3.99/-3.83	0.00/0.00/0.00	Serine (or cysteine) peptidase inhibitor, clade A, member 4, pseudogene 1
Serpinb6b	20708	1.72	0.01	Serine (or cysteine) peptidase inhibitor, clade B, member 6b
Serpine1	18787	1.77	0.03	Serpin peptidase inhibitor, clade E (nexin, plasminogen activator inhibitor type 1), member 1
Serpine2	20720	-2.28	0.01	Serpin peptidase inhibitor, clade E (nexin, plasminogen activator inhibitor type 1), member 2
Sertad1	55942	1.40	0.00	SERTA domain-containing protein 1
Sfpq	71514	1.09	0.00	Splicing factor proline/glutamine-rich
Sfxn5	94282	-1.29	0.00	Sideroflexin 5
Sgsm1	52850	1.70/2.90	0.00/0.00	Small G protein signaling modulator 1
Sh3bgrl	56726	1.07/1.11	0.01/0.00	SH3 domain binding glutamic acid-rich protein like
Sh3bp4	98402	1.27	0.00	SH3-domain binding protein 4
Sh3pxd2b	268396	1.68	0.00	SH3 and PX domains 2B
Shc2	216148	1.10	0.01	SHC transforming protein 2
Shcbp1	20419	1.07	0.02	SHC SH2-domain binding protein 1
Shroom3	27428	1.29	0.00	Shroom family member 3
Sidt1	320007	1.23	0.01	SID1 transmembrane family, member 1
Sik1	17691	1.15	0.02	Salt-inducible kinase 1
Sirpa	19261	1.46	0.01	Signal-regulatory protein alpha
Sirt3	64384	-1.26	0.01	Sirtuin 3
Slc10a1	20493	-1.68/-1.67	0.01/0.00	Solute carrier family 10 (sodium/bile acid cotransporter family), member 1
Slc12a2	20496	-1.44	0.04	Solute carrier family 12 (sodium/potassium/chloride transporters), member 2
Slc13a3	114644	-1.22	0.04	Solute carrier family 13 (sodium-dependent dicarboxylate transporter), member 3
Slc16a10	72472	-1.68/-1.41	0.00/0.01	Solute carrier family 16, member 10 (aromatic amino acid transporter)
Slc16a6	104681	1.23	0.00	Solute carrier family 16, member 6
Slc16a9	66859	-1.12	0.04	Solute carrier family 16, member 9
Slc17a2	218103	-1.23/-1.20	0.00/0.02	Solute carrier family 17 (sodium phosphate), member 2
Slc1a2	20511	-2.21/-2.05/-1.81	0.02/0.01/0.00	Solute carrier family 1 (glutamate/neutral amino acid transporter), member 1
Slc1a4	55963	1.17/1.61/1.72	0.02/0.01/0.03	Solute carrier family 1 (glutamate/neutral amino acid transporter), member 4
Slc20a1	20515	1.33	0.01	Solute carrier family 20 (phosphate transporter), member 1
Slc22a27	171405	2.16	0.00	Solute carrier family 22 (organic anion transporter), member 27
Slc22a30	319800	-1.76	0.00	Solute carrier family 22 (organic anion transporter), member 30
Slc22a4	30805	-1.19	0.02	Solute carrier family 22 (organic anion transporter), member 4
Slc22a7	108114	-3.34	0.01	Solute carrier family 22 (organic anion transporter), member 7
Slc24a3	94249	1.91	0.01	Solute carrier family 24 (sodium/potassium/calcium exchanger), member 3
Slc25a15	18408	-1.13	0.01	Solute carrier family 25 (mitochondrial carrier; ornithine transporter) member 15
Slc25a30	67554	1.37/1.67/1.70	0.00/0.01/0.00	Solute carrier family 25, member 30
Slc25a42	73095	-1.50	0.00	Solute carrier family 25, member 42
Slc26a1	231583	-1.29/-1.14	0.01/0.00	Solute carrier family 26, member 1
Slc26a4	23985	-1.26	0.00	Solute carrier family 26, member 4
Slc27a5	26459	-1.09	0.01	Solute carrier family 27 (fatty acid transporter), member 5
Slc29a1	63959	-1.12	0.01	Solute carrier family 29 (nucleoside transporters), member 1
Slc35e3	215436	-1.13	0.00	Solute carrier family 35, member E3
Slc35f2	72022	1.40	0.00	Solute carrier family 35, member F2
Slc37a3	72144	1.01	0.01	Solute carrier family 37 (glycerol-3-phosphate transporter), member 3
Slc39a2	214922	-1.11	0.01	Solute carrier family 39 (zinc transporter), member 2
Slc39a4	72027	2.36	0.00	Solute carrier family 39 (zinc transporter), member 4
Slc41a2	338365	1.10	0.01	Solute carrier family 41, member 2
Slc41a3	71699	1.25/2.79	0.00/0.00	Solute carrier family 41, member 3
Slc44a3	213603	1.11	0.00	Solute carrier family 44, member 3
Slc48a1	67739	1.26/1.40	0.00/0.00	Solute carrier family 48 (heme transporter), member 1
Slc6a8	102857	1.09	0.00	Solute carrier family 6 (neurotransmitter transporter, creatine), member 8

Gene symbol	EntrezGene ID	Log-ratio	p-value	Gene name
Slc7a7	20540	1.65	0.00	Solute carrier family 7 (cationic amino acid transporter, y+ system), member 7
Slc7a9	30962	1.14	0.01	Solute carrier family 7 (cationic amino acid transporter, y+ system), member 9
Slco1a1	28248	-4.26/-4.23	0.01/0.01	Solute carrier organic anion transporter family, member 1A2
Slco1b2	28253	-3.24/-3.22/-3.03	0.00/0.00/0.00	Solute carrier organic anion transporter family, member 1B2
Slco2b1	101488	-3.42/-2.30	0.00/0.00	Solute carrier organic anion transporter family member 2B1
Slpi	20568	4.15	0.00	Secretory leukocyte peptidase inhibitor
Smoc2	64074	1.95/2.66	0.01/0.00	SPARC-related modular calcium-binding protein 2
Smox	228608	1.01/2.79	0.00/0.00	Spermine oxidase
Smpd3	58994	1.78	0.00	Sphingomyelin phosphodiesterase 3, neutral membrane
Smpdl3b	100340	2.62	0.00	Sphingomyelin phosphodiesterase, acid-like 3B
Sned1	208777	-1.03	0.02	Sushi, nidogen and EGF-like domains 1
Snhg11	319317	-2.92	0.00	Small nucleolar RNA host gene 11 (non-protein coding)
Sntb2	20650	1.23	0.00	Syntrophin, beta 2
Sntg2	268534	-1.79	0.00	Syntrophin, gamma 2
Snx6	72183	1.00	0.01	Sorting nexin 6
Socs5	56468	1.34/1.54	0.00/0.00	Suppressor of cytokine signaling 5
Sod2	20656	-1.08	0.00	Superoxide dismutase 2, mitochondrial
Sod3	20657	-1.17	0.01	Superoxide dismutase 3, extracellular
Sorbs2	234214	1.13	0.02	Sorbin and SH3 domain-containing protein 2
Sord	20322	-1.59	0.04	Sorbitol dehydrogenase
Sox4	20677	1.15/1.39/2.74	0.01/0.00/0.00	SRY (sex determining region Y)-box 4
Spa17	20686	1.17	0.00	Sperm autoantigenic protein 17
Sparc	20692	2.45/2.46	0.00/0.00	Secreted protein, acidic, cysteine-rich (osteonectin)
Spc25	66442	1.61	0.01	NDC80 kinetochore complex component, homolog
Specc1	432572	1.95	0.00	Sperm antigen with calponin homology and coiled-coil domains 1
Spin2	278240	1.21	0.00	Spindlin family, member 2
Spink3	20730	4.98	0.00	Serine protease inhibitor Kazal-type 3
Spna2	20740	1.18/1.27	0.00/0.00	Spectrin alpha 2
Spred1	114715	1.31/1.44	0.00/0.00	Sprouty-related, EVH1 domain-containing protein 1
Spred2	114716	1.16	0.00	Sprouty-related, EVH1 domain-containing protein 2
Sprr1a	20753	1.72	0.00	Small proline-rich protein 1A
Spry2	24064	2.45	0.00	Sprouty homolog 2
Spry4	24066	1.25	0.03	Sprouty homolog 4
Sptlc2	20773	1.31	0.00	Serine palmitoyltransferase, long chain base subunit 2
Spty2d1	101685	1.14	0.01	Suppressor of Ty, domain containing 1
Sqle	20775	2.17	0.02	Squalene epoxidase
Srd5a1	78925	-2.71/-2.28/-2.15	0.00/0.00/0.00	Steroid-5-alpha-reductase, alpha polypeptide 1
Srd5a2	94224	1.08	0.00	Steroid-5-alpha-reductase, alpha polypeptide 2
Srr	27364	-1.21/-1.20/-1.12/-1.09/-1.06	0.00/0.00/0.00/0.01/0.01	Serine racemase
Srxn1	76650	1.01	0.01	Sulfiredoxin 1
Sstr2	20606	1.37	0.00	Somatostatin receptor 2
St6gal1	20440	1.09	0.00	ST6 beta-galactosamide alpha-2,6-sialyltranferase 1
Stambpl1	76630	1.54	0.00	STAM binding protein-like 1
Stard5	170460	-1.19/-1.06	0.03/0.02	StAR-related lipid transfer protein 5
Steap2	74051	-1.15	0.01	STEAP family member 2, metalloreductase
Stmn1	16765	1.04/1.60	0.02/0.01	Stathmin 1
Sulf2	72043	-1.16/-1.13	0.00/0.00	Sulfatase 2
Sult1b1	56362	-2.02	0.00	Sulfotransferase family 1B, member 1
Sult2a2	100043194	3.63	0.02	Sulfotransferase family 2A, member 2
Sult4a1	29859	1.19	0.01	Sulfotransferase family 4A, member 1
Sult5a1	57429	-2.13	0.00	Sulfotransferase family 5A, member 1
Suox	211389	-1.91	0.00	Sulfite oxidase
Susd1	634731	-1.42	0.01	Sushi domain containing 1
Susd4	96935	-2.68/-2.64	0.00/0.00	Sushi domain containing 4
Sybu	319613	1.84	0.00	Syntabulin (syntaxin-interacting)
Sycp3	20962	-1.24	0.02	Synaptonemal complex protein 3
Synj2	20975	1.13	0.00	Synaptojanin 2
Synm	233335	1.08	0.00	Synemin, intermediate filament protein
Tagln2	21346	1.51/1.90	0.00/0.00	Transgelin-2
Tanc1	66860	1.23	0.00	tetratricopeptide repeat, ankyrin repeat and coiled-coil containing 1
Tax1bp3	76281	1.03	0.00	Tax1-binding protein 3
Tbc1d2b	67016	1.08	0.00	TBC1 domain family, member 2B
Tbx20	57246	-1.37	0.01	T-box 20
Tbx3	21386	-2.59/-2.14	0.00/0.00	T-box 3
Tc2n	74413	2.15/2.39/2.80	0.00/0.00/0.00	Tandem C2 domains nuclear protein
Tceal8	66684	2.75	0.00	Transcription elongation factor A (SII)-like 8
Tcf21	21412	-1.76	0.00	Transcription factor 21
Tcf4	21413	1.00	0.01	Transcription factor 4
Tes	21753	1.25	0.00	Testin
Tex12	66654	-1.49	0.01	Testis expressed 12
Tff3	21786	4.50	0.00	Trefoil factor 3 (intestinal)

Gene symbol	EntrezGene ID	Log-ratio	p-value	Gene name
Tgfa	21802	1.04	0.01	*Transforming growth factor alpha*
Tgfb2	21808	1.64/1.87/1.97	0.00/0.00/0.00	Transforming growth factor, beta 2
Tgfbr2	21813	2.65	0.00	Transforming growth factor, beta receptor II
Tgif1	21815	1.34	0.00	TGFB-induced factor homeobox 1
Thsd4	207596	1.03	0.01	Thrombospondin, type I, domain containing 4
Tifa	211550	-1.42	0.01	TRAF-interacting protein with forkhead-associated domain
Timeless	21853	1.01	0.01	Timeless homolog
Timp2	21858	-1.37/-1.20	0.04/0.03	TIMP metallopeptidase inhibitor 2
Tinag	26944	3.11	0.00	Tubulointerstitial nephritis antigen
Tjp2	21873	1.19/1.20	0.02/0.00	Tight junction protein 2
Tlr1	21897	4.33	0.00	Toll-like receptor 1
Tlr5	53791	-1.25	0.01	Toll-like receptor 5
Tm4sf4	229302	1.14	0.00	Transmembrane 4 superfamily member 4
Tm9sf2	68059	-1.04	0.02	Transmembrane 9 superfamily member 2
Tmc5	74424	2.25	0.00	Transmembrane channel-like protein 5
Tmed6	66269	2.12	0.03	Transmembrane emp24 protein transport domain containing 6
Tmem146	106757	3.00	0.00	Transmembrane protein 146
Tmem158	72309	1.04	0.03	Transmembrane protein 158
Tmem191c	224019	1.25	0.01	Transmembrane protein 191C
Tmem229a	319832	1.96	0.04	Transmembrane protein 229A
Tmem45b	235135	3.69	0.00	Transmembrane protein 45B
Tmem62	96957	1.34	0.00	Transmembrane protein 62
Tmem63a	208795	-1.17	0.00	Transmembrane protein 63A
Tmem71	213068	2.56	0.00	Transmembrane protein 71
Tmem86a	67893	2.49	0.00	Transmembrane protein 86A
Tnfrsf11b	18383	-2.12	0.00	Tumor necrosis factor receptor superfamily member 11b
Tnfrsf12a	27279	2.98/3.17	0.00/0.00	Tumor necrosis factor receptor superfamily member 12a
Tnfrsf18	21936	2.17	0.00	Tumor necrosis factor receptor superfamily member 18
Tnfrsf21	94185	1.50/1.77	0.00/0.00	Tumor necrosis factor receptor superfamily member 21
Tnik	665113	2.10	0.00	TRAF2 and NCK-interacting protein kinase
Tns1	21961	1.00	0.03	Tensin 1
Tox2	269389	1.38	0.05	TOX high mobility group box family member 2
Tox3	244579	1.46	0.02	TOX high mobility group box family member 3
Tpcn1	252972	-1.03	0.01	Two pore segment channel 1
Tpd52	21985	1.07	0.00	Tumor protein D52
Tpm1	22003	1.62/1.84	0.00/0.00	Tropomyosin alpha-1 chain
Tppp	72948	-1.26	0.02	Tubulin polymerization-promoting protein
Tpra1	24100	1.11	0.00	Transmembrane protein, adipocyte asscociated 1
Tprkb	69786	-1.25/-1.20	0.00/0.00	TP53RK binding protein
Trfr2	50765	-1.02	0.00	Transferrin receptor protein 2
Trib2	217410	1.22	0.01	Tribbles homolog 2
Trib3	228775	1.93/1.99	0.01/0.01	Tribbles homolog 3
Trim2	80890	1.31/1.52	0.01/0.03	Tripartite motif-containing protein 2
Trim68	101700	1.13	0.00	Tripartite motif-containing protein 68
Trip13	69716	1.30	0.00	Thyroid hormone receptor interactor 13
Trip4	56404	-1.24	0.00	Thyroid hormone receptor interactor 4
Trp53inp1	60599	1.16	0.01	p53-dependent damage-inducible nuclear protein 1
Trpm4	68667	2.10	0.00	Transient receptor potential cation channel subfamily M member 4
Tsc22d2	72033	1.17	0.00	TSC22 domain family, member 2
Tsc22d4	78829	1.04	0.02	TSC22 domain family, member 4
Tspan15	70423	1.23	0.00	Tetraspanin-15
Tspan2	70747	1.41/2.50	0.01/0.01	Tetraspanin-2
Tspan8	216350	2.20/2.20/3.99/4.91/ 5.03	0.02/0.00/0.00/0.00/0.00	Tetraspanin-8
Tspyl4	72480	-2.60	0.00	TSPY-like 4
Tstd1	226654	2.64	0.00	Thiosulfate sulfurtransferase (rhodanese)-like domain containing 1
Ttc39c	72747	-2.03/-1.91/-1.85	0.01/0.02/0.00	Tetratricopeptide repeat domain 39C
Ttc7b	104718	-1.81	0.00	Tetratricopeptide repeat domain 7B
Tuba1b	22143	1.41	0.00	Tubulin, alpha 1b
Tuba8	53857	1.04/1.06	0.02/0.02	Tubulin, alpha 8
Tubb2a	22151	1.97/2.82	0.00/0.00	Tubulin, beta 4B class IVa
Tubb2b	73710	1.48	0.04	Tubulin, beta 4B class IIb
Tubb4b	227613	1.62	0.01	Tubulin, beta 4B class IVb
Tubb6	67951	2.36	0.00	Tubulin, beta 6 class V
Tuft1	22156	1.80	0.00	Tuftelin 1
Tulp2	56734	-1.01	0.00	Tubby like protein 2
Twf2	23999	1.33/1.38	0.02/0.00	Twinfilin, actin-binding protein, homolog 2
Uap1l1	227620	2.05	0.00	UDP-N-acteylglucosamine pyrophosphorylase 1-like 1
Ubtd2	327900	1.90	0.00	ubiquitin domain containing 2
Uggt2	66435	1.10	0.01	UDP-glucose glycoprotein glucosyltransferase 2
Ugt2a3	72094	-1.34	0.00	UDP glycosyltransferase 2 family, polypeptide A3
Ugt2b1	71773	-2.21	0.00	UDP glycosyltransferase 2 family, polypeptide B1
Ugt3a1	105887	-2.13	0.02	UDP glycosyltransferase 3 family, polypeptide A1
Ugt3a2	223337	-1.65	0.00	UDP glycosyltransferase 3 family, polypeptide A2
Ulk1	22241	1.03	0.00	Unc-51-like kinase 1

Gene symbol	EntrezGene ID	Log-ratio	p-value	Gene name
Unc119	22248	2.28	0.00	Unc-5 homolog 119
Unc13b	22249	1.04	0.01	Unc-5 homolog 13B
Unc5b	107449	1.27	0.00	Unc-5 homolog B
Upp2	76654	-3.48/-3.44/-2.57	0.01/0.01/0.02	Uridine phosphorylase 2
Uvrag	78610	-1.18	0.01	UV radiation resistance-associated gene
Vasp	22323	1.55	0.00	Vasodilator-stimulated phosphoprotein
Vipr1	22354	-1.63	0.00	Vasoactive intestinal polypeptide receptor 1
Vnn1	22361	4.05/4.16	0.00/0.00	Vanin 1
Vnn3	26464	2.94	0.00	Vanin 3
Vrk2	69922	-1.19/-1.13	0.01/0.03	Vaccinia related kinase 2
Vsig10	231668	1.91	0.00	V-set and immunoglobulin domain containing 10
Wbp5	22381	1.56	0.00	WW domain binding protein 5
Wdr1	22388	1.10/1.24/1.26	0.00/0.00/0.00	WD repeat domain 1
Wdr67	210544	1.78/2.48	0.00/0.00	WD repeat domain 67
Wdr91	101240	-1.22	0.01	WD repeat domain 91
Wfdc12	192200	1.68	0.01	WAP four-disulfide core domain protein 12
Wfdc15b	192201	4.33	0.00	WAP four-disulfide core domain protein 15b
Wfdc2	67701	-1.19	0.01	WAP four-disulfide core domain protein 2
Wnk4	69847	1.89	0.00	WNK lysine deficient protein kinase 4
Wnt2	22413	-1.61	0.00	Wingless-type MMTV integration site family, member 2
Wnt5b	22419	-1.58/-1.20	0.01/0.03	Wingless-type MMTV integration site family, member 5B
Wsb1	78889	1.27	0.01	WD repeat and SOCS box containing 1
Wsb2	59043	1.01	0.00	WD repeat and SOCS box containing 2
Zc3h12d	237256	1.30	0.03	Zinc finger CCCH-type containing 12D
Zeb2	24136	-1.09	0.04	Zinc finger E-box-binding homeobox 2
Zfand3	21769	1.02	0.00	Zinc finger, AN1-type domain 3
Zfp157	72154	-1.02	0.01	Zinc finger protein 137
Zfp318	57908	-1.18	0.01	Zinc finger protein 318
Zfp385b	241494	-1.02	0.02	Zinc finger protein 385b
Zfp386	56220	1.04	0.01	Zinc finger protein 386
Zfp462	242466	1.97	0.02	Zinc finger protein 462
Zfp53	24132	1.40	0.05	Zinc finger protein 53
Zfp54	22712	1.10	0.01	Zinc finger protein 54
Zfp618	72701	1.16	0.00	Zinc finger protein 618
Zfp7	223669	1.94	0.00	Zinc finger protein 7
Zfp704	170753	1.01/1.52	0.00/0.00	Zinc finger protein 704
Zfp750	319530	1.23	0.01	Zinc finger protein 750
Zfp871	208292	-1.06	0.02	Zinc finger protein 871
Zfp9	22750	1.30	0.00	Zinc finger protein 9
Zfp948	381066	1.08	0.01	Zinc finger protein 948
Zik1	22775	1.08	0.04	Zinc finger protein interacting with K protein 1 homolog
Zmat3	22401	1.31	0.00	Zinc finger, matrin-type 3

C) miRNAs significantly dysregulated in *Ctnnb1*-mutated tumors vs. adjacent non-tumor tissue (log-ratio >1.0, p-value <0.05).

miRNA name	Ensembl Gene ID	Log-ratio	p-value
mmu-miR-680	ENSMUSG00000076253	6.11	0.00
mmu-miR-425	ENSMUSG00000065579	4.01	0.00
mmu-miR-199a-3p	ENSMUSG00000070126	-1.25	0.04

D) miRNAs significantly dysregulated in *Ha-ras*-mutated tumors vs. adjacent non-tumor tissue (log-ratio >1.0, p-value <0.05).

miRNA name	Ensembl Gene ID	Log-ratio	p-value
mmu-miR-96	ENSMUSG00000065586	7.21	0.00
mmu-miR-199a-5p	ENSMUSG00000070126	-5.45	0.00
mmu-miR-455	ENSMUSG00000070102	-5.74	0.00
mmu-miR-146b	ENSMUSG00000070127	4.75	0.01
mmu-miR-199a-3p	ENSMUSG00000070126	-1.23	0.05
mmu-miR-338-3p	ENSMUSG00000065600	-1.54	0.05
mmu-miR-139-5p	ENSMUSG00000065446	-1.21	0.05
mmu-miR-193	ENSMUSG00000065395	-1.41	0.05

E) Differentially methylated DNA regions in *Ctnnb1*-mutated tumors vs. adjacent non-tumor tissue (log-ratio >1.0, p-value <0.05).

Probeset ID	Gene symbol	Gene name	Strand	Chromosome	Start	End	Log-ratio	p-value
ENSMUSG00000066584	Abpb	Androgen binding protein beta	-1	7	34796951	34798961	-1.02	0.04
ENSMUSG00000030168	Adipor2	Adiponectin receptor 2	-1	6	119303168	119367501	1.55	0.01
ENSMUSG00000044033	Ccdc141	Coiled-coil domain containing 141	-1	2	76847960	77008693	1.26	0.05
ENSMUSG00000059554	Ccdc28a	Coiled-coil domain containing 28A	-1	10	17933482	17954804	1.34	0.05
ENSMUSG00000004709	Cd244	Cluster of differentiation 244	1	1	173489324	173515449	-1.59	0.02
ENSMUSG00000016756	Cmah	Cytidine monophosphate-N-acetylneuraminic acid hydroxylase-like	1	13	24419289	24569154	1.36	0.01
ENSMUSG00000079415	Cntf	Ciliary neurotrophic factor	-1	19	12838150	12840122	1.01	0.05
ENSMUSG00000046516	Cox17	Cytochrome c oxidase assembly homolog	1	16	38347077	38362383	1.09	0.02
ENSMUSG00000025991	Cps1	Carbamoyl-phosphate synthase 1	1	1	67169600	67277833	1.5	0.03
ENSMUSG00000029014	Dnajc2	DnaJ (Hsp40) homolog, subfamily C, member 2	-1	5	21263085	21291069	1.2	0.05
ENSMUSG00000003235	Eif2b5	Eukaryotic translation initiation factor 2B, subunit 5 epsilon, 82kDa	1	16	20498890	20510028	1.2	0.03
ENSMUSG00000019989	Enpp3	Ectonucleotide pyrophosphatase/phosphodiesterase family member 3	-1	10	24493620	24556001	1.25	0.02
ENSMUSG00000075703	Ept1	Ethanolaminephosphotransferase 1 (CDP-ethanolamine-specific)	1	5	30559121	30598558	1.13	0.05
ENSMUSG00000061286	Exosc5	Exosome component 5	1	7	26444172	26453050	1.27	0.05
ENSMUSG00000043230	Fam124b	Family with sequence similarity 124B	-1	1	80195281	80215048	-1.34	0.05
ENSMUSG00000069911	Fam196b	Family with sequence similarity 196b	1	11	34214822	34322640	-1.13	0.05
ENSMUSG00000026835	Fcnb	Ficolin b	-1	2	27931898	27940405	-1.37	0.05
ENSMUSG00000042993	Ifnk	Interferon kappa	1	4	35099305	35101254	1.07	0.03
ENSMUSG00000020155	Kcnmb1	Potassium large conductance calcium-activated channel, subfamily M, beta member 1	1	11	33863013	33873641	-1.17	0.02
ENSMUSG00000058354	Krt6a	Keratin 6A	-1	15	101520363	101524738	-1.39	0.04
ENSMUSG00000019906	Lin7a	Lin-7 homolog A	1	10	106708899	106862199	1.22	0.05
ENSMUSG00000041673	Lrrc18	leucine rich repeat containing 18	1	14	33804568	33828478	-1.41	0.04
ENSMUSG00000045854	Lyrm2	LYR motif containing 2	1	4	32887228	32888534	1.33	0.03
ENSMUSG00000040003	Magi2	Membrane-associated guanylate kinase, WW and PDZ domain-containing	1	5	18732864	20210616	1.44	0.05
ENSMUSG00000045973	Mcart1	Mitochondrial carrier triple repeat 1	-1	4	45408795	45421633	1.01/1.01	0.04/0.04
ENSMUSG00000065437	Mir30d	microRNA 30d	-1	15	68172770	68172851	1.48	0.02
ENSMUSG00000039956	Mrap	Melanocortin 2 receptor accessory protein	1	16	90738569	90750030	1.07	0.05
ENSMUSG00000023967	Mrps18a	Mitochondrial ribosomal protein S18A	1	17	46247935	46265859	1.01	0.05
ENSMUSG00000061952	Olfr1377	Olfactory receptor 1377	1	11	50798160	50799222	-1.6	0.03
ENSMUSG00000042849	Olfr1414	Olfactory receptor 1414	-1	1	94407625	94415092	-1.15	0.03
ENSMUSG00000036381	P2ry14	Purinergic receptor P2Y, G-protein coupled, 14	-1	3	58918548	58934546	-1.01	0.05
ENSMUSG00000005069	Pex5	Peroxisomal targeting signal 1 receptor	-1	6	124346834	124365085	1.34	0.05
ENSMUSG00000020464	Pnpt1	Polyribonucleotide nucleotidyltransferase 1	1	11	29030744	29061828	1.46	0.04
ENSMUSG00000030643	Rab30	RAB30, member RAS oncogene family	1	7	99890113	99985627	1.29	0.04
ENSMUSG00000032387	Rbpms2	RNA binding protein with multiple splicing 2	1	9	65477455	65508335	1.18	0.03
ENSMUSG00000032050	Rdx	Radixin	1	9	51855255	51896842	1.02	0.03
ENSMUSG00000072945	Ripply1	*Ripply1* homolog	-1	X	136314088	136316892	1.05	0.04
ENSMUSG00000021403	Serpinb9b	Serine (or cysteine) peptidase inhibitor, clade B, member 9b	1	13	33119285	33133753	1.06	0.05
ENSMUSG00000030382	Slc27a5	Solute carrier family 27 (fatty acid transporter), member 5	-1	7	13573695	13583541	1.21	0.02
ENSMUSG00000032548	Slco2a1	Solute carrier organic anion transporter family, member 2A1	1	9	102910817	102990179	1.19	0.05
ENSMUSG00000060429	Sntb1	Beta-1-syntrophin	-1	15	55470398	55738504	1.43	0.02
ENSMUSG00000022658	Tagln3	Transgelin 3	-1	16	45711343	45724721	1.23	0.04
ENSMUSG00000024287	Thoc1	THO complex 1	1	18	9958178	9995482	1.22	0.03
ENSMUSG00000046688	Tifa	TRAF-interacting protein with forkhead-associated domain	1	3	127492790	127535053	1.2	0.05
ENSMUSG00000002032	Tmem25	Transmembrane protein 25	-1	9	44601858	44607390	1.71	0.01
ENSMUSG00000038984	Tspyl5	TSPY-like 5	-1	15	33613631	33617638	1.02	0.05
ENSMUSG00000038172	Ttc39b	Tetratricopeptide repeat domain 39B	-1	4	82866204	82970159	1.22	0.03
ENSMUSG00000001924	Uba1	Ubiquitin-like modifier activating enzyme 1	1	X	20235452	20260305	1.17	0.02
ENSMUSG00000034429	Zfp707	Zinc finger protein 707	1	15	75799553	75806298	1.25	0.04
ENSMUSG00000056019	Zfp709	Zinc finger protein 709	1	8	74411163	74414811	1.57	0.03
ENSMUSG00000071267	Zfp942	Zinc finger protein 942	-1	17	22063927	22099431	1.26	0.02
ENSMUSG00000018820	Zfyve27	Zinc finger, FYVE domain containing 27	1	19	42238441	42269080	-1.59	0.03

F) Differentially methylated DNA regions in *Ha-ras*-mutated tumors vs. adjacent non-tumor tissue (log-ratio >1.0, p-value <0.05).

Probeset ID	Gene Symbol	Gene name	Strand	Chromosome	Start	End	Log-ratio	p-value
ENSMUSG00000028545	Bend5	BEN domain containing 5	1	4	111087611	111132903	-1.67	0.03
ENSMUSG00000024647	Cbln2	Cerebellin 2 precursor	1	18	86880502	86887675	-1.35	0.04
ENSMUSG00000057110	Cep110	Centriolin	1	2	34965012	35034342	1.79	0.02
ENSMUSG00000042248	Cyp2c37	Cytochrome P450 2C37	1	19	40066909	40086738	-1.26	0.04
ENSMUSG00000082932	Cyp2j8	Cytochrome P450 2J8	-1	4	96111287	96174077	-1.31	0.04
ENSMUSG00000017688	Hnf4g	Hepatocyte nuclear factor 4 gamma	1	3	3508030	3659775	-1.34	0.04
ENSMUSG00000019774	Mtrf1l	Mitochondrial translational release factor 1-like	1	10	4522631	4534654	-1.57	0.04
ENSMUSG00000035177	Nlrp2	NLR family, pyrin domain containing 2	-1	7	5250156	5302637	-1.51	0.04
ENSMUSG00000034738	Nostrin	Nitric oxide synthase trafficker	1	2	68973857	69027387	1.45	0.04
ENSMUSG00000059857	Ntng1	Netrin G1	-1	3	109582958	109938426	-1.66	0.04
ENSMUSG00000051200	Olfr513	Olfactory receptor 513	1	7	115898372	115899301	-1.32	0.04
ENSMUSG00000032099	Pate4	Prostate and testis expressed 4	-1	9	35414678	35419520	-1.64	0.04
ENSMUSG00000042700	Sipa1l1	Signal-induced proliferation-associated 1 like 1	1	12	83270407	83552769	-2.00	0.02
ENSMUSG00000021830	Txndc16	Thioredoxin domain containing 16	-1	14	45754123	45840003	-1.39	0.04
ENSMUSG00000019772	Vip	Vasoactive intestinal peptide	-1	10	4698927	4707323	-1.45	0.04

G) Differentially expressed protein and phophoprotein in *Ha-ras*-mutated tumors vs. adjacent non-tumor tissue (log-ratio >1.0, p-value <0.05).

Analyte ID	Gene symbol	Gene name	Modification	EntrezGene ID	Log-ratio	p-value
BAX	BAX	BCL2-associated X protein	basic	12028	1.25	0.02
CYP1A2	CYP1A2	Cytochrome P450 1A2	basic	13077	-1.72	0.02
CYP2C8	CYP2C8	Cytochrome P450 2C8	basic	n/a	-1.39	0.03
CYP2E1	CYP2E1	Cytochrome P450 2E1	basic	13106	-2.45/ -3.81	0.00/0.01
GSK3B_P-S9	GSK3B	Glycogen synthase kinase 3 beta	P-S9	56637	2.01	0.01
JUN	JUN	Jun oncoprotein	basic	16476	1.54	0.01
MAP2K1_P-S217/S221	MAP2K1	Dual specificity mitogen-activated protein kinase kinase 1	P-S217/S221	26395	1.07	0.04
MAP2K1_P-S217/S221	MAP2K2	Dual specificity mitogen-activated protein kinase kinase 2	P-S217/S221	26396	1.07	0.04
MAPK3_P-T202/Y204	MAPK	Mitogen-activated protein kinase	P-T202/Y204	n/a	2.23	0.01
MAPK8_P-T183/Y185	MAPK10	Mitogen-activated protein kinase 10	P-T183/Y185	26414	1.33	0.02
MAPK3_P-T202/Y204	MAPK3	Mitogen-activated protein kinase 3	P-T202/Y204	26417	2.23	0.01
MAPK8_P-T183/Y185	MAPK8	Mitogen-activated protein kinase 8	P-T183/Y185	26419	1.33	0.02

Analyte ID	Gene symbol	Gene name	Modification	EntrezGene ID	Log-ratio	p-value
MAPK8_P-T183/Y185	MAPK9	Mitogen-activated protein kinase 9	P-T183/Y185	26420	1.33	0.02
MTOR_P-S2448	MTOR	Mammalian Target of Rapamycin	P-S2448	56717	1.09	0.01
RPS6KA1_P-S380	RPS6KA1	Ribosomal protein S6 kinase, 90kDa, polypeptide 1	P-S380	20111	2.05	0.02
RPS6KA1_P-T573	RPS6KA1	Ribosomal protein S6 kinase, 90kDa, polypeptide 1	P-T573	20111	1.17	0.03